UNIVERSITY OF SOUTHAMPTON

METHODS FOR ASSESSING THE SEAKEEPING PERFORMANCE OF HIGH SPEED DISPLACEMENT MONOHULLS AND CATAMARANS

By
Dominic John Taunton

Doctor of Philosophy

FACULTY OF ENGINEERING AND APPLIED SCIENCE
SCHOOL OF ENGINEERING SCIENCES, FLUID-STRUCTURE INTERACTION RESEARCH GROUP

March 2001

UNIVERSITY OF SOUTHAMPTON

ABSTRACT

FACULTY OF ENGINEERING AND APPLIED SCIENCE

SCHOOL OF ENGINEERING SCIENCES, FLUID-STRUCTURE INTERACTION RESEARCH GROUP

Doctor of Philosophy

METHODS FOR ASSESSING THE SEAKEEPING PERFORMANCE OF HIGH SPEED DISPLACEMENT MONOHULLS AND CATAMARANS

by Dominic John Taunton

The research programme has investigated methods for assessing the seakeeping performance of high speed vessels. This has included a review and assessment of seakeeping attributes, the development of a suitable database of motion characteristics using experimental and numerical techniques and proposals for assessing the seakeeping characteristics of alternative vessels. An experimental test programme was carried out in regular head and oblique waves as well as irregular open seas on two different hull forms of fast displacement catamarans.

The results of the experiments in oblique waves are extended to beam and following headings using the transfer functions from a 3D pulsating source code at headings from head to following seas in regular waves. This effectively provides a means of generating 3D transfer functions.

The methodology used to compare and assess the seakeeping performance of vessels at an early design stage is discussed. The use of short crested seas as opposed to long crested is assessed and the differences compared. This leads to the use of spreading relationships to generate 3D transfer functions from the database of transfer functions in regular head waves. This allows the motion prediction method to be greatly enhanced by allowing any heading to be assessed. The proposed attributes and criteria suitable for assessing the seakeeping performance of high speed vessels are summarised.

Contents

Acknowledgements

Thanks to the staff and students of the Department of Ship Science for there support and help throughout my time in the Department. Especially to those who gave up many hours to help with the experiments.

Dr. A.F. Molland, who supervised this project, for his continual help, support and guidance.

Dr. J.F. Wellicome, for all his help with the experiments and the open water analysis.

Dr. D.A. Hudson, for his help and friendship over the last few years. Also for all his advice since my transfer viva and during the last few months.

Mr. P.A. Wilson, for his helpful advice since the transfer viva.

The experimental test programme was funded by EPSRC and part of the the Fast Craft Research programme funded by EPSRC and Industry and managed by Marinetech South Ltd.

Douglas Bradshaw, for his friendship and competition both on and off the river over the past few years.

Thanks also to the scullers of Southampton University for their friendship and putting up with me for so long. They have provided a welcome distraction from my work.

Finally to my family who have always given their support when it was needed.

Nomenclature

A	Static wetted surface area [m^2], I.T.T.C. spectrum coefficient
A_p	Total passenger area [m s^{-1}]
AR	Added resistance as % of calm water resistance
A_s	Seating area [m s^{-1}]
a_y	Lateral acceleration [m s^{-2}]
a_z	Vertical acceleration [m s^{-2}]
B	Beam [m], or I.T.T.C. spectrum coefficient
b	Demihull beam [m]
B/T	Breadth draught ratio
C_B	Block coefficient
C_m	Midship section coefficient
C_p	Prismatic coefficient
Demihull	One of the hulls which make up the catamaran
$f(\mu)$	Spreading function
F_N	Froude number, $\left[\frac{u}{\sqrt{gL}}\right]$
g	Acceleration due to gravity [9.80665 m s^{-2}]
H_0	Heave amplitude [m]
$H_{\frac{1}{3}}$	Significant wave height [m]
L	Length on waterline [m]
LCB	Longitudinal centre of bouyancy
LCG	Longitudinal centre of gravity
L/B	Length to breadth ratio
$L/\nabla^{1/3}$	Length displacement ratio
$M(\omega_e)$	Response spectral amplitude, in the encounter frequency domain
m_0	Motion variance
m_2 , m_4	Velocity and acceleration variance
MII	Motion induced interruptions
MSDV	Motion sickness dose value [m $s^{-1.5}$]
N_p	Number of passengers
N_v	Number of vehicles
P	Factor used to calculate MSDV for different tasks
P_0	Pitch amplitude [rad]
P_I	Installed power [kW]
$RAO(\omega_e)$	Response amplitude operator, in the encounter frequency domain

RMS	Root mean square
R_N	Reynolds number, $[\frac{uL}{\nu}]$
S	Separation of centrelines of demihulls [m]
S/L	Separation to length ratio
SM	Subjective motion index
$S_\zeta(\omega)$	Spectral ordinate of wave amplitude
t	Voyage duration, time [s]
T	Draught [m]
TF	Transfer function
$\overline{T}$	Wave modal period [s]
u, U	Velocity [m s^{-1}]
V	Service speed (Knots), [m s^{-1}]
VI	Vomiting incidence [%]
w_f	Frequency weighting for motion sickness
WSA	Static wetted surface area [m^2]

β	Normalising factor
β_1, β_2	Phase of heave and pitch [rad]
ζ_a	Wave amplitude [m]
ζ_0	Forced heave amplitude [N]
θ_0	Forced pitch ampliude [Nm]
μ	Ship heading [rad] (0=following seas, π=headseas)
π	3.142
ρ	Fluid density [Kg m^{-3}]
ω_e	Wave encounter frequency [rad s^{-1}]
ω, ω_0	Wave circular frequency [rad s^{-1}]
Δ	Displacement mass [kg or Tonnes]
∇	Displacement volume [m^3]

Chapter 1

Introduction

In recent years the demand for fast marine transport between centres of population has resulted in the development of fast catamarans and monohulls, together with a number of hybrid vessels. The development of these types of vessel has lead to greater and greater speeds. Typical speeds are of the order of 30-40 knots, with the fastest vessels achieving speeds of 50 knots. In order to achieve such speeds the vessels must be of light construction, high strength and have good calm water resistance properties. Progress has been made in developing techniques for the prediction of power for these vessels. At the same time there has been a need to develop techniques for the prediction of the seakeeping performance of such vessels. It is likely, judging by the growth in the last ten years, that the number of such vessels will continue to increase. Table 1 shows the fast ferry growth by type in the period from 1990 to 1995 and Table 2 shows a breakdown of the worldwide fleet of catamarans and monohulls by length in 1997.

The environment in which these vessels operate is unpredictable and the sea state can develop in a short period of time into conditions which are far from ideal for the operation of high speed vessels. It is therefore necessary for such vessels to be able to operate in conditions other than calm water and this will impose additional loads on the structure of the vessel, the equipment and people on board. Many high speed vessels make use of ride control or stabilizing mechanisms. These can either be included in the original design to improve an area of operation which is known to be bad, or retro-fitted after trials have shown up an area of weakness. At the same time, these control mechanisms can lead to a significant addition to the ship resistance. If areas of weakness in the operation can be predicted early in the design cycle, this need for mechanical ride-control may be reduced or eliminated.

The design of high speed vessels is a complicated procedure. From the initial outline of a new service the procedure runs through a concept design stage, then through a feasibility study before the final design stage. It is apparent that the seakeeping performance can have

a significant influence on the design and operation of these vessels and should be addressed at an early stage of the design process. The aim of this research has been to focus on and improve the prediction of seakeeping performance of high speed vessels at the concept design stage. At the concept design stage a number of different vessel types, hull shapes and dimensions will be created from the initial service requirements. Figure 1 illustrates a typical concept design process for high speed ferries. After selecting preliminary dimensions, determining the powering requirements, calculating the masses, carrying out some preliminary stability and manoeuvring checks the seakeeping performance of the suitable vessels is assessed. At this stage there may be up to 20-30 alternative vessels. The current approaches, either physical model tests or numerical methods, are too costly in terms of both expense and time. What is needed is a simple approach which will determine the relative seakeeping performance of a number of vessels at little cost. Such an approach has now been developed. It uses the large database of existing model head sea transfer functions and suitable relationships to determine the transfer functions at the other required headings. The level of detail required at this stage in the design will relate to how well the vessels perform relative to each other at the required heading and speed and to indicate any likely areas of weakness in their operating conditions. Later in the design process, when the number of alternative vessels has been reduced to say two or three, experimental and theoretical methods of seakeeping performance prediction which provide more detail may be necessary to help decide on the final design.

In order to be able to select between the seakeeping performance of alternative high speed vessels at the concept design stage, a number of diverse attributes, such as motions, velocities and accelerations, must be quantified. Once these attributes have been quantified, the vessels are assessed based on how these attributes compare with selected limiting criteria which depend on the role of the vessel. In order to improve the assessment procedure it would be helpful if these attributes could be simplified by grouping together some of the similar attributes.

Seakeeping performance prediction methods generally rely on using the various motion, velocity and acceleration transfer functions at the desired ship heading, and a suitable wave energy spectrum. The transfer functions relate the transfer of wave energy to the vessel's response over a range of frequencies. Typical transfer functions show three characteristic regions. A low frequency contouring region, where the vessel follows the wave surface. A region of resonance where the ship experiences an output greater than the input. A high frequency region where the output tends to zero relative to the input. The data base of such transfer functions is increasing with every new vessel built. Unfortunately there is very little parametric or systematic series data available, especially at high speeds. This lack of systematic series data led to the development of this programme of research at Southampton University into the seakeeping performance of high speed vessels. This programme has

comprised the physical testing of a number of different models in regular head and oblique waves. In addition to the regular wave test novel experiments, such as testing in open water and building a Vertical Planar Motion Mechanism, have been developed. These data have been used to validate numerical methods which in turn have been used to extend the data base of transfer functions to beam and following waves.

The objectives of this research are summarised as follows:

- To investigate and propose methods of predicting and assessing the seakeeping performance of alternative high speed vessels at the concept design stage.
- To increase the data base of high quality experimental results for such vessels in both head and oblique seas.
- To apply numerical techniques to extend the data base in oblique seas.
- To develop new and novel experimental procedures for use with high speed vessels, which will help to extend the data base and improve the understanding of the physical processes involved in the seakeeping of high speed vessels.

The review of the literature in Chapter 2, examines the existing sources of high speed vessel transfer functions determined from the available physical and numerical techniques. This highlights the deficiencies in the data base of high speed vessel motions and the limitations of the techniques used to determine these motions. The existing approaches to performance assessment are described and some key attributes for high speed vessels are discussed.

The attributes and criteria used to assess the seakeeping performance of high speed vessels are described and methods of condensing these into appropriate subsets is described in Chapter 3. A review of typical limiting values is presented.

The physical experimental programme is described in Chapter 4. Details of the models tested and their configurations are given. The results in head and oblique waves are presented. Novel experimental techniques are described at the end of the Chapter.

Chapter 5 describes the numerical methods used to extend the physical test results in regions which were not possible to test due to physical constraints. The limitations of these numerical results are shown and an approach which circumvents these limits is proposed.

Chapter 6 describes how both the physical and numerical results are use to determine relationships which describe how the transfer functions change with heading from head seas to following seas. The application of these transfer function spreading relationships is then validated.

The methods of predicting the seakeeping performance are described in Chapter 7. The

benefits and deficiencies of the various approaches are described. These are then illustrated in the form of a number of case studies in Chapter 8.

The summary at the end of each Chapter are drawn together and the important aspects expanded upon in Chapter 9 to form the conclusions. Some recommendations for future work are proposed.

Chapter 2

Review of literature

The literature review has focused on seakeeping data and their availability, particularly for high speed vessels in oblique waves, together with the use of suitable criteria to assess or rank the seakeeping performance of high speed vessels.

A good starting point for this research is with the concept design of high speed vessels. Some recent work carried out by Karayannis et al. [1] - [4] has automated the procedure of determining the principal particulars of fast ferries based on data for existing vessels. Alternatively an inverse design procedure can be used such as that developed by Hearn et al [5]. This uses a genetic algorithm based inverse analysis procedure to improve the design of catamarans. Both of these methods require a method of determining the motions of the vessel and criteria by which to assess the seakeeping performance.

The classical work of Bales [6] describes a model which has been developed relating ship hull geometry to an index of seakeeping merit. The work was carried out using destroyer type hulls. The characteristics of the hull geometry used were L, B, T, C_{WF}, C_{WA}, T/L, c/l, C_{VPF} and C_{VPA}. An investigation was carried out by the ABCD working group on human performance at sea [7] to determine the effects of ship motions on the crew performance of naval vessels in a wide variety of shipboard tasks, the results of which provide help to designers and operators. Graham et al. [8] describes a frequency domain method of predicting the incidence of events which may degrade the performance of shipboard tasks, as well as giving suitable seakeeping criteria in the form of limits on the incidence of these events.

Motion sickness is a severe problem for passenger vessels. An extensive investigation into motion sickness on board passenger vessels, by the use of simulators and various ships has been carried out by Lawther and Griffin [9] - [11]. Some twenty ships were investigated with journey times from one to six hours. The motions of the vessels were measured and questionnaires were filled in by passenger in predetermined seating areas. The questionnaires were then analysed and compared with the measured motions. In addition to the conventional

ships that were tested a hovercraft and a hydrofoil were included in the investigation. The work carried out showed that the worst frequencies for motion sickness tend to be the same as the most common frequencies for vertical accelerations on many ships.

Having selected suitable criteria by which to determine the seakeeping performance of the vessels at the concept design stage, the seakeeping attributes of the vessels must be determined. The methods available to the designer include both physical experiments and numerical experiments. A concise summary of the available physical techniques is given in Conolly [12]. He firstly describes the use of long crested regular waves to determine ship motions, going on to describe short crested irregular waves. The paper also describes the experimental methods used to determine the motions of ships in regular and irregular waves. An important technique highlighted in this paper was how to investigate ship motion in oblique short-crested irregular seas by means of a 3D transfer function generated from regular wave tests at various heading angles. Examples of the application of motion prediction methods in long-crested head seas is given in Wright [13]. This work describes how this motion prediction method can be used to investigate the influences of a change in principal dimensions on the seakeeping performance of high speed monohulls and catamarans.

Having discussed how to determine the motions of the ship in a suitable sea, it is now necessary to generate the ship motions. There is an overlap between physical and numerical experiments, with physical experiments often being used to validate numerical experiments. The most useful experimental data is that which has been determined for a systematic series. A classical reference is the work of Blok and Beukelman [14]. This work describes a programme of physical experiments in head seas on monohulls. The data from these experiments are incorporated into design charts. The tests were carried out at four speeds (Fn=0.285, 0.570, 0.855 and 1.140). A more recent programme of monohull physical experiments is being carried out by Grigoropoulos and Loukakis [15]. Three hull forms have been tested to date. The models were tested for resistance and seakeeping performance in head waves. The results presented are for pitch motion, acceleration and mean added resistance at two speeds (Fn=0.34 and 0.68). Another systematic series of five monohulls was tested by Lahtiharju et al [16]. These hull forms are suited to shallow water operation with water jets and were tested in head seas using two versions of a modified strip theory program. Two of the models were physically tested in regular waves.

A systematic series of catamarans was tested at Southampton University by Wellicome et al. [17]. This work was carried out on three NPL based models with round bilge, transom stern hull forms. The models were tested in three configurations, (demihull, S/L=0.2 and S/L=0.4), all at three speeds (Fn=0.2, 0.53 and 0.8). The results are presented in the form of transfer functions for heave, pitch, accelerations and added resistance. These models were also tested in calm water by Insel and Molland [18]. An experimental and theoretical

investigation into the resistance and seakeeping of the same models was carried out by Couser [19]. The experimental results were incorporated into a seakeeping performance prediction program which was later used by Wright [13] and Karayannis [1]. A recent investigation into the seakeeping performance of catamarans was carried out by Soares et al. [20]. This work was carried out on a catamaran in oblique regular waves. The headings tested were 180°, 165° and 150° at a variety of speeds, but the width of the tank resulted in a maximum speed of Fn=0.4 at all headings. The model was towed using a planar carriage, which is able to traverse the tank whilst towing the model. Results are presented in the form of transfer functions for heave, pitch and roll.

Another source of seakeeping data, other than systematic series data, is that derived to assess the performance of numerical methods, such as the work carried out by Boccalatte et al. [21] on two catamarans for the Italian Navy. Two models were tested in head seas at two speeds and in beam and in stern quartering seas at zero speed. The results were used to assess the performance of three seakeeping codes, two 2D methods and a 3D method. Another example of physical experiments being used to validate numerical experiments is the work carried out by Rocco and Grossi [22]. This work was carried out to improve the design of fast monohulls in terms of their seakeeping and comfort performance. The problem of monohulls operating at speeds greater than 40 knots in severe seas is a difficult problem for designers to solve. The designers at Fincantieri have introduced computational tools to improve the passenger comfort early in the design stage. The motions were determined by a strip theory based program. Physical experiments were carried out in head seas and the numerical and physical experiments were compared with sea trials of the completed ships. Boot et al. [23] carried out numerical and physical experiments to determine the seakeeping performance of monohulls using physical experiments to validate their numerical code. The code used was linear strip theory based, which allowed the motions to be calculated at various headings in regular and irregular waves using long or short-crested wave spectra. Particular consideration was given to passenger comfort and operability. The seakeeping criteria had to satisfy the worst reasonable sea state that the ship might encounter in the mediterranean. The use of wave recorder buoys combined with wave statistics were used to determine the likely range of sea states.

Kvålsvold et al of DNV, [24] compares two large high speed catamarans in terms of their seakeeping comfort levels. One catamaran was a conventional semi-displacement hull form and the other a semi-swath hull form of approximately the same length and displacement. The comparison is based on standard ISO 2631 curves for motion sickness. The acceleration levels at any point in the ship can be investigated. The seakeeping comfort analysis is part of the "Comfort Class" concept recently launched by DNV. Other optional elements include noise and vibration and indoor climate effects on comfort.

A number of seakeeping data for high speed vessels have been established using numerical investigations. Chan [25] describes the use of two mathematical models for calculating ship motions. One is a three-dimensional oscillating source distribution method, and the other a three-dimensional translating-pulsating source distribution technique. The comparison of numerical results of ship motions and wave loads for two fast catamarans are discussed. The Research group at the University of Southampton [26] has investigated different methods of evaluating the motions of monohulls and catamarans. Three methods were considered, a pulsating source and two translating pulsating source methods. The results are compared with experimental results at speeds up to Fn=0.5. Two papers by Fang et al [27] and [28] describe an analytical technique based on the two dimensional Greens function method taking into account viscous effects in order to estimate the motion response of catamarans in the frequency domain. Experimental results obtained for two different catamaran models are used to validate the results, with both towed and free running model experiments being carried out. A third catamaran was used in experiments to determine non-linear effects. Following on from the first paper by the same authors, the theory was extended to include a quasi-non-linear time-domain technique in order to investigate the large amplitude motions of catamarans in regular waves. The theoretical results are validated using results from experiments in head seas at three forward speeds (Fn=0, 0.226, 0.677). Kring and Sclavounos [29] carried out work using a three-dimensional Rankine panel method to investigate the wave patterns and motions for multi-hulled ships in head seas.

More recent work that is of interest concerns oblique waves and open water experiments. Some experiments carried out by Cook et al [30], in both regular head waves and in open water, have given some information on catamaran motion in oblique seas. The open water tests were carried out using an 8m free-running model with all the instrumentation and driver on board. Unfortunately the results in open water are only given at zero speed and the regular head seas results do not tend to the correct value at low frequencies. Some numerical oblique regular wave experiments were carried out by Wellicome et al. [31], using both a pulsating source code and a translating-pulsating source code. The results are compared with experimental data and the results show a fairly good correlation, the translating-pulsating source code giving the better results.

The extent of the available seakeeping data is presented in Figures 2 to 5. This data shows the lack of systematic series data and how most of the monohulls are grouped together at similar B/T ratios. The catamaran data are even more sparse and most at the same B/T ratio, with only one systematic series of data.

2.1 Summary

The existing work on improving the concept design of high speed vessels clearly requires an efficient and reliable method of assessing the seakeeping performance of suitable vessels. Currently, the numerical and experimental methods available which allow a large number of vessels to be examined are not entirely suited to high speeds or are demanding on time and resources.

Large gaps in the data base of vessels are clear from Figures 2 to 5. A data base of transfer functions is required for suitable vessels which can be updated with every new design or every new cycle of the design process. Data for some vessels which fail to reach the final design stage may be suited to other design requirements. Such results should be available in the data base to provide as broad a base of vessels as possible.

The literature review shows the lack of systematic seakeeping data available for both fast monohulls and catamarans. It does however also indicate a quantity of physical and numerical tests which have been carried out on new designs. These provide data on a wide variety of different hull forms but lack the ability to vary essential parameters systematically.

The literature also shows the current trend in designing high speed vessels with a high level of passenger comfort. Most fast ferry builders are looking at methods of improving passenger comfort.

The literature indicates available numerical methods for predicting seakeeping performance and the amount of work that has gone into validating such methods with physical results. The numerical methods are still unable to provide all of the solutions, especially for high speeds and novel designs. They do however offer an alternative to physical experiments when a variety of headings are required.

Chapter 3

Assessment of seakeeping performance

3.1 Introduction

At some stage in the concept design process it is necessary to decide between a number of vessels based on their seakeeping performance. The assessment of their seakeeping performance will have to be judged on suitable attributes. A number of criteria will be needed in order to evaluate these attributes. The attributes are likely to be common to all vessels and include motions, accelerations and added resistance, but the criteria by which the vessels are assessed will be role specific and applicable to high speed vessels. Figure 123 provides an overview of this process.

Fast vessels, often operating in the semi-displacement regime, present particular problems in the assessment of seakeeping which are often not necessarily present with slower and larger displacement vessels. Higher speeds lead to potentially larger relative motions, velocities and accelerations which have to be addressed and coped with. Such vessels are often concerned with the carriage of people and cars, with all the inherent problems and requirements and, as a necessary part of their design and operational viability, normally have lightweight structures.

3.2 Seakeeping attributes

3.2.1 Motions

The motions of a vessel as it travels at speed U relative to its intended heading are defined by a right handed axis system, which is centred at the centre of gravity of the vessel and travels with the vessel. The six motions, three translational and three rotational, are defined

in terms of the body axis system. Table 3 gives the positive directions and units of the six motions.

If the wave depression at the origin is defined as:

$$\zeta = \zeta_0 \sin(\omega_e t) \ \ [\text{m}] \tag{1}$$

and the ship motions as:

$$x_i = x_{i0} \sin(\omega_e t + \delta_i) \ \ [\text{m or rad}] \ \ (i = 1, 6) \tag{2}$$

The six motions can be divided into vertical and lateral motions. The vertical motions are heave, pitch and roll. The lateral motions are surge, sway and yaw. A vessel with six degrees of freedom can have absolute motions described by the sum of the vertical and lateral motions at the desired point in the vessel. For example the vertical displacement of the port bow of a catamaran will be the sum of the heave, pitch and roll at that point. By considering the motions at or about the centre of gravity of the vessel, all the motions are absolute. The relative motions are dependent on the magnitude of the motions of the vessel and the seas surface and the phasing between them.

The most important motions for seakeeping are the vertical motions:

3.2.1.1 Heave

Heave is a measure of the vertical displacement of the vessel. If measured at the centre of gravity it is an absolute measurement of the vertical displacement. Measured at any other point it will have contributions from the other vertical motions. Heave can also be found from measurements of vertical acceleration.

3.2.1.2 Pitch

Pitch is a measure of the rotation about the y-axis of the ship. It is an absolute measurement of the rotation and can be measured at any point in the vessel.

3.2.1.3 Roll

The roll motion is a rotation about the longitudinal centreline of the vessel, the x-axis. It also can be measured at any point in the vessel.

3.2.2 Velocities

The velocities can be found by differentiating the motions with respect to time or frequency. The equation of velocity obtained from the equation of motion, Equation 2 is:

$$\dot{x_i} = x_0 \omega_e \cos(\omega_e t + \delta) \quad [\text{m s}^{-1} \text{ or } \text{rad s}^{-1}] \tag{3}$$

The velocities are useful when considered along with the wave motion as this will give the relative velocities used for slamming and deck wetness.

3.2.3 Accelerations

The accelerations can be found by differentiating twice the motions with respect to time or frequency or by direct measurement using accelerometers. In the same way as heave motion, acceleration is an absolute motion measurement at the lcg, but anywhere else has contributions from roll and pitch accelerations.

Differentiating twice Equation 2 with respect to frequency gives:

$$\ddot{x_i} = x_0 \omega_e^2 \sin(\omega_e t + \delta) \quad [\text{m s}^{-2} \text{ or rad s}^{-2}] \tag{4}$$

3.2.3.1 Vertical accelerations

The vertical acceleration at the LCG and at the bow are required. This is very important when trying to determine the seasickness or comfort levels in a particular area of the ship. For example passenger ships have several seating areas and these may have very different acceleration levels. The acceleration at the bow is the sum of the vertical motions and if the acceleration at the centre of gravity is known, the pitch angle can be determined.

3.2.3.2 Lateral accelerations

The lateral accelerations are required for determining the motion induced interruptions or MII. However in long-crested head waves, where the model is restrained in roll and yaw, there will be no lateral accelerations. The lateral acceleration could be determined from the measurement of roll motion, or from the direct measurement of lateral accelerations.

3.3 Derived attributes

3.3.1 Structural loading/strength

The design vertical accelerations described by Det Norske Veritas [32] in their high speed light craft Rules for displacement and semi-planing craft ($V/\sqrt{L} < 5$) are as follows:

$$a_v = k\frac{C_w}{L}\left(0.85 + 0.25\frac{V}{\sqrt{L}}\right)g \tag{5}$$

k = 9 aft of 0.2L from FP
= 15 fwd. of 0.2L from FP

C_w = wave coefficient for high speed displacement craft ($V < 3\sqrt{L}$)
=0.08L for unrestricted service.

V = maximum speed (knots).

Tentative formula relating instantaneous values of vertical acceleration a_v, significant wave height H_s and maximum speed is V:

$$a_v = 0.67k\frac{H_s}{L}\left(0.85 + 0.35\frac{V}{\sqrt{L}}\right)g \tag{6}$$

3.3.2 Safety

The vessel will need to operate safely with respect to its structure, cargo, crew, passengers and navigation. The high speed craft code (HSC code, [33]), gives rules for the safe operation of high speed vessels in terms of limits on lateral and vertical accelerations. These limits are shown in Table 5. There are several limits for lateral acceleration relating to increasing degradation of safety. However there is only one limit for vertical acceleration which is set to 1.0g, corresponding to the level of acceleration which would result in people and objects loosing contact with the deck.

3.3.3 Motion sickness

The estimation of the level of motion sickness on board a high speed vessel is of great interest to both designers and operators. The predominant cause of motion sickness is due to vertical acceleration at low frequencies. That is frequencies between 0.16 and 0.8 Hz, (1.005 to 5.026 rad/s). The worst frequency for motion sickness is about 0.2 Hz or 1.257 rad/s. Unfortunately this low frequency corresponds to the typical encounter frequency of many high speed vessels.

Some work is currently being carried out at the Institute of Sound and Vibration Research (ISVR) at Southampton University to determine if lateral accelerations have a similar affect at low frequencies. Motion sickness is influenced predominantly by the duration (exposure time), amplitude and frequency of the acceleration.

3.3.3.1 Motion sickness index

The most common method of determining the level of motion sickness is to calculate the motion sickness index (MSI). This method relates the level of motion sickness to the encounter frequency and acceleration amplitude Equation 7, O'Hanlon and McCauley [34].

$$MSI = 100\left[0.5 + erf\left(\frac{\log_{10}\left(\frac{|\ddot{s}_3|}{g}\right) - \mu_{MSI}}{0.4}\right)\right] \tag{7}$$

where, $|\ddot{s}_3|$ is the vertical acceleration averaged over a half motion cycle and $\mu_{MSI} = -0.819 + 2.32(\log_{10}\omega_e)^2$

In order to apply the MSI to real life situations it is assumed that $|\ddot{s}_3| = 0.798\sqrt{m_4}$, where m_4 is the acceleration variance. Unfortunately this method does not take into consideration the voyage duration.

3.3.3.2 ISO 2631

Another method of determining the motion sickness is to determine the RMS level of vertical acceleration, frequency and duration at the required position along the length of the ship. This is then compared with the ISO 2631/3 curves Figure 6 [35] which relate acceleration levels, frequency and duration to the percentage of people who will be seasick.

3.3.3.3 Vomiting incidence

A more comprehensive method involves weighting the RMS acceleration level as a function of frequency. The weighting that is suggested in British Standard BS6841 [36] are for frequencies of 0.1 to 0.5 Hz, (0.6 to 3.15 Rad/s). It must be noted that when dealing with motions sickness the frequency is the encounter frequency, ω_e or f_e, as this is what the passenger will experience.

The reason that the RMS accelerations must be weighted is that the human body transfers accelerations of different frequencies, magnitudes and directions in slightly different ways. Above and below these frequencies there will be almost no motion sickness but the body will experience discomfort. The frequency weighting w_f is shown in Figure 7.

The RMS of the weighted accelerations can the be used to calculate the dose value, Equation 8.

$$\text{Motion Dose} = \left[\int a^n(t)\, dt\right]^{1/n} \tag{8}$$

The British Standard BS6841 defines a motion sickness dose value MSDV, in m $s^{-1.5}$ as:

$$\text{MSDV} = (a^2 t)^{1/2} \tag{9}$$

where:
a [m s^{-2}] is the RMS value of the weighted acceleration,
t [s] is the duration over which the measurement was taken.

Some recent work carried out by Arribas et al [37] has included a factor P^2 in the motion sickness dose value. This factor P is to allow for the different levels of motion sickness whilst performing different tasks and in different environments. Their suggested values are 1 for standing inside, 0.6-1 for seated, 1.5-2.5 for eating, 0.2-0.6 for lying down, and 0.5-1 for passengers standing outside. It may be possible to reduce the motion sickness by change of posture, but the reasoning behind this is not understood sufficiently, it may be due to the different transfer of accelerations in different directions or the movement of the head when unsupported. However it is acknowledged that motions sickness is dependent on a number of factors such as age, sex, motion experience, head movement, visual environment, odours and drugs. These values give an indication of the influence of some of these factors on motion sickness, even if the range of values is too broad to provide a useful prediction method.

From this the vomiting incidence can be found as a percentage of mixed unadapted adults, Equation 10. It was found that the incidence of motion sickness reduces with age and that women and children were more susceptible than men.

$$\text{Vomiting Incidence (\%)} = \text{K*motion dose} \tag{10}$$

Lawther and Griffin suggest a K factor of 1/3 for a mixed population of unadapted adults, and that this value is valid for durations of 30 mins. to 6 hours. This was adopted in BS6841. The K factor will vary for different populations, with age and sex being the principle factors. The value was determined as a fraction of the number of people in a sample who experienced motion sickness, ie (30/90).

There are a number of frequency weightings for motion sickness and comfort as defined in BS 6841 [36] which were adopted in the later draft of ISO 2631, [38].

Habituation is used to describe how the response of an individual or individuals to stimulation changes with time. In the case of responses to vertical accelerations at sea, there will be a trend for the motion sickness to decrease with time. In some cases where the motion is continuous the response can tend to zero, but any change in this motion might trigger an increase in motion sickness.

3.3.4 Subjective motion magnitude

An experienced acclimatised crew will have a reduced sensitivity to motion sickness but their work will still be impaired by the ships motions. The degree to which their work may be impaired is rated on a subjective motion magnitude scale as described in Lloyd [39]. The use of the subjective magnitude scale is illustrated in Andrew and Lloyd [40].

$$SM = A\left(\frac{\ddot{s}_{30}}{g}\right)^{1.43} \tag{11}$$

where, $A = [1 - exp(-1.65\omega_e^2)] * [75.6 - 49.6\log_e \omega_e + 13.5(\log_e \omega_e)^2]$
and $\ddot{s}_{30} = 2\sqrt{m_4}$

3.3.5 Motion induced interruptions (MII)

Motion induced interruptions are a measure of the number of times an individual would have to stop the task they were performing and hold on to some convenient anchor point. This gives an indication of how both the ship and the crew perform in rough weather. The MII's can be divided in to two groups those due to tipping and those due to sliding, as described in Graham et al. [8].

3.3.5.1 Sliding

The number MIIs caused by slides to port are given in Equation 12.

$$MII_{sp} = \frac{60}{T_z} exp\left(-\frac{(\mu g)^2}{2m_0}\right) \quad min^{-1} \tag{12}$$

There will be a similar number of MIIs caused by slides to starboard, the total MIIs caused by sliding is given in Equation 13.

$$MII = MII_{sp} + MII_{ss} \quad min^{-1} \tag{13}$$

3.3.5.2 Tipping

The number of MIIs caused by tipping to port per minute is described in Equation 14.

$$MII_{tp} = \frac{60}{T_z} exp\left(-\frac{\left(\frac{Lg}{h}\right)^2}{2m_0}\right) \quad min^{-1} \tag{14}$$

There will be a similar equation for MIIs due to tipping to starboard. The total MIIs due to tipping will be given by Equation 15.

$$MII = MII_{tp} + MII_{ts} \quad min^{-1} \tag{15}$$

The MIIs due to tipping are likely to be much greater than for sliding, especially in most high speed vessels where most of the interior will be carpeted or at least non slip. Many high speed vessels have aircraft style interiors with limited opportunity for walking without some convenient handhold nearby.

3.3.6 Deck wetness

Deck wetness occurs when the relative motion of the bow is greater than the freeboard of the vessel. Deck wetness may occur anywhere along the length of the ship, but is most likely to occur at the bow. The worst conditions will be in head seas at high speeds. The effects of deck wetness may be to damage equipment on the bow, reduce visibility and in the most severe cases the weight of water on the deck might be sufficient to cause the bow to submerge. The probability of deck wetness occurring can be calculated using Equation 16.

$$P = 1 - e^{-F^2/2m_0} \tag{16}$$

where F is the freeboard at the bow of the vessel and m_0 is the variance of the relative motion of the bow.

3.3.7 Slamming

Slamming occurs when the relative motion of the bow is greater than the draught of the vessel, the keel emerges and then impacts with the surface of the wave causing decelerations, local structural damage and transient vibrations through the rest of the hull.

The probability of slamming occurring can be predicted in a similar way to deck wetness, but this time replacing freeboard with the local draught, as shown in Equation 17.

$$P = 1 - e^{-T^2/2m_0} \tag{17}$$

A more realistic model uses the prediction of forefoot emergence and the probability of relative velocity exceeding a given value, as shown in Equation 18

$$P = 1 - e^{-0.5(T^2/m_0 + \dot{\xi}_{RC}/m_2)} \tag{18}$$

where T is the local draught, m_0 is the variance of the relative bow motion, $\dot{\xi}_{RC}$ is the critical velocity and m_2 is the variance of the relative bow velocity.

Also of interest to high speed multihulls is wetdeck slamming, where the cross-structure impacts the wave surface.

3.3.8 Power increase/added resistance

The added resistance is a measure of how the waves effect the resistance of a vessel relative to its calm water resistance. This added resistance will mean that for a vessel to maintain an operating speed it will have to increase its power. This information can be used to calculate what the economic impacts to the operator will be of operating in various sea states. By expressing the added resistance as a percentage of the calm water resistance different ships can be compared.

3.3.9 Windows of operation

The window of operation is an indication of the availability and the overall economic viability of a vessel. If the window of operation is expressed as a percentage of the time a vessel will be able to operate, the greater that value the better. Unfortunately, the window of operation is generally determined by the worst attribute. For example, if the limiting criterion for motions sickness is exceeded for 80% of the time and all other criteria are only exceeded for say 40% of the time, then the window of operation is reduced to a value of 20%.

3.3.10 Selection of attributes

Methods of condensing the seakeeping performance attributes into a single criterion, such as that proposed by Bales [6], have been explored. The seakeeping responses are normalised by dividing by the largest response and then the values summed. The best ship, the one with

the lowest summed value is assigned an index of 10 and the worst an index of 1. To improve this method, the seakeeping responses can be weighted, as suggested in Wijngaarden, [41].

The general weighting given in Wijngaarden, [41] uses the probability of occurrence of the wave period for which the responses were calculated. This would assume that for a given wave height the response is determined by the wave period. This can be seen due to wave matching where there is a maximum response when the wave period coincides with the resonant period of the ships transfer function as illustrated in Figure 136.

The more specialist nature of the high speed vessels under consideration suggests that the attributes should be retained in their individual forms, or suitably chosen subsets. In this way the output can be more transparent, offering increased flexibility in evaluating competing designs. For example, such an approach offers the facility to vary the weighting between the chosen attributes.

Whilst the retention of all of the attributes would be desirable, in order to establish a workable approach it is useful to decrease or rationalise the number of attributes. For example, the six motions and their respective velocities and accelerations are used to derive other attributes. These derived attributes can then be rationalised into subsets as demonstrated in Table 4. For example motion sickness, subjective motion magnitude and motion induced interruptions can be rationalised to an attribute of comfort. Safety, structural loading, slamming and deck wetness can be reduced to a single attribute of operational availability. Added resistance/ power increase will remain the same.

3.4 Seakeeping criteria

The seakeeping performance of a vessel once assessed needs to be presented in a form that designers and operators will understand and can interpret. It has sometimes been the case just to compare the transfer functions of different vessels, but this takes no account of the sea state. Criteria which overcome these problems are described in the following sections.

3.4.1 RMS responses

The data generated from seakeeping prediction programs is usually in the form of RMS motions, velocities and accelerations. These provide a direct comparison between one vessel and another.

The Root Mean Square (R.M.S.) value is

$$RMS = \left[\frac{1}{N}\sum x^2(i)\right]^{\frac{1}{2}} \tag{19}$$

The RMS value can either be expressed as an amplitude or motion.

3.4.2 Probability of exceedance

The RMS responses can be used to determine the probability of exceeding given criteria. This probability is determined using the Rayleigh Probability.

$$p = 100 * exp\left\{\frac{-0.5 * lim^2}{(0.5 * RMS)^2}\right\} \tag{20}$$

where RMS is the RMS value and lim is the limiting criterion.

This probability of exceedance can, for example, be interpreted as the likely percentage of the time the vessel is not available for operation.

3.5 Suitable limits

There are several proposals for the limiting values for the assessment criteria. These start with the limits for structural strength specified by the classification societies which deal with high-speed light craft, such as DNV. These limiting values may be high enough to allow the ship to operate even when it is not safe for the crew and passenger on board to do so. The next set of limiting values are those specified for the safe operation of the vessel. These are set by organisations such as the International Maritime Organisation who have defined the High-Speed craft Code [33] and various national Coastguard Agencies around the world. The final set of limiting values are those for passenger and crew comfort. These are defined by international and national standards, such as ISO 2631 [38] and BS 6841 [36], as well as from other research carried out for specific vessel types such as the ABCD Working Group [7] and Chan & Incecik [42]. The decision as to which set of limits to use is complicated and will be incorporated in the overall decision making process as discussed by Karayannis [1].

The various proposals for the limiting criteria are presented in Tables 6 to 12. The main differences between the proposed values are that some are for naval vessels, others for merchant or passenger vessels. Some of the limiting values for naval vessels are to enable weapons systems to operate and helicopters to operate. Despite this it is clear from the values that the crew of the naval vessels will be acclimatised to the motions and so be able to cope with higher limiting values. The crew of the merchant vessels will be able to cope with a higher

level than passengers on ferries. It is also seen that there are very high limiting values on the conventional cross-channel ferries, the only limit given being for an acceleration of 1.0g.

Table 13 summarises the limits for fast vessels, proposed to be used in the case studies in Chapter 8. These limits are based on four ship roles. The first case considers a ship with returning passengers, such as a commuter vessel. The limits were selected to be at the minimum of the various ranges of values in Tables 6 to 12. This ensures that the motion sickness values are as low as possible. The second case is for a ship with non-returning passengers. The limits are set at the mid to maximum range for passenger vessels. In this case a higher level of motion sickness can be tolerated to allow the vessel to have a greater availability. The third case is a mixed passenger/freight vessel, which is determined from the lower end of the merchant vessel range of limiting values and the maximum values for the passenger vessels. Finally, a freight vessel is considered, the values being selected from the merchant limiting values and the naval vessel values. These values take into consideration some degree of crew acclimatisation.

3.6 Summary

There exist a number of seakeeping attributes from which further practical attributes can be derived. These are used to assess the seakeeping performance of vessels. The seakeeping performance may be judged by comparing suitable limiting criteria for these attributes.

In order to simplify the seakeeping assessment of the vessels at the concept design stage, a condensed set of attributes may be used, which incorporates strength, safety, operability and comfort.

It is not necessary to set limiting criteria for added resistance/power increase because this is directly comparable between the competing vessels.

The available limiting criteria have been examined and, from them, a set of role specific values proposed for use at the concept design stage of fast vessels. These are summarised in Table 13 and are used in the case studies described later.

Chapter 4

Physical experiments

4.1 Introduction

In order to assess the seakeeping performance of high speed catamarans a data base of motion characteristics is needed based either on experimental or theoretical sources. As mentioned in Chapter 1, the experimental data base for these types of vessels is relatively sparse. In order to extend the existing data base an experimental test programme has been carried out. A number of models had been tested earlier in regular and irregular waves in head seas by Couser [19]. The influence of increasing $L/\nabla^{1/3}$ on the seakeeping performance was investigated. The models were designated 4b, 5b and 6b and their principal particulars are shown in Table 15. The models were tested in three configurations, with two catamaran separations and as a monohull. The experimental test programme has been extended in the current research to investigate the infiuence of hull form on the seakeeping performance. This has involved testing a model at the same $L/\nabla^{1/3}$ as one of the existing models but with a different hull form. The new model designated Model 5s was tested under the same conditions as the earlier Model 5b.

Model 5b is a round bilge/ transom stern form based on the NPL Series [43]. Its body plan is shown in Figure 9 and its principal particulars of the demihulls are given in Table 15.

Like Model 5b, Model 5s is also a round bilge/ transom stern form but has a distinctly different prismatic coefficient and hull shape. This model is based on the Series 64 hull form [44]. Its body plan is shown in Figure 8 and its principal particulars are also given in Table 15.

Model 5s has been tested at a range of speeds in calm water [45]. This allows the added resistance in waves to be calculated.

Both models 5b and 5s were tested in regular head waves with 1.6m captive models and in

regular head and oblique waves with 4.5m self propelled models. The details of the 4.5m models are given in Table 17. The principal particulars of the 4.5m models when tested were slightly different from the designed values. The results from the experiments in regular head and oblique waves have been presented in Molland et al. [46].

4.2 Head sea experiments

Tests on the 1.6m model were carried out in the Southampton Institute Ship Tank.

Model 5s was tested in both catamaran and monohull configurations and in all cases at Froude number = 0.20, 0.53, 0.65 and 0.80. In the catamaran configuration separation/length ratios (S/L) of 0.2 and 0.4 were tested. Model 5b had been tested in the same monohull and catamaran configurations as Model 5s and at the same Froude numbers with the exception of 0.65. The longitudinal moment of inertia in pitch was set such that the longitudinal radius of gyration was 25% of the model length.

4.2.1 Facilities and tests

4.2.1.1 Tank facilities

The tank is fitted with flap type wavemakers at one end, capable of generating both regular and irregular waves of various heights and frequencies, and has a passive beach at the other. Details of the tanks dimensions and the maximum carriage speed are given in Table 14.

4.2.1.2 Instrumentation and measurements

Heave motions were measured with a linear potentiometer attached to the heave post, which in turn was mounted at the longitudinal centre of gravity. Pitch was measured with an angular potentiometer incorporated into the tow fitting. Accelerations were measured using piezoresistive accelerometers at the longitudinal centre of gravity and 15% of the model length aft of the forward perpendicular. The wave system encountered during the run was measured with a stiff, sword type resistance probe mounted on the carriage ahead and to the side of the model. The signals were recorded using a PC based data acquisition system and an analogue to digital converter on the carriage. The accelerometers and potentiometers signals were also low-pass filtered. This system enabled detailed analysis of the results from each run to be carried out between each run. Typical examples of the records for the motions and accelerations are presented in Figures 10 to 13.

The speed of the model is determined by measuring the time the test carriage takes to cover

the constant run length between two switches. These switches are 15m apart. The switches also start and stop the data acquisition process.

The wave maker was found to produce waves of the requested period but wave amplitudes showed some variation with frequency.

4.2.1.3 Test conditions

Tests were carried out in head seas of three hull configurations: monohull (catamaran demi-hull), and two catamarans, S/L=0.2 and S/L=0.4. Measurements in each model configuration were taken at four Froude numbers (Fn=0.20, 0.53, 0.65 and 0.80) and over an encounter frequency range of 6 rad s^{-1} to 18 rad s^{-1}. The steady speed run length was 15m. The wave frequencies were set for each Froude number so that it gave a constant encounter frequency range.

4.2.2 Data reduction and corrections

During regular wave tests the models were allowed to encounter at least five to six waves before the responses were recorded, so as to allow transients in the response to die out. The models then encountered a minimum of six waves during which the measurements were recorded. At high frequencies many more waves were encountered.

Regular wave tests were analysed using RMS values of the measured motions and the programmed wave and encounter frequencies were used to calculate the transfer functions.

Transfer functions from the regular wave experiments were calculated as follows:

$$\text{Pitch TF} = \frac{\text{Pitch Amplitude RMS [rad]}}{\text{Wave Amplitude RMS [m]}} * \frac{g[ms^{-2}]}{\omega_0^2[rads^{-1}]} \tag{21}$$

$$\text{Heave TF} = \frac{\text{Heave Amplitude RMS [m]}}{\text{Wave Amplitude RMS [m]}} \tag{22}$$

$$\text{Accel. TF} = \frac{\text{Accel. Amplitude RMS } [ms^{-2}]}{\text{Wave Amplitude RMS [m]}} * \frac{1}{\omega_e^2[rads^{-1}]} \tag{23}$$

where encounter frequency ω_e is related to wave frequency ω_0 by the following equation,

$$\omega_e = \omega_0 - \cos\mu \frac{\omega_0^2 u}{g} \tag{24}$$

where u is the ship speed and μ is the ship heading, with $\mu = 0°$ for the following sea case and $\mu = 180°$ for the head sea case.

Added resistance was calculated from the regular wave data, noting the model was kept fixed in surge. The dynamometer was sufficiently stiff for the rise and fall in resistance during each wave cycle to be clearly visible on the resistance measurement trace. Added resistance was assumed to be proportional to wave height squared and has been presented in terms of the added resistance coefficient given in Equation 25. This is similar to that proposed and used by Blok and Beukelman, [14].

$$\text{Added Res. Coeff.} = \frac{R_{reg.\ waves} - R_{calmwater}}{2\zeta_{RMS}^2 \rho g B^2 / L} \tag{25}$$

4.2.3 Discussion of results

4.2.3.1 Motions

The derived transfer functions for heave, pitch and vertical accelerations are given in Figures 14 to 25. Due to the failure of one accelerometer the monohull has only results for forward accelerations. However, the accelerations at LCG can be derived from the heave measurements by differentiating twice with respect to frequency. The graphs are plotted to a base of non dimensional encounter frequency ω_e', Equation 26.

$$\omega_e' = \omega_e \sqrt{L/g} \tag{26}$$

Three dummy points at 0, 1 and 2 rads^{-1} have been added to the transfer function curves in order to force the transfer functions to show the model contouring the waves at low frequencies. The figures are plotted showing all four Froude numbers.

The results for Model 5s have been compared with Model 5b, an NPL based model tested by Couser [19]. This model was tested at the same Froude numbers except, Fn=0.65, and the results are shown in Figures 30 to 41. The results show many similarities and it can be seen that form has relatively little effect on the seakeeping performance of the vessel. This is probably due to the models having the same pitch inertia and displacement. The graphs do indicate some differences, mainly between the heave response of the two different models. Most notable is the difference between the heave for the monohulls shown in Figures 14 and 30, with 5b having a greater peak heave response. This is also true for the narrow spaced catamaran shown in Figures 18 and 34 but not for the wide spaced catamaran Figures 22 and 38.

At low Froude numbers for the narrow spaced catamaran, there is some wave interaction. The waves generated by one demihull interact with the other demihull. This causes some secondary low amplitude peaks in the transfer function, such as those shown in Figure 18 at the lowest Froude number. At higher speeds and at wider separations the waves have passed behind the stern before they reach the other demihull so no wave interaction occurs.

The transfer functions for all of the motions and accelerations at the lowest Froude number has a very low resonant response compared with the transfer functions at Fn=0.5 and Fn=0.8. The reasons behind this have not been investigated, but a possible influencing factor is the different running trim of the vessel at the lowest speed, as shown in Figure 26.

4.2.3.2 Added resistance

The added resistance for the model in the various test conditions is given in Figures 27 to 29. The data are plotted to a base of non dimensional encounter frequency. The added resistance has been non-dimensionalised according to Equation 25, noting that B^2/L was the same for the monohull and catamaran.

These results for Model 5s can again be compared with the results obtained by Couser for Model 5b in Figures 42 to 44. The results again show similar trends and values. The results for both models have been smoothed to indicate the trends rather than the absolute values. Because of the small differences between the resistance in waves and in calm water, the experimental points show some scatter.

4.3 Oblique sea experiments

A series of model tests were carried out on two 4.5m catamarans in regular head and oblique waves in the Ocean Basin/Manoeuvring Tank at DERA Haslar.

4.3.1 Description of models

Models 5b and 5s were tested at separation to length ratios (S/L) of 0.2 and 0.4. Both models have a waterline length of 4.5m, a test displacement in fresh water of 324kg and are constructed in GRP. They are free running, propelled by gas fuelled internal combustion engines, radio controlled, and instrumented to record pitch, roll and vertical accelerations at LCG and 7.5% aft of FP. Measured values of the radii of inertia of the models in pitch, yaw and roll are given in Table 18. Further details are given in Wellicome et al. [47].

4.3.2 Facilities and tests

4.3.2.1 General

The model tests were carried out in the Ocean Basin at DERA Haslar. The basin has a length of 120m, breadth of 60m and water depth of 5.5m. Regular and irregular waves can be generated at various wave heights and frequencies. A schematic view of the tank and model tracks at the three headings tested is shown in Figure 45.

For each test run, the model engines were firstly started, then the waves started, data acquisition started and the model released at the required heading. The correct heading was maintained manually by the radio control operator. This heading was maintained as long as possible in order to capture sufficient wave encounters before turning out of the run. The lowest number of wave encounters occurred at a heading of 120°, when the number of full encounters (at the lowest wave frequency) was seven.

4.3.2.2 Instrumentation and measurements

Pitch and roll were measured using a pitch/roll gyro mounted in the port hull. Accelerations were measured using piezoresistive or integrated circuit accelerometers; these were mounted in both hulls at the LCG for Model 5b and in both hulls at the LCG and at 7.5% aft of FP for Model 5s. The wave system encountered during each run was measured by a wave probe mounted in the tank. Its approximate position is indicated in Figure 45. The waves were measured over a time of 60 secs, the mean values of frequency and wave height were calculated for each run. The wavemaker was found to produce waves of the requested frequency, but wave amplitude tended to be larger than set.

All measurement signals on the model were acquired using an on-board laptop computer via an analogue to digital converter. The system enables analysis and checking of the results of each run to be carried out between test runs, during a period of about 15 to 20 minutes which was required to let the waves in the basin die out. Typical examples of the time histories for vertical acceleration, pitch and roll are presented in Figures 48 to 51. The reason the pitch motion time history is not symmetrical about the x-axis is because it was not possible to zero the gyro at the running trim of the model. In the figures it is clear when the model has reached its full speed and a regular sinusoidal response is obtained, the region from 25s to 50s. The region after this is when the model was executing its turn and returning slowly to the landing stage in the remainder of the waves. Figures 46 and 47 are photographs of Model 5s in the basin at headings of 180° and 150°.

4.3.2.3 Test conditions

The models were tested in head seas (180°) and oblique seas at headings of 150° and 120°, Figure 45. Hull separation to length ratios (S/L) of 0.2 and 0.4 were tested at each heading over an encounter frequency range of 3 rad/s to 13 rad/s.

The wavemaker set wave height for each set frequency was based on a nominal wave slope of 2°. It should be noted that for both models at a heading of 120°, tests were not carried out at frequencies less than 0.4 Hz since there would not have been an adequate number of wave encounters. Similarly some tests were carried out in beam seas, (90°), but the time taken to cross the width of the tank was so short that the model did not encounter enough waves and it was difficult to turn the model out of the run without hitting the tank sides. For Model 5b at S/L=0.4, tests at the highest and lowest frequencies were curtailed by the time limitations of the test programme.

The test were carried out at mean calm water speeds of 4.35 m/s for S/L=0.2 and 4.45m/s for S/L=0.4. These speeds were derived for both models from time trials over a measured distance in the basin. The nominal Froude numbers for these speeds are Fn=0.65 for S/L=0.2 and Fn=0.67 for S/L=0.4.

4.3.3 Reduction and presentation of data

RMS values of the measured motions and wave frequency were used to calculate the transfer functions. The values were taken from the records where regular motions had been established and, at the lower frequencies, using a minimum of seven wave encounters. At the higher frequencies many more waves were encountered.

Pitch and roll were derived as direct calibrated measurements from potentiometers coupled to the pitch/roll gyro. Roll was also estimated using the difference of the acceleration measurements port and starboard and was found to correlate well with the direct measurements. Heave was derived from double integration of the mean accelerations at LCG for each hull. Accelerations at LCG and forward were obtained from the mean of the port and starboard measurements.

Transfer functions were calculated as for the head sea experiments, Equations 21 to 23. In addition to these, roll transfer functions were calculated as follows:

$$\text{Roll TF} = \frac{\text{Roll Amplitude RMS [rad]}}{\text{Wave Amplitude RMS [m]}} * \frac{\text{g [ms}^{-2}\text{]}}{\omega_0^2 \text{ [rads}^{-1}\text{]}} \tag{27}$$

4.3.4 Discussion of results

4.3.4.1 Model 5b (NPL hull form)

The results for Model 5b are shown in Figures 52 to 57. These show the transfer functions for heave, pitch and roll to a base of non-dimensional encounter frequency for the three headings and two separation ratios.

The pitch transfer functions, Figures 53 and 56, show a small reduction when going from a heading of 180° to 150°, but a significant reduction when going from 150° to 120°. This trend is similar for both separations, although greater for the wider separation ratio of S/L=0.4.

The heave transfer functions, Figures 52 and 55, shows a much greater reduction for S/L=0.4 than for S/L=0.2 when going from 150° to 120°.

The roll transfer functions, Figures 54 and 57, as expected shows a marked increase when going from 150° to 120°. Its value at a heading of 120° and S/L=0.2 is of the order of 18% higher than that for S/L=0.4, whilst at 150° and S/L=0.2 is of the order of 12% lower than that for S/L=0.4.

It should be noted that, due to the way the heave and acceleration transfer functions have been defined, Equation 22 and Equation 23, the acceleration transfer function at LCG will be identical to that for heave, Figures 52 and 55, and therefore has not been plotted. Accelerations forward were not measured for Model 5b.

4.3.4.2 Model 5s (Series 64 hull form)

The results for Model 5s are shown in Figures 58 to 65. These show the transfer functions for heave, pitch, roll and forward acceleration to a base of non-dimensional encounter frequency for the three headings and two hull separations, together with speed loss to a base of non-dimensional encounter frequency for S/L=0.4.

The pitch transfer functions, Figures 59 and 63, show relatively small reductions when going from a heading of 180° to 150°, but a significant reduction when going from 150° to 120°. This trend is similar for both spacings although, like Model 5b, the reduction is greater for the larger spacing, S/L=0.4.

The results for the heave transfer functions, Figures 58 and 62, show similar trends to those for Model 5b. Namely, when going from a heading of 150° to 120° there is a greater reduction in transfer function for S/L=0.4 than for S/L=0.2.

The roll transfer functions, Figures 60 and 64, shows a marked increase when going from 150° to 120°. Its value at a heading of 120° and S/L=0.2 is of the order of 19% higher than that for S/L=0.4. This is similar to Model 5b. At 150° the transfer function at S/L=0.2 shows little change from that for S/L=0.4.

Transfer functions for accelerations forward for Model 5s are shown in Figures 61 and 65. At S/L=0.2 there is little change in forward acceleration with change in heading whereas at S/L=0.4 there is a marked decrease when going from 150° to 120°.

4.3.4.3 Comparison between models 5b and 5s

Inspection of the results for Model 5b in Figures 52 to 57 and Model 5s in Figures 58 to 65 indicate that, in the main, the differences in performance between the two hull shapes is not large. However, roll response, Figures 54, 57, 60 and 64 does show a significant difference in that at S/L=0.2 the roll transfer function for Model 5s is 19% higher at a heading of 120° and 14% higher at 150°, and at S/L=0.4 Model 5s is 18% higher at 120° and about the same at 150°.

4.3.4.4 Comparison between the 1.6m and 4.5m models

Comparisons of the data for head seas at the common Froude number of 0.65 indicate broad agreement in most cases, although the 4.5m model exhibits larger heave transfer functions and smaller pitch transfer functions then those for the 1.6m model. There were a number of differences in the experiments: the free running 4.5m model was self propelled whilst the 1.6m model was towed and its tow post, which made up 10% of the displacement mass, moved only in the vertical direction and was not free to pitch; the Southampton Institute tank used for the 1.6m model may have had some wall effects; the wave probe on the towed carriage may have been influenced by the model.

4.3.4.5 Reduced wave height

Model 5s, S/L=0.4 was run at encounter frequencies near to resonance at a smaller wave height, in order to check the linearity of the transfer functions. The result are presented in Figures 66 to 68 superimposed on the existing transfer functions. It is clear that allowing for some experimental inaccuracies that the results are very similar to the existing transfer functions for Model 5s. This would indicate that there is a linearity of response with wave height.

4.3.4.6 Speed loss

In the available experimental setup, direct measurement of model speed was not possible. A novel indirect method of obtaining the speed in regular waves was therefore adopted. The speed loss for both models is shown in Figures 69 to 72. This has been derived from Equation

24, where ω_0 is the measured wave frequency, ω_e the actual measured encounter frequency and using nominal values of heading μ, whence speed is derived as follows:

$$u = \frac{g}{\omega_0^2} \frac{\{\omega_0 - \omega_e\}}{\cos \mu} \tag{28}$$

The curves in Figures 69 to 72 show a maximum decrease in speed at about the resonant frequency. It should be noted that estimates of speed would be affected by the deviations from the nominal heading which were not recorded. Except for Model 5s at S/L=0.4, the results showed a large amount of scatter at 120° heading and have not been presented. Typically, the speed loss for Model 5b, Figures 69 and 70 is of the order of 4% to 8% of the calm water speed. For Model 5s, Figures 71 and 72, the speed loss for S/L=0.2 is about 8% whilst for S/L=0.4 is about 7% at headings of 120° and 150°, increasing to about 10% at 180°. These speed reductions correspond to increases in resistance of the order of 10% to 20%. They are in broad agreement with the added resistance recorded in the head sea tests, Figures 27 to 29 and Figures 42 to 44.

The influence of deviations from the nominal heading on speed loss is presented in Figures 73 to 75. These figures show the influence of a 5° change in heading on the speed loss. The results at 180° are seen to be reliable, but at 150° deviations are large and it is clear that the results at 120° are most dependent on deviations from the set heading. This approach has been validated by differentiating Equation 28 with respect to μ. Both approaches show good agreement.

$$\frac{du}{d\mu} = u\ tan(\mu) \tag{29}$$

The influence of a 5% change in the measured encounter frequency is shown in Figures 76 to 78, it can be seen that any encounter frequency errors have most effect at low encounter frequencies. Differentiating Equation 28 with respect to ω_e shows very good results. It can be seen that the technique is suitable for use in head, or close to head seas. However for the reasons mentioned, the results are treated as being indicative rather than definitive.

$$\frac{du}{d\omega_e} = \frac{-g}{\omega_0^2 \cos(\mu)} \tag{30}$$

4.4 Open water experiments

Open water tests can provide more scope in investigating different model headings and speeds than the controlled, but sometimes limiting seakeeping tests in a test tank. As well as

providing information on a vessels behaviour in the more realistic short-crested seas.

4.4.1 Description of model

Model 5b was tested in open water. The model has a waterline length of 4.5m, a test displacement of 324kg and is constructed in GRP and details are given in Table 17. For the open water tests in irregular seas the engines were run on petrol. Further details of the construction, equipment and layout of the model is given in Wellicome et al. [48] and Appendix A.

4.4.2 Open water tests

4.4.2.1 Location

The open water model tests in irregular seas were carried out on Southampton Water. The tests were carried out over a number of days when suitable wave conditions were available. Wave properties at the test location were measured with a wave buoy designed and built for the purpose and described in Wellicome et al. [49]. In all the open sea tests the model was accompanied by a high speed support boat in order to service the model and equipment and to deploy the wave buoy.

4.4.2.2 Instrumentation and measurements

Pitch and roll were measured using a pitch/roll gyro mounted in the port hull. Accelerations were measured using piezoresistive accelerometers; these were mounted in both hulls at the LCG. Model speed was derived using a small portable GPS in the support boat which followed, and travelled at the same speed as, the model during a test run.

All measurement signals on the model were acquired using an on-board laptop computer via an analogue to digital converter. The system enabled analysis and checking of the results of each run to be carried out during the experiments.

The wave buoy [49], is fitted with three accelerometers mounted on top of a lifebelt to measure buoy heave, pitch and roll responses to waves, together with a flux-gate compass to measure buoy heading. A full description of the wave buoy calibration and analysis is given in Appendix B. Power supplies to the instrumentation and output signals are carried along a 50m umbilical cable to the support boat. The buoy deployed directly to windward of the support boat at the end of the extended, but not taught, umbilical cable. During buoy deployment wind speed was monitored using a hand held wind gauge. Wind direction and the cable lead angle from the support boat to the buoy were measured with a hand bearing

compass. Broadly, the wind direction and mean cable agreed within 5 to 10 degrees. Since the support boat was used to follow the model during each test run, it was not possible to test the model and measure wave properties simultaneously.

4.4.2.3 Test conditions

The tests were carried out at separation to length ratios, (S/L) of 0.2 and 0.4 and at a nominal calm water Froude number of 0.65, (4.3m s^{-1}). The wind direction provided a reasonable indication of the mean wave direction and runs were made at various headings to the mean. Prior to, and immediately after, each test run the wave properties were measured, as described in [49]. For each test run the model engines were started, data acquisition started and the model released at the required heading. A time lag was built into the data acquisition, so that it did not start to acquire until the model was clear of the support boat and on the correct heading. The correct heading was maintained manually by the radio control operator. During each test run the support boat followed the model (at speeds of the order of 3m $s^{-1}$to 4m s^{-1}) in order to monitor model speed. A typical test run was of 4 or 5 minutes duration and covered some 1000m.

4.4.3 Reduction and presentation of data

An attempt to generate transfer functions from the recorded motions and the wave record was made. The analysis for the wavebuoy is explained in Appendix B. Unfortunately the attempt to use a directional approach to the analysis did not give results which could be trusted. A problem highlighted in the wavebuoy analysis and in Harris et al. [50] which is applicable to both the analysis of the wavebuoy and the vessel motions is that care must be taken when integrating the accelerations to determine displacements. The integration is achieved by dividing the accelerations by frequency squared, if the low frequency components have not been filtered or removed correctly any noise at these low frequencies will be amplified resulting in unrealistically large displacements. This has given the appearance of the 4.5m model heaving so much that it was clear of the water surface by some 0.3 of a metre. The generation of transfer functions was abandoned until a more reliable approach could be found.

Examples of typical result are presented in the form of RMS motions and accelerations in Tables 19 and 20. These RMS responses were obtained from a time history 165 seconds long at a sample rate of 10Hz. In some of the time histories there were large amplitude spikes caused by a fault in the roll/pitch gyro. These spikes had a large influence on the RMS values and, in order to achieve more realistic values, the data had to be windowed. The most accurate RMS values are obtained by windowing the longest section of record possible. In some cases this meant that the record had to be windowed in several successive sections and

then averaged. A typical example of measured and windowed data is shown in Figures 81 and 82.

In order to allow comparison of RMS responses with those available for a similar full scale vessel, the data were normalised. This involved dividing the RMS value at a particular heading by a reference RMS value as shown in Equations 31 to 33. This would then show the relative changes with heading rather than RMS value.

$$\text{Normalised Pitch} = \text{RMS Pitch}(\mu)[deg]/\text{RMS Pitch}(180°)[deg] \tag{31}$$

$$\text{Normalised Accel.} = \text{RMS Accel.}(\mu)[g]/\text{RMS Accel.}(180°)[g] \tag{32}$$

$$\text{Normalised Roll} = \text{RMS Roll}(\mu)[deg]/\text{RMS Roll}(90°)[deg] \tag{33}$$

With $\mu = 0°$ for the following sea case and $\mu = 180°$ for the head sea case.

4.4.4 Discussion of results

4.4.4.1 General

Several days of testing took place, but for many reasons only two days produced usable results from both the wavebuoy and the catamaran model. A range of headings were tested from head to following seas.

After much initial trial and investigation a successful open water test procedure was established. The following results, for particular days in April 1998 which are presented and discussed, illustrate and confirm the satisfactory nature of the test procedures which were finally achieved and adopted.

4.4.4.2 Model with S/L=0.4

The results for this configuration are shown in Table 19 which gives RMS values and Figure 84 which gives normalised values of pitch, roll and acceleration. Other than the 180° heading, roll shows very similar levels and changes with heading. Pitch also shows similar levels and trends. Open water acceleration values are higher in head (180°) seas than the regular wave tests. The average values are however likely to be questionable since the port acceleration values seem to be in error. The normalised curves presented in Figure 84 show the changes in model pitch, roll and acceleration with change in heading. These can be compared with the results in Figures 86 to 88 for a full scale vessel of similar form (at Fn=0.76). These full scale

results were provided by one of the industrial sponsors of the fast craft research programme at Southampton. It is seen when comparing Figures 84 and 88 that the roll characteristics show a very similar form. The ship pitch shows a much larger variation and with higher following sea values than for the model. The full scale ship shows a significantly larger reduction in acceleration in following seas.

4.4.4.3 Model with S/L=0.2

The results are shown in Table 20. The normalised results are not plotted since there is not a value close enough to 180° with which to do the normalising. Like the S/L=0.4 data, the roll values close to head sea conditions are larger in the open sea tests, although reasonable agreement is achieved as they approach beam seas. Pitch results are comparable, but the acceleration results are larger in the open sea case. Again, the port acceleration results are questionable.

4.4.4.4 Speed loss

Model speed loss with heading is shown in Figure 85. The results for S/L=0.4 and 178° heading is questionable, since the most severe motions would be in head seas and so added resistance should be highest. Otherwise, the results show expected trends although they are a little higher than the speed losses estimated from the regular oblique wave tests of Model 5b shown in Figures 69 and 70. This is most likely due to the larger wave amplitudes in the open water trials.

4.5 Vertical planar motion mechanism (V.P.M.M.)

Traditional seakeeping experiments, such as those described earlier, give the total response to an input force. A V.P.M.M. can be used to find the component forces on a model due to an input oscillation. This device force oscillates the model in heave or pitch as it progresses down the tank. The vertical oscillations are imparted on the model by means of motor driven vertical posts located near the ends of the model. This is especially useful for the validation of numerical methods, where the hydrodynamic coefficients in the equation of motion, Equation 34, can be determined experimentally. It was also considered important that a VPMM should be designed and built which would be capable of testing high speed craft, and contribute to the model seakeeping data base for these vessels.

$$\sum_{k=1}^{6} \left\{ -\omega_e^2 (M_{jk} + A_{jk}) + \mathrm{i}\omega_e B_{jk} + C_{jk} \right\} \eta_k = F_j \quad \text{for j=1,2,.....,6.} \tag{34}$$

Such a device is currently being developed at the University of Southampton.

4.6 Summary

Model 5s has been tested in regular head waves and the results have been compared with model 5b, a model of the same $L/\nabla^{1/3}$ ratio, which was tested by Couser [19]. This allowed the influence of different hull forms to be assessed and the differences were found to be small.

4.5m versions of Models 5b and 5s have been tested in regular head and oblique bow waves. Again the difference between the seakeeping performance of two different hull forms was small.

The differences in the seakeeping performance between a towed model and a free-running model were also investigated. It was found that the heave motion of the 4.5m model was slightly higher and the pitch slightly less than the 1.6m towed model.

A method of determining the speed loss of a free-running model in regular waves has been investigated.

Very little published data has been available for oblique seas, and the oblique wave experiments reported make an important contribution to the experimental data base.

An open water test methodology has been established, although the results to date are very limited.

The gathered experimental data, together with theoretical prediction, are used later in Chapter 7 to assess vessel performance in long-crested seas and to establish 3D transfer functions.

Chapter 5

Numerical investigations

5.1 Introduction

The physical experiments described in the previous chapter have provided results in oblique regular waves at headings from 180° to 120°. The results from the tests carried out in open water did not give the transfer functions at headings round the clock as hoped. Consequently there are no results in beam and following waves. The successful use of existing theoretical packages available and/or under development at the University of Southampton, including strip theory, pulsating and translating-pulsating source codes, may be used to investigate the transfer functions in beam and following waves. The results from the pulsating and translating-pulsating source code have been compared with experimental results in beam seas, Wellicome et al. [31] and show good correlation.

A theoretical method was required which will allow a large number of variations to be carried out and still provide a good representation of the physical result. Of the methods available, it was decided that the simpler pulsating source code would be used as this would allow a fuller investigation to be carried out.

5.2 Description of models

The seakeeping performance of Models 5b and 5s was investigated using the theoretical methods. Details of the principal particulars of the models are given in Table 17 and their body plans are given in Figures 8 and 9. The panelled hulls, up to the waterline, as used in the seakeeping code are shown in Figures 89 and 90. Both models were tested at four Froude numbers, Fn=0.2,0.53, 0.65 and 0.8. Only the lowest Froude number allowed more than one wave frequency for a given encounter frequency and this Froude number was low enough not to be considered at great length in this research.

5.3 Outline of theory

The theory behind the numerical methods available has not been reported in much detail, because the codes available were used only as a numerical tool. The work carried out to develop these codes is reported better by others, such as Hudson [51].

5.3.1 Equations of motion

The equations of a rigid vessel undergoing small perturbations, in regular sinusoidal waves, about an equilibrium axis system 0xyz situated in the calm water surface vertically above or below the centre of gravity can be represented by the coupled linear equations of motion:

$$\sum_{k=1}^{6} \left\{ -\omega_e^2 (M_{jk} + A_{jk}) + \mathrm{i}\omega_e B_{jk} + C_{jk} \right\} \eta_k = F_j \quad \text{for j=1,2,.....,6,} \tag{32}$$

where, η_k is the complex motion amplitude,
ω_e is the encounter frequency
C_{jk} is an element of the hydrostatic restoring matrix,
A_{jk} is the added mass in the jth mode due to unit motion in the kth direction,
B_{jk} is the damping coefficient in the jth mode due to unit motion in the kth direction,
F_j is the complex amplitude of the wave exciting force,
M_{jk} is an element of the generalised mass matrix, which for a body with lateral symmetry may be written as:

$$M_{jk} = \begin{pmatrix} M & 0 & 0 & 0 & M_{zG} & 0 \\ 0 & M & 0 & -M_{zG} & 0 & 0 \\ 0 & 0 & M & 0 & 0 & 0 \\ 0 & -M_{zG} & 0 & I_{44} & 0 & -I_{46} \\ M_{zG} & 0 & 0 & 0 & I_{55} & 0 \\ 0 & 0 & 0 & -I_{46} & 0 & I_{66} \end{pmatrix} \tag{35}$$

where, M is the mass of the vessel,
I_{jj} is the moment of inertia in the jth mode of motion about the centre of gravity G situated at (0,0,z_G) and I_{jk} is the cross-product of inertia. For a body with lateral symmetry the only non-zero elements in the hydrostatic restoring matrix are $C_{33}, C_{35} = C_{53}, C_{44}$ and C_{55}.

The terms in Equation 34 can be evaluated by a number of methods; such as two-dimensional strip theory and three-dimensional potential flow analysis, each assuming the fluid inviscid, incompressible and the fluid flow is irrotational. The fluid motion can be represented by

velocity potential function satisfying Laplace's equation throughout the fluid domain. Unfortunately calculating the total velocity potential in its most general form is difficult and, for practical use, some simplification is necessary. Thus, the total potential can be expressed as a linear summation of components,

$$\phi(x, y, z, t) = (Ux + \phi_s(x, y, z)) + \phi_T e^{i\omega_e t} \tag{36}$$

where,

U is the forward speed,
ϕ_s is the perturbation potential due to steady translation and
ϕ_T is the unsteady perturbation potential which may be decomposed to give:

$$\phi_T = \phi_I + \phi_D + \sum_{j=1}^{6} \phi_j \eta_j, \tag{37}$$

with,

ϕ_I as the incident wave potential,
ϕ_D as the diffraction potential and
ϕ_j denoting the radiation potential due to unit motion in the jth direction.

In Equation 36 the first two terms represent the problem of the ship advancing at steady forward speed in calm water. These may be determined separately from the unsteady potentials. Using Equation 37 and appropriate boundary condition solutions to Equation 34 are obtained.

5.3.2 Method of evaluation

Evaluation of the radiation and diffraction potentials in Equation 37, which are used to calculate the added mass and damping coefficients and the diffraction component of the wave exciting force respectively, may be carried out in several ways. For this study a three-dimensional method using a pulsating source distribution was used, Bishop et al. [52].

The three-dimensional analysis is a boundary element method, whereby the problem of modelling the whole fluid domain can be reduced to that of the boundaries of the fluid, in this case by application of Green's 2nd theorem. By suitable choice of the singularities to be used, the problem can be further reduced to modelling the body surface only. Thus, in the three-dimensional method adopted the wetted surface of the hull is represented by four-cornered panels, each with a singularity at its centre. For Model 5b 640 panels were used, 320 per demihull and for Model 5s 700 panels were used, 350 per demihull.

5.4 Presentation of data

The results of the theoretical investigation are presented in the form of transfer functions. This allows the RMS response at any encounter frequency and in any wave condition to be calculated.

The transfer functions are defined in Equations 21 to 27 where encounter frequency ω_e is related to wave frequency ω_0 by Equation 24. Graphs were plotted of transfer function to a base of non-dimensional encounter frequency, Equation 26.

The results are also presented in the form of normalised RMS motions against ship heading. These are obtained from the peak RMS responses and are defined in Equations 31 to 33.

5.5 Results

The average computation times for each heading consisting of 25 encounter frequencies using the pulsating source code was between 90 and 130 minutes running on a Sparc 10. This allowed a large number of cases to be investigated. Examples of the typical transfer functions for Model 5s at S/L=0.2 and for a Froude number of 0.65 are shown in Figures 92 to 94.

Only at the lowest Froude number of 0.2 was there more than one wave frequency for a given encounter frequency in following seas, as shown in Figure 91. This indicates that some of the waves were able to pass the ship from astern. The results at this speed have been considered to be too slow for the normal operation of high speed craft and are not considered in detail. At the other speeds the ship was travelling fast enough to encounter the waves from ahead.

The general trends indicated by the transfer functions for heave and roll are as expected. However the magnitudes of the peak response at the resonant frequency are very large and unrealistic when compared with the experimental results available such as those in Figures 95 and 97. The results for pitch, Figure 96, were not predicted well by the theory. The theoretical method over predicted the peak response and shifted the resonant frequency. Consequently it was necessary to try and remove this inaccuracy built into every transfer function by normalising the results. This meant dividing the peak response by an appropriate value. The most suitable value is the peak response in head seas. This works for heave and pitch but roll presents a problem because the transfer function in both head and following seas is zero in regular long-crested waves. The next best solution was to normalise roll using the beam seas value as this would be close to the maximum. It was later decided, that normalising using the 150° value was better. This was a consequence of the spreading relationship discussed in the next chapter.

5.5.1 Model 5s

The results for this model at both S/L of 0.2 and 0.4 are shown in the form of normalised results, Figures 98 to 110. The experimental results are plotted on the graphs for Fn=0.65, Figures 102 and 109 these indicate a good correlation between the experimental and theoretical results.

Figures 104 to 106 indicate the effect of Froude number on peak response with heading. It is clear that the effect of Froude number is minimal except for the Fn of 0.2. For both separation ratios the results for Fn=0.2 show a different trend for heave, which increases to a maximum at 90° and then decreases, rather than having a maximum at 180°. Pitch shows expected trends and is similar to the other Froude numbers. Roll is smaller in magnitude than at the other Froude numbers and peaks at a heading of 90° rather than 120°.

5.5.2 Model 5b

The results for this model are very similar to the results for Model 5s, and normalised results are shown in Figures 114 and 115. Again the results for the Fn=0.2 were significantly different from the other Froude numbers, but the trends for Model 5s and 5b at this Froude number are the same.

5.5.3 Comparison with full scale data

The results show reasonable comparison with data obtained from sea trials of a 35m catamaran, [53]. The peak RMS responses have been normalised as for the theoretical results. These graphs can be seen in Figures 86 to 88. The most noticeable difference is the results for roll, which has a non zero result in head and following seas. This is because the full scale results were not obtained in regular long-crested waves but in a sea with some degree of wave spreading.

5.6 Summary

It can be seen from the results that it is possible to produce transfer functions for a range of encounter frequencies at headings from $\mu = 180°$ (head seas) to $\mu = 0°$ (following seas) using the pulsating source method. Unfortunately experimental data is only available to validate the results in head and bow seas, but these results show a good correlation when presented in the form of normalised RMS motions.

The comparison with the available full scale data, was fairly good considering that the full

scale ship was operating in irregular seas.

The next chapter describes how the normalised RMS motions form the basis for developing the spreading relationships required to develop three-dimensional transfer functions.

Chapter 6

Transfer function spreading relationships

6.1 Introduction

The current methods of assessing the seakeeping performance of high speed vessels, as described in Chapters 4 and 5, are not feasible at the concept design stage due to time or computing power restraints. A method of assessing the seakeeping performance for a large number of vessels is required. This Chapter describes a suitable approach for use at the concept design stage which allows oblique headings to be investigated from a data base of head sea transfer functions.

The creation of a sea spectrum, which is a more realistic representation of what occurs in the open ocean is desirable from the point of view of predicting seakeeping performance. This can be achieved by creating a short-crested sea spectrum from a long-crested spectrum using a suitable spreading function, such as that given in Equation 38, for headings within $\pm 90°$ of the wind direction.

$$f(\mu) = \beta \cos^n \mu \tag{38}$$

In a similar manner, it would be very useful to develop suitable relationships between the transfer functions at headings from $\mu = 180°$ to $\mu = 0°$. This approach has been suggested by Goodrich [54]. This "spreading" relationship should allow the larger data base of head sea transfer functions to be developed into three dimensional transfer functions. This would then allow more realistic, and consequently, more accurate predictions of seakeeping performance to be made.

The relationships were developed by examining sources of transfer functions from both numerical and physical experiments.

6.2 Motion prediction

The methodology used to assess the seakeeping performance is presented in Figure 123 and this involves multiplying the wave spectrum by the RAO or transfer function squared. This produces a motion response spectrum. From this motion response spectrum various statistics and derived statistics can be determined. Conolly [12], suggested that a number of transfer functions for different headings could be combined to generate a three-dimensional transfer function together with a spreading function to create a short-crested sea spectrum to get a more realistic motion response spectrum.

A further idea developed following the discussions with Goodrich [54] was that if a relationship between the transfer functions at different headings could be found, then the head sea transfer functions could be "spread" in a similar manner to the wave spectrum. An important advantage of this approach is that there are many more transfer functions for head seas than for oblique seas and such spreading relationships could be applied to this relatively large data base of head sea transfer functions.

6.3 Methodology

In order to apply this "spreading relationship" to the head sea transfer functions the relationship between the transfer functions at different headings was required to be found and the influence of various parameters on these relationships determined.

6.3.1 Transfer functions

The transfer functions used to determine this spreading relationship need to be consistent in form. The use of an encounter frequency base is important since it will mean that the shape of the transfer function is similar at different headings with the peak occurring at the same frequency. This can be seen in the transfer functions for a catamaran in oblique regular waves in Figure 58. This also means that the spreading relationship will not have any influence on the shape of the transfer function, only the relative amplitudes.

A number of transfer functions at headings from head to following seas were generated using a pulsating source code, as described in Chapter 5. This enabled a large number of variations and investigations to be carried out. Experimental data from head and oblique wave tests,

as described in Chapter 4 are used to assess the validity and, where necessary, empirically adjust the numerically derived values.

6.3.2 Normalising

In order to be able to spread the head sea transfer function, the spreading relationship has to relate each heading to this head sea case. This means that the change in the transfer function has to be divided by the head sea value for heave, pitch and accelerations. For roll the 150° value is used since there is no roll in head seas in regular waves. At this point the question arises as to what value should be selected to represent the change in transfer function at each heading. A frequency by frequency determination of the normalised values would be the most precise. From a practical viewpoint the peak value could be used as this is where the most significant changes occur. The initial low frequency value is 1 for heave, $\cos\mu$ for pitch or $\sin\mu$ for roll, where μ is the heading angle. A frequency by frequency determination of the normalised motion can be seen in Figure 124. This figure shows that there is relatively little change in the spreading relationship with frequency except in following seas. It should be noted that the values were only shown for the first 15 frequencies of the 25 evenly spaced frequencies which make up the transfer function, after which the values of the transfer function are so small that the spreading relationship begins to deteriorate. Also, the transfer function values in following seas are small, such as those in Figure 92. The use of a single normalising value based on peak values will not lead to any significant errors. The results of the investigation indicate that the use of the ratios of the peak values would provide a satisfactory normalising approach.

6.3.3 Spreading relationship

The influence of $L/\nabla^{1/3}$, S/L, Fn and hull form on the spreading relationship were investigated using the data generated in Chapters 4 and 5. Three length-displacements, two separations, six Froude numbers and two hull forms were tested. The results of these investigations are presented in Figures 104 to 106, 120 to 122 and 126 to 131.

6.3.3.1 Froude Number

The influence of Froude number on the spreading relationships is presented in Figures 104 to 106. These figures show that increasing speed results in a reduction in the value of the spreading relationship. This is most clear in the Froude number range of 0.2 to 0.4. After this point the curves tend to bunch more closely together. This is most obvious for heave and roll motion. It is therefore assumed for this study that, for the speeds to be considered,

(Fn=0.53,0.65 and 0.8), the spreading relationship is independent of Froude number changes. The influences at the lower Froude numbers are retained for possible use at a later stage.

6.3.3.2 $L/\nabla^{1/3}$

The influence of $L/\nabla^{1/3}$ on the spreading relationships is presented in Figures 120 to 122. The theoretical results show significant inconsistencies, e.g. in Figure 120 a small change in heave going from $L/\nabla^{1/3}$ of 7.4 to 8.5 and a large change from 8.5 to 9.5. In Figure 122 the changes are similar in inconsistency. The reason for these inconsistencies in the theoretical values is not clear. In the example application of the approaches the influence of $L/\nabla^{1/3}$ has therefore been set aside.

6.3.3.3 S/L

The influence of separation is presented in Figures 126 to 128. These figures show that there is a clear difference between the two separations. The heave motion shows some irregularities when the two curves cross over at a heading of 100° but the pitch and roll show more clearly defined differences.

6.3.3.4 Hull shape

The influence of hull shape on the spreading relationships is presented in Figures 129 to 131. It is clear from these graphs that there is almost no difference in the spreading relationships for two different hull shapes at the same Froude number, S/L and $L/\nabla^{1/3}$. It is therefore assumed for this study that hull shape has no influence on the spreading relationships. The results also suggest that the spreading function might be suitable for a wider range of hull shapes having similar speed, $L/\nabla^{1/3}$ and S/L.

6.3.4 Generic spreading relationship

The investigations into which parameters may influence the spreading relationships has shown that the only parameter of significance is that of separation. It is therefore possible to generate a set of generic spreading relationships dependent only on separation-length ratio.

The question arises as to whether these generic spreading relationships should be fitted with a numerical approximation, curve-fitted or using a linear interpolation method. Currently, the methodology uses a linear interpolation of the data in a look up table.

6.4 Application and validation

The current spreading relationships have been applied to the experimental data for Model 5s, S/L=0.2 at Fn=0.65, in order to check the accuracy of this method. A polynomial fit through the spreading relationship for heave is shown in Figure 132. It would be expected to under predict the 160° transfer function and over predict the 130° transfer function. Given the limited number of data points, the use of the linear interpolation method provides a better fit to the data and this is also shown in Figure 133. This may be compared with the more complicated frequency by frequency determination of the spreading relationship shown in Figure 134. The difference in accuracy between the two approaches is small and the more complicated approach is considerably more time consuming and therefore less applicable at the concept design stage.

If the simpler approach is used a potential problem is the low frequency section of the curve, where the curve for heave would normally run into a value of 1. The scaling of the curve results in this section being altered and usually lowered. This is not so much of a problem for pitch since this section will change with $\cos\mu$ and so reduce with heading change from head seas. It is found that for practical purposes, the results can be forced to the correct low frequency values without any undue loss in accuracy.

6.5 Added resistance in waves

The change of added resistance with heading, would be very useful to designers. Just as the use of a spreading function can be used to determine the motions at any heading from head sea motions data, added resistance at any heading would be determined from head sea data.

The resulting forces from the numerical experiments could be used in a simple added resistance formula, Equation 39, such as that proposed by Havelock [55]. This formula is however intended for calculating added resistance in head seas and, as a result, would not generate a sensible variation of added resistance with heading.

$$R = \frac{\pi}{\lambda} H_0 \zeta_0 \sin\beta_1 + \frac{\pi}{\lambda} P_0 \theta_0 \sin\beta_2 \tag{39}$$

Where H_0 and P_0 are the amplitudes of heave and pitch moments. ζ_0 and θ_0 are the amplitudes of the forced heaving and pitching. β_1 and β_2 are the phase lags of oscillation.

It was decided not to continue to investigate a spreading relationship for added resistance for two reasons. Firstly in order to obtain the added resistance at different headings, modifications to the numerical prediction program would have to be made to integrate the pressures

on the hull. Secondly, it is anticipated that the added resistance in head seas would be the worst case, and that this could be used in the assessment of competing designs.

6.6 Summary

The data base of head sea transfer functions may be enhanced by adopting a three-dimensional approach applying a "spreading relationship" to the head sea transfer functions and using short-crested wave spectra.

The generic spreading relationships depend only on separation and, for the cases considered in this study, are assumed to be independent of Froude number, $L/\nabla^{1/3}$ and hull form.

The application of these generic spreading relationships requires the transfer functions to be a function of encounter frequency, so that all of the transfer functions have the same overall shape.

It has been found to be more satisfactory to use a linear interpolation method rather than a curve fit, which may incorrectly represent the spreading relationship in areas of high curvature. Using this approach the spreading relationship produces a good representation of the experimental data used to validate the methodology.

It was not possible to derive a spreading relationship for added resistance from either physical or numerical experiments. It is therefore proposed that the head sea values be used as the determining values for practical design considerations.

Chapter 7

Motion prediction

7.1 Introduction

The straightforward comparison of transfer functions in order to assess the seakeeping performance of competing vessels is not a satisfactory method, since no influence of the sea state is considered. Similarly, when comparing monohulls and catamarans for the same service, different size vessels will normally be required and have to be assessed. The experimental results in Figures 66 to 68 indicate that the response will increase linearly with increasing wave height. However, the effect of the modal period of the wave spectrum and the resonant period of the transfer function coinciding is not considered. The approach illustrated in Figure 123 shows how the response spectrum is determined from the following combinations of transfer function and wave spectrum:

Transfer function^2 at desired heading angle $\times$ long-crested wave spectrum

or 3D transfer function^2 $\times$ short-crested wave spectrum

Relevant statistics can then be derived from the response spectrum.

7.2 Representation of the sea state

The likely sea state that the vessels under consideration will encounter can be determined from published data on global wave statistics such as Hogben et al. [56] or from more precise data such as local wave measurements. This data is presented in the form of a wave period, a significant wave height and a probability of occurrence. These values need to be used to generate an irregular seaway. This can be achieved by using a wave spectrum. The wave spectrum needs to be selected to represent the real sea state as well as possible, since the incorrect spectrum may result in the wrong vessel being selected at the concept design stage.

There are a number of wave spectra available varying in complexity from the single-parameter Pierson-Moskowitz to the Ochi six-parameter spectrum. Most of the wave energy is located in an area around the modal period of the spectrum. The greater the modal period the narrower the band that contains most of the energy as illustrated in Figure 135. This will create problems for vessels if the resonant period of their motion is located at or near the same period as the modal period of the wave spectrum as the resulting response will be more severe. Figure 136 shows the influence on the RMS motions of the resonant period of the transfer function and the mean wave period of the wave spectrum coinciding.

7.2.1 Long-crested wave spectrum

The wave spectrum is representative of a statistical analysis of time histories of irregular waves. A time history of length T_H might be represented by a Fourier series of the form given in Equation 40 from Lloyd [39].

$$\zeta(t) = \overline{\zeta} + \sum_{n=1}^{\infty} A_n \cos(\omega_n t) + B_n \sin(\omega_n t) \quad [m] \tag{40}$$

with equally space frequencies given by Equation 41

$$\omega_n = \frac{2\pi n}{T_H} \quad [rad\ s^{-1}] \tag{41}$$

with n=1,2,....∞

Rewriting Equation 40 as Equation 42

$$\zeta(t) = \overline{\zeta} + \sum_{n=1}^{\infty} \zeta_{n0} \cos(\omega_n t + \epsilon_n) \quad [m] \tag{42}$$

This implies that an irregular wave record may be represented by an infinite number of regular sine waves of amplitude ζ_{n0}, frequency ω_n and phase ϵ_n.

7.2.2 Wave energy spectrum

The relative importance of the component sine waves making up an irregular wave time history may be quantified in terms of a wave energy spectrum. The energy per square metre of the sea surface of the nth wave component is $(\rho g \zeta_{n0}^2)/2 \quad [kJ\ m^2]$. The wave energy spectrum is defined so that the area bounded by a frequency range is proportional to the

total energy of all the wave components within that range of frequencies. It follows that the total area enclosed by the wave spectrum is proportional to the total energy per square metre of the complete wave system.

There will be only one component frequency ω_n in the range $\omega_a - \omega_b$ and the wave amplitude spectral ordinate $S_\zeta(\omega_n)$ corresponding to the frequency ω_n is defined by

$$\rho g S_\zeta(\omega_n)\delta\omega = \frac{\rho g \zeta_{n0}^2}{2} \tag{43}$$

so the spectral ordinate is

$$S_\zeta(\omega_n) = \frac{\zeta_{n0}^2}{2\delta\omega} \tag{44}$$

7.2.2.1 Idealised spectra

Suitable wave spectra for open oceans include the I.T.T.C. 2-parameter spectrum. This uses values of Period, $\overline{\mathrm{T}}$ and Mean wave height $\mathrm{H}_{\frac{1}{3}}$, as described in Lloyd, [39]. The I.T.T.C. 2-parameter spectrum is shown:

$$S_\zeta(\omega) = \frac{A}{\omega^5}\exp\left\{\frac{-B}{\omega^4}\right\} \tag{45}$$

Where:

$$A = \frac{173\overline{H}_{\frac{1}{3}}^2}{\overline{T}^4}$$

$$B = \frac{692}{\overline{T}^4}$$

This produces an irregular wave spectrum of long-crested waves. A long-crested wave is one in which all the crests travel parallel to each other. This rarely happens if at all. There will always be some degree of wave spreading caused by fluctuations in the wind direction, changes in depth and the presence of coastlines. These factors will all result in a number of long-crested wave systems being generated. When these wave systems meet there will be interference between the systems which will result in a short-crested wave system, where the wave crests are travelling in different directions. There will be a primary wave direction usually aligned with the local wind direction.

7.2.3 Short-crested wave spectrum

In order to represent a short-crested wave spectrum, a long-crested spectrum is spread using a suitable spreading function, as described in Lloyd [39]. The spreading function used is a $\cos^n$ function, Equation 46. The greater the value of n, the closer the result to a unidirectional sea. This can be seen in Figure 137, where at an n value of 8, almost all of the wave energy will be at a heading of $\mu = 180$, (head seas). The $\cos^2$ function has been shown to be quite appropriate for many ocean waves and a typical spectrum is illustrated in Figure 138.

$$f(\mu) = \beta \cos^n \mu \tag{46}$$

The generalised form of the normalising factor β is shown in Equation 47.

$$\beta = \frac{2.4.6...n}{1.3.5...n{-}1} . \frac{1}{\pi} \tag{47}$$

The normalising factor is necessary to insure that, for all values of n.

$$\int_{-\pi/2}^{\pi/2} f(\mu)\, d\mu = 1$$

such that the short-crested sea spectrum has the same total energy as the long-crested sea spectrum.

To illustrate this, the simplest case is for an n value of 2 when:

$$S_\zeta(\omega, \mu) = \frac{2}{\pi} cos^2 \mu . S_\zeta(\omega) \tag{48}$$

7.3 Transfer functions

The transfer functions for the various motions, velocities and accelerations required can be determined either experimentally or numerically. Chapters 4 and 5 describe the derivation of various two-dimensional transfer functions. In order to use the short-crested wave spectrum a three-dimensional transfer function is required.

7.3.1 Three-dimensional transfer functions

The generation of a three-dimensional transfer function can be achieved in one of two ways. The first is to group together a number of individual transfer functions at different heading

angles. This method was used with the oblique experimental data for head seas in order to assess the relative merits of the different methods, Molland and Taunton [57]. The second method uses the generic spreading relationships, described in Chapter 6, to generate three-dimensional transfer functions from the head sea two-dimensional transfer functions described in Chapters 4 and 5. An example of a three-dimensional transfer function for vertical accelerations at lcg is given in Figure 139.

7.4 Response spectrum

The response spectrum is determined by multiplying the square of the transfer function by the wave spectral energy, Equation 49.

$$M(\omega_e, \mu) = RAO(\omega_e, \mu).S_\zeta(\omega_e, \mu) \tag{49}$$

This 3-D approach allows the motions to be calculated at any heading angle. It also shows what influence the ship's response to waves at other headings has on the total response of the ship. This is most significant when roll motion is considered. There will be no roll in head and following seas if the waves are long crested, but if the waves are short crested the roll response in the bow quarter will produce some roll in head seas, likewise in the stern quarter. Typical examples of 3D response spectra for heave and midship acceleration are shown in Figures 140 to 143. It can be seen from Figure 143 that the short crested approach gives the peak of the heave response in beam seas at a heading of 110°. This is because the 3D heave transfer function is higher towards head seas than in following seas which will skew the result in beam seas.

7.4.1 Roll in short-crested head and following seas

Using the short-crested approach it is possible to predict the roll motion of a ship with centreline symmetry in a short-crested head or following sea which has been generated using a symmetric spreading function. The wave spectra used to describe the sea state are derived from measurements of wave records. These wave records will all have random phasing of the wave components. When the spectra are generated this random phasing is part of the spectra. Hence when the roll response function is generated for identical port and starboard transfer functions and identical wave spectra, then the resulting roll response spectra are added to give the total roll energy.

7.5 Statistics

The statistics for both the 2D and 3D prediction methods are determined in a similar way. This involves calculating the area under the response spectrum for the 2D case and the volume under the response spectrum for the 3D case. The RMS values can then be determined from the areas and volumes. The variance (m_n) for the 2D and 3D methods are determined using Equations 50 and 51.

$$m_n = \int_0^\infty \omega_e^n M(\omega_e) d\omega_e \tag{50}$$

$$m_n = \int_0^{2\pi} \int_0^\infty \omega_e^n M(\omega_e, \mu)\, d\omega_e d\,\mu \tag{51}$$

where, n=0, for the motion, 2 for the velocity and 4 for the acceleration of the response. This has its basis in differentiation, where the motion can be differentiated by dividing by the frequency or time. The RMS values are determined using Equation 52.

$$\sigma_0 = \sqrt{m_n} \tag{52}$$

7.5.1 Comparison of short-crested and long-crested statistics

The effect of wave spreading on the response of a vessel is illustrated in Figures 144 to 146. The effect of wave spreading on heave and pitch is to reduce the response in head and following seas and to smooth the change in response with heading. The effect of wave spreading on the roll response results in some roll in head and following seas, as described earlier in this Chapter, and reduced roll motion in beam seas. The waves were spread using a $\cos^2$ spreading function.

7.6 Methods available

The methods available are determined by the transfer functions available. The current data base of experimental and theoretical data allows the following methods to be applied:

- Long-crested head seas
- Long-crested oblique seas (180°, 150° & 120°)

- Short-crested (from head sea data base - no roll)
- Short-crested (from oblique sea data base - with roll)

Currently due to the lack of data for monohull roll motion the fourth method, is only applicable to catamarans.

7.6.1 Significance to the designer

The first approach, which uses long-crested head seas, provides good insight into the overall seakeeping performance of different vessels at the concept design stage. This is likely to be the most severe case for vertical motions of heave and pitch, but roll motion is not considered. Currently it is the only method which gives the added resistance of the vessel. There is a large data base of suitable vessels for a wide range of speeds.

The second approach, which uses long-crested oblique seas, provides information on the performance at different headings. If route information is known at the concept design stage then this approach will provide more useful information of the seakeeping performance. This approach is limited by the number of suitable vessels and headings.

The third and fourth approaches use the easily generated or existing large data base of head sea transfer functions coupled with a suitable transfer function spreading relationship and a short-crested wave spectrum. This approach provides the designer with more accurate information of the seakeeping performance at any heading when only head wave transfer function are available, as illustrated in Figure 147. This approach will also provide information of the roll motion, but only if there are transfer functions for the 150° heading in regular waves.

7.7 Summary

The prediction of seakeeping performance requires a suitable wave spectrum and transfer function. These can either be a simple long-crested wave spectrum and transfer function for the required heading or a three-dimensional transfer function and short-crested wave spectrum.

The most accurate method of predicting the seakeeping performance of a vessel is to use a short-crested sea spectrum and three-dimensional transfer functions constructed from a number of individual transfer functions at headings from 180° to 0°.

If individual transfer functions are not available then implementing an appropriate spreading relationship to generate a three-dimensional transfer function from an appropriate head sea transfer function is an alternative.

Some examples of the use of and differences between the methods is presented in the next Chapter in the form of a number of case studies.

Chapter 8

Example applications

8.1 Introduction

A number of example ships are used as case studies in order to demonstrate the use of the various approaches and evaluate their effectiveness. For each case study a number of competing ships are used along with suitable and typical sea states from global wave statistics, such as those given in Hogben et al [56]. A typical heading is also suggested to show the benefit of the short-crested three-dimensional approach. The performance of these ships is assessed based on suitable criteria for the role of the ship, as already discussed in Chapter 3.

It is deduced from the experimental tests carried out that the transfer functions are linear with respect to wave height. The effect of increasing wave height will simply be to increase the motions and is therefore not investigated. The influence of wave period is, however, investigated for the long-crested head sea approach. It is assumed that the short-crested approach will show the same trends with different wave periods as the long-crested approach, since the short-crested approach involves applying a spreading function to the long-crested wave spectra.

8.2 Case one: Passenger only ferry

The first case study is for two competing ships, a monohull (M1) and catamaran (C1) whose details are given in Table 23, operating a passenger only service in the English Channel. The results are presented for four of the more typical wave periods and for a single wave height.

The results in long-crested seas are presented in Tables 24 and 25. M1 has values of non-availability which increase with wave period. Added resistance is highest at a wave period of 6s and vomiting incidence is highest at a period of 7.1s. C1 has values of non-availability

which increase with wave period. The added resistance is highest at a period of 6s and vomiting incidence is highest at a period of 8s. The levels of non-availability are similar between the two vessels but the catamaran C1 is marginally better. The vomiting incidence is also similar with the catamaran being marginally better. The added resistance, however, is significantly greater for the catamaran.

The results in short-crested seas are presented in Tables 26 to 29. Tables 26 and 27 show the RMS values and probabilities for the seakeeping attributes. Tables 28 and 29 show the condensed attributes. It can be seen that the values used in the condensed attributes for non-availability are those for vertical accelerations at the LCG or forward. This is because these had the highest probabilities of exceedance. If headings of 135° and 45° are assumed in order to illustrate the benefits of the short-crested approach, then there is little difference between the two vessels in terms of their non-availability and vomiting incidence. At both headings the catamaran's seakeeping performance was better. It should be noted that if the added resistance from head seas is considered then the catamaran has considerably greater added resistance than the monohull.

8.2.1 Reduced speed operation

Ships M1 and C1 were run at a reduced speed as might be required when operating in an estuary or in bad weather. The results are presented in Tables 30 to 33. In long-crested seas the catamaran C1 performed better than the monohull M1 in the criteria of non-availability and vomiting incidence but was again inferior with its higher added resistance. In short-crested seas the monohull again performed better than the catamaran. Performance polar plots for M1 and C1 in short crested seas are shown in Figures 148 to 151.

Overall, it can be concluded that the monohull M1 has better seakeeping performance.

8.3 Case two: Passenger/vehicle ferry

The second case study is for two competing ships a monohull (M2) and a catamaran (C2), operating a passenger/car service in the Irish Sea. The typical wave statistics are shown in Table 34 and the ships' details are shown in Table 35. The results have been presented for long-crested head seas and short-crested seas.

The results in long-crested seas are presented in Tables 36 and 37. The mean results for monohull M2 and catamaran C2 over the four wave periods are that the much longer monohull is significantly better in terms of its availability and added resistance, but its mean vomiting incidence is only marginally better. This is most likely due to a favourable frequency weighting

of the vertical accelerations for the catamaran.

The results in short-crested seas are presented in Tables 38 and 39. The shorter catamaran has considerably higher non-availability, but only marginally worse vomiting incidence. The seakeeping performance polar plots, Figures 152 to 155 show the seakeeping performance in short-crested seas at headings from 180° to 0°. The graphs are plotted using the RMS motions for each heading. The inner of the two lines in Figure 154 represent the frequency weighted acceleration used to determine the vomiting incidence. Figure 152 shows the roll motion present in short-crested head and following seas.

8.4 Case three: Variation of catamaran hull separation

The third case study is a variation of the second case study and attempts to improve on the seakeeping performance of the catamaran C2. Two competing catamarans C3 and C4 are considered, C3 is a longer more slender hull than C2. C4 is a shorter hull with a greater separation. Again the two vessels are operating a passenger service in the Irish Sea. The ships' details are given in Table 40.

The results in long-crested seas are presented in Tables 41 and 42. The mean results for the four wave periods show that the two catamarans C3 and C4 have very similar seakeeping performance. The main difference between the two ships is that the more slender catamaran C3 has a higher added resistance.

The results in long-crested oblique seas Table 43 show the seakeeping performance of catamarans C3 and C4 at headings angles of 180°, 150° and 120°. Catamaran C4 has the overall better seakeeping performance, with a slightly worse performance in head seas but increasingly better performance with change of heading.

The results in short-crested seas are presented in Tables 44 and 45. These results show very similar seakeeping performance at the four wave periods. Catamaran C4 is always slightly better except at the lowest wave period, where the performance is very close.

The results in short-crested seas with roll are presented in Tables 46 and 47. The catamaran C4 performs better than C3 over the four wave periods. The results are again similar to the short-crested results without roll. This is because in almost all cases vertical acceleration is the deciding factor.

Performance polar plots for C3 and C4 in short-crested seas are shown in Figures 156 to 158.

8.5 Case four: Fast freight service

The fourth case study is a variation of the third case study but instead of operating a passenger service for a voyage duration of 2 hours the ships are operating a freight service for 6 hours. This case study uses ships C3 and C4 to illustrate the effect of changing the limiting criteria on the seakeeping performance.

The results in long-crested seas are presented in Tables 48 and 49. These results show the same trends as for the passenger service with catamaran C4 having the better seakeeping performance, but the values for the non-availability are reduced. The values of vomiting incidence are of the order of 40% but this is based on values for unadapted adults. It is likely that the crew of a fast vessel will have a greater tolerance of motion sickness.

8.6 Case five: Hullform variation

For this case study the substantially better seakeeping performance of the longer monohull M2 over the competing catamaran C2 has lead to different hull forms at the same length displacement ratio being investigated.

The mean results for the four wave periods are presented in Table 50 and show the second variant, M2-c, to have slightly better seakeeping performance than either the original M2 or the other variant M2-b.

8.7 Case six: Variations of passenger area

The program used to generate the vessels, written by Williams [4], has the ability to modify the seating area and passenger area. The initial values for M1 and C1 were set to the mean values in the appropriate ranges for these types of vessel. The second set of ships designated M1′ and M2′ had the passenger and seating area set to the maximum values. Both resulting ships are considerably longer than their original variations, and their details are presented in Table 51. It can be seen that the catamaran is now longer than the monohull rather than the other way round for M1 and C1.

The mean results for the four wave periods in long-crested head seas are presented in Table 52 and show that the longer catamaran C1′ has better seakeeping performance than the monohull M1′. This is the reverse of the original outcome for M1 and C1. The results are however much closer for the ships M1′ and C1′ than for the originals M1 and C1.

8.8 Summary

The long-crested results give an indication of the overall performance of the competing vessels, as well as providing information on the added resistance of the vessel. The minimum required for assessing the seakeeping performance is a transfer function in regular head waves. The short-crested approach requires at least the head wave transfer function.

The long-crested oblique results give an indication of how the vessels performance changes with heading. This approach is probably adequate for assessing the seakeeping performance of competing vessels, but at the concept design stage is limited by the data available and the time required to generate the transfer functions.

The two short-crested approaches allow the influence of heading to be fully investigated in the absence of experimental or numerical transfer functions for the required heading. The short-crested roll requires a roll transfer function at 150°. The simpler approach is probably the most useful at the concept design stage.

When the seakeeping performance of two vessels is similar it is preferable to keep all seakeeping attributes in order to help with the final selection.

The case studies show that the longer vessel will have better motions. In most cases a monohull competing with a catamaran will be longer and so have better motions. The monohull will always have better added resistance than the catamaran.

Chapter 9

Conclusions and recommendations

9.1 Two categories of attributes, (seakeeping and derived attributes), have been described. The sources of proposed limiting criteria have been examined for their usefulness in assessing the seakeeping performance of high speed passenger and commercial vessels. A method of condensing the relevant attributes has been proposed in order to simplify the assessment procedure at the concept design stage. A set of limiting criteria values have been selected from the proposed values to illustrate their use in the assessment procedure in a number of case studies.

9.2 An experimental test programme has been undertaken to extend the data base of motions for suitable high speed vessels. Model 5s (based on Series 64) has been tested in three configurations, monohull, and catamaran at S/L=0.2 and 0.4, at four speeds in regular head waves. This model has also been tested in the same configurations at a much wider range of speeds in calm water. The results for Model 5s have been compared with those for Model 5b (based on the NPL Series), a model of the same $L/\nabla^{1/3}$ ratio, which had been tested earlier. This allowed the influences of different hull shapes to be assessed but the differences were found to be small.

4.5m free-running versions of the Models 5b and 5s have been tested in regular head and oblique bow waves. The difference between the seakeeping performance of the two different hull shapes at headings of 180°, 150° and 120° was found to be small.

9.3 The differences in the seakeeping performance between a towed model and a free-running model have been investigated. It has been found that the heave or vertical acceleration at LCG of the 4.5m model was higher than that of the 1.6m towed model and that the pitch motion of 4.5m model was less than that of the 1.6m model. This is most likely due to the following differences in the experiments: The 4.5m model was self propelled rather than towed. The tow post for the 1.6m model made up 10% of the displacement mass and moved only in the vertical direction and was not free to pitch.

The wave probe used for the 1.6m model tests in the Southampton Institute tank was mounted on the carriage and may have been influenced by the presence of the model. There may have been some wall effects in the Southampton Institute tank.

9.4 The direct measurement of added resistance for the 4.5m free running models was not possible. As an alternative, speed loss has been determined using a novel approach which, uses a modified wave frequency to encounter frequency relationship at different headings. The results, particularly in head seas, showed good agreement with the towed 1.6m model tests. The influence of variations in heading during the run, were investigated and it was found that small changes in course at headings of 180° and 150° have only a small influence on the determination of speed but at a heading of 120° the results are not reliable because of the large error involved.

9.5 The data base of motion transfer functions in oblique seas is very limited. The oblique wave experiments carried out as part of this research make an important contribution to the experimental data base. In order to overcome the restrictions on speed and heading imposed by testing in test tanks and ocean basins, a successful open water methodology has been established. The results to date are limited, but the platform and analysis techniques are available for future tests which should facilitate the collection of further model seakeeping data for high speed vessels.

9.6 The limited headings tested in the Ocean Basin at Haslar and the limited data available from the open water tests required the use of numerical methods to extend the data base of transfer functions to beam and following waves. The numerical code was selected based on the accuracy and computation time. The accuracy of the numerical methods can be improved by validating the hydrodynamic coefficients with data from a V.P.M.M. which is currently under development.

9.7 The head wave transfer function and long-crested wave spectrum provides most of the information required for assessing the relative seakeeping performance at the concept design stage. A better approach to predicting seakeeping performance is to use a short-crested sea spectrum and to construct a three-dimensional transfer function from transfer functions at a number of headings from 180° to 0°. This approach, although the most accurate, is not considered to be applicable at the concept design stage.

9.8 The concept of a spreading relationship for transfer functions relating the change in the transfer function to heading angle has been investigated. This is a new concept and, such an approach would greatly enhance the use of the existing data base of head sea transfer functions. For this purpose, the normalised experimental data in oblique waves has been used in conjunction with the normalised data from the numerical investigation. The influence of Froude number, $L/\nabla^{1/3}$, S/L and hull shape on the spreading

relationship have been investigated. Within the scope of the investigation it was determined that only S/L has a significant influence on the spreading relationships. This has led to the development of generic spreading relationships with the potential for much wider applications. Two approaches to the generation and use of these spreading relationships have been investigated. The first a frequency by frequency approach, where a transfer function spreading relationship is determined for each frequency. The second, much simpler, approach uses a transfer function spreading relationship determined from the values at resonance. The small increase in accuracy given by the first approach is not considered to be worth the increase in time required to apply it, and the simpler approach is therefore used. The use of mathematical functions to represent the spreading relationships has also been investigated. With only a limited number of headings for each relationship there was not enough data to enable a good mathematical representation to be fitted to the data. Instead. a much simpler look-up table and linear interpolation method was successfully applied.

In order to detect relative difference in the seakeeping performance, other than those shown by the head wave long-crested approach, there must be a significant difference in the spreading relationships used. At present for a given displacement the only variable for the spreading relationship is the hull separation. At present therefore, the spread transfer function is not able to distinguish between competing monohulls or catamarans of the same separation.

9.9 The possibility of applying a spreading relationship to added resistance has been considered. The numerical code used does not calculate added resistance and attempts to calculate added resistance from the generated hydrodynamic coefficients have been unsuccessful.

9.10 A number of case studies have been used to illustrate the methods available at the concept design stage. The simplest method involves using transfer functions for the desired heading and a long-crested wave spectrum for the appropriate sea state. Alternatively, the head sea data can be used in conjunction with a transfer function spreading relationship. This is then used in conjunction with a short-crested wave spectrum, created by spreading a long-crested wave spectrum. This method has been found to produce more realistic motions and allows for roll motions. It is suitable for application at the concept design stage and therefore provides a powerful tool for comparing the seakeeping attributes early in the design process.

9.11 The parameters which influence the transfer function spreading relationships have only

been investigated for certain vessel types, namely semi-displacement round bilge catamarans with transom sterns. A more diverse range of model transfer functions is required. Transfer functions for head to following waves will be needed for these vessels in order to validate existing spreading relationships or determine new ones.

9.12 The vertical planar motion mechanism needs to be commissioned and a suitable experimental procedure developed. Once this has been carried out it is expected that useful data for high speed craft will be gathered and improvements to the numerical model can be made where necessary.

9.13 Modifications to the numerical model will allow the added resistance to be determined at different headings. This will allow a spreading relationship for added resistance to be developed in a similar manner to those for transfer functions. This would enhance the investigation process when comparing the added resistance/ speed loss for different high speed vessels.

9.14 Increasing the number of headings used to define the spreading relationship would allow a mathematical fit to be applied to the data. This might allow a mathematical function similar to that used to spread long-crested wave spectra to be developed.

APPENDICES

Appendix A

Details of 4.5m model

Principal dimensions of the 4.5m are given in Table 17.

A.1 Construction

The hulls were constructed from GRP. Each hull has a wooden gunwale glassed in and is fitted with three 6mm plywood bulkheads. Platforms carrying the engines, shaft bearings and rudder bearings were made of 18mm plywood and glassed into the hulls. The two cross beams joining/separating the hulls were of continuous section aluminium alloy mast material (kindly provided free of charge by Kemps Masts). These spars were bolted to each hull via a GRP fitting which was glassed to the hull and an adjacent bulkhead. This set-up allowed adjustment of the separation of the hulls, and removal of the spars for transportation of the models to test sites. The GRP hulls were constructed outside the University and fitted out in the University Engineering Faculty Workshops. The model was weighed prior to testing, including fuel and necessary ballast, leading to an all-up weight of 324kg.

A.2 Pitch, roll and yaw inertias

Model 5b was swung in its test condition in pitch and roll to obtain the relevant radii of gyration. The radius of gyration in yaw was estimated from the inertia in pitch assuming the demi-hull inertias in pitch and yaw to be the same. A summary of the radii of gyration for Model 5b is given in Table 18.

A.3 Engines, transmission and propellers

Engines: One per hull. Honda GX160QX4. Maximum power output: 4.1kW @ 3600 rpm. Continuous power output: 3.5 kW @ 3600 rpm. Capable of operation on petrol or propane gas (gas used when operating under cover in the Haslar Model Basin).

Shafting: Stainless steel 19mm (3/4") diameter.

Propellers: Brass. Diameter 152mm, Pitch 178mm. One right handed, one left handed. Propellers, shafting, brass stern tubes and stuffing boxes supplied by Norris Marine Equipment Ltd.

Gear Ratios: Transmission from engine to shaft is achieved using a pulley-belt system. Vee belts and pulleys are used with three gear ratios as shown in Table 53.

All tests to date have been carried out using the mid gear ratio (1:1.695), leading to a speed in calm water of the order of 4.40 m/s (Fn=0.67) at full engine throttle setting.

An electric clutch was originally fitted but proved to be unsuccessful, due mainly to misalignment problems. It was subsequently removed at an early stage of model commissioning and replaced with a direct drive fitting.

A.4 Electrical power/remote control

Electrical power for instrumentation and data acquisition equipment is provided by a 12v battery. Power for all on-board radio controlled equipment is provided by a 6v battery. The following operations are controlled by radio: Rudder winches; Throttle servos; Engine hold; Engine off, together with channels for data acquisition trigger etc as required. The rudder winches (one in each hull) are controlled simultaneously from a single rudder control signal. Similarly, the throttle servos (one in each hull) are controlled simultaneously.

Appendix B

Wave buoy analysis

B.1 Calibration of the buoy

Prior to the construction of the buoy some theoretical responses were investigated for a number of possible buoy geometries, seeking a configuration that would have a flat, unit response operator in both pitch and heave over the range of wave frequencies of interest. The ring configuration appeared to satisfy this requirement. It should be pointed out, however, that neither the fluxgate compass nor the umbilical cable was modelled in the theoretical calculations.

The buoy as finally constructed was calibrated in the Lamont tank at the University of Southampton, moored in its intended orientation to the dominant wave direction (along the tank centreline in this case) and also at a heading of 90 degrees to this direction. The first orientation provided heave and pitch calibration data and the second provided additional roll calibration data. Because of the restricted water depth in the towing tank and also its short length, the maximum wavelength that could sensibly be generated was only 5m (corresponding to a wave frequency of 0.55 hz). The shortest wavelength was 1.5m, or about twice the outer diameter of the buoy (corresponding to a wave frequency of 1.1 hz).

Measured catamaran model responses indicate the desirability of measuring wave data for wavelengths up to about 4 times model length, or about 20m (corresponding to a wave frequency of 0.3 hz). To date it has not been possible to calibrate the buoy in a facility permitting the generation of such waves. However, the buoy heave response operator clearly tends towards unity in long waves and this is readily apparent in the wave lengths actually tested.

Table 54 gives transfer functions for buoy responses in regular waves, based on RMS values of buoy accelerations, as tested in the Lamont tank. These results are shown graphically

in Figures 159 to 161. The heave response of the buoy is more or less as expected, being a flat response at a few percent above wave amplitude at low frequencies and falling off at frequencies above 1.0 hz. The roll and pitch responses appear to be quite large at low frequencies and to fall to values comparable with wave slope as frequency increases. This was not expected from the preliminary theoretical studies and seems to indicate larger rotary motions than were apparent from visual observation. However, the indicated pitch and roll responses seem qualitatively to match measurements made in open water in irregular waves. At present there is no obvious explanation for these calibration characteristics.

Qualitatively the roll and pitch results are similar. If the pitch transfer function results are shifted by 0.1 hz to lower frequencies the ratio of roll transfer function to pitch transfer function is reasonably constant over the range of frequencies tested. The roll T.F. being, on average, about 90% of the pitch T.F. This is shown in Figure 162. The calibration analysis assumed that the accelerometers were placed exactly at 120 degree intervals round the buoy. In fact measurement of the actual positions of the accelerometers shows the precise locations to differ slightly from this requirement in such a way as to reduce the roll signal and increase the pitch signal from the buoy. The true roll and pitch responses could in fact be equal or nearly so. This possibility is made use of in estimating the directional properties of a wave spectrum.

Ideally, it would be desirable to have phase information for the buoy motions relative to the wave passage. Unfortunately the calibration data was not of sufficiently good quality to allow the estimation of phase.

B.2 Analysis of buoy data from tests in open water

The elevation of the sea surface can be represented by an equation of the form:

$$\eta = \sum_n \sum_m \alpha_{n,m} \left[k_n x \cos\theta_m + k_n y \sin\theta_m - \omega_n t + \phi_{n,m} \right] \tag{53}$$

where:

ω_n = Component wave frequency (rad/s)
K_n = Component wave number (1/m)
θ_m = Component wave direction
α_{nm} = Component wave amplitude (m)
$\phi_{n,m}$ = Random component phase angle (rad)

In this equation the x-axis is along the reference wave direction $\theta_m = 0$, which will be taken to be the mean direction of the buoy longitudinal axis.

The directional spectral density for the wave elevation, $S(\omega_n, \theta_m)$, can be defined in terms of the component wave amplitudes by the equation:

$$S(\omega_n, \theta_m)\delta\theta_m\delta\omega_n = 1/2(\alpha_{n,m})^2 \tag{54}$$

Because the wave buoy provides rather limited information about the sea surface, in particular because the buoy measures data at only one point in space, the directional spectrum will be simplified to the form:

$$S(\omega_n, \theta_m) = S(\omega_n).D_n(\theta_m - \mu_n) \tag{55}$$

Here $D_n(\theta_m - \mu_n)$ is a spreading function assumed to be symmetric about a given mean wave direction and having the property that

$$\int_{-\pi/2}^{\pi/2} D_n(\theta)d\theta = 1.0 \tag{56}$$

The choice of spreading function is somewhat arbitrary. A convenient and common choice is to use the form given in Equation 57:

$$D(\theta') = a\cos^{2p}(\theta') : \frac{\pi}{2} < \theta' < \frac{\pi}{2} \tag{57}$$

The objective of the buoy analysis procedure is to determine $S(\omega_n)$, μ_n and $D_n(\theta)$ for each wave frequency present in the spectrum. This is accomplished by examining the auto- and cross-correlations of wave elevation and the wave slopes along the reference wave direction and across it. The wave elevation and slopes are determined from the buoy heave, pitch and roll responses via the buoy calibrations. The auto- and cross- correlations are determined from fast Fourier transforms of the time histories of the buoy motions. The details of the identification of wave spectral information are set out in A.3.

Because of changes of buoy heading (due to yaw effects), the instantaneous accelerometer records do not directly give pitch and roll data about the reference buoy direction. It is necessary to convert the acceleration data into vertical displacements at the accelerometers and subsequently, by a suitable co-ordinate rotation allowing for the instantaneous buoy

heading, to compute the buoy pitch and roll about the reference axes. This process is detailed in Section A.4.

The use of a fluxgate compass to monitor buoy heading is not ideal. The output voltage from the compass is somewhat unsteady, does not react correctly to rapid changes of heading and is sensitive to buoy motions (particularly pitch and roll). In order to obtain a useable output from the compass, the raw signal was heavily smoothed digitally by performing an FFT and retaining only those frequency components below that of the longest wave of interest from the viewpoint of model motions. The inversion of the truncated FFT yields a slowly varying yaw motion similar to that observed visually, as shown in Figure 169.

In converting accelerometer data into vertical displacements the method adopted is to perform an FFT of the accelerometer data, to remove any slow drift by deleting frequency components below the minimum frequency of interest from the point of view of catamaran model responses, to remove high frequency components associated with signal noise and to divide the remaining components by frequency squared. Predicted vertical displacements were found by inverting the truncated FFT. If the low frequency components are not removed the buoy can appear to be displaced several meters from the mean sea level. Once they are removed the buoy appears to oscillate, correctly, about a zero mean level.

Analysis of wave buoy data has been carried out in three different ways:

a) Buoy accelerometer data was used directly to calculate the power spectral density of buoy heave acceleration as a route to estimating $S(\omega_n)$ by itself.

b) Smoothed time series data of accelerometer displacements and compass heading, as outlined above, were converted to time series data for buoy heave, pitch and roll referred to the compass zero direction, as set out in Section A.4. The FFT of auto- and cross-correlations of the motions required for the estimation of wave spectral density, mean wave direction and spreading function (as set out in A.3.) were found from these time series.

c) An analysis using the mean value of compass heading as a constant heading angle replaced the co-ordinate transformation on a point by point basis of method b). In this case, since the effects of yaw rate and yaw acceleration are suppressed, the coefficients of the auto- and cross-correlations can be obtained directly from the accelerometer acceleration data without the need to construct time series of accelerometer displacements.

The analysis procedures outlined above can be carried out using the mathematical routines available within the DASYLab software used for all data acquisition purposes.

B.3 Measurements of wave spectra

Figures 163 to 172 show a sample of a wave spectral estimates from data obtained in Southampton Water. This particular set of data has been used as illustration of each of the analysis methods mentioned in the previous section of this report.

B.3.1 Frequency spectra from power spectral density of acceleration data (method (a))

Figures 163 and 164 shows the result of estimating the power spectral density of the buoy vertical acceleration and its subsequent transformation to a displacement spectral density (method (a) of the previous section). For comparison purposes, a standard ITTC two parameter wave spectrum has been superimposed on both spectral density distributions. The parameters for the ITTC spectrum were chosen to match the zero crossing period and significant height of the measured spectrum. In comparison to the ITTC spectrum, the measured amplitude spectrum lacks the energy peak at the modal frequency and is substantially flat up to 0.5 hz. Beyond this frequency there is slightly more energy than expected from the ITTC spectrum. This characteristic of the amplitude spectrum is less evident in the acceleration spectrum, which seems to follow fairly well the form of the ITTC spectrum. It should be born in mind that it is the acceleration spectrum that is derived directly from the buoy measurements and that conversion to the amplitude spectrum involves division by ω^2. At the low frequencies there is only a small acceleration to measure and scatter in the experiment data can easily dominate the estimated amplitude spectrum. With this in mind the measured wave spectra look very plausible. It should be noted that the buoy acceleration spectrum and the wave slope spectrum have similar forms.

For the record, the wave spectra have been derived from a record of 2048 points digitised at a sample rate of 10 hz. In order to smooth the data, the calculated power spectral components were aggregated into frequency bands of 0.05 hz each containing the sum of approximately 10 components.

B.3.2 The estimation of spectral directional properties (methods (b) and (c))

Attempts to obtain further details of the wave, including directional properties, have been based on FFT of the of the auto- and cross-correlations of buoy heave, pitch and roll signals. For the wave record used in this report the auto-correlations are shown in Figures 165 to 167. The cross-correlations are complex and have not been plotted.

Frequency Spectra estimated by analysis methods (b) and (c), from the auto-correlation of buoy heave via Equation 60, produced results identical to those shown in Figures 163 and 164 based on the power spectrum of heave acceleration.

Satisfactory identification of the mean wave direction and the directional spreading function from Equations 58 and 59 depend on the phase relations between heave, pitch and roll. Identification of these relations from buoy calibration data has proved unobtainable and reliance had to be placed on the assumption that wave slope/pitch and wave slope/roll phase relationships were likely to be the same.

The cross-correlations of pitch/heave and roll/heave are given by Equations 58 and 59 respectively:

$$A_{1,0,n} = \frac{\mathrm{i}}{2} P(\omega_n)\overline{H(\omega_n)} k_n S(\omega_n) \cos\mu_n \int_{-\pi}^{\pi} D_n(\theta') cos\theta' d\theta' \delta\omega_n \tag{58}$$

and

$$A_{2,0,n} = \frac{\mathrm{i}}{2} R(\omega_n)\overline{H(\omega_n)} k_n S(\omega_n) \sin\mu_n \int_{-\pi}^{\pi} D_n(\theta') \cos\theta' d\theta' \delta\omega_n \tag{59}$$

Dividing Equation 59 by Equation 58 gives

$$\frac{A_{2,0,n}}{A_{1,0,n}} = \frac{R(\omega_n)}{P(\omega_n)} \cdot \tan(\mu_n)$$

Since $R(\omega_n)$ and $P(\omega_n)$ are complex transfer functions for roll and pitch, respectively, the result of this division is complex and the argument is the phase difference between pitch and roll. Figure 168 shows this phase difference as a function of component wave frequency. Up to about 1.0 hz the difference is small (up to about 10 degrees), above 1.0 hz the difference becomes rather erratic. The smallness of this phase difference justifies the use of a working assumption that wave slope/pitch and wave slope/roll responses have the same phase.

Assuming, further, that the amplitudes of $R(\omega_n)$ and $P(\omega_n)$ should be identical, $\tan(\mu_n)$ can be estimated from the modulus of $A_{2,0,n}/A_{1,0,n}$. Figure 169 shows values of μ_n estimated by this method. For the particular wave data analysed in this report the mean wave direction appears to be between 50 and 70 degrees to the buoy axis for component waves up to 1.0 hz and to vary erratically above that frequency. Visual observation at the time indicated a mean wave direction close to the buoy axis. A 60 degree error in estimation of wave heading could arise if the accelerometer channels had been miss-identified when recording the wave data. Efforts to investigate this possibility by cyclically interchanging the accelerometer data channels were not successful.

The auto-correlations for heave, pitch and roll are given by Equations 60 to 62 respectively:

$$A_{0,0,n} = \frac{1}{2} H(\omega_n)\overline{H(\omega_n)} S(\omega_n)\delta\omega_n \tag{60}$$

$$A_{1,1,n} = \frac{1}{4} P(\omega_n)\overline{P(\omega_n)} k_n^2 S(\omega_n)\left\{1 + \cos(2\mu_n)\int_{-\pi}^{\pi} D_n(\theta')\cos(2\theta')d\theta'\right\}\delta\omega_n \tag{61}$$

$$A_{2,2,n} = \frac{1}{4} R(\omega_n)\overline{R(\omega_n)} k_n^2 S(\omega_n)\left\{1 - \cos(2\mu_n)\int_{-\pi}^{\pi} D_n(\theta')\cos(2\theta')d\theta'\right\}\delta\omega_n \tag{62}$$

If it is assumed that $|H(\omega_n)|$ and that μ_n and the spreading function integrals $I_n = \int_{-\pi}^{\pi} D_n(\theta')\cos(2\theta')d\theta'$ are constants, the values of $\sqrt{A_{1,1,n}/k_n^2 A_{0,0,n}}$ and $\sqrt{A_{2,2,n}/k_n^2 A_{0,0,n}}$ are proportional to pitch and roll amplitude transfer functions. The similarity between these quantities and the buoy calibration data is shown in Figures 170 and 171. Figure 170 compares $\sqrt{A_{1,1,n}/k_n^2 A_{0,0,n}}$ with the pitch calibration data including the raw calibration data and smoothed calibration data frequency shifted by 0.1 hz to a lower frequency range. Figure 171 compares $\sqrt{A_{2,2,n}/k_n^2 A_{0,0,n}}$ with the raw roll calibration data. Qualitatively the comparison is quite good. It serves to show that the buoy calibration data for pitch and roll, although varying with frequency in a totally unexpected way, is probably correct.

The final step in the analysis of directional properties is to take the estimate of μ_n and to estimate the value of the spreading function integral I_n from Equations 61 and 62. the result is shown in Figure 172. According to A.3., a spreading function of the form $D(\theta') = acos^{2p}(\theta')$ leads to the conclusion that $I_n = \frac{p}{p+1}$. From this result I_n has a value 0.5 for p=1 and increases towards 1.0 as p becomes larger, or as the wave system becomes unidirectional. In Figure 172 I_n is approximately 1.0 at low frequencies, but above 1.0 hz the values erratic and not very plausible. On the face of it, this suggests a long crested wave system. However, this conflicts with visual impressions at the time of recording the wave data. It is possible that, although each wave frequency is long crested, individual frequencies vary in direction (since μ_n varies) and that this produced the short crested appearance of the wave system. This interpretation is not totally convincing. The analysis presented here assumed that the transfer functions for buoy roll and pitch have the same amplitude. Attempts to improve results by assuming a ratio of roll response to pitch response less than 1.0 did not significantly change the result. Neither did the use of a mean value of μ_n for all frequencies, nor did the reanalysis of the data using a fixed mean buoy heading rather than allowing for the modulation due to buoy yaw motion.

As noted earlier for the wave spectra, the FFT's of the auto- and cross-correlation functions have been derived from a record of 2048 points digitised at a sample rate of 10 hz. In order to

smooth the data, the calculated power spectral components were aggregated into frequency bands of 0.05 hz each containing the sum of approximately 10 components.

B.4 Estimation of buoy motions relative to datum directions based on compass zero heading

z1, z2, z3 Accelerometer vertical displacements

x, y Reference axes for wave buoy defining the roll and pitch axes

ψ Wave buoy yaw angle from compass zero heading

r Radius of accelerometers from buoy centre

In terms of the heave displacement at the centre of the buoy (z), the roll angle about the x axis (ϕ) and the pitch angle about the y axis (θ) , the vertical displacements of the accelerometers are given by:

$$z_1 = z - r\theta\cos\psi + r\phi\sin\psi \tag{63}$$

$$z_2 = z - r\theta\cos(\psi + 120) + r\phi\sin(\psi + 120) \tag{64}$$

and

$$z_3 = z - r\theta\cos(\psi - 120) + r\phi\sin(\psi - 120) \tag{65}$$

From these equations :

$z_2 + z_3 = 2z + r\theta\cos\psi - r\phi\sin\psi$

and

$z_2 - z_3 = \sqrt{3}r\theta\cos\psi + \sqrt{3}r\phi\sin\psi$

It follows that the buoy attitude is given by:

Heave displacement

$$z = (z_1 + z_2 + z_3)/3 \tag{66}$$

Roll displacement

$$\phi = B\cos\psi + A\sin\psi \tag{67}$$

and Pitch displacement

$$\theta = B\sin\psi - A\cos\psi \tag{68}$$

where $A = \frac{[2z_1-(z_2+z_3)]}{3r}$ and $B = \frac{(z_2-z_3}{\sqrt{3}r}$ and Equation (A1.1) can be differentiated to give

$$\begin{aligned} \ddot{z_1} &= \ddot{z} - r\ddot{\theta}\cos\psi + \left\{2r\dot{\theta}\dot{\psi}\sin\psi + r\theta\ddot{\psi}\sin\psi + r\theta(\dot{\psi})^2\cos\psi\right\} \\ &+ r\ddot{\phi}\sin\psi + \left\{2r\dot{\phi}\dot{\psi}\cos\psi + r\phi\ddot{\psi}\cos\psi - r\phi(\dot{psi})^2\sin\psi\right\} \end{aligned} \tag{69}$$

The terms in brackets {} represent the effects of yaw rate and yaw acceleration on accelerometer acceleration data. If the yaw rate $\dot{\psi}$ and yaw acceleration $\ddot{\psi}$ are sufficiently small, these terms may be neglected. In this case:

$$\ddot{z_1} = \ddot{z} - r\ddot{\theta}\cos\psi + r\ddot{\phi}\sin\psi \tag{70}$$

Similar equations can be found for $\ddot{z_2}$ and $\ddot{z_3}$. It follows that:

$$\ddot{z} = (\ddot{z_1} + \ddot{z_2} + \ddot{z_3})/3 \tag{71}$$

$$\ddot{\phi} = \ddot{B}\cos\psi + \ddot{A}\sin\psi \tag{72}$$

and

$$\ddot{\theta} = \ddot{B}\sin\psi - \ddot{A}\cos\psi \tag{73}$$

where $\ddot{A}$ and $\ddot{B}$ follow directly from the earlier definitions of A and B.

This makes it possible to estimate buoy heave, pitch and roll data directly from accelerometer acceleration data without the need to estimate accelerometer displacement data first.

B.5 Summary

A wave buoy has been built and calibrated in heave, pitch and roll over a limited range of frequencies. The heave transfer function is close to unity at low frequencies and falls off at frequencies above 1.0 Hz. The pitch and roll calibrations show unexpectedly high output at low frequencies in a manner similar to the output of pitch and roll in random waves in open

water. Clearly the transfer functions for pitch and roll motions relative to wave slope must approach unity as wave frequency approaches zero. The failure of the buoy output to behave in this manner requires further investigation.

One dimensional frequency spectra for the measured waves derived from records taken over a 200 second period proved to be satisfactory. The estimated spectra compared well with standard ITTC two parameter spectra and gave significant wave heights in line with visual estimates made during measurement.

Estimates of mean wave direction and directional spread have been made based on FFT of auto- and cross-correlations of wave buoy heave, pitch and roll output. These estimates rely on assumptions regarding the phase relationships between buoy pitch and roll and the assumption of unity heave response. Results are encouraging but not yet satisfactory and further work is needed in this area.

Appendix C

The design of a vertical planar motion mechanism

C.1 Background

The first Planar Motion Mechanism was developed in the USA by Gertler and Goodman in 1960, as a means of measuring the hydrodynamic forces and derivatives involved in ship motions. The first PMMs were the vertical type designed to test submarine models. Both vertical and horizontal manoeuvres were carried out. The horizontal manoeuvres by turning the model on its side. The earlier PMMs were mechanically driven and only produced sinusoidal motions.

Considerable work has been done on the horizontal motions of the "Mariner" hull form at Delft University, using a horizontal planar motion mechanism [58].

The Department has a horizontal PMM. It has computer controlled motors which will allow both sinusoidal and non-sinusoidal motions to be produced. These motors allow tests to be carried out at a wide range of frequencies. This HPMM has been used to validate manoeuvring models for slow speed monohulls such as the "Mariner". A vertical PMM is also currently under development in the Department of Ship Science.

C.2 Specifications

A vertical planar motion mechanism [VPMM] is used to measure the hydrodynamic derivatives of surface ship models in order to determine their seakeeping and manoeuvring characteristics.

The performance requirements of the VPMM were defined as follows:

1. The device is to be capable of carrying out experiments in pure heave, pure pitch and pure roll modes and in any combination thereof.

2. Software is to be designed or adapted to control the mechanism and analyse experimental results from a PC.

3. The mechanism must be suitable for use with conventional ship models, yachts and high-speed catamarans.

4. Motions must be performed to amplitudes large enough to induce hydrodynamic non-linearity in pitch and heave.

5. The mechanism should be capable of oscillating the model about a prescribed mean heel angle.

6. Target specifications for the VPMM are:

Model lengths	1.5 - 2.5 m
Model displacement mass	10 - 75 kg
Model support separation	0.6 - 1.0 m
Motion frequencies	0 - 3.0 Hz
Heave motion maximum	0 - 100mm
Pitch angle maximum	7.5°
Roll amplitude	0 - 15°

C.3 Design requirements

C.3.1 Components

The original design was carried out by a group of M.Eng. students [59] when it was decided that the V.P.M.M. should measure two force components and one moment (heave/pitch, drag and roll). It was later decided that it should measure three force components and one moment. This additional force was the sideforce component on the model for use when testing yacht models or when rolling the model.

C.3.2 Forces

The magnitudes of the forces were determined in the original report using the Wolfson Unit's Ship Motions software. An NPL Round Bilge (NPL-RB) hullform and a General Purpose Cargo Carrier were used to determine suitable forces these are given in Table 55.

When these forces were reviewed with high-speed catamarans and yacht models in mind it was decided that the sideforce acting on the model would be required. Calculations in order to determine the maximum force that a model might experience were carried out and it was determined that a yacht hull with keel at a maximum heel angle of 20° would experience the greatest sideforce and that this force would be of the order of 100N. It was also decided that the drag force could be equal in magnitude to the sideforce.

C.3.3 Accuracy

The frame of the V.P.M.M. was built to give a maximum deflection of 0.1mm in order to transmit the required motion to the model. The dynamometers measure the deflection due to an imposed force. It was decided that the dynamometers should have a maximum deflection of 0.2mm in normal operation. The output signal from the measuring device (Linear Variable Differential Transformers) would determine the accuracy of the force measurements.

C.3.4 Dimensional constraints

The space into which the dynamometers have to fit is limited by the height above the water to the bottom of the frame. For the case of a conventional monohull form the height restriction is not a problem since the baseplate is mounted inside the model and could be mounted below the waterline. A problem arises when a catamaran model is to be fitted, because the baseplate has to be mounted on the crossbeams rather than inside the model.

The frame of the VPMM was designed to allow models of various sizes to be used. This is achieved by having the frame built in two modules separated by channel beams. The spacing of the two heave posts can increase from a minimum of 600mm to 1000mm. This means that the entire baseplate should fit into the 600mm space. Because the V.P.M.M. is built in two modules any length of channel section could be used to separate the modules allowing much larger models to be used. The only consideration then is the forces involved.

Appendix D

Design and calibration of the force blocks for a vertical planar motion mechanism

D.1 Force block arrangement

The ideal arrangement for the force blocks would be a stack as used in the PMM at the Admiralty Experimental Works, Haslar [60]. Here three identical force blocks were stacked horizontally at either end of the baseplate. This arrangement is only really possible if the forces being measured are similar in magnitude. In the case of the Southampton University VPMM, the vertical heave force was two and a half times greater than the drag or side force. So this arrangement was not possible.

As a result of the height restriction and the height of the baseplate when using catamaran models, it is not possible to stack the force block vertically as three separate blocks. This meant that some sort of nested arrangement would have to be used.

It was possible to separate the force blocks into two planes; the vertical plane and the horizontal plane. By combining the two horizontal forces a force block was designed which measures both drag and side forces.

D.2 Block dimensions and material

An iterative process using the space constraints as a maximum determined the dimensions of the force blocks. The forces and the limiting deflection of 0.2mm determined the dimensions of the flexures, Table 56. The material selected for the force blocks was Aluminium alloy

and it was decided that the blocks should be machined from a solid block instead of being fabricated.

The final dimensions are:

Heave block: Block = 72.0mm x 63.0mm x 40.0mm Flexures = 47.0mm x 10.0mm x 3.5mm

Drag/sway block: Block = 60.5mm x 63.0mm x 63.0mm Flexures = 42.0mm x 3.25mm x 3.25mm

The general arrangement of the baseplate and the dynamometers are shown in Figures 173 and 174. The scale drawings of the heave and combined drag/sideforce dynamometers are shown in Figures 175 and 176.

D.3 Force measurement

The forces on the model are determined by either measuring the deflection of the force block dynamometers or the strain in the four flexures. The deflection is measured using linear variable differential transformers [LVDT's]. These devices are mounted as close to the centre of the force block to reduce the effect of moments on the reading. The strain in the flexures is measured by siting foil strain gauges on the flexures.

The dimensions of the flexures determine the strain levels or the amount of deflection. For accurate measurement of strain a maximum of $1000\mu\epsilon$ is required with acceptable levels greater than $700\mu\epsilon$. The strain levels in the flexure are calculated using Equation 74. The maximum deflection of the force blocks was decided to be 0.2mm in order not to alter the imposed motion of the model. The deflection of the force blocks was calculated using Equation 75.

$$\text{strain} = \frac{Fl}{2E(I/Y)} \tag{74}$$

$$\text{deflection} = \frac{Fl^3}{12EI} \tag{75}$$

where: F is the force applied to each flexure in [N],
l is the length of the flexure in [m],
E is the Young's Modulus in [N m^{-2}],
$I/Y = \frac{bt^2}{6}$, where: t is the thickness and b is the breadth of the flexure in [m].

LVDT's operate by providing a primary winding with an a.c. excitation voltage, typically of 5V RMS at 5KHz. Two secondary windings are connected so that their combined output

represents the difference in the voltage induced into them. With the armature in the central position, the output is zero. Movement of the armature from this position produces an output which is proportional in phase and magnitude to the armature displacement.

D.4 Strain gauges or LVDT'S

The decision as to which measuring device to use was dependent on the following:

- Dimensions of flexures
- accuracy
- repeatability

The dimensions of the flexures were important because it would be difficult to mount the strain gauges on square or narrow flexures. The accuracy and repeatability of the measuring device was also important as this determined that accuracy of the whole system, especially at high frequencies.

It was decided to use L.V.D.T.s to measure the deflection of the force blocks as they provided better repeatability and the siting of the strain gauges might be difficult on the square flexures.

D.4.1 Ac or Dc energised LVDT'S

The type of L.V.D.T. to be used needed to be considered. The Department has had some problems with the a.c. L.V.D.T.s used on the dynamometer in the Lamont Test Tank. The problem being that of the slight difference in the oscillating frequencies used to energise the L.V.D.T.s causing cross talk resulting in the L.V.D.T.s oscillating. This could partly be due to the length of cable to the l.v.d.ts and the cable movement as the carriage moves down the tank.

One possibility would be to use D.C. energised L.V.D.T.s, where the supply voltage is d.c. and the L.V.D.T. has a built in modulator/demodulator.

It was decided that the space limitations on the force blocks might make the d.c.-L.V.D.T.s a problem, as the d.c. type are considerably larger than the a.c. type. The manufacturer of the L.V.D.T.s [R.D.P. Electronics] have said that there should be no problems using a.c energised L.V.D.T.s as the cable is screened and this will eliminate cross talk when several cables are run next to each other. Also, the short cable length, 3 metres, required for use on the Southampton Institute carriage would not cause a problem.

D.5 Instrumentation

The L.V.D.T.s have to be provided with an excitation voltage, which is a.c. and sinusoidal and the a.c. sinusoidal voltage output has to be conditioned. The conditioning module compares the phase and magnitude of the output voltage with the phase and magnitude of the input voltage. The output from the conditioning module is then amplified and sent to the computer through an Analogue to Digital board, (A to D).

There are two methods of achieving this one is to have individual conditioning units for each L.V.D.T. and then put the output of these in to the A to D board in the computer. The other method is to have a combined conditioning/excitation module and A to D card and have the whole system inside the computer.

There are advantages and disadvantages to both systems. The main advantage of the Combined system is that it can be software controlled.

D.6 Position of LVDT'S

In order that the L.V.D.T. measures the displacement of the flexures as accurately as possible it is important to mount the sensor of the L.V.D.T. as close to the geometric centre of the four flexures. Unfortunately for both the drag/sway block and the heave block it was not possible to position the sensor at the exact centre of the block.

The position of the sensors for the drag/sway block is vertically at the centre of the block but because both the drag and the sway sensor read relative to the same central pillar they could not be positioned on the horizontal centreline.

In order to reduce the amount of the L.V.D.T.'s body exposed below the heave block it was necessary to move the position of the sensor above the vertical centre of the block. The sensor is positioned on the horizontal centre of the block.

D.7 Calibration

The two pairs of dynamometers, (two heave and two combined drag/sideforce), were calibrated individually. Each dynamometer was bolted to an aluminium plate, which was clamped to a heavy calibration frame. A steel wire was attached to the dynamometer, running over a pulley to a weight carrier. The pulley could be adjusted vertically to ensure that the wire was always parallel to the frame. The dynamometer was then incrementally load to its maximum design load and then unloaded to determine any hysteresis. A digital voltmeter was used to measure the conditioned output voltage from the l.v.d.t.s and a dial gauge was

used to measure the deflection of the flexures. The results for the four dynamometers show a linear relationship for voltage against mass and voltage against deflection. The results are shown in Figures 177 to 182. All four dynamometers achieved their designed deflection of 0.2mm for the full load.

D.8 Summary

The successful calibration of the force blocks has completed the hardware aspects of the V.P.M.M. .

Development of the controllers for the forced vertical motions is being carried out as a separated project. When this part of the work has been completed, the overall VPMM will be tested and commissioned.

TABLES

Type	Number		Growth	% of total fleet	
	1990	1995	%	1990	1995
Catamaran	312	500	60.3	34.4	41.9
Hovercraft	45	52	15.6	5.0	4.3
Hydrofoil	368	408	10.9	40.6	33.4
Monohull	118	165	39.8	13.0	13.7
SES	61	81	28.6	7.0	6.6
TOTAL	906	1206	32.6	100	100

Table 1: Fast ferry fleet growth by type 1990-1995, Shipping World and Shipbuilding 1996 [61]

L_{OA} [m]	Monohulls	%	Catamarans	%
< 20	12	5	22	7
20-30	95	37	48	15
30-40	84	33	149	46
40-50	22	9	49	15
50-60	15	6	5	2
60-80	6	2	26	8
80-100	9	4	17	5
> 100	12	5	6	2
Total	255	100	322	100

Table 2: Worldwide fleet compiled by Bertorello [62]

Motion	**Direction**	**Units**	**Positive Direction**
Surge	X	Metres	Forward
Sway	Y	Metres	To Starboard
Heave	Z	Metres	Down
Roll	X	Radians	Starboard Side Down
Pitch	Y	Radians	Bow Up
Yaw	Z	Radians	Bow to Starboard

Table 3: Motions and their positive directions in the body axis system

Attributes		
Seakeeping	Derived	Condensed
Motions	Motion Sickness	
	SM	Comfort
	MII	
Velocities	Power Increase/ Added Res.	Speed Loss/Power Increase
	Slamming	
Accelerations	Deck wetness	Availability
	Safety	
	Structural Loading	

Table 4: Seakeeping performance attributes

EFFECT	CRITERIA NOT TO BE EXCEEDED		COMMENTS
	Type of load	Value	
Level 1 Minor Effect Moderate degradation of safety	Maximum acceleration measured horizontally	0.20g	0.08g and $0.20g/s^3$: Elderly persons will keep balance when holding 0.15g and $0.20g/s$: Mean person will keep balance when holding 0.15g and $0.80g/s$: Sitting person will start holding
Level 2 Major Effect Significant degradation of safety	Maximum acceleration measured horizontally	0.35g	0.25g and $2.0g/s$: Maximum load for mean person keeping balance when holding 0.45g and $10g/s$: Mean person falls out of seat when not wearing seat belts
Level 3 Hazardous Effect Major degradation of safety	Collision design condition calculated. Maximum structural design load, based on vertical acceleration at centre of gravity		Risk of injury to passengers; safety emergency operation after collision. 1.0g: Degradation of passenger safety
Level 4 Catastrophic Effect			Loss of craft or/and fatalities

Table 5: Criteria not to be exceeded -HSC code [33]

Vert. Acc.	Lat. Acc.	Roll	Description
0.275 g			Simple light work. Most of the attention must be devoted to keeping balance. Tolerable only for short periods on high speed craft.
0.20 g	0.10 g	6.0 deg	Light manual work to be carried out by people adapted to ship motions. Not tolerable for long periods. Causes fatigue quickly.
0.15 g	0.07 g	4.0 deg	Heavy manual work, carried out on work ships.
0.10 g	0.04 g	3.0 deg	Intellectual work by people not so well adapted to ship motions. Long-term tolerable for the crew. Tolerable for half an hour exposure period for people unused to ship motions (ISO standard 2631/3)
0.05 g	0.03 g	2.5 deg	Passengers on a ferry. Tolerable for two hours exposure period for people unused to ship motions. Causes symptoms of motion sickness in approximately 10% of unacclimatized adults.
0.02 g	0.03 g	2.0 deg	Passengers on a cruise liner. threshold Older people. Close to lower below which vomiting is unlikely to take place.

Table 6: Human effectiveness limit values , Karppinen [63]

Vessel	Naval	Monohull	Gen Cargo	Cross-Channel
Source	Olson	Comstock	Aertssen	
RMS Roll [deg]	9.6	4.0	-	-
RMS Pitch [deg]	-	1.5	-	-
RMS Vert Acc g	-	0.2	0.9	1.0
RMS Lat Acc g	-	0.1	-	-
MSI	20% in 2hrs	-	-	-
Slam Acc g	0.2	-	0.2	0.4
slam freq	3/100	20/hr	4/100	5/100
Deck wetness freq	30/hr	30/hr	5/100	-

Table 7: Suggested typical limiting criteria I, Lewis [64]

Vessel	Swath	Planing Craft	Hydrofoil	SES
Source	Olson	Allen et al	Stark	Mandel
RMS Roll [deg]	9.6	-	1.25	1.5
RMS Pitch [deg]	-	-	1.5	1.5
RMS Vert Acc g	-	-	0.11	0.1
RMS Lat Acc g	-	-	0.06	0.1
MSI	20% in 2hrs	-	10% in 4hrs	10% in 2hrs
Slam Acc g	-	4*	0.5*	0.6*
Deck wetness freq	-	-	-	-

Table 8: Suggested typical limiting criteria II, Lewis [64]

Location	Criterion	Duration	Significant Value
F.P.	Vertical acceleration	Continuous	0.55 g
Bridge	Lateral acceleration	Continuous	0.20 g
	Vertical acceleration		0.40 g
	GLFE		0.28 g
	MSI		20%
	SMI		5
Helicopter	Roll amplitude	Limited periods	5.0 deg
Deck	Pitch amplitude		3.0 deg
	Vertical velocity		2.0 m/s
Global	Roll amplitude		8.0 deg
Vessel	Pitch amplitude		3.0 deg
Motion	Occurrence of slams		20/hour
	Occurrence of deck wetness		30/hour

Table 9: Limiting criteria for the operability of a trimaran vessel, Chan et al. [42]

RESPONSE	MERCHANT SHIPS
Vertical acceleration at fwd perpendicular (rms)	0.275 g (L≤100m)
	0.05 g (L≥330m)*
Vertical acceleration at bridge (rms)	0.15 g
Lateral acceleration at bridge (rms)	0.12 g
Roll (rms)	6.0°
Slamming criteria (probability)	0.03 (L≤100m)
	0.01 (L≥330m)*

Table 10: NORDFORSK, 1987, comfort criteria concerning merchant ships, [65]

Application	**Performance Limitations**		
	Motion	**Limit**	**Location**
General	Roll	8°	CG
	Pitch	3°	CG
	Vertical Acceleration	0.4g	Bridge
	Lateral Acceleration	0.2g	Bridge
Specific Task	Motion Sickness Index (MSI)	20% of Crew	Task Location
	Motion Induced Interruption (MII)	1/min	Task Location
	Relative Wind	35 Kts	Flight Deck

Table 11: ABCD suggested typical limiting criteria for personnel performance [7]

Response	Mobility	Helicopter Operation
Roll [deg]	8	5
Pitch [deg]	3	2
Vertical Acceleration at CIC [g]	0.4	-
Vertical Vel. at Helo. Deck [m/s]	-	2
Deck Wetness [/hour]	30	-
Bow slamming [/hour]	20	-

Table 12: Selected responses and seakeeping criteria for high speed warships, Sariöz and Narli [66]

Criteria	Returning Passengers	Non-returning Passengers	Pass/Freight	Freight
Pitch [deg]	1.5	2.0	3	3
Roll [deg]	2	2.5	3	6-8
Mid a_z [g]	0.1	0.1	0.2	0.4
Fwd a_z [g]	0.2	0.2	0.4	0.6
Mid a_y [g]	0.1	0.1	0.2	0.2
Availability	90%	80%	60%	80%
MSI	10%	10-30%	20-40%	50%
MII $[min^{-1}]$	0.3	0.5	< 1	1

Table 13: Role specific limiting criteria values.

Item	Dimension
Length	60m
Breadth	3.7m
Depth	1.8m
Carriage Speed	4.2m/s

Table 14: SIHE: Tank Dimensions

Model	4b	5b	5s	6b
Length [m]	1.6	1.6	1.6	2.1
$\frac{L}{\nabla^{1/3}}$	7.4	8.5	8.5	9.5
L/B	9.0	11.0	12.8	13.1
B/T	2.0	2.0	2.0	2.0
C_B	0.397	0.397	0.537	0.397
C_P	0.693	0.693	0.633	0.693
C_M	0.565	0.565	0.848	0.565
WSA [m^2]	0.338	0.276	0.261	0.401
LCB [%]	-6.4	-6.4	-6.4	-6.4

Table 15: Hullform principal particulars (demi-hull)

Model	Fn	S/L	Regular Head Waves	Regular Oblique waves	Open Water	Theoretical Oblique Waves
4b	0.2 0.53	demi 0.2 0.4	•			•
5b	0.2 0.53 0.8	demi 0.2 0.4	•	•	•	•
5s	0.2 0.53 0.65, 0.8	demi 0.2 0.4	•	•	•	•
6b	0.2 0.53 0.8	demi 0.2 0.4	•			•

Table 16: Data base of models tested in the experimental and theoretical programmes.

	DESIGN		AS TESTED	
	5b	5s	5b	5s
L/B	11.0	12.8	11.0	12.8
B/T	2.0	2.0	1.9	1.9
$\frac{L}{\nabla^{1/3}}$	8.5	8.5	8.3	8.3
C_B	0.397	0.537	0.4	0.540
C_P	0.693	0.633	0.698	0.637
C_M	0.573	0.848	0.573	0.848
A/L^2	0.1078	0.1095	0.1131	0.1149
LCB[%x]	-6.4%	-6.4%	-6.4%	-6.4%

Table 17: Principal particulars of the two 4.5m models in the design and as tested condition

S/L	Pitch	Yaw	Roll
0.2	0.26L	0.28L	0.11L
0.4	0.26L	0.32L	0.20L

Table 18: Radii of inertia for both 4.5m Models 5b and 5s (catamaran configurations)

Heading		178	160	124	121	88	19
Roll	deg	1.114	0.803	1.499	1.841	1.9265	1.569
Pitch	deg	2.040	1.264	1.598	1.684	2.026	2.172
Acc_p	g	0.023	0.011	0.020	0.026	0.024	0.012
Acc_s	g	0.614	0.724	0.523	0.425	0.629	0.641

Table 19: RMS Motions and Accelerations for Model 5b, $S/L = 0.4$, approx. Sea State: $T_0 = 2.6s$, $H_{1/3} = 0.2m$

Heading		160	145	96	41	37
Roll	deg	1.7473	0.9187	1.827	1.6089	0.6275
Pitch	deg	2.4915	1.3565	1.972	1.5824	1.183
Acc_p	g	0.1436	0.0923	0.123	0.0854	0.050
Acc_s	g	0.6048	0.6041	0.634	0.6438	0.575

Table 20: RMS Motions and Accelerations for Model 5b, $S/L = 0.2$, approx. sea state: $T_0 = 2.6s$, $H - 1/3 = 0.2m$

μ [deg]	90	120	150	180	210	240	270		
μ [rad]	1.57	2.094	2.618	3.142	3.665	4.189	4.712		
$\cos^n$	$f(\mu)$							$\sum$	$\int$
2	0	0.16	0.48	0.64	0.48	0.16	0	1.91	1
4	0	0.05	0.48	0.85	0.48	0.05	0	1.91	1
6	0	0.02	0.43	1.02	0.43	0.02	0	1.91	1
8	0	0.00	0.37	1.16	0.37	0.00	0	1.91	1

Table 21: $\cos^n$ spreading function, for $d\mu = 0.524$ rad or 30°

$H_{1/3}$	Total	-	12	78	211	283	224	121	49	16	5	1000
	9-10	-	-	-	-	-	-	-	-	-	-	0
	8-9	-	-	-	-	-	1	-	-	-	-	1
	7-8	-	-	-	-	1	1	1	-	-	-	3
	6-7	-	-	-	1	2	2	1	1	-	-	6
	5-6	-	-	1	2	3	3	3	2	1	-	12
	4-5	-	-	1	8	21	26	19	9	3	1	88
	3-4	-	-	3	21	46	47	28	11	3	1	160
	2-3	-	-	11	49	82	66	31	10	3	1	252
	1-2	-	2	29	85	**93**	52	18	5	1	-	285
	0-1	1	9	34	43	25	8	2	-	-	-	121
		< 4	4-5	5-6	6-7	7-8	8-9	9-10	10-11	11-12	12-13	Total

$\overline{T}$ [s]

Table 22: Wave statistics for the English Channel in all seasons and all directions, Hogben et al. [56]

	M1	C1
Np	400	400
Nv	0	0
V [Knots]	33	33
$L/\nabla^{1/3}$	7.0	8.0
B/T	4.5	2.0
C_B	0.4	0.5
S/L	0	0.22
L [m]	39.9	37.0
B [m]	7.22	11.41
b [m]		3.27
T [m]	1.60	1.63
S [m]		3.27
$\triangle_1$ [Tonnes]	188	202
P_I [kW]	4600	5200

Table 23: Ship details for M1 and C1

$\overline{T}[s]$	$H_{1/3}[m]$	Non-availability	Added Resistance	Vomiting Incidence
4.9	1.5	27.12	3.56	14.94
6	1.5	45.05	5.38	20.05
7.1	1.5	48.62	5.24	21.11
8	1.5	49.85	4.40	20.77
Mean Values		42.66	4.64	19.22

Table 24: M1 in long-crested head seas, Fn=0.8

$\overline{T}[s]$	$H_{1/3}[m]$	Non-availability	Added Resistance	Vomiting Incidence
4.9	1.5	28.25	100.00	13.58
6	1.5	38.93	103.99	16.76
7.1	1.5	37.57	85.90	17.48
8	1.5	42.19	72.15	17.51
Mean Value		36.74	90.51	16.33

Table 25: C1 in long-crested head seas, Fn=0.8

μ [°]	Heave [m]	Heave Prob.	Pitch [deg]	Pitch Prob.	A_z lcg [g]	A_z lcg Prob.	A_z fwd [g]	A_z. fwd Prob.
180	0.37	0.00	0.14	0.00	0.12	26.93	0.21	16.42
165	0.36	0.00	0.14	0.00	0.12	26.66	0.21	16.18
150	0.35	0.00	0.13	0.00	0.12	24.45	0.20	14.37
135	0.33	0.00	0.12	0.00	0.11	20.14	0.19	11.00
120	0.30	0.00	0.10	0.00	0.10	14.21	0.17	6.80
105	0.26	0.00	0.07	0.00	0.09	7.82	0.15	2.99
90	0.22	0.00	0.05	0.00	0.07	2.79	0.13	0.72
75	0.26	0.00	0.07	0.00	0.09	7.82	0.15	2.99
60	0.30	0.00	0.10	0.00	0.10	14.21	0.17	6.80
45	0.32	0.00	0.11	0.00	0.11	17.32	0.18	8.94
30	0.34	0.00	0.12	0.00	0.12	22.54	0.20	12.85
15	0.36	0.00	0.14	0.00	0.12	25.83	0.21	15.49
0	0.07	0.00	0.03	0.00	0.02	0.00	0.04	0.00

Table 26: RMS values and probabilities of exceedance for monohull M1

μ [°]	Heave [m]	Heave Prob.	Pitch [deg]	Pitch Prob.	A_z lcg [g]	A_z lcg Prob.	A_z fwd [g]	A_z fwd Prob.
180	0.42	0.00	0.22	0.00	0.12	24.60	0.24	25.06
165	0.42	0.00	0.21	0.00	0.12	24.36	0.24	24.82
150	0.41	0.00	0.20	0.00	0.12	22.48	0.23	22.92
135	0.39	0.00	0.18	0.00	0.11	18.70	0.22	19.12
120	0.35	0.00	0.15	0.00	0.10	13.28	0.20	13.64
105	0.31	0.00	0.12	0.00	0.09	7.16	0.18	7.41
90	0.26	0.00	0.09	0.00	0.07	2.26	0.15	2.38
75	0.31	0.00	0.12	0.00	0.09	7.16	0.18	7.41
60	0.35	0.00	0.15	0.00	0.10	13.28	0.20	13.64
45	0.37	0.00	0.17	0.00	0.10	16.16	0.21	16.56
30	0.40	0.00	0.19	0.00	0.11	20.82	0.23	21.26
15	0.42	0.00	0.21	0.00	0.12	23.66	0.24	24.11
0	0.07	0.00	0.03	0.00	0.02	0.00	0.04	0.00

Table 27: RMS values and probabilities of exceedance for catamaran C1

μ	Non-availability	Vomiting Incidence
180	26.93	15.65
165	26.66	15.59
150	24.45	15.11
135	20.14	14.16
120	14.21	12.83
105	7.82	11.23
90	2.79	9.48
75	7.82	11.23
60	14.21	12.83
45	17.32	13.54
30	22.54	14.69
15	25.83	15.41
0	0.00	2.81
Mean Value	16.21	12.66

Table 28: M1 in short-crested oblique seas, Fn=0.8, $\overline{T} = 7.1s$, $H_{1/3} = 1.5m$

μ	Non-availability	Vomiting Incidence
180	25.06	14.70
165	24.82	14.65
150	22.92	14.24
135	19.12	13.44
120	13.64	12.25
105	7.41	10.72
90	2.38	8.94
75	7.41	10.72
60	13.64	12.25
45	16.56	12.89
30	21.26	13.89
15	24.11	14.50
0	0.00	2.29
Mean value	15.26	11.96

Table 29: C1 in short-crested oblique seas, Fn=0.8, $\overline{T} = 7.1s$, $H_{1/3} = 1.5m$

$\overline{T}[s]$	$H_{1/3}[m]$	Non-availability	Added Resistance	Vomiting Incidence
4.9	1.5	37.72	4.67	15.48
6	1.5	40.11	8.00	17.14
7.1	1.5	33.20	8.30	16.65
8	1.5	29.72	7.40	15.54
Mean Value		35.19	7.09	16.20

Table 30: M1 in long-crested head seas, Fn=0.5

$\overline{T}[s]$	$H_{1/3}[m]$	Non-availability	Added Resistance	Vomiting Incidence
4.9	1.5	42.62	45.47	15.92
6	1.5	40.69	55.34	17.73
7.1	1.5	44.10	52.57	18.39
8	1.5	48.76	46.93	18.19
Mean Value		44.04	50.08	17.56

Table 31: C1 in long-crested head seas, Fn=0.5

μ	Non-availability	Vomiting Incidence
180	14.95	12.67
165	14.73	12.62
150	13.00	12.23
135	9.81	11.47
120	5.92	10.39
105	2.49	9.09
90	0.56	7.67
75	2.49	9.09
60	5.92	10.39
45	7.89	10.96
30	11.55	11.89
15	14.07	12.48
0	0.00	2.27
Mean Value	7.95	10.25

Table 32: M1 in short-crested seas, Fn=0.5, $\overline{T} = 7.1s$, $H_{1/3} = 1.5m$

μ	Non-availability	Vomiting Incidence
180	31.09	15.39
165	30.84	15.34
150	28.83	14.92
135	24.74	14.08
120	18.60	12.83
105	11.11	11.22
90	4.26	9.36
75	11.11	11.22
60	18.60	12.83
45	21.91	13.50
30	27.05	14.55
15	30.09	15.18
0	0.00	2.40
Mean Value	19.86	12.52

Table 33: C1 in short-crested seas, Fn=0.5, $\overline{T} = 7.1s$, $H_{1/3} = 1.5m$

$H_{1/3}$	Total	7	75	234	314	225	103	35	9	2	-	1000
	9-10	-	-	-	-	1	1	-	-	-	-	2
	8-9	-	-	-	1	1	1	1	-	-	-	3
	7-8	-	-	-	1	2	2	1	-	-	-	6
	6-7	-	-	1	3	4	3	2	1	-	-	13
	5-6	-	-	2	7	9	7	3	1	-	-	29
	4-5	-	1	6	18	21	13	6	2	-	-	66
	3-4	-	2	17	42	42	23	8	2	-	-	136
	2-3	-	7	46	85	67	30	9	2	-	-	246
	1-2	1	22	91	**114**	64	21	5	1	-	-	319
	0-1	6	44	71	44	14	3	-	-	-	-	181
		< 4	4-5	5-6	6-7	7-8	8-9	9-10	10-11	11-12	12-13	Total

$\overline{T}$ [s]

Table 34: Wave statistics for the Irish Sea in all seasons and all directions, Hogben et al. [56]

	M2	C2
Np	650	650
Nv	150	150
V [Knots]	36	36
$L/\nabla^{1/3}$	8.5	8.0
B/T	6.0	2.2
C_B	0.35	0.5
S/L	0	0.24
L [m]	89.3	68.0
B [m]	14.9	22.7
b [m]		6.31
T [m]	2.49	2.87
S [m]		16.32
$\triangle_1$ [Tonnes]	1189	1264
P_I [kW]	22000	26000

Table 35: Ship details for M2 and C2

$\overline{T}[s]$	$H_{1/3}[m]$	Non-availability	Added Resistance	Vomiting Incidence
4.9	1.5	0.00	0.15	5.96
6	1.5	3.20	1.25	19.92
7.1	1.5	23.94	3.45	31.54
8	1.5	35.24	5.30	36.59
Mean Value		15.60	2.54	23.50

Table 36: M2 in long-crested head seas, Fn=0.8

$\overline{T}[s]$	$H_{1/3}[m]$	Non-availability	Added Resistance	Vomiting Incidence
4.9	1.5	0.02	6.02	10.60
6.0	1.5	15.48	18.89	24.71
7.1	1.5	33.92	25.55	32.86
8.0	1.5	38.71	25.20	35.07
Mean Value		22.03	18.92	25.81

Table 37: C2 in long-crested head seas, Fn=0.8

μ	Non-availability	Vomiting Incidence
180	2.59	19.73
165	2.52	19.65
150	1.98	19.04
135	1.16	17.85
120	0.44	16.17
105	0.08	14.15
90	0.00	11.94
75	0.08	14.15
60	0.44	16.17
45	0.76	17.06
30	1.58	18.51
15	2.31	19.42
0	0.00	3.54
Mean Value	1.07	15.95

Table 38: M2 in short-crested seas, Fn=0.68, $\overline{\mathrm{T}} = 7.1\mathrm{s}$, $\mathrm{H}_{1/3} = 1.5\mathrm{m}$

μ	Non-availability	Vomiting Incidence
180	12.54	23.71
165	12.36	23.63
150	10.97	22.99
135	8.36	21.69
120	5.03	19.76
105	2.02	17.29
90	0.37	14.43
75	2.02	17.29
60	5.03	19.76
45	6.73	20.80
30	9.80	22.42
15	11.83	23.39
0	0.00	3.69
Mean Value	6.70	19.30

Table 39: C2 in short-crested seas, Fn=0.8, $\overline{\mathrm{T}} = 7.1\mathrm{s}$, $\mathrm{H}_{1/3} = 1.5\mathrm{m}$

	C3	C4
Np	650	650
Nv	150	150
V [Knots]	36	36
$L/\nabla^{1/3}$	8.5	7.3
B/T	2.4	2.0
C_B	0.44	0.53
S/L	0.2	0.3
L [m]	72.4	62.2
B [m]	21.3	24.8
b [m]	6.8	6.13
T [m]	2.85	3.06
S [m]	14.48	18.66
$\triangle_1$ [Tonnes]	1266	1268
P_I [kW]	24800	27700

Table 40: Ship details for C3 and C4

$\overline{T}[s]$	$H_{1/3}[m]$	Non-availability	Added Resistance	Vomiting Incidence
4.9	1.5	0.34	2.00	14.49
6	1.5	30.04	9.03	33.32
7.1	1.5	48.82	17.82	43.88
8	1.5	54.32	22.36	47.02
Mean Value		33.38	12.80	34.68

Table 41: C3 in long-crested seas

$\overline{T}[s]$	$H_{1/3}[m]$	Non-availability	Added Resistance	Vomiting Incidence
4.9	1.5	1.22	3.00	16.79
6	1.5	32.17	7.45	34.88
7.1	1.5	48.14	9.27	43.90
8	1.5	51.63	9.07	45.61
Mean Value		33.29	7.20	35.30

Table 42: C4 in long-crested seas

$\overline{T}$	$H_{1/3}$	C3		C4	
$[s]$	$[m]$	Non-availability	VI	Non-availability	VI
180°					
4.9	1.5	0.10	9.30	9.24	21.69
6	1.5	19.56	27.38	49.50	41.17
7.1	1.5	48.65	44.74	58.27	47.97
8	1.5	59.30	53.07	58.03	48.47
Mean Value		31.90	33.62	43.76	39.83
150°					
4.9	1.5	2.30	14.84	7.76	19.83
6	1.5	36.05	35.24	42.95	37.19
7.1	1.5	57.70	49.78	54.42	45.59
8	1.5	63.04	55.16	55.32	47.09
Mean Value		39.77	38.75	40.11	37.43
120°					
4.9	1.5	35.50	24.69	4.46	15.71
6	1.5	54.85	35.33	17.43	23.62
7.1	1.5	57.12	38.96	27.34	30.26
8	1.5	54.64	39.38	35.89	35.74
Mean Value		50.53	34.59	21.28	26.33

Table 43: Ships C3 and C4 in long-crested oblique waves, Fn=0.65

μ	Non-availability	Vomiting Incidence
180	24.05	31.12
165	23.82	31.02
150	21.95	30.17
135	18.21	28.47
120	12.86	25.94
105	6.86	22.70
90	2.13	18.94
75	6.86	22.70
60	12.86	25.94
45	15.70	27.30
30	20.31	29.42
15	23.12	30.70
0	0.00	4.85
Mean Value	14.52	25.33

Table 44: C3 in short-crested seas, $\overline{T} = 7.1s$, $H_{1/3} = 1.5m$

μ	Non-availability	Vomiting Incidence
180	21.07	30.07
165	20.81	29.95
150	18.78	29.02
135	14.92	27.21
120	9.86	24.66
105	4.85	21.57
90	1.43	18.20
75	4.85	21.57
60	9.86	24.66
45	12.48	26.01
30	17.05	28.22
15	20.04	29.60
0	0.00	5.39
Mean Value	12.00	24.32

Table 45: C4 in short-crested seas, $\overline{T} = 7.1s$, $H_{1/3} = 1.5m$

μ	Non-availability	Vomiting Incidence
180	36.42	34.46
165	36.17	34.34
150	34.13	33.40
135	29.90	31.52
120	23.37	28.72
105	14.97	25.13
90	6.53	20.97
75	14.97	25.13
60	23.37	28.72
45	26.91	30.23
30	32.30	32.58
15	35.41	33.99
0	0.00	5.37
Mean Value	24.19	28.04

Table 46: C3 in short-crested seas with roll, Fn=0.65, $\overline{T} = 7.1$s, $H_{1/3} = 1.5$m

μ	Non-availability	Vomiting Incidence
180	12.10	24.36
165	11.90	24.26
150	10.35	23.51
135	7.58	22.04
120	4.32	19.97
105	1.65	17.47
90	0.31	14.75
75	1.65	17.47
60	4.32	19.97
45	5.94	21.07
30	9.08	22.86
15	11.31	23.98
0	0.00	4.37
Mean Value	6.19	19.70

Table 47: C4 in short-crested seas with roll, Fn=0.65, $\overline{T} = 7.1$s, $H_{1/3} = 1.5$m

$\overline{T}$	$H_{1/3}$	Non-availability	Added Resistance	Vomiting Incidence
4.9	1.5	0.00	2.00	14.49
6	1.5	0.82	9.03	33.32
7.1	1.5	5.68	17.82	43.88
8	1.5	8.70	22.36	47.02
Mean Value		3.80	12.80	34.68

Table 48: Catamaran C3 operating as a fast freight vessel in long-crested seas.

$\overline{T}$	$H_{1/3}$	Non-availability	Added Resistance	Vomiting Incidence
4.9	1.5	0.00	3.00	16.79
6	1.5	1.07	7.45	34.88
7.1	1.5	5.37	9.27	43.90
8	1.5	7.10	9.07	45.61
Mean Value		3.38	7.20	35.30

Table 49: Catamaran C4 operating as a fast freight vessel in long-crested seas.

	M2			M2-b			M2-c		
$\overline{T}$ $[s]$	AR	UnA	VI	AR	UnA	VI	AR	UnA	VI
4.9	0.15	0	5.94	-	0	8.71	0.22	0	5.67
6.0	1.25	3.20	19.92	-	15.87	27.51	1.49	3.74	18.65
7.1	3.45	23.94	31.54	-	52.39	46.78	3.13	21.72	29.23
8.0	5.30	35.24	36.59	-	66.30	57.40	3.88	29.37	33.56
Mean	2.54	15.60	23.50	-	43.29	35.10	2.18	13.71	21.78

Table 50: M2 hullform variations

	M1′	C1′
Np	400	400
Nv	0	0
V [Knots]	33	33
$L/\nabla^{1/3}$	7.75	8.98
B/T	4.5	2.0
C_B	0.3	0.42
S/L	0	0.22
L [m]	48.66	57.79
B [m]	8.81	17.38
b [m]	-	4.66
T [m]	1.96	2.33
$\triangle_1$ [Tonnes]	253	546.45
P_I [kW]	7254	13608

Table 51: Ship details for M1′ and C1′

	M1′		C1′	
$\overline{T}$ [s]	UnA	VI	UnA	VI
4.9	1.10	8.75	17.12	12.35
6.0	26.76	16.05	34.97	16.96
7.1	50.94	20.95	36.99	17.90
8.0	61.34	22.82	34.01	17.21
Mean	35.04	17.14	30.77	16.08

Table 52: M1′ and C1′ in long-crested head seas.

Ratio	Engine pulley diameter	Prop. shaft pulley diameter
1:2.5	80mm	200mm
1:1.695	118mm	200mm
1:1	200mm	200mm

Table 53: The available gear ratios for the 4.5m model.

freq Hz	heave TF	pitch TF	freq. Hz	roll TF
0.565	0.9132	3.728	0.391	7.712
0.599	0.866	2.663	0.469	3.645
0.625	1.155	3.277	0.547	2.325
0.667	1.017	2.213	0.625	1.625
0.676	0.986	2.075	0.703	1.163
0.719	1.041	1.631	0.780	0.747
0.833	1.026	1.160	0.859	1.160
0.909	1.006	1.153	0.938	1.153
0.990	0.962	1.135	1.016	1.135
1.110	0.866	0.950	1.094	0.950

Table 54: Buoy calibration data

Heave	250 N
Drag	100 N
Sideforce	100 N
Roll moment	13 Nm

Table 55: V.P.M.M. Forces

	E N/m^2	**P** N	**l** mm	**b** mm	**t** mm	**I/y**	**I** mm^4	**def.** mm	**strain** $\mu\epsilon$	**stress** MPa	$\mathbf{P_{crit}}$ N
Fx	68900	25	38	3.25	3.25	5.7	9.3	0.18	1205	83	4378
Fy	68900	25	38	3.25	3.25	5.7	9.3	0.18	1205	83	4378
Fz	68900	62.5	44	10	3.5	20.4	35.7	0.18	978	67	12550

Table 56: Force block flexure properties

FIGURES

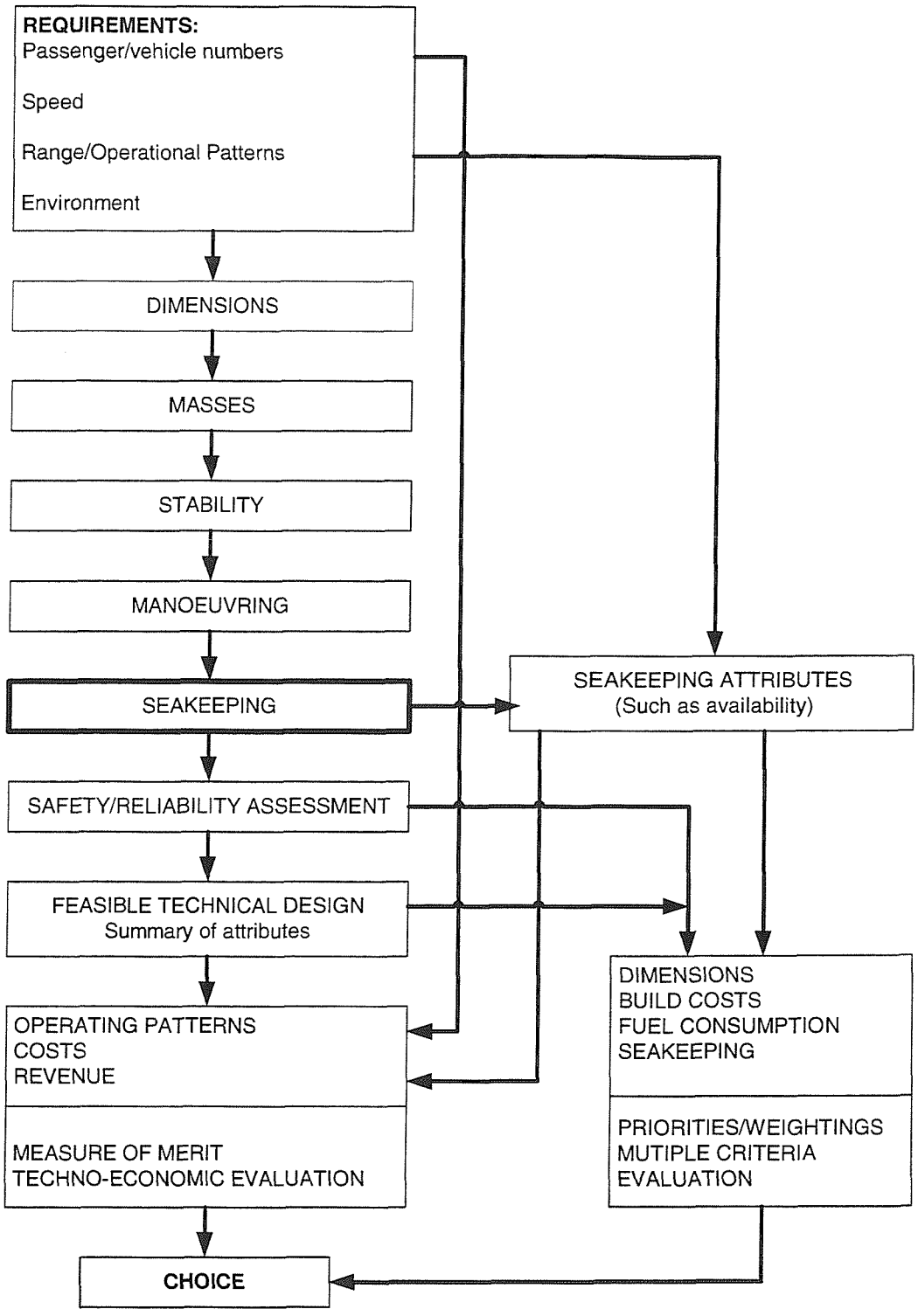

Figure 1: Conceptual Exploration of High Speed Ferry Types, Wright [13]

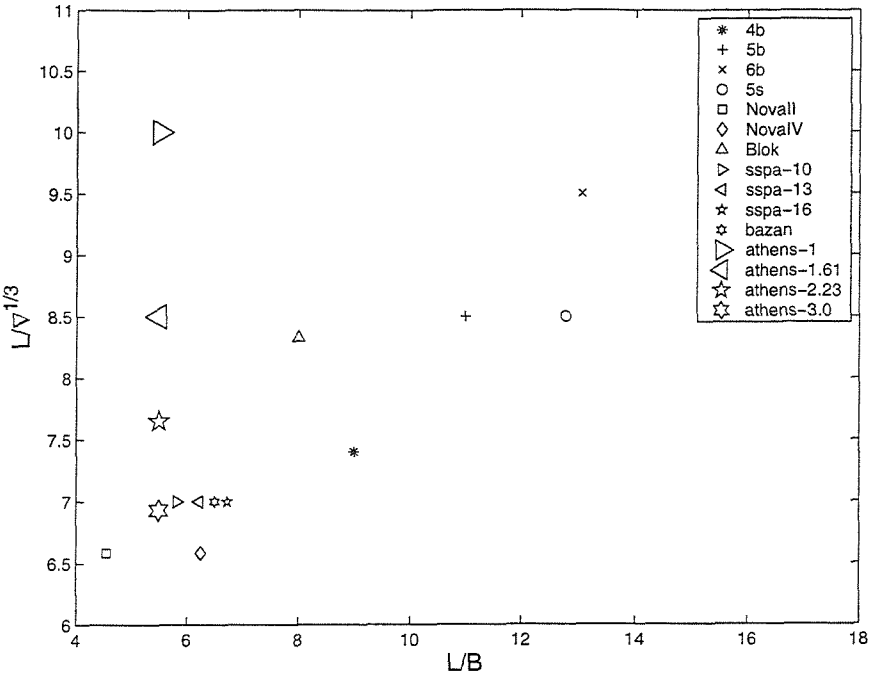

Figure 2: Extent of seakeeping data: Monohull L/B against $L/\nabla^{1/3}$

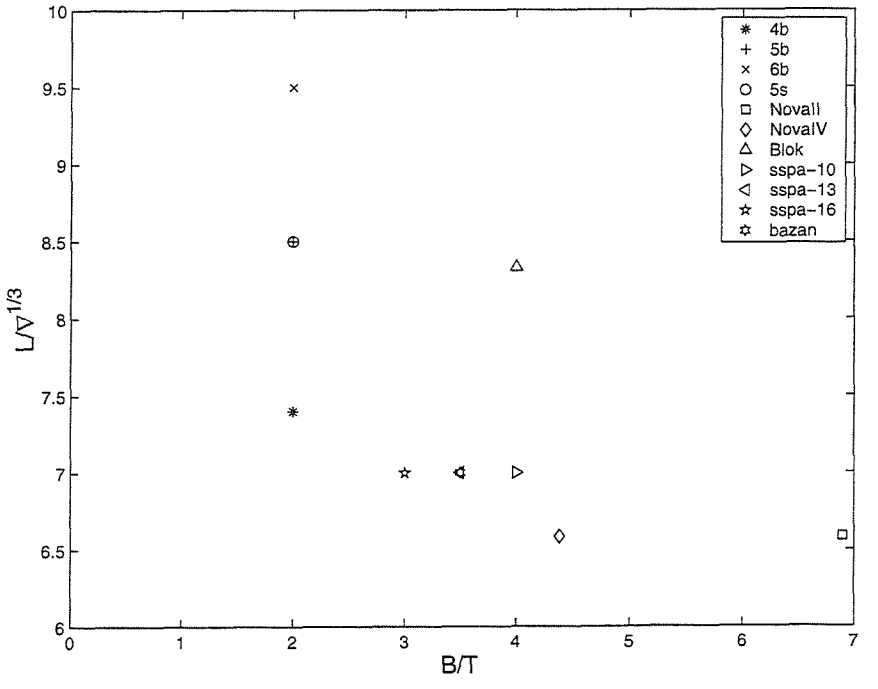

Figure 3: Extent of seakeeping data: Monohull B/T against $L/\nabla^{1/3}$

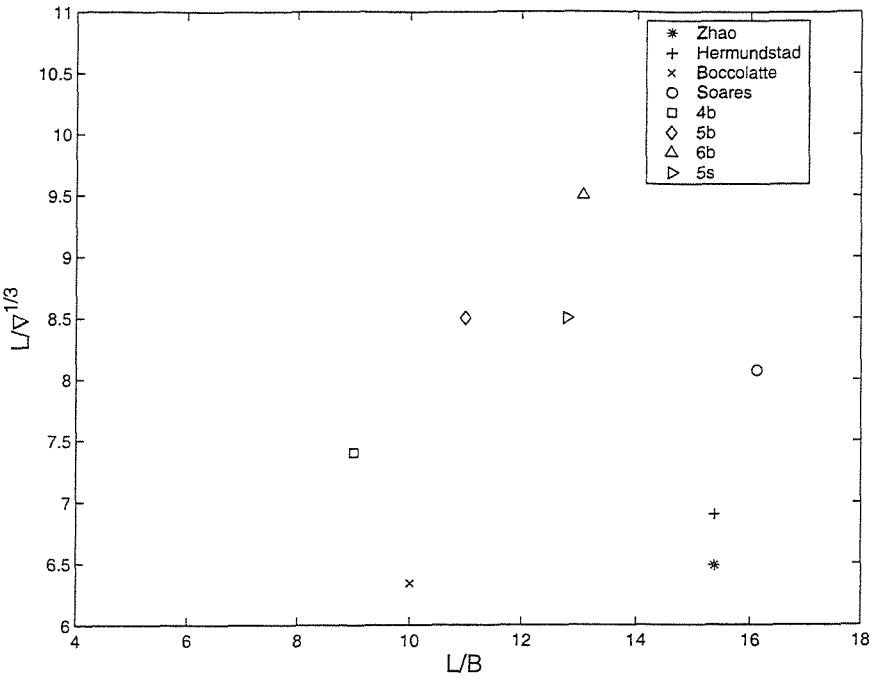

Figure 4: Extent of seakeeping data: Catamaran B/T against $L/\nabla^{1/3}$

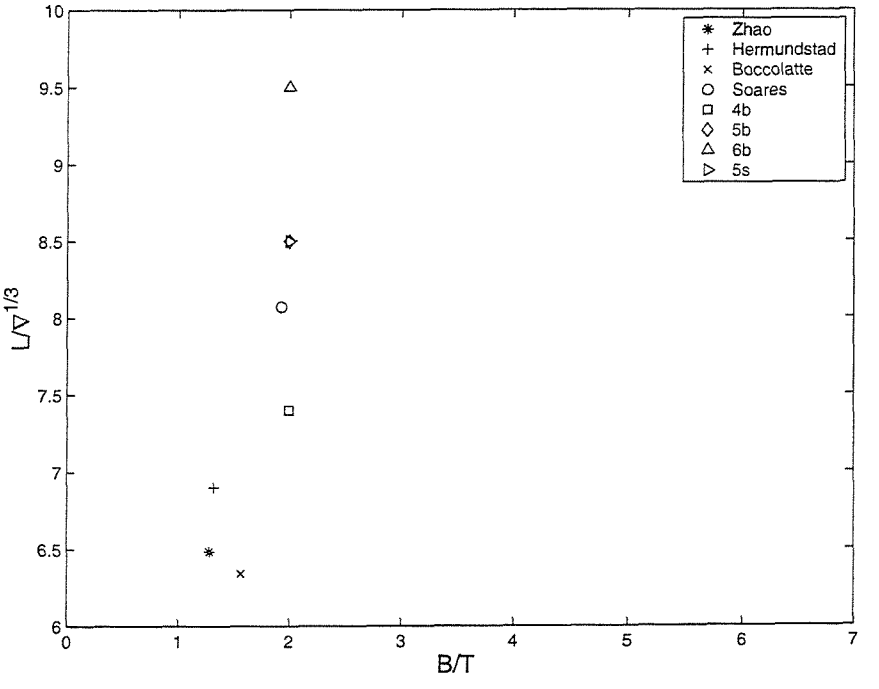

Figure 5: Extent of seakeeping data: Catamaran B/T against $L/\nabla^{1/3}$

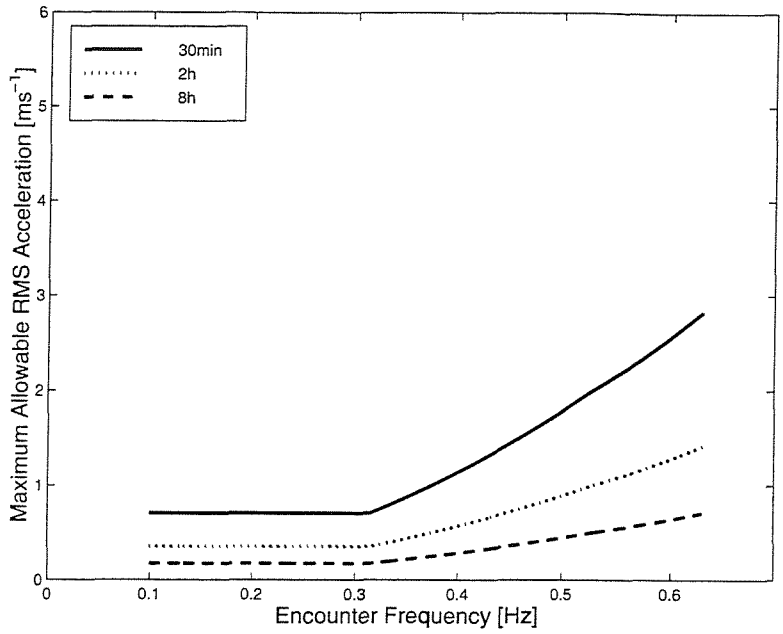

Figure 6: Relationship between acceleration level, duration and frequency for an MSI of 10%

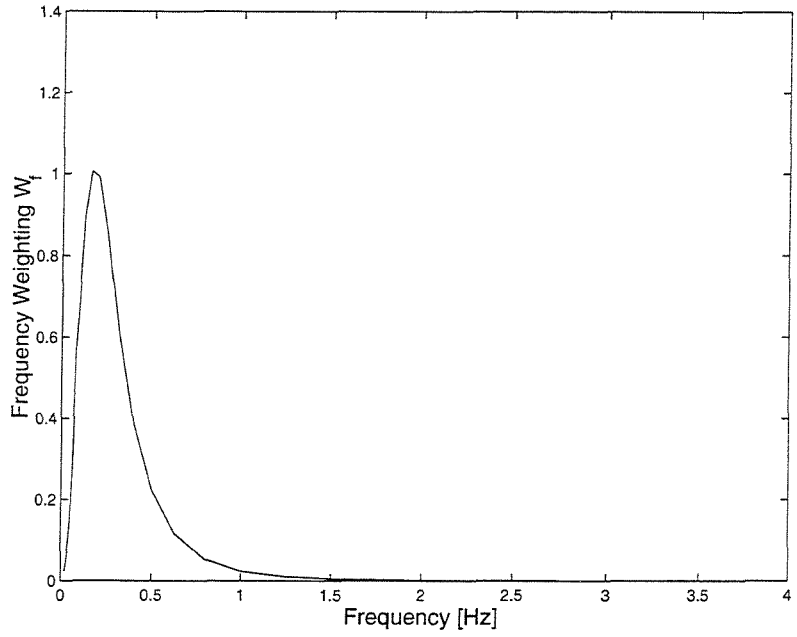

Figure 7: Frequency weighting wf of vertical acceleration for motion sickness, from ISO 2631-1997 [38]

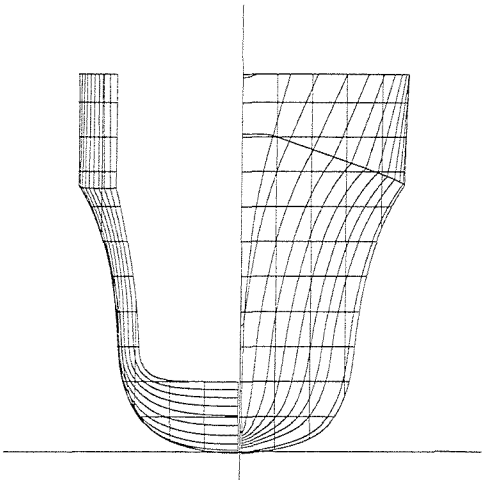

Figure 8: Bodyplan for Model 5s demihulls

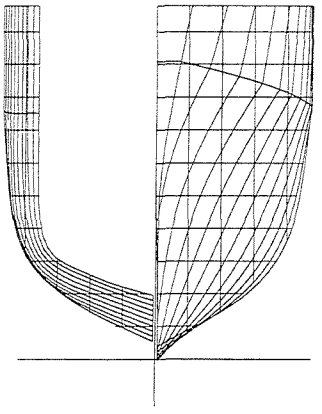

Figure 9: Bodyplan for Model 4b,5b and 6b demihills

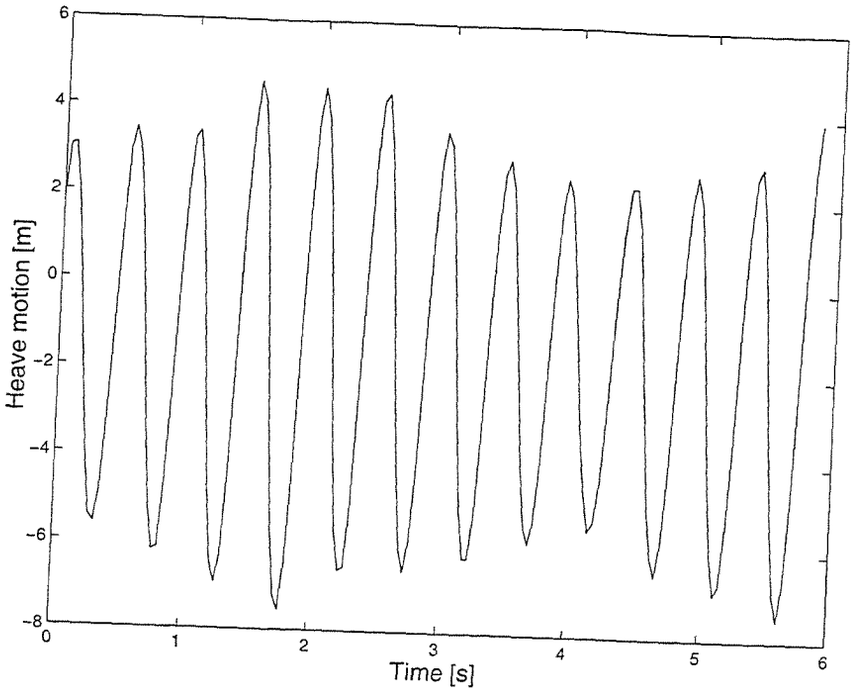

Figure 10: Example of heave record from model test at Southampton Institute on model 5s, S/L=0.2, Fn=0.65

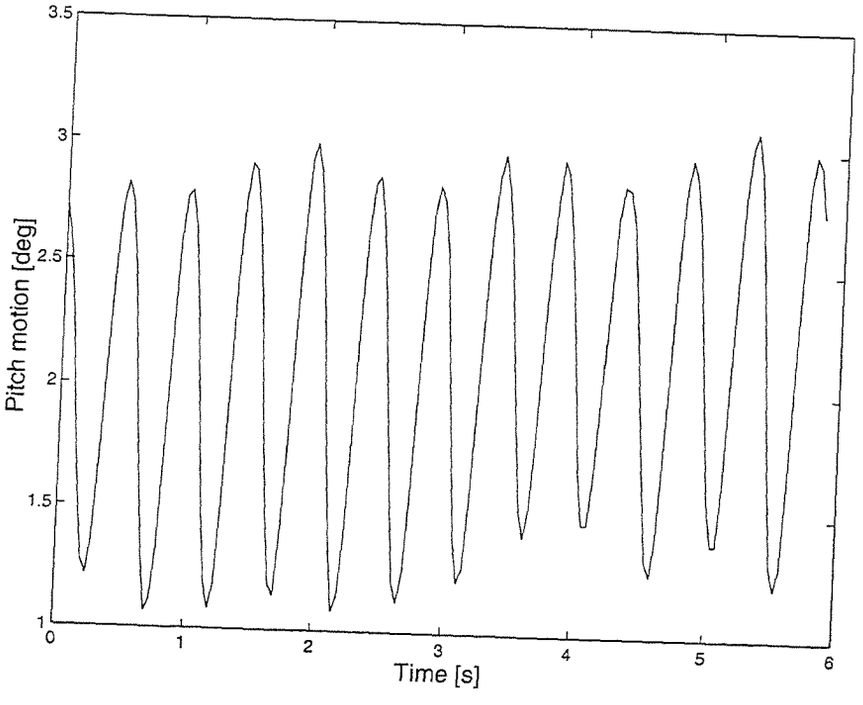

Figure 11: Example of pitch record from model test at Southampton Institute on model 5s, S/L=0.2, Fn=0.65

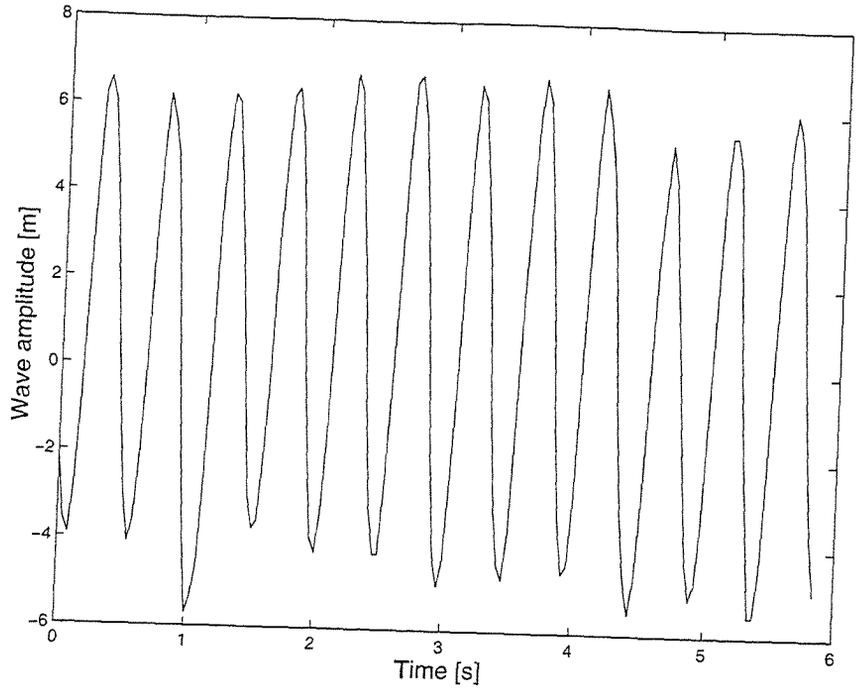

Figure 12: Example of wave record from model test at Southampton Institute on model 5s, S/L=0.2, Fn=0.65

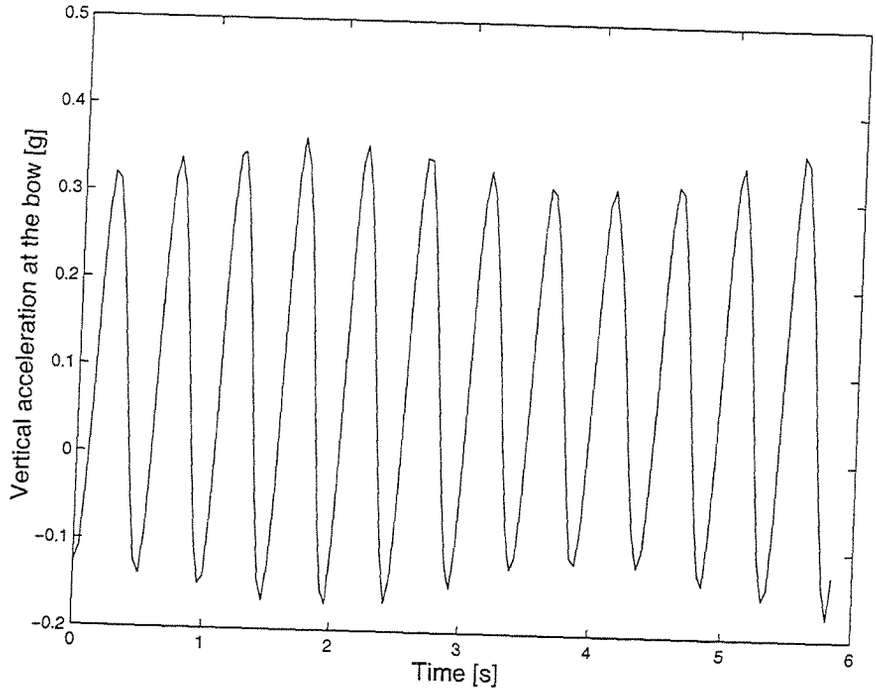

Figure 13: Example of vertical acceleration at the bow record from model test at Southampton Institute on model 5s, S/L=0.2, Fn=0.65

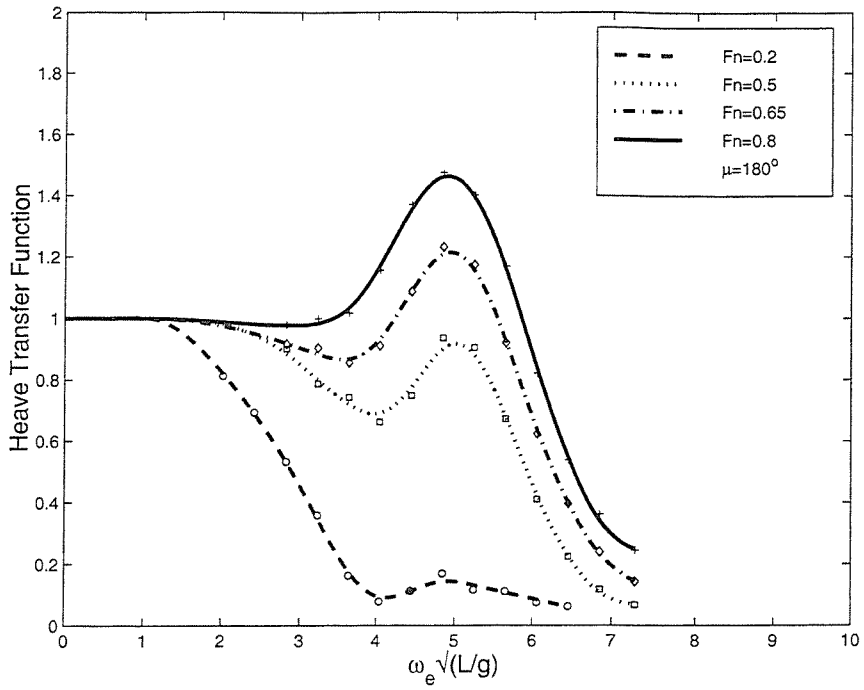

Figure 14: Heave transfer function, Model 5s, monohull, in head seas.

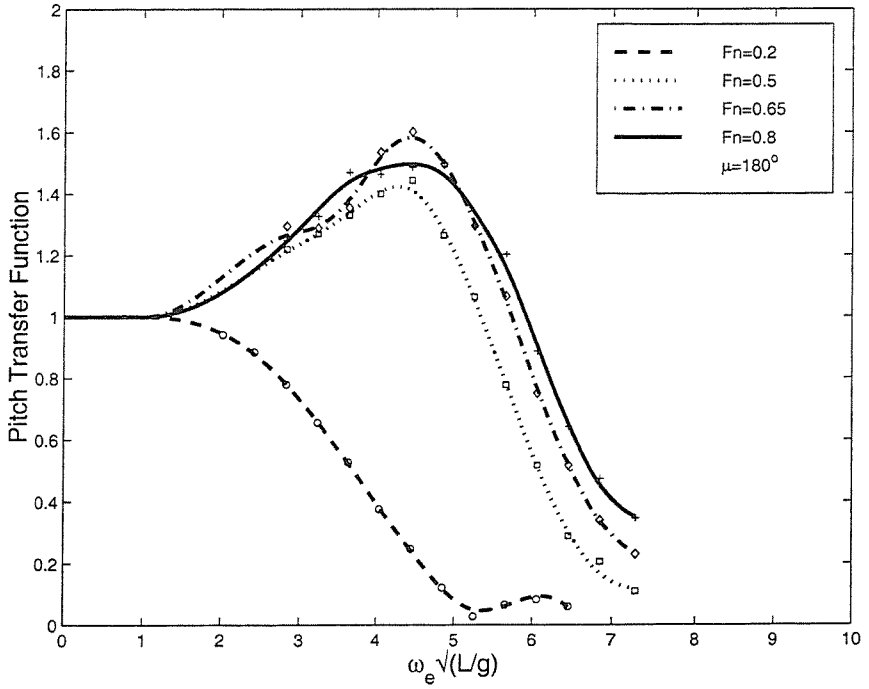

Figure 15: Pitch transfer function, Model 5s, monohull, in head seas.

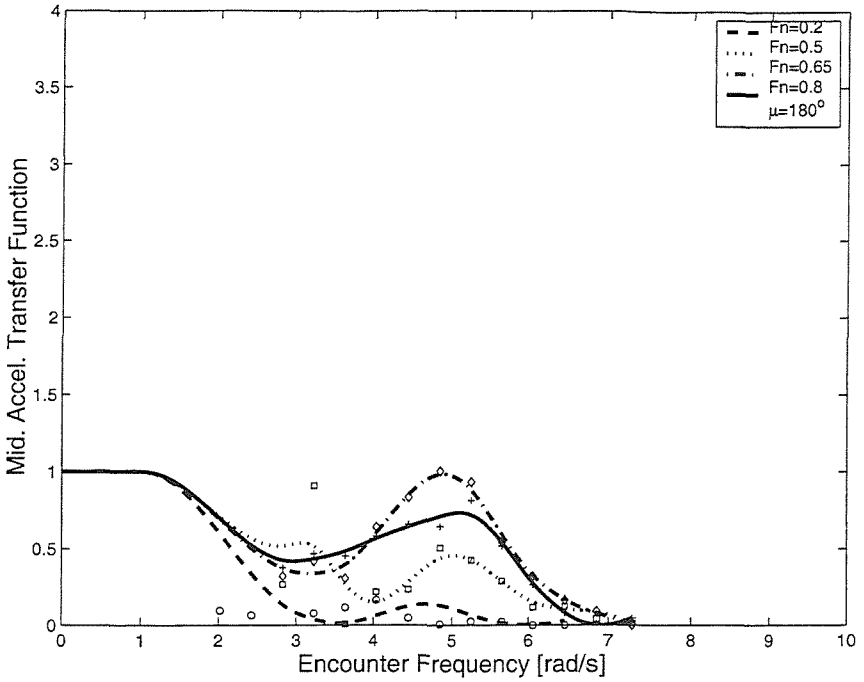

Figure 16: Acceleration at LCG transfer function derived from $\ddot{a}_z mid = \ddot{a}_z fwd - \ddot{\phi} l$, Model 5s, monohull, in head seas.

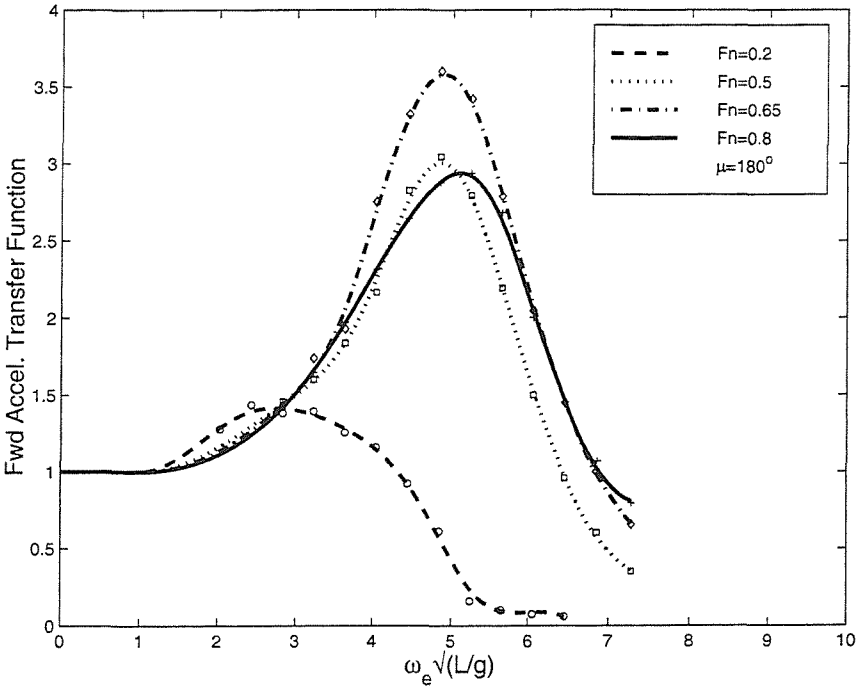

Figure 17: Acceleration at Bow transfer function, Model 5s, monohull, in head seas.

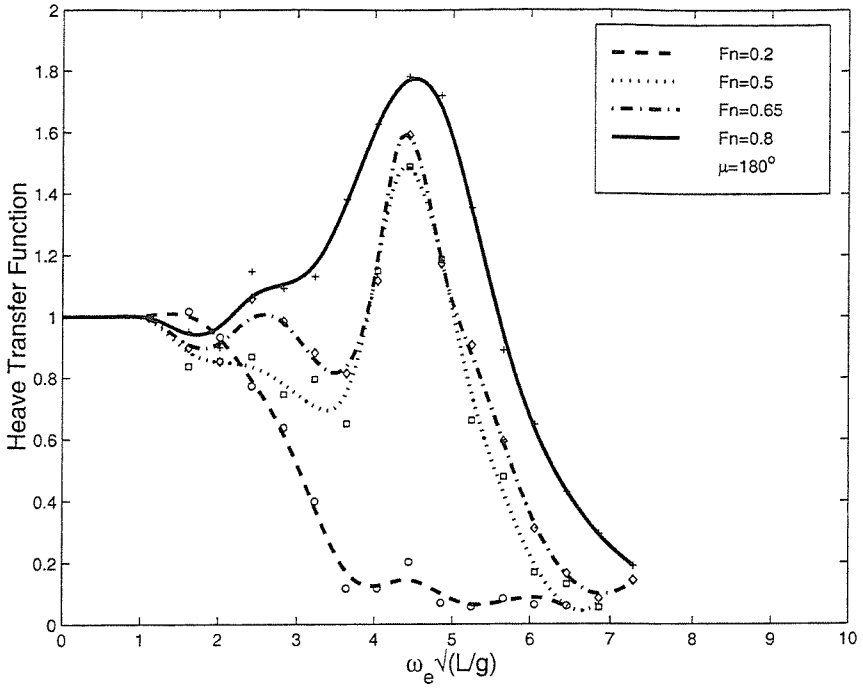

Figure 18: Heave transfer function, Model 5s, S/L=0.2, in head seas.

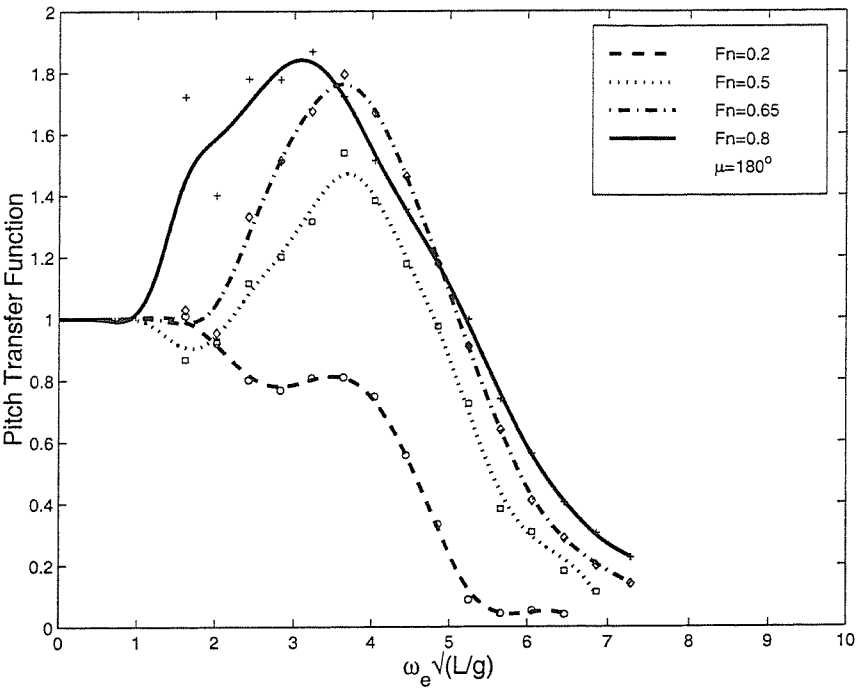

Figure 19: Pitch transfer function, Model 5s, S/L=0.2, in head seas.

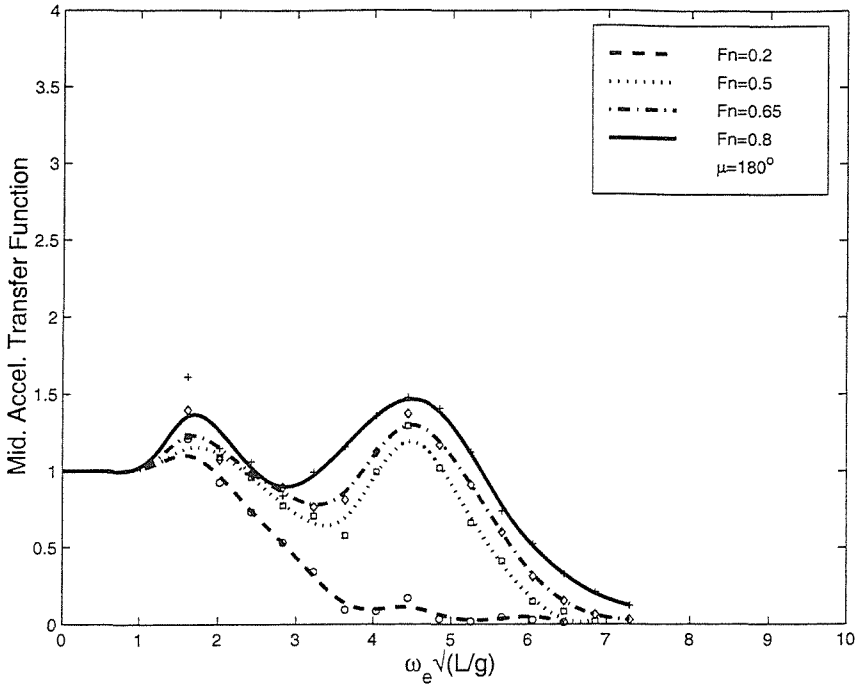

Figure 20: Acceleration at LCG transfer function, Model 5s, S/L=0.2, in head seas.

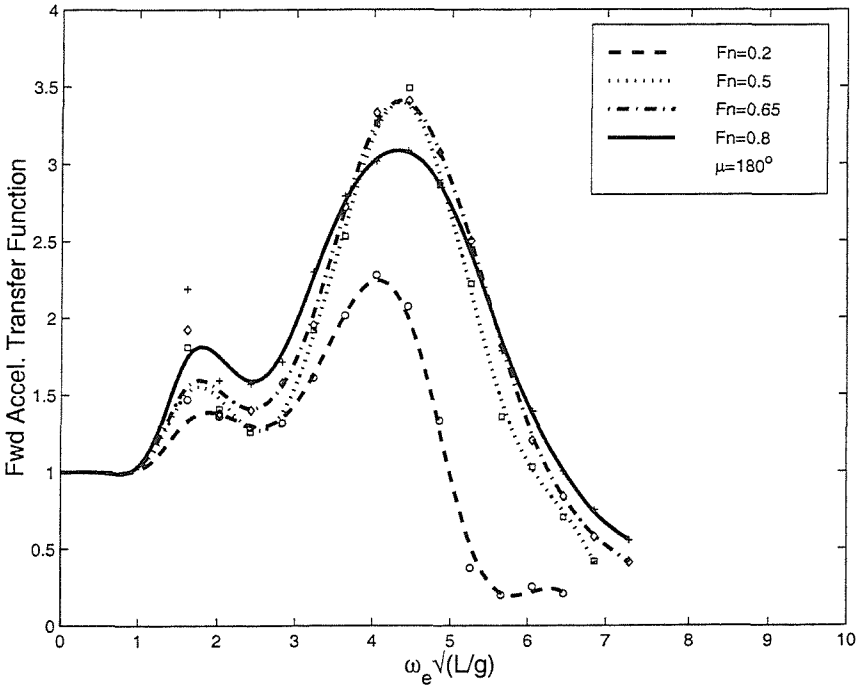

Figure 21: Acceleration at Bow transfer function, Model 5s, S/L=0.2, in head seas.

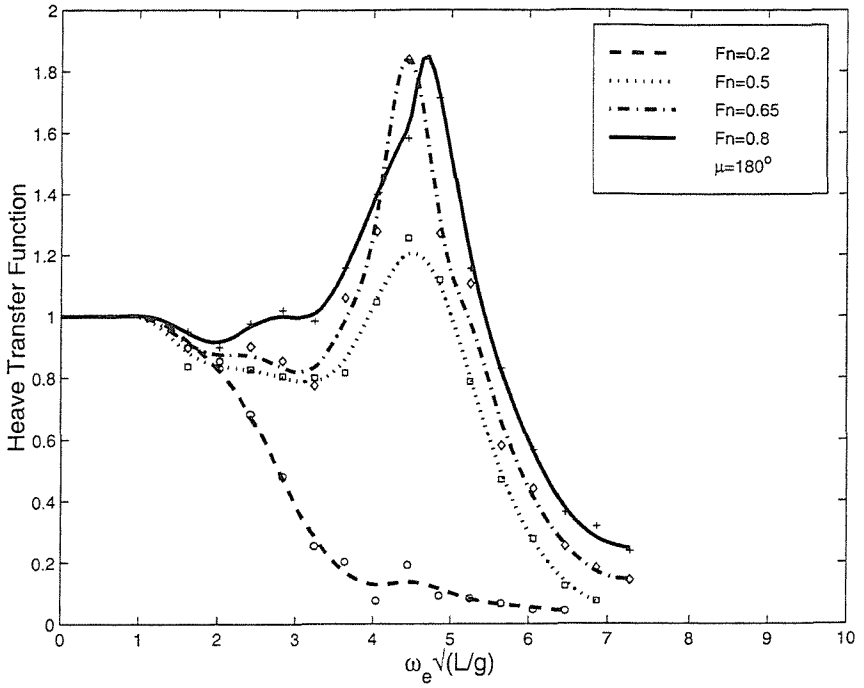

Figure 22: Heave transfer function, Model 5s, S/L=0.4, in head seas.

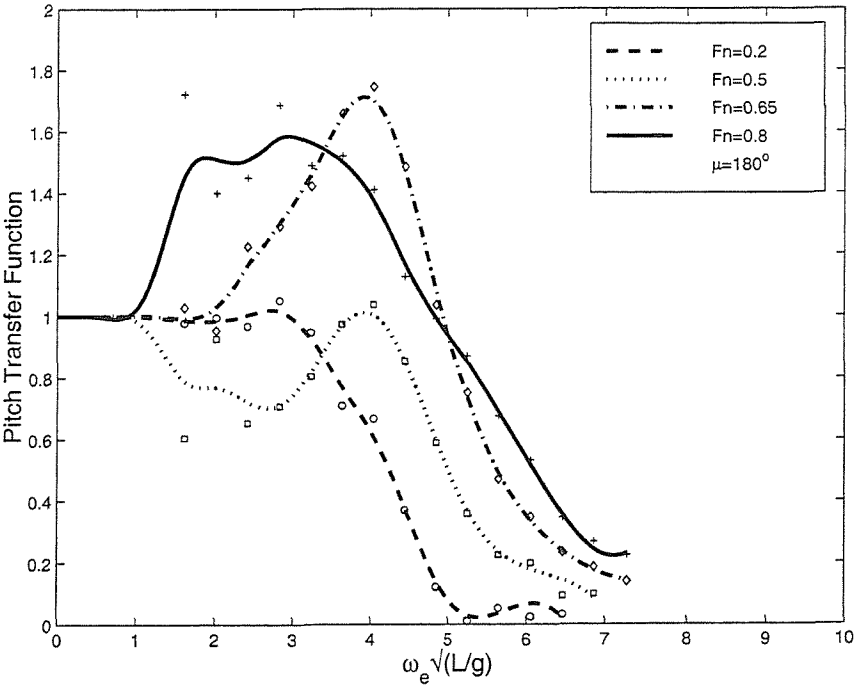

Figure 23: Pitch transfer function, Model 5s, S/L=0.4, in head seas.

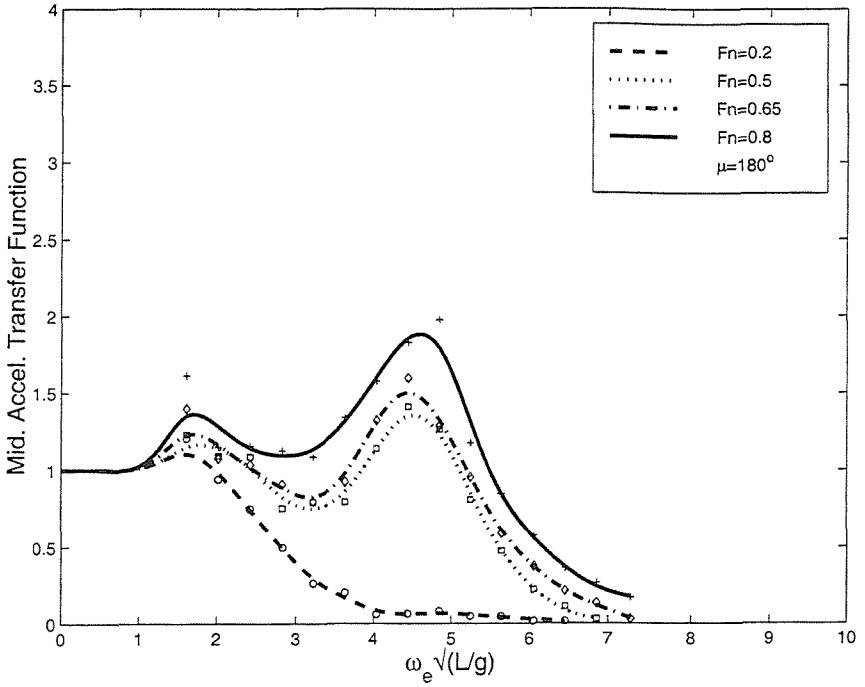

Figure 24: Acceleration at LCG transfer function, Model 5s, S/L=0.4, in head seas.

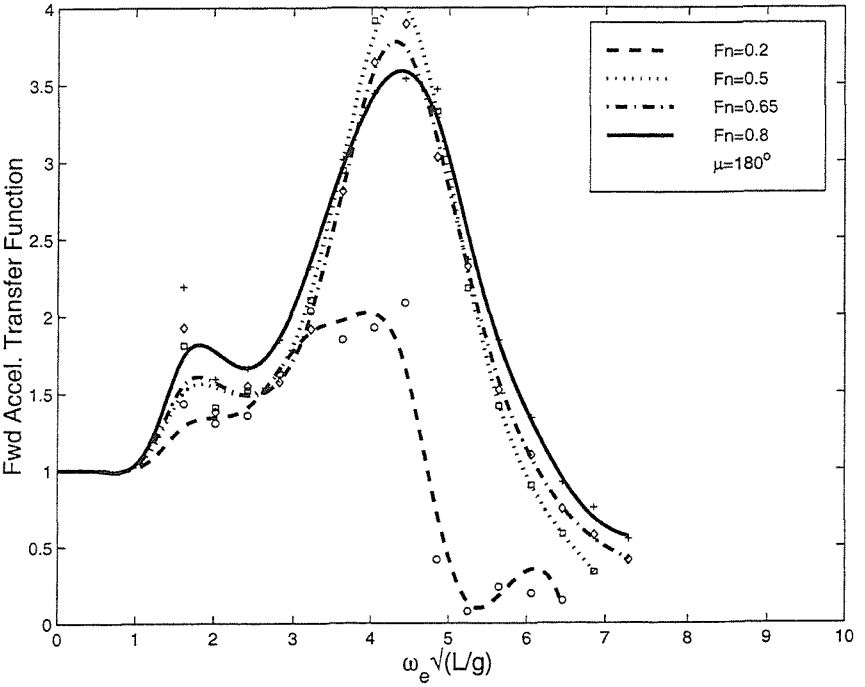

Figure 25: Acceleration at Bow transfer function, Model 5s, S/L=0.4, in head seas.

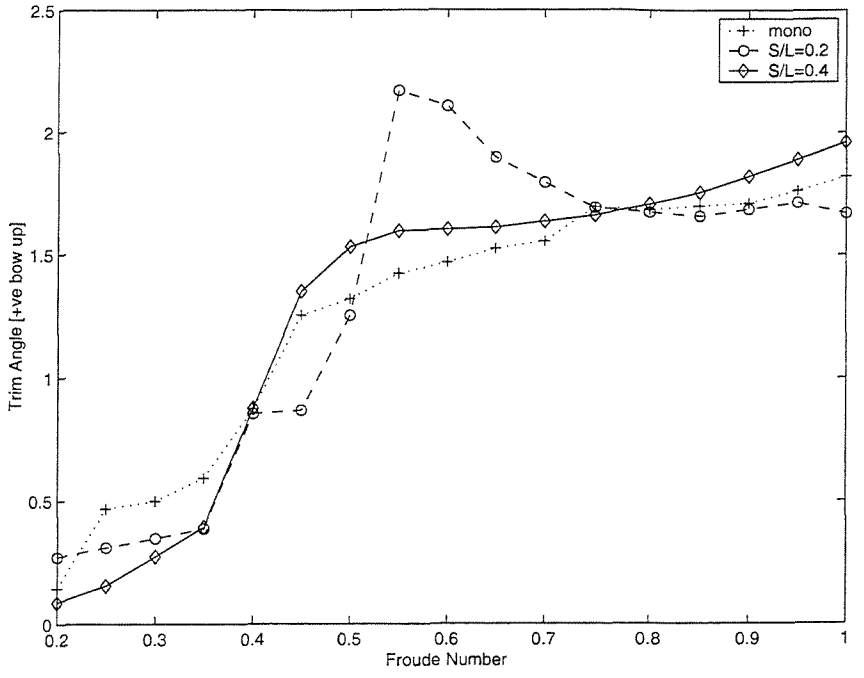

Figure 26: Trim angles for Model 5s in calm water.

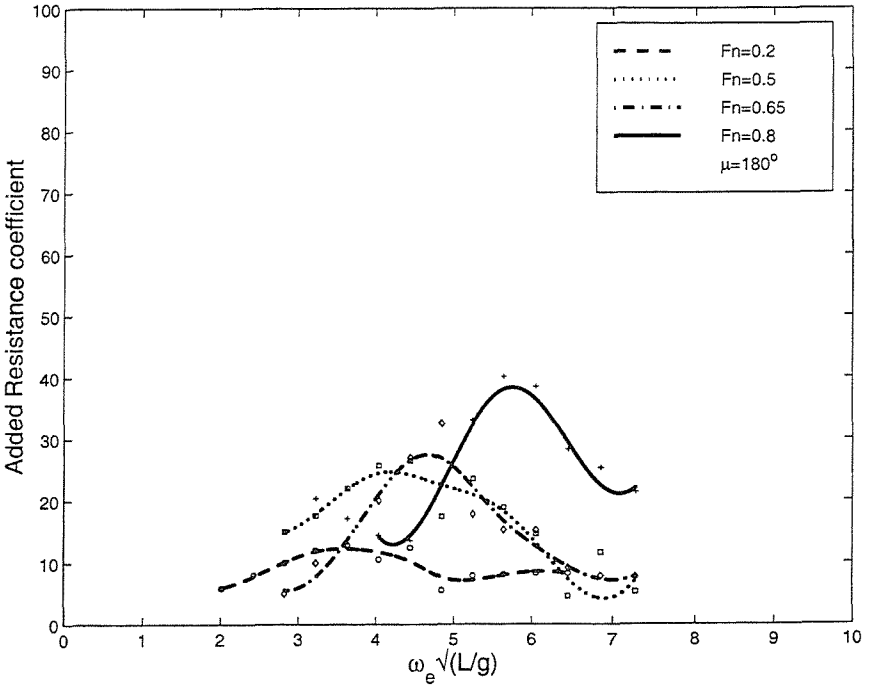

Figure 27: Added resistance, Model 5s, monohull, in head seas.

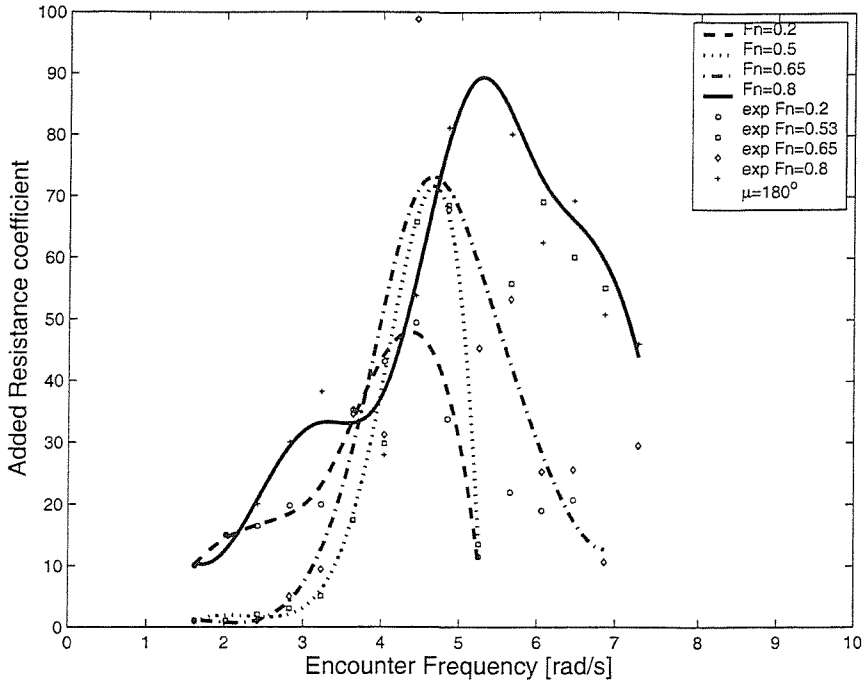

Figure 28: Added resistance, Model 5s, S/L=0.2, in head seas.

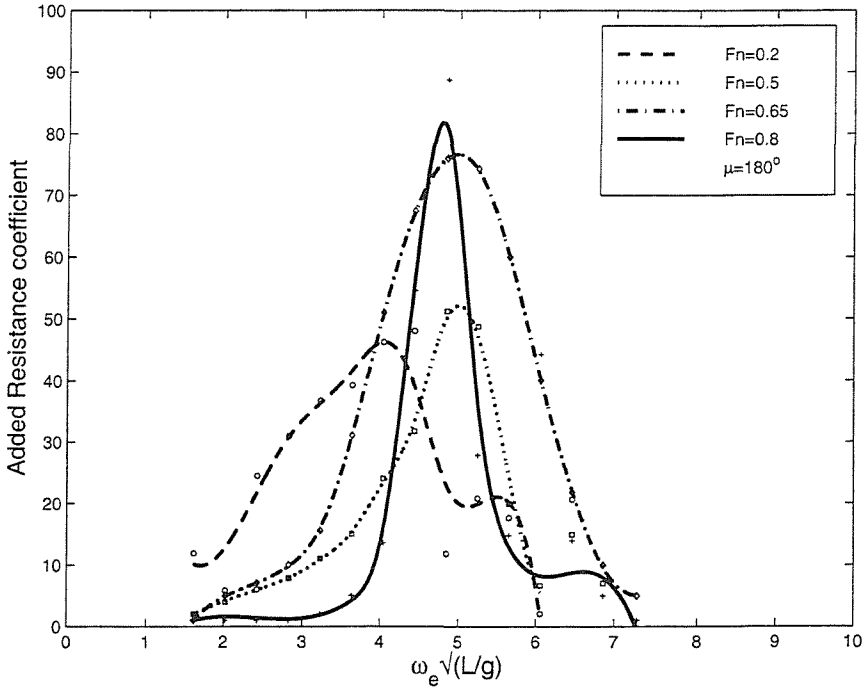

Figure 29: Added resistance, Model 5s, S/L=0.4, in head seas.

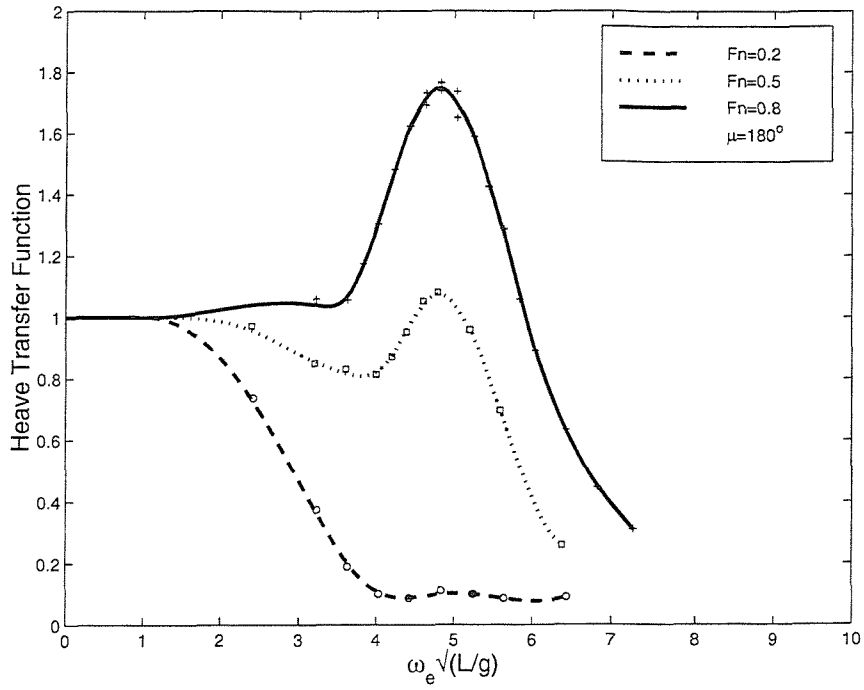

Figure 30: Heave transfer function, Model 5b, monohull, in head seas, Couser [19].

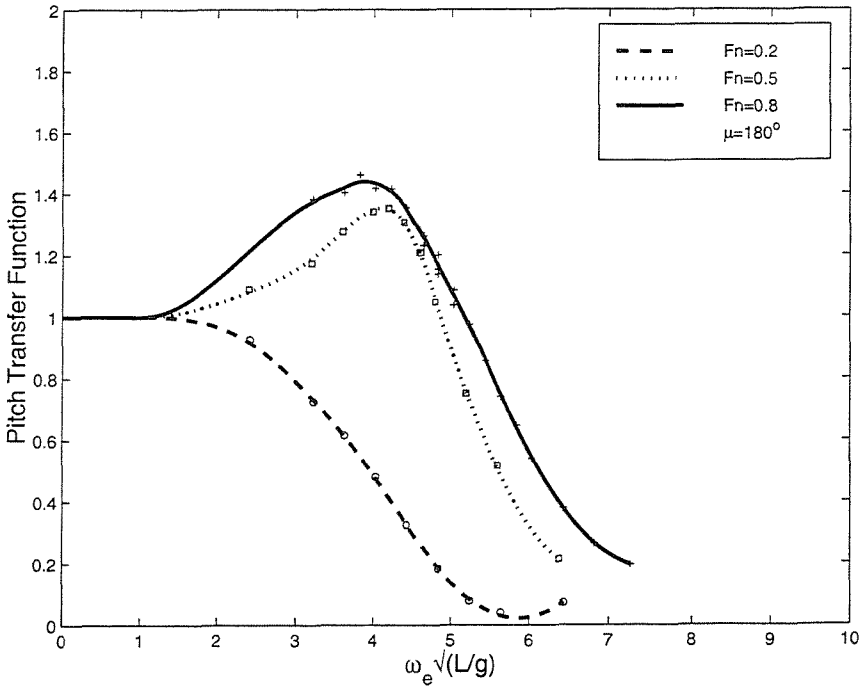

Figure 31: Pitch transfer function, Model 5b, monohull, in head seas, Couser [19].

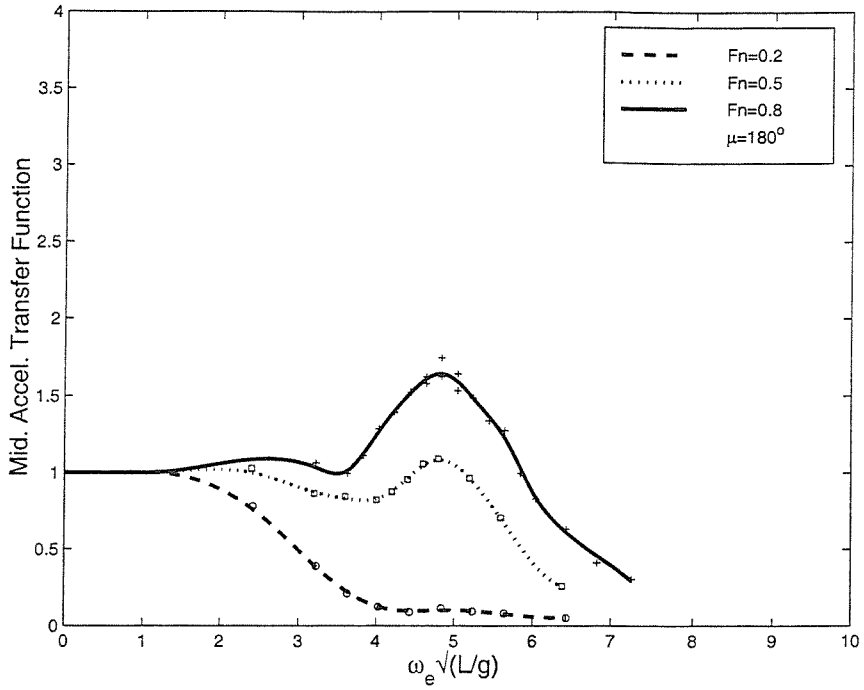

Figure 32: Acceleration at LCG transfer function, Model 5b, monohull, in head seas, Couser [19].

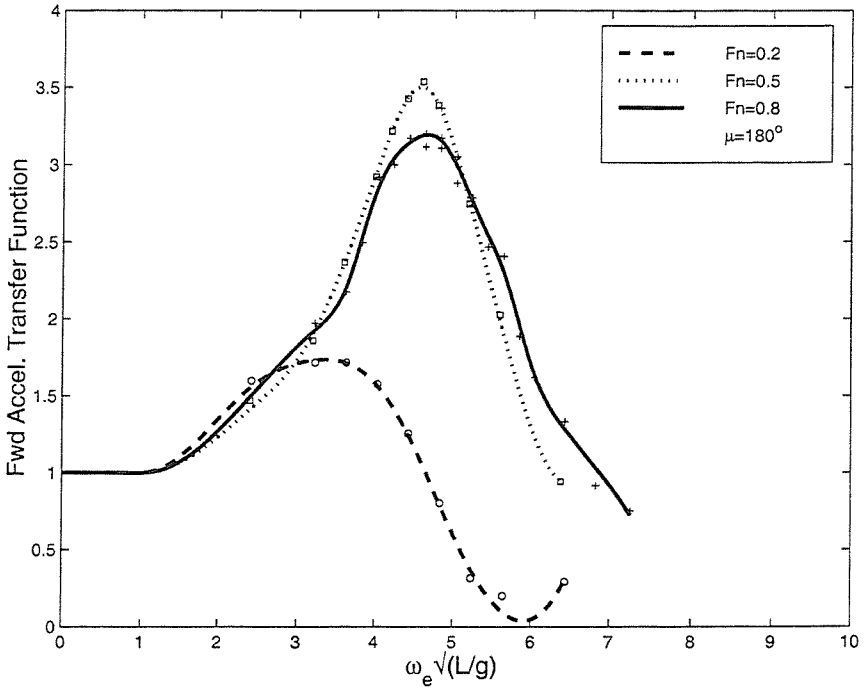

Figure 33: Acceleration at Bow transfer function, Model 5b, monohull, in head seas, Couser [19].

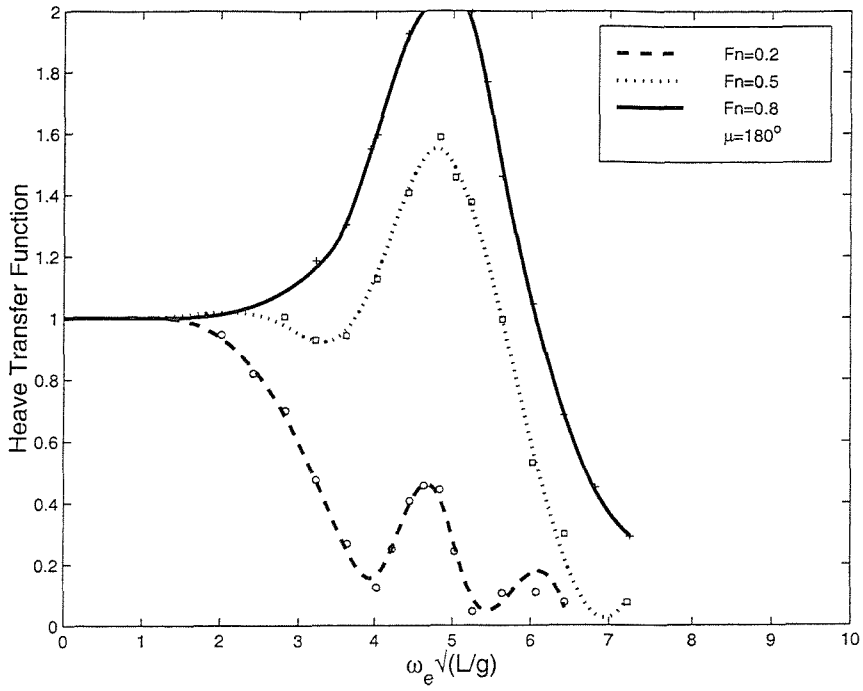

Figure 34: Heave transfer function, Model 5b, S/L=0.2, in head seas, Couser [19].

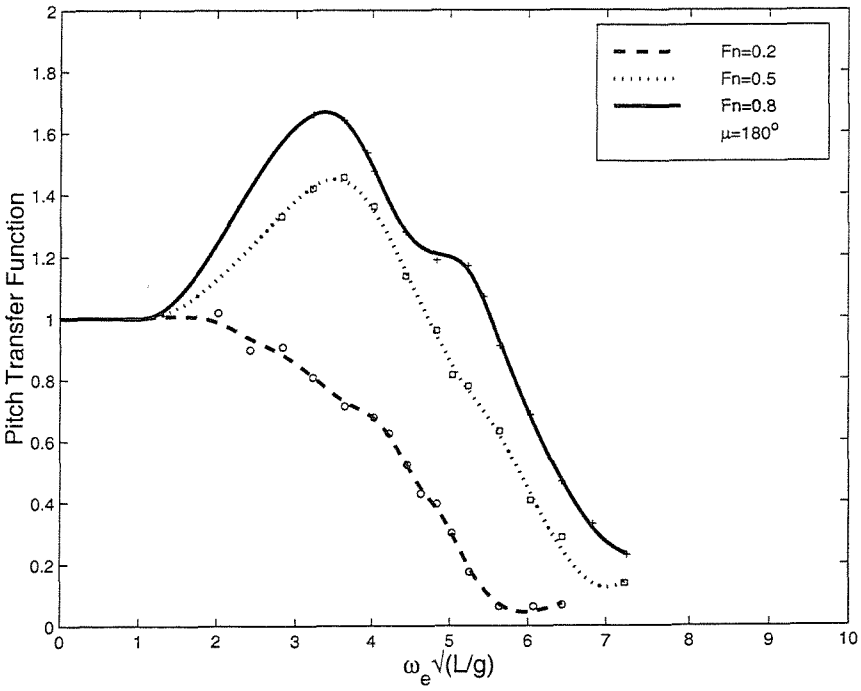

Figure 35: Pitch transfer function, Model 5b, S/L=0.2, in head seas, Couser [19].

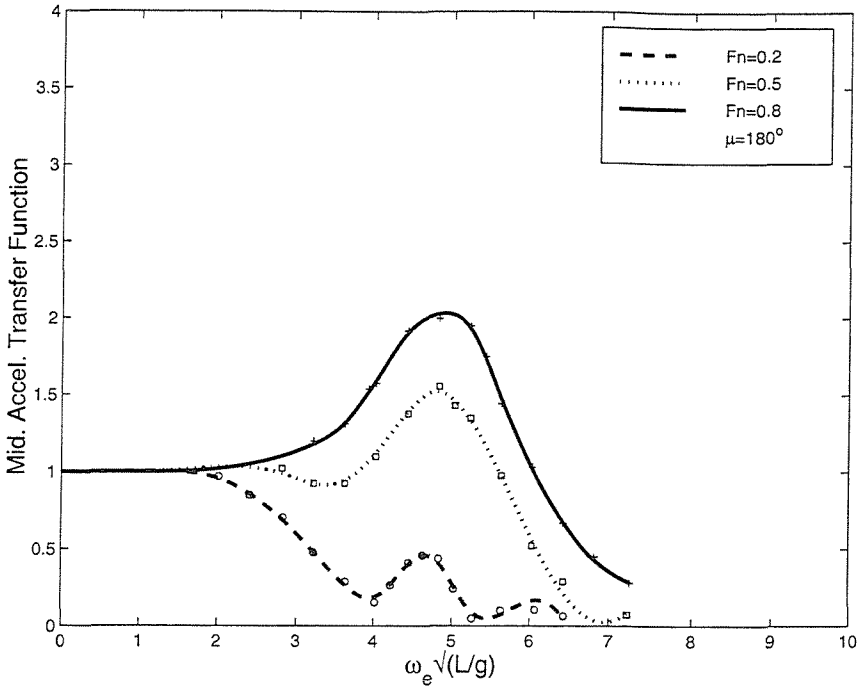

Figure 36: Acceleration at LCG transfer function, Model 5b, S/L=0.2, in head seas, Couser [19].

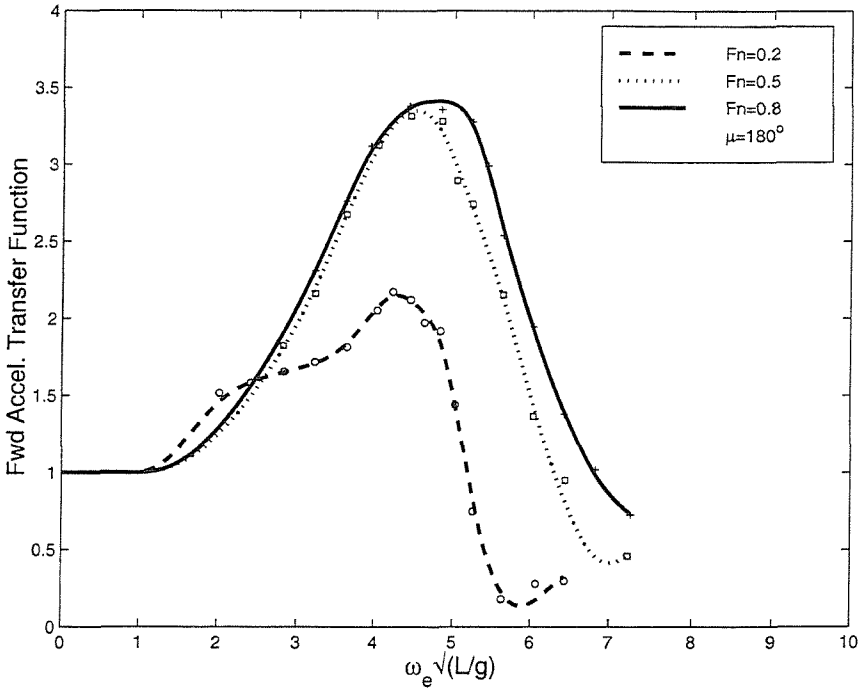

Figure 37: Acceleration at Bow transfer function, Model 5b, S/L=0.2, in head seas, Couser [19].

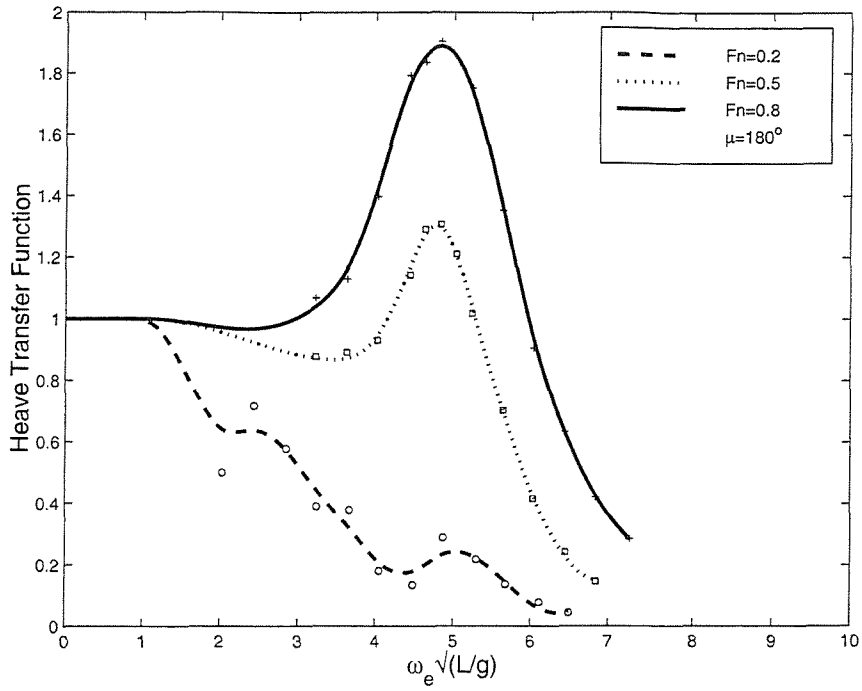

Figure 38: Heave transfer function, Model 5b, S/L=0.4, in head seas, Couser [19].

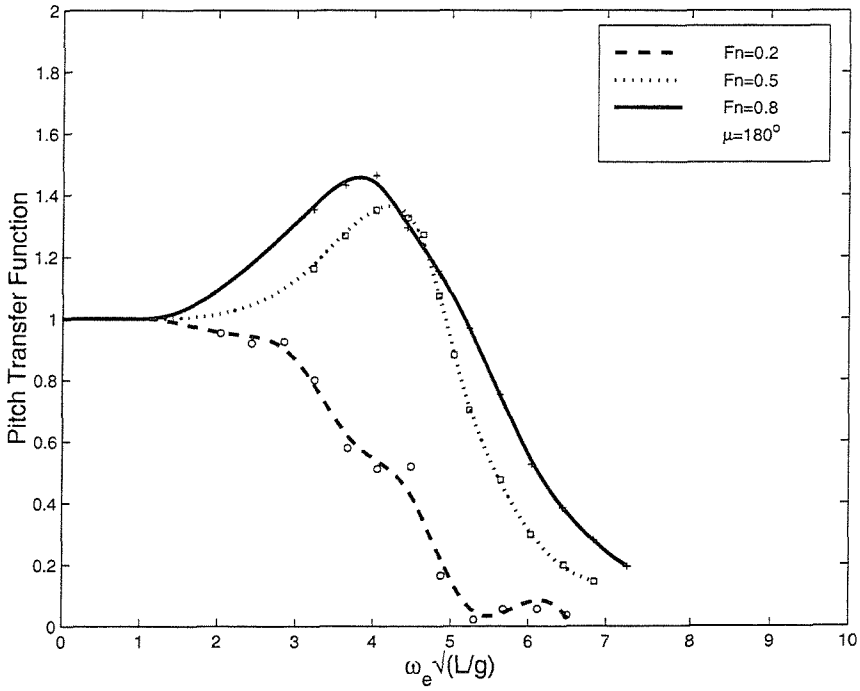

Figure 39: Pitch transfer function, Model 5b, S/L=0.4, in head seas, Couser [19].

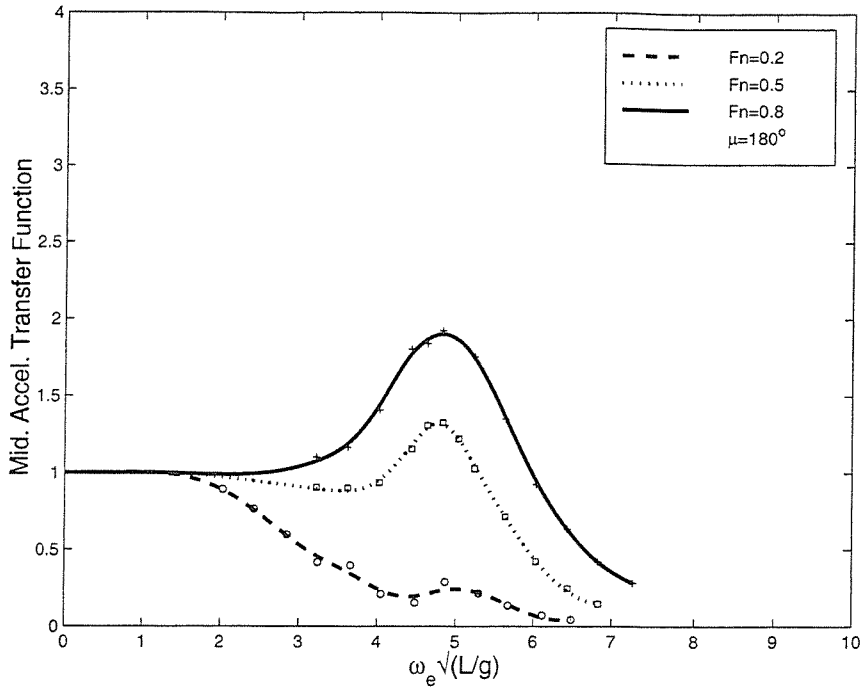

Figure 40: Acceleration at LCG transfer function, Model 5b, S/L=0.4, in head seas, Couser [19].

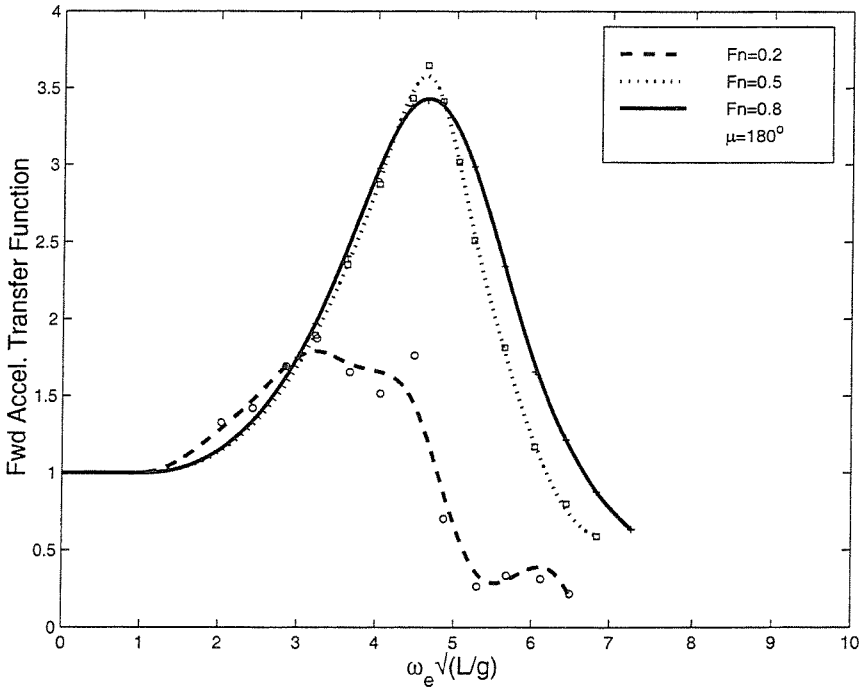

Figure 41: Acceleration at Bow transfer function, Model 5b, S/L=0.4, in head seas, Couser [19].

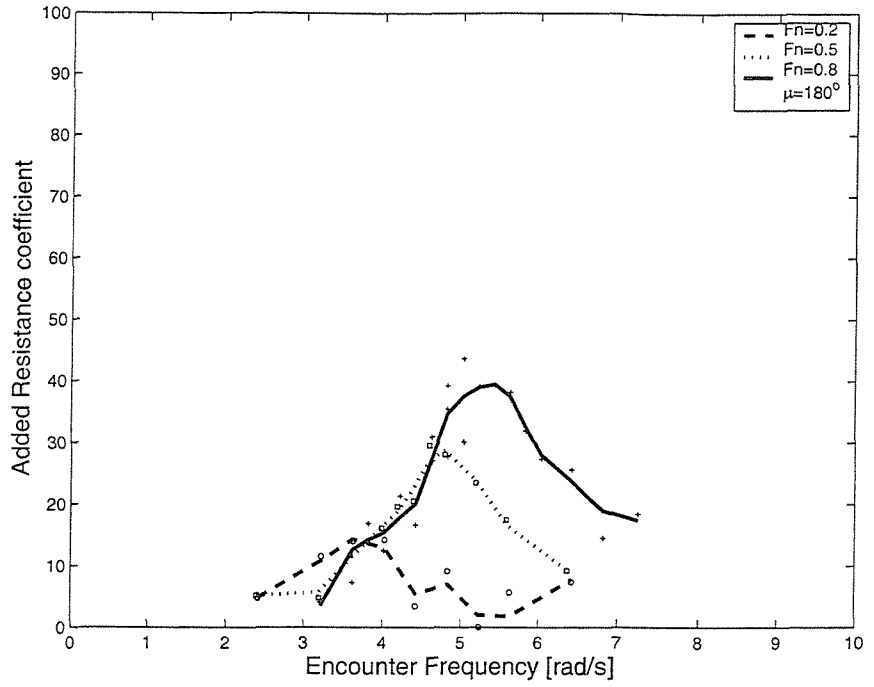

Figure 42: Added resistance, Model 5b, monohull, in head seas, Couser [19].

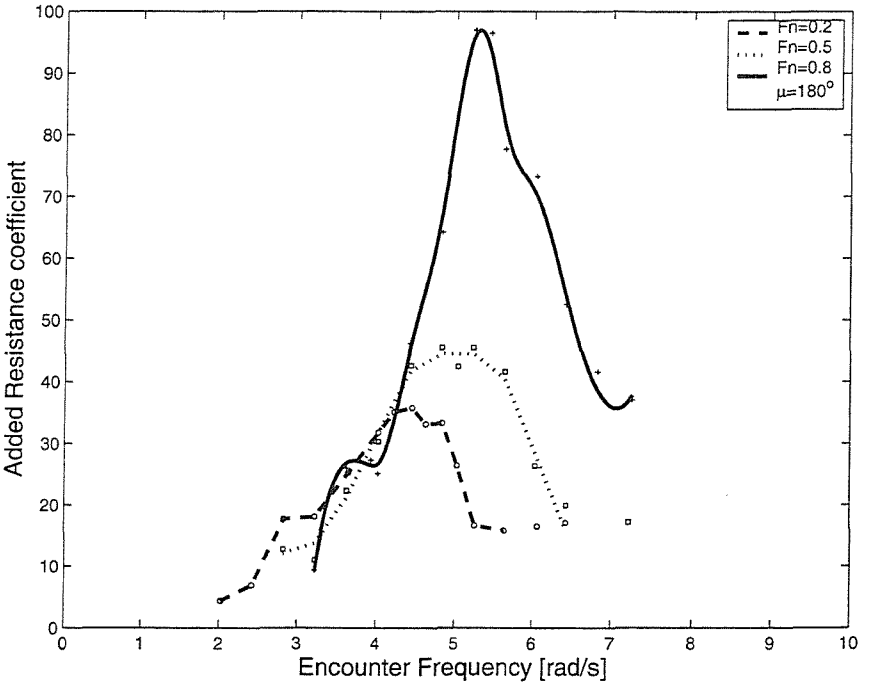

Figure 43: Added resistance, Model 5b, S/L=0.2, in head seas, Couser [19].

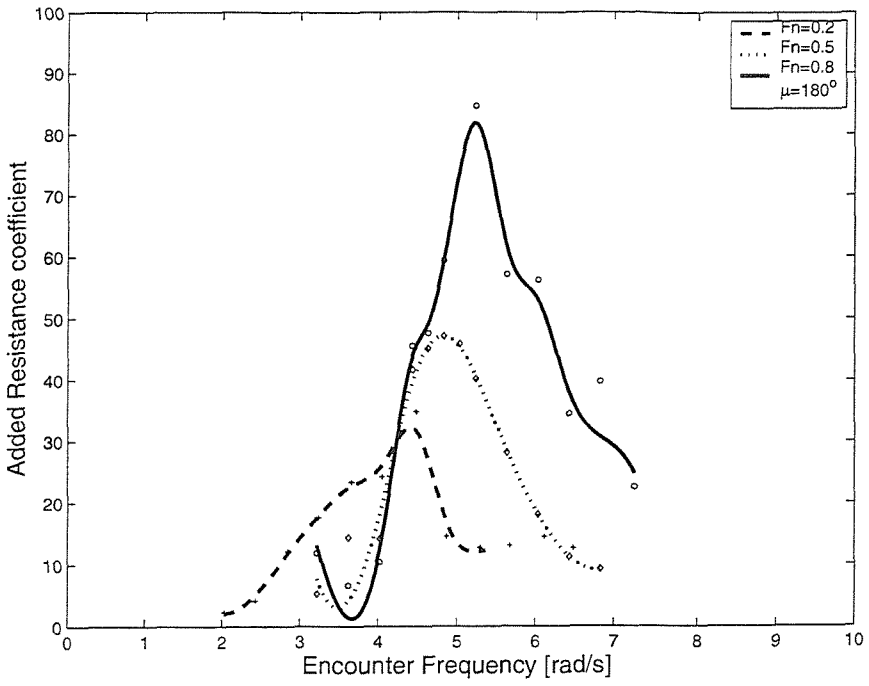

Figure 44: Added resistance, Model 5b, S/L=0.4, in head seas, Couser [19].

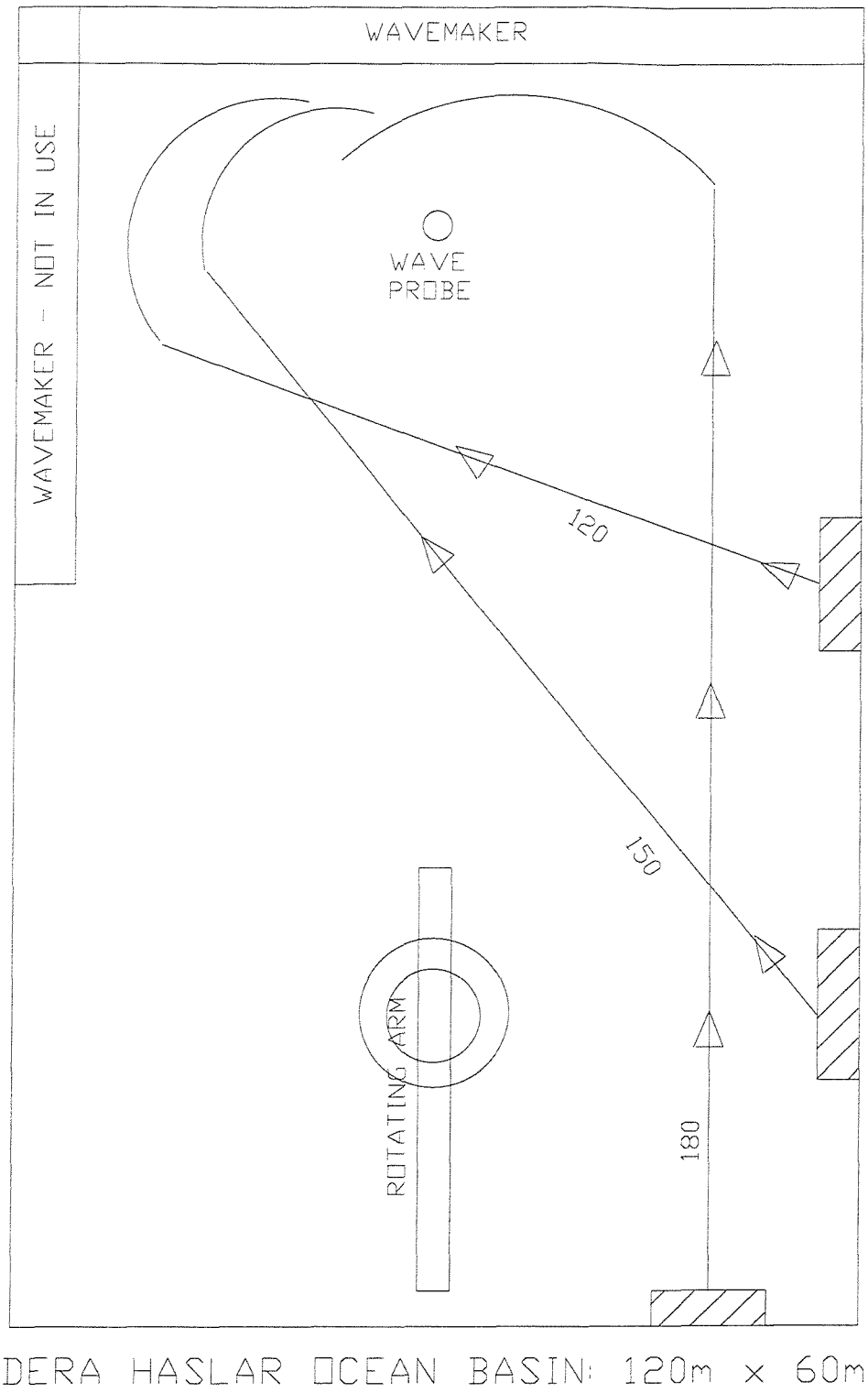

Figure 45: Schematic layout of basin and headings of test runs.

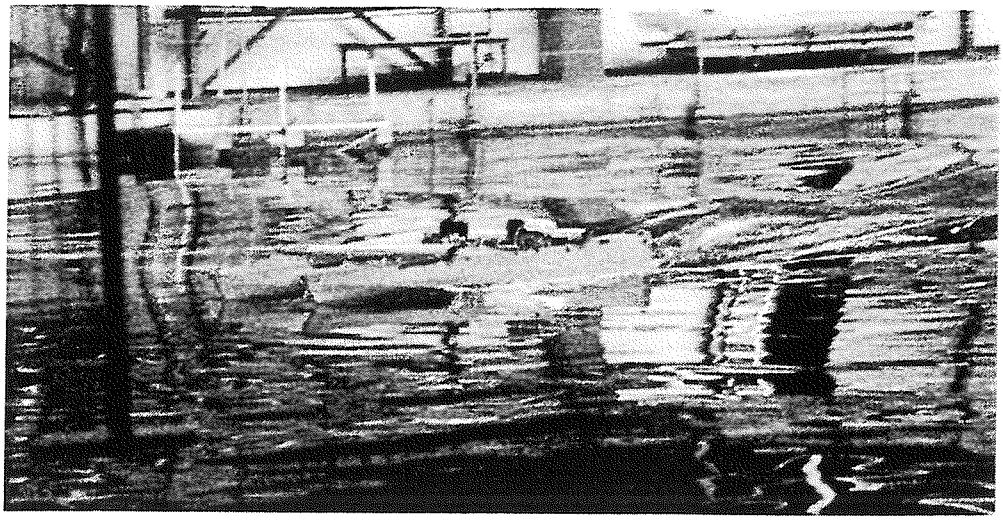

Figure 46: Catamaran 5b, S/L=0.2 in the Ocean Basin at DERA Haslar at a heading of $\mu = 180°$.

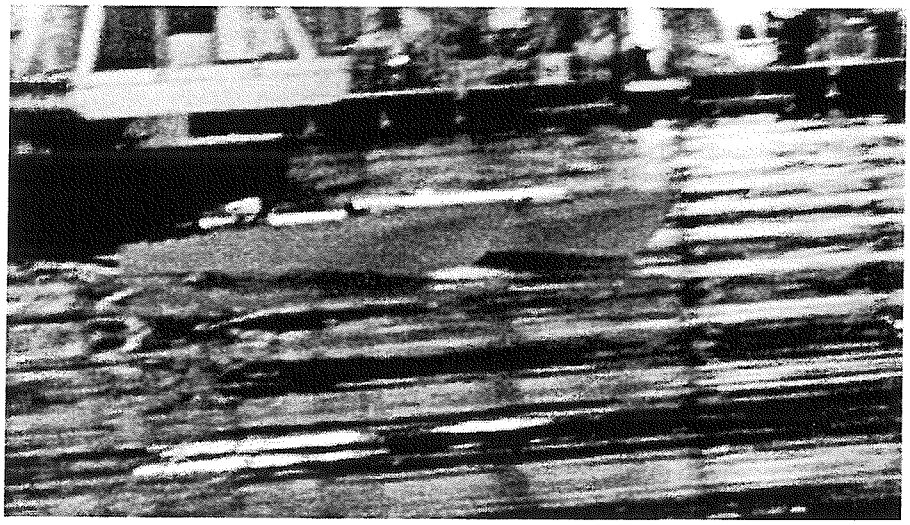

Figure 47: Catamaran 5b, S/L=0.4 in the Ocean Basin at DERA Haslar at a heading of $\mu = 150°$.

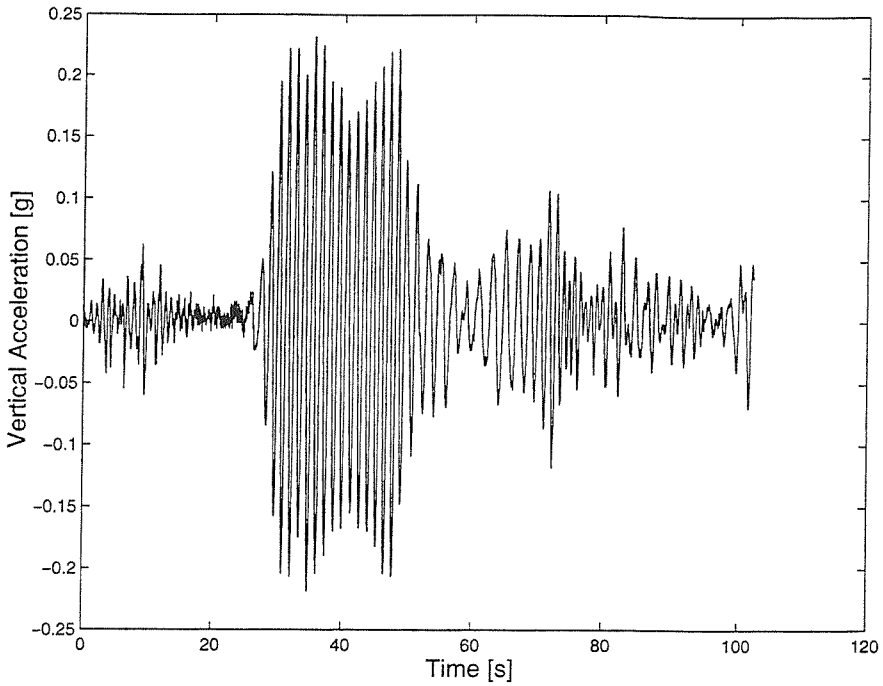

Figure 48: Example vertical acceleration at LCG, record for Catamaran 5s in the Ocean Basin at DERA Haslar

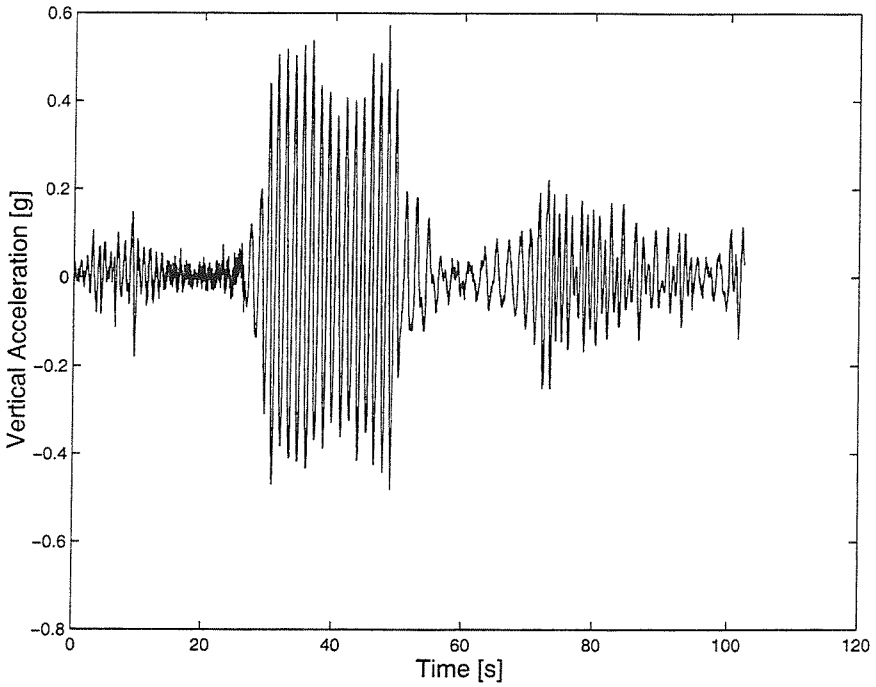

Figure 49: Example vertical acceleration at bow, record for Catamaran 5s in the Ocean Basin at DERA Haslar

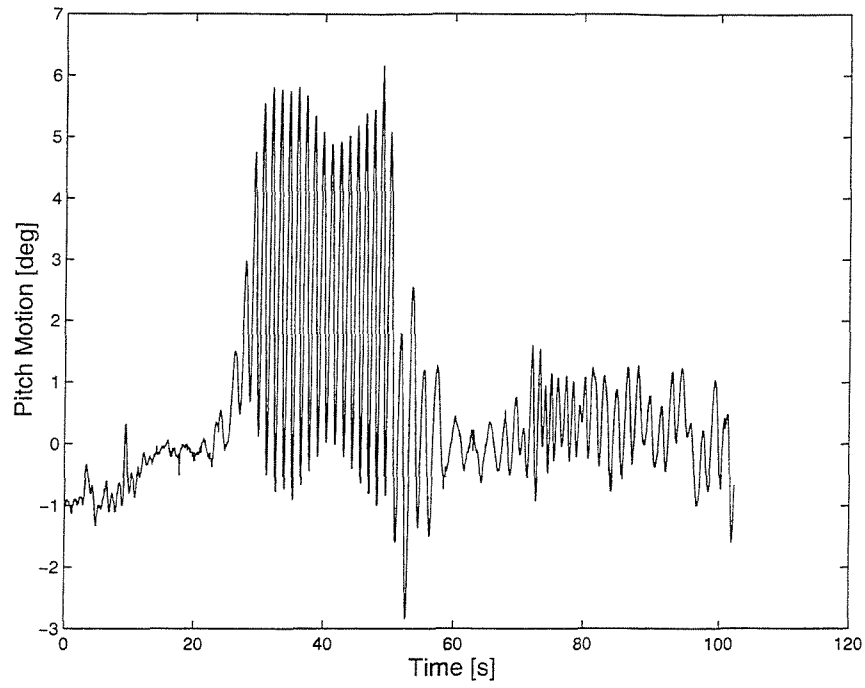

Figure 50: Example pitch record for Catamaran 5s in the Ocean Basin at DERA Haslar

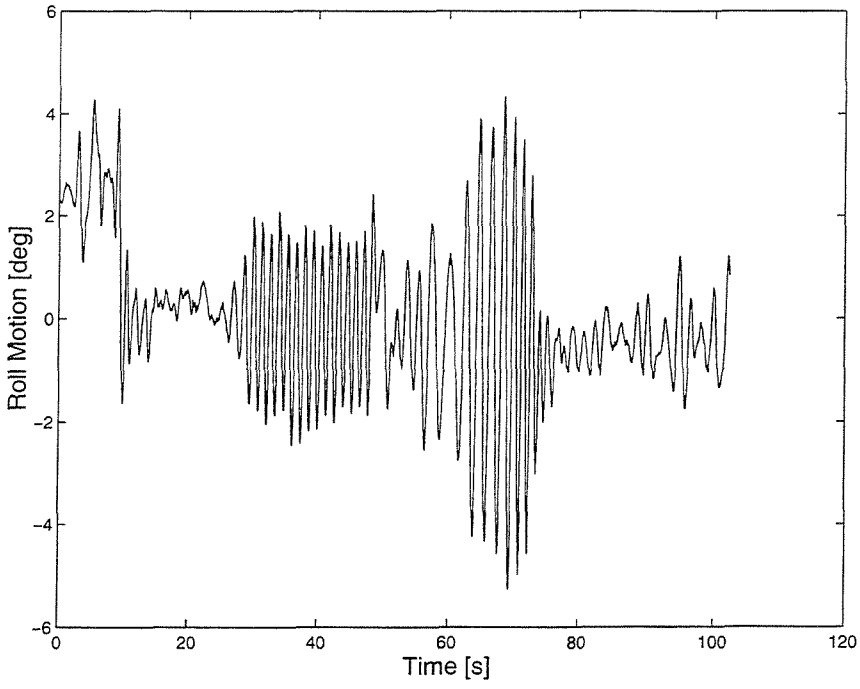

Figure 51: Example roll record for Catamaran 5s in the Ocean Basin at DERA Haslar

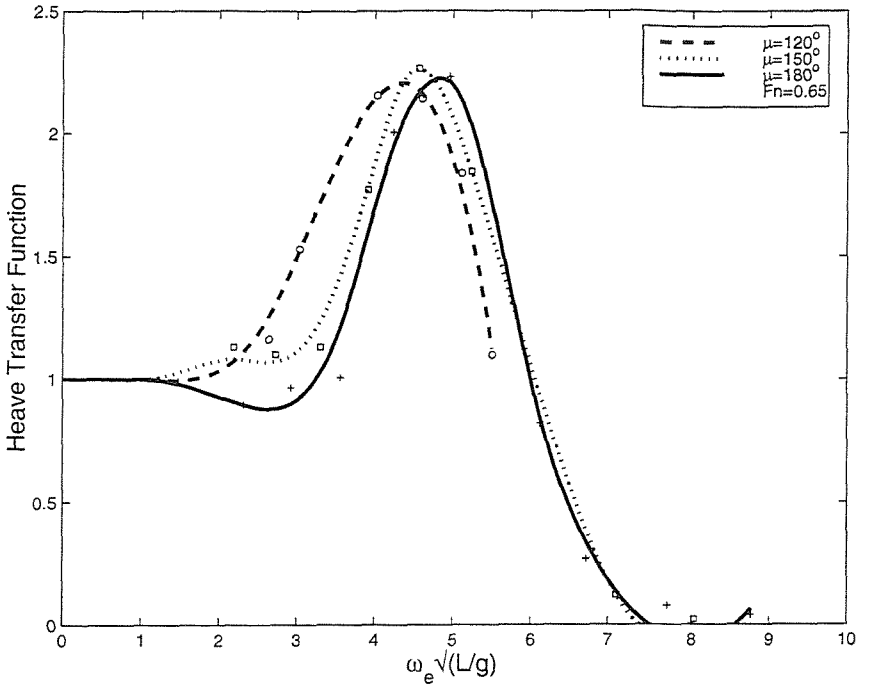

Figure 52: Heave transfer function, Model 5b, S/L=0.2, in oblique seas.

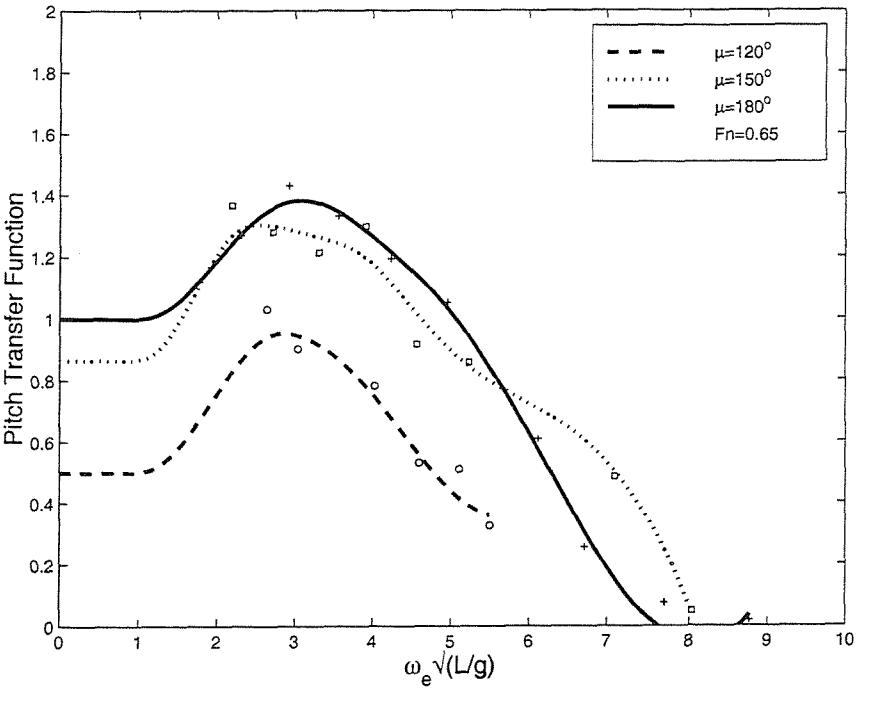

Figure 53: Pitch transfer function, Model 5b, S/L=0.2, in oblique seas.

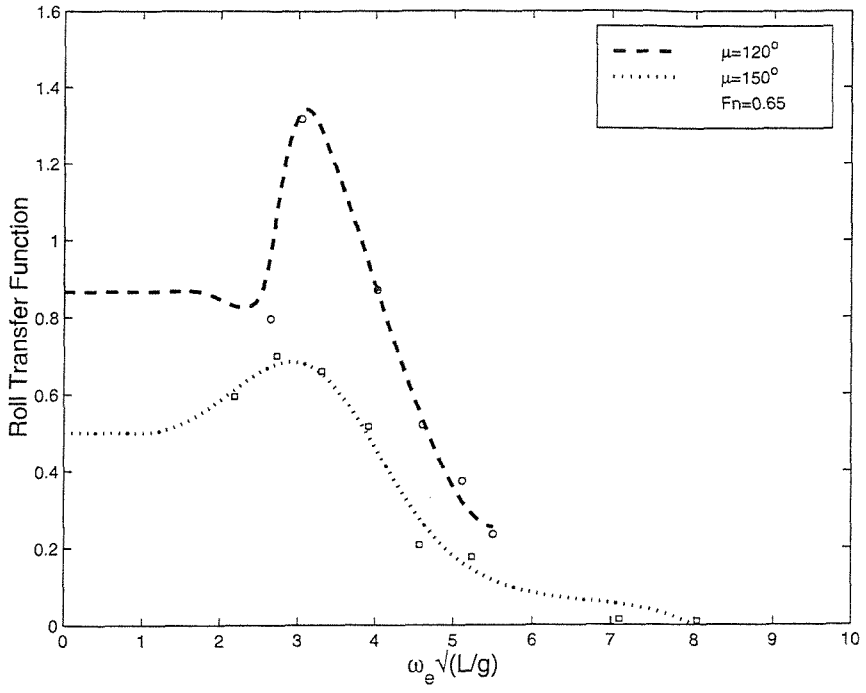

Figure 54: Roll transfer function, Model 5b, S/L=0.2, in oblique seas.

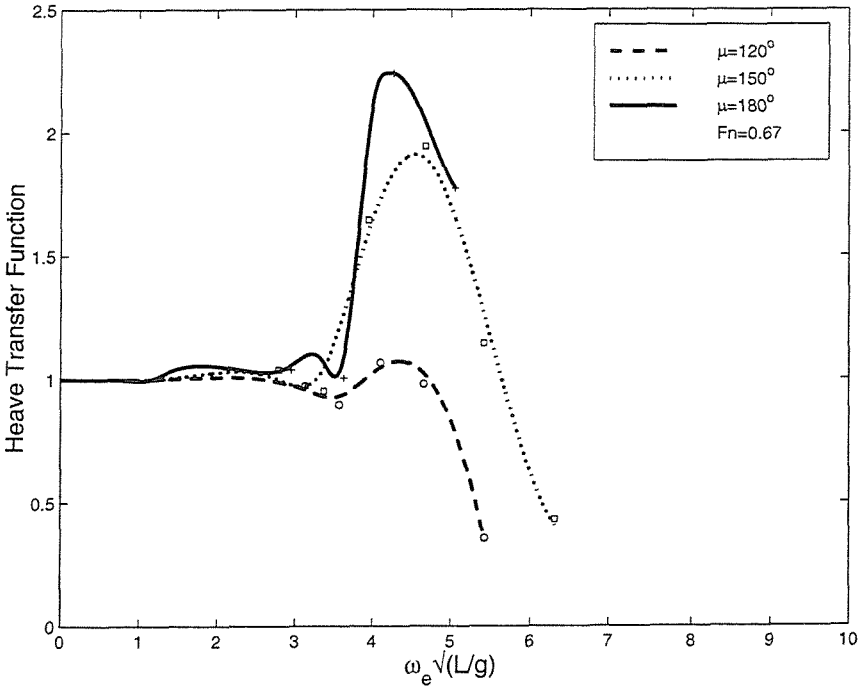

Figure 55: Heave transfer function, Model 5b, S/L=0.4, in oblique seas.

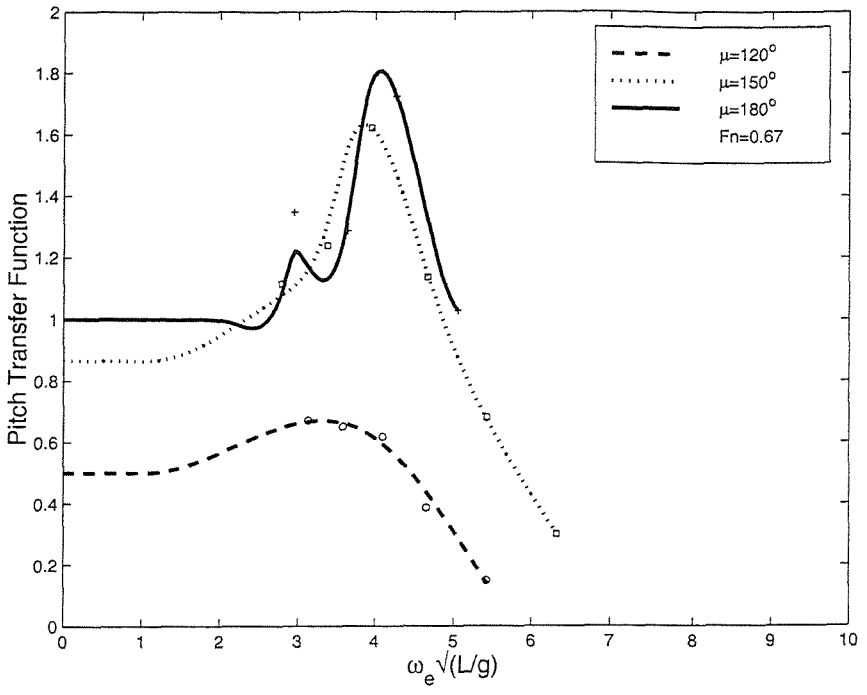

Figure 56: Pitch transfer function, Model 5b, S/L=0.4, in oblique seas.

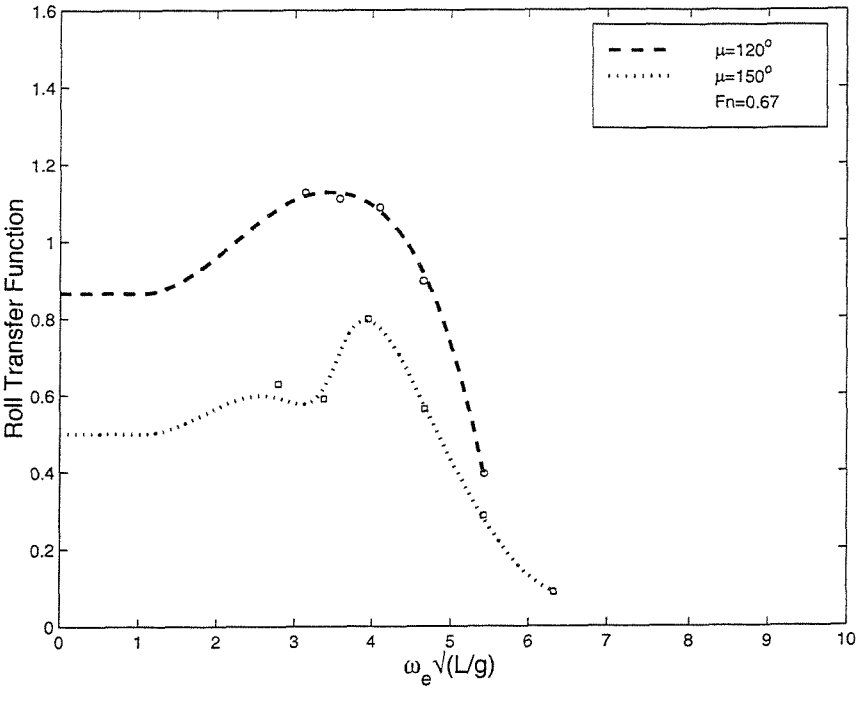

Figure 57: Roll transfer function, Model 5b, S/L=0.4, in oblique seas.

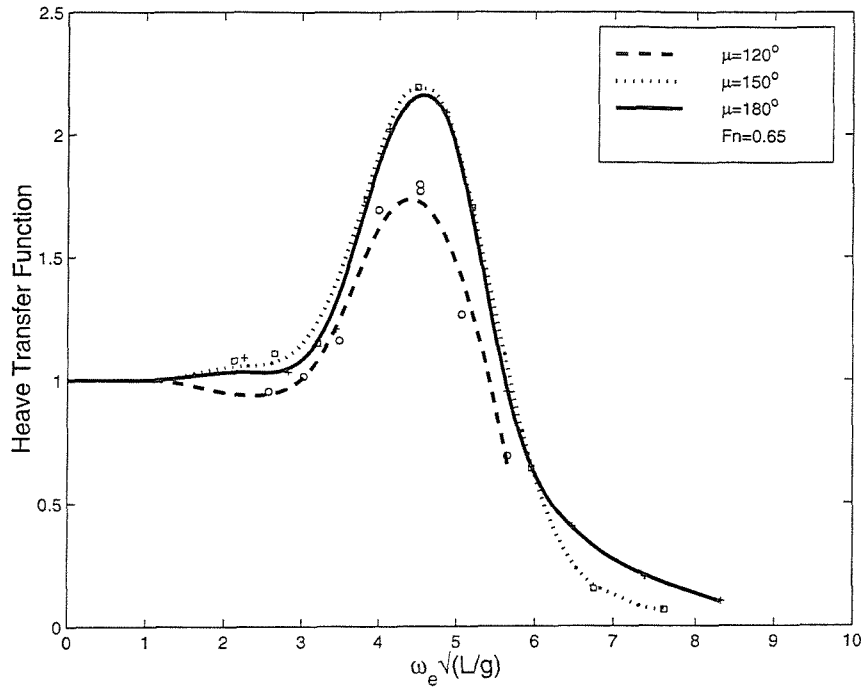

Figure 58: Heave transfer function, Model 5s, S/L=0.2, in oblique seas.

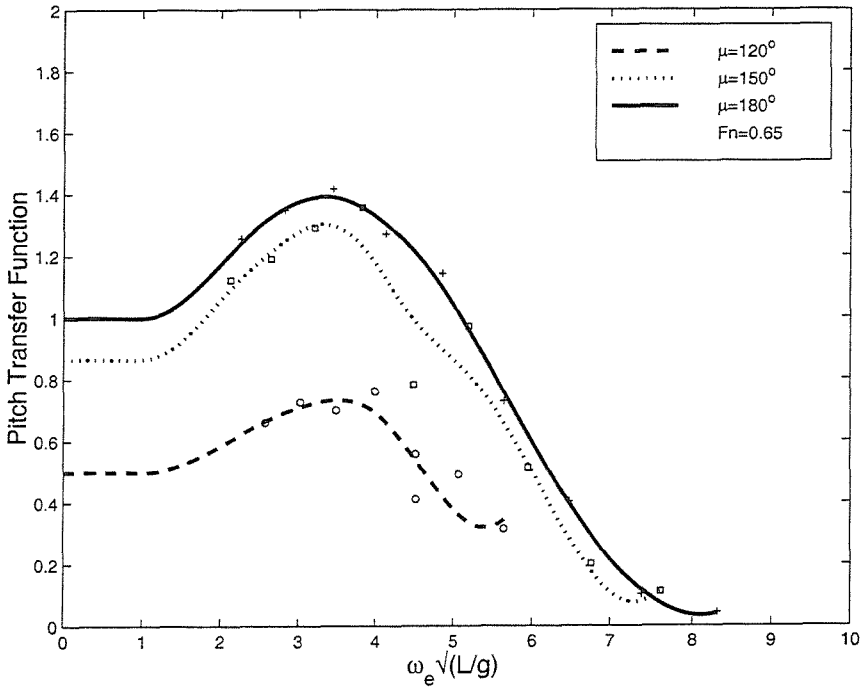

Figure 59: Pitch transfer function, Model 5s, S/L=0.2, in oblique seas.

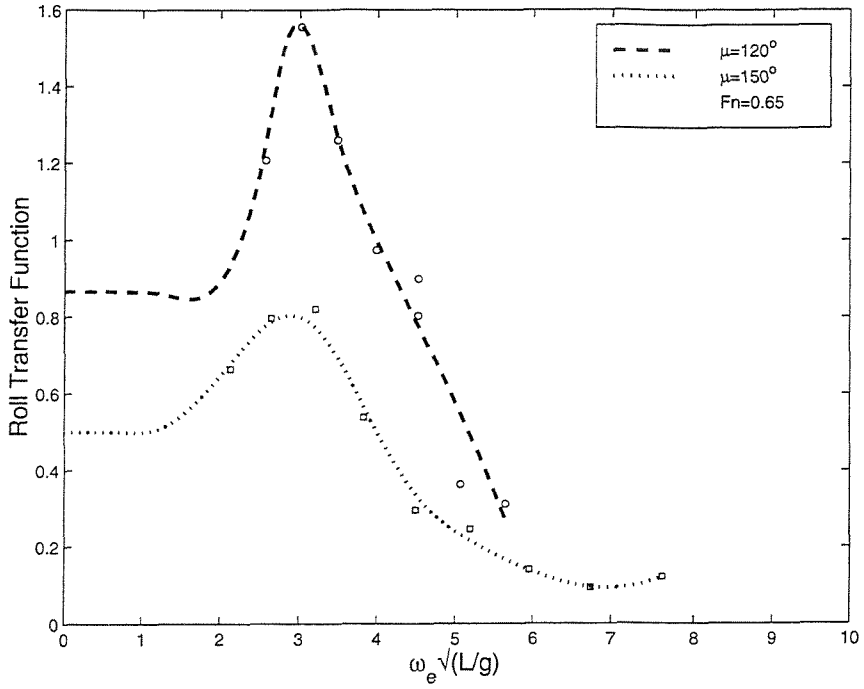

Figure 60: Roll transfer function, Model 5s, S/L=0.2, in oblique seas.

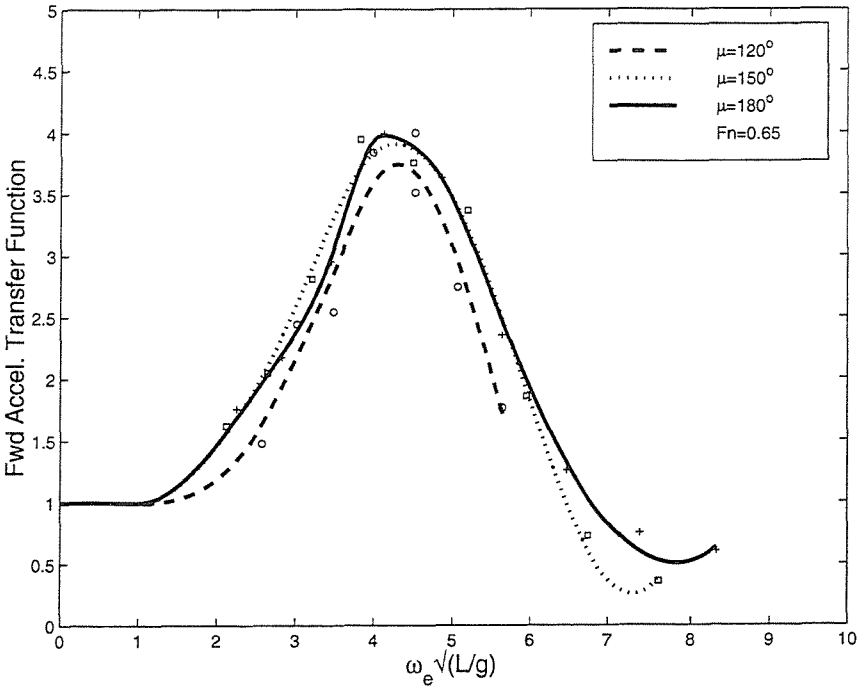

Figure 61: Acceleration at Bow transfer function, Model 5s, S/L=0.2, in oblique seas.

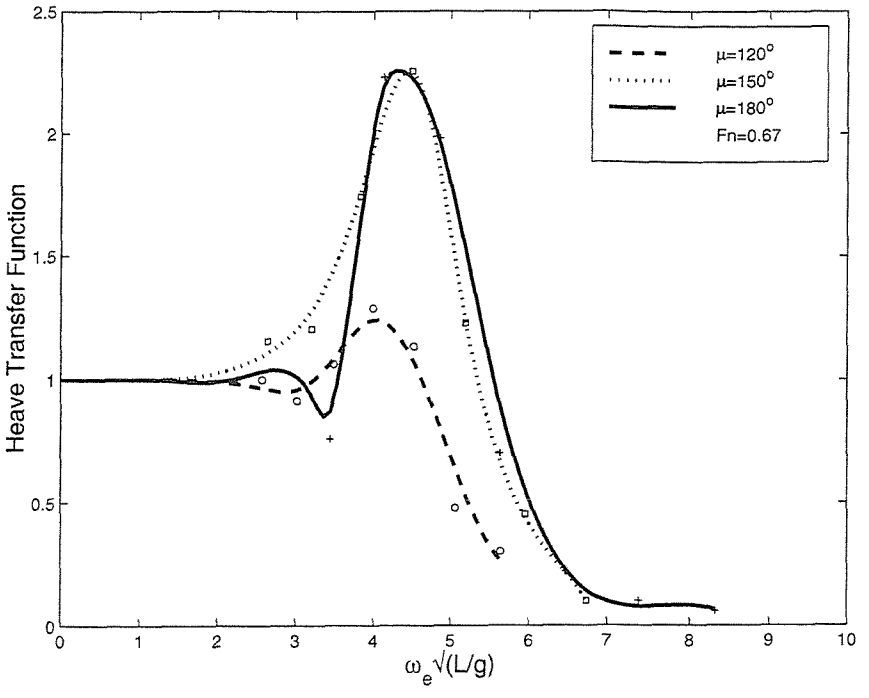

Figure 62: Heave transfer function, Model 5s, S/L=0.4, in oblique seas.

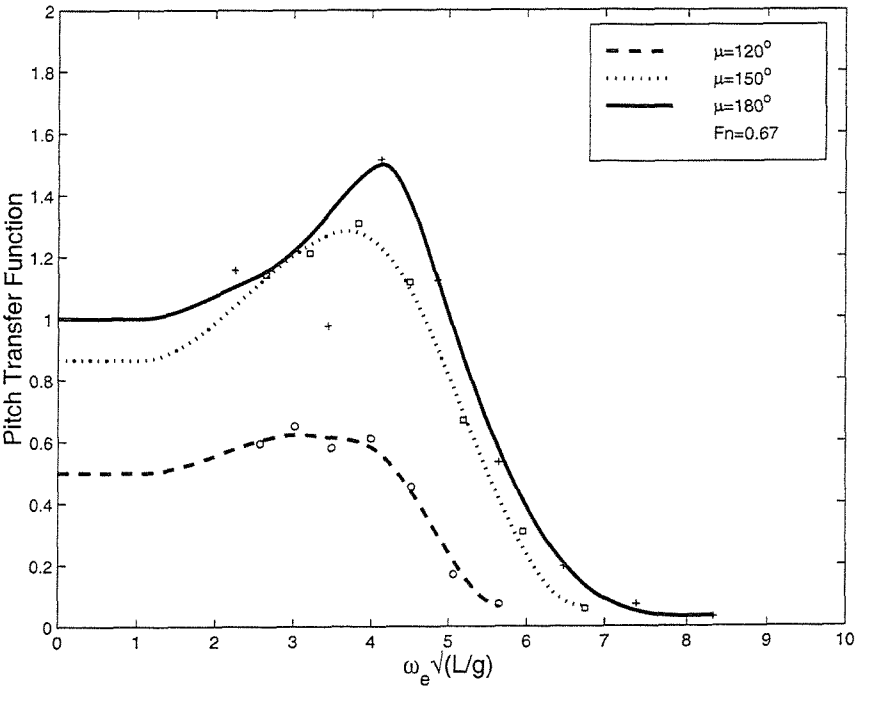

Figure 63: Pitch transfer function, Model 5s, S/L=0.4, in oblique seas.

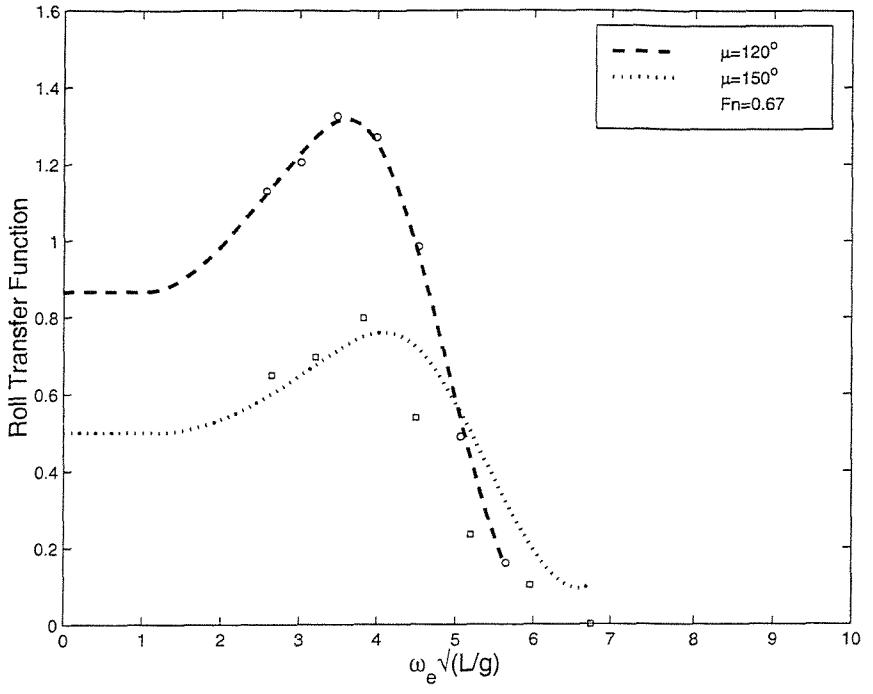

Figure 64: Roll transfer function, Model 5s, S/L=0.4, in oblique seas.

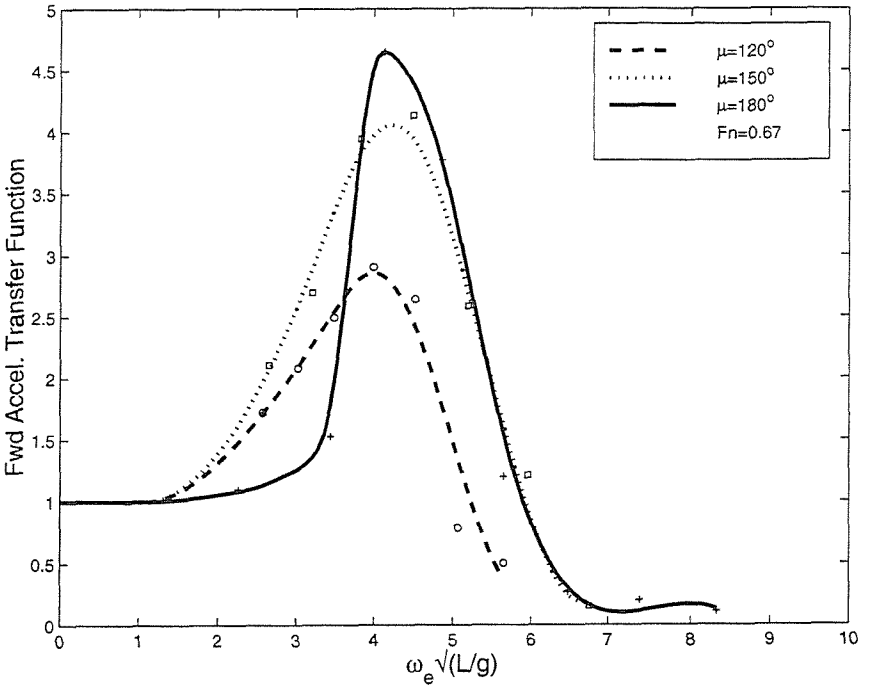

Figure 65: Acceleration at Bow transfer function, Model 5s, S/L=0.4, in oblique seas.

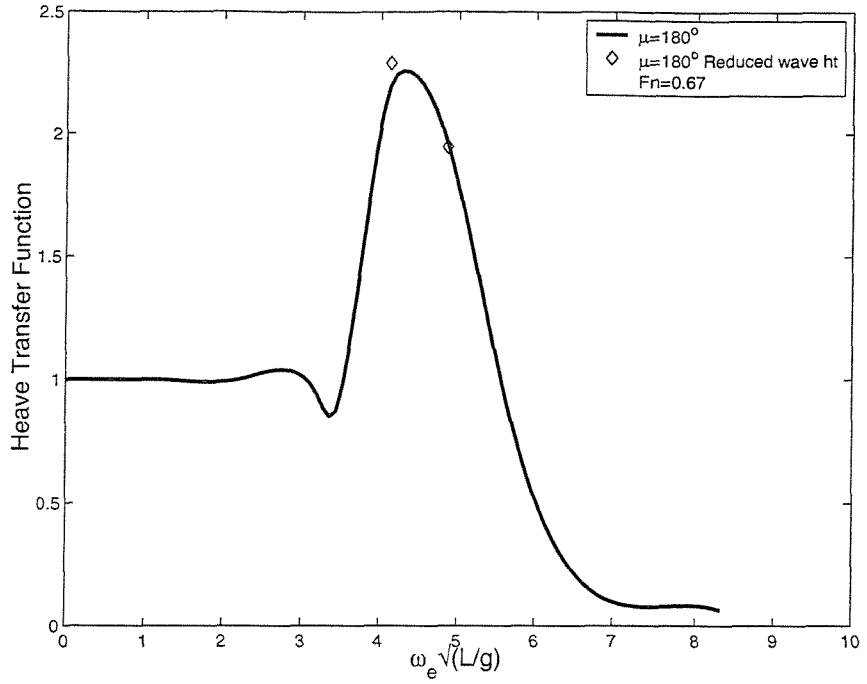

Figure 66: Heave transfer function, Model 5s, S/L=0.4, $\mu =$ 180° showing the influence of reducing the wave height on the transfer function

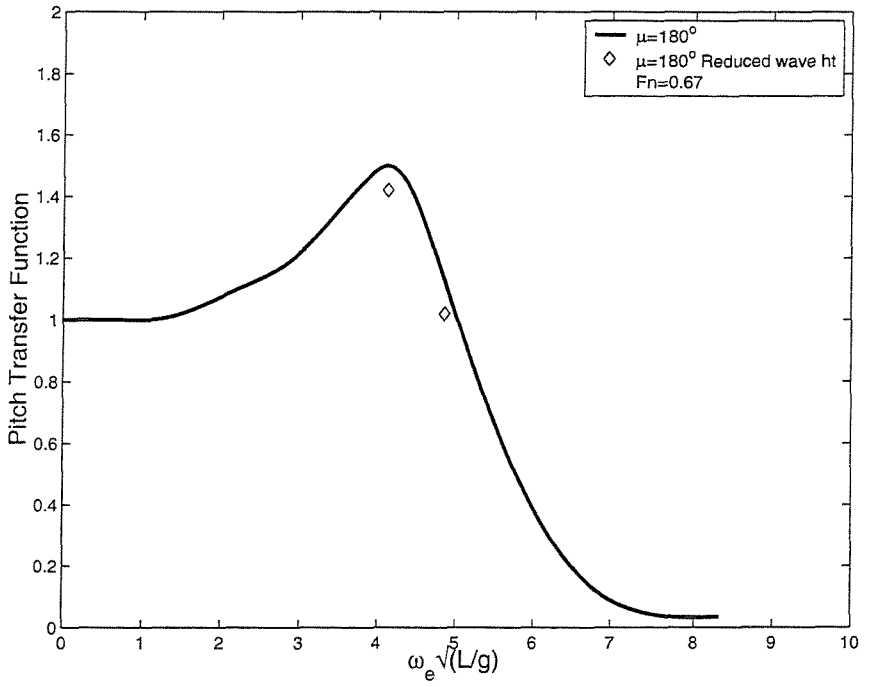

Figure 67: Pitch transfer function, Model 5s, S/L=0.4, $\mu =$ 180° showing the influence of reducing the wave height on the transfer function

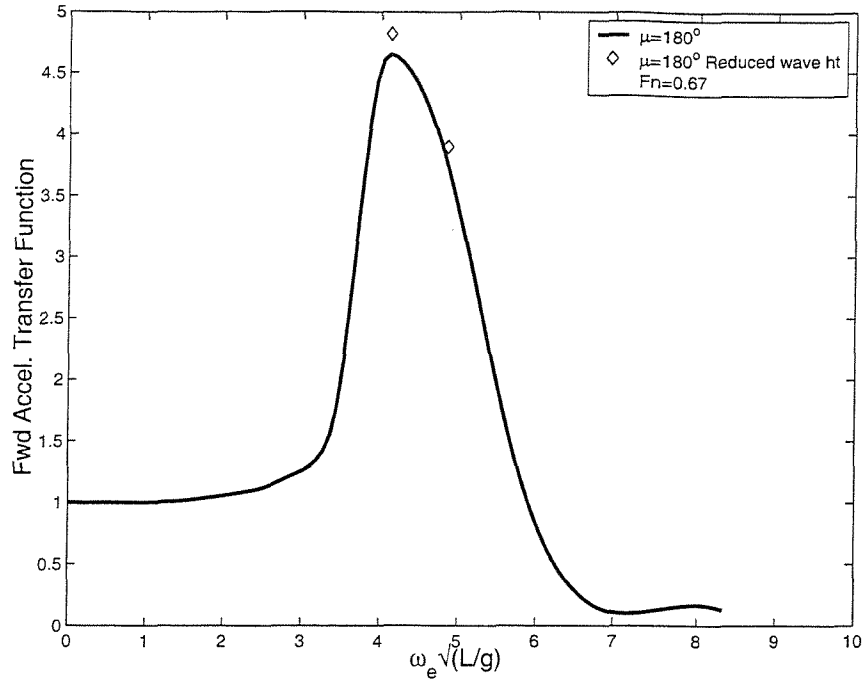

Figure 68: Fwd Accel. transfer function, Model 5s, S/L=0.4, $\mu = 180°$ showing the influence of reducing the wave height on the transfer function

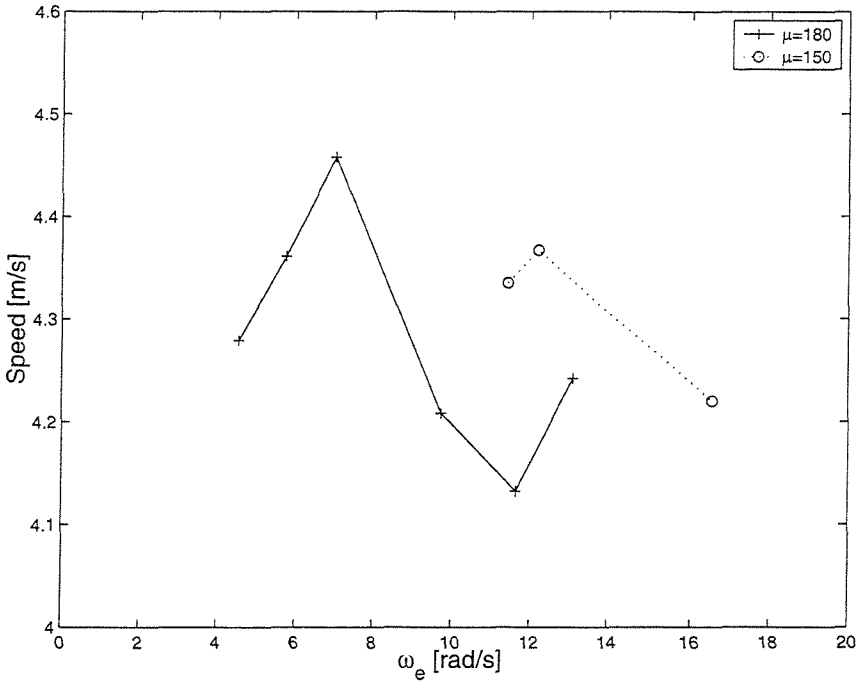

Figure 69: Model 5b, S/L=0.2 Speed Loss

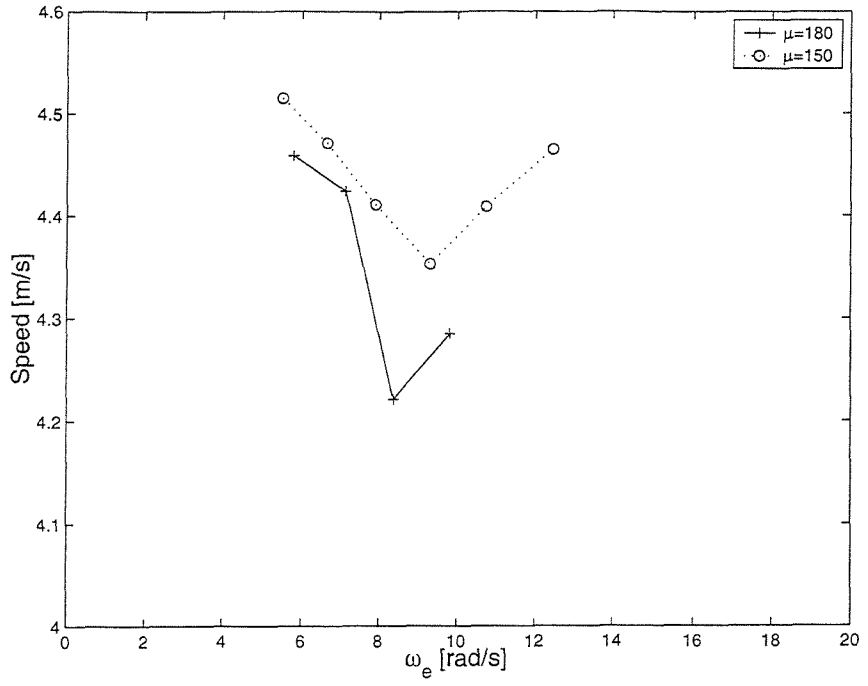

Figure 70: Model 5b, S/L=0.4 Speed Loss

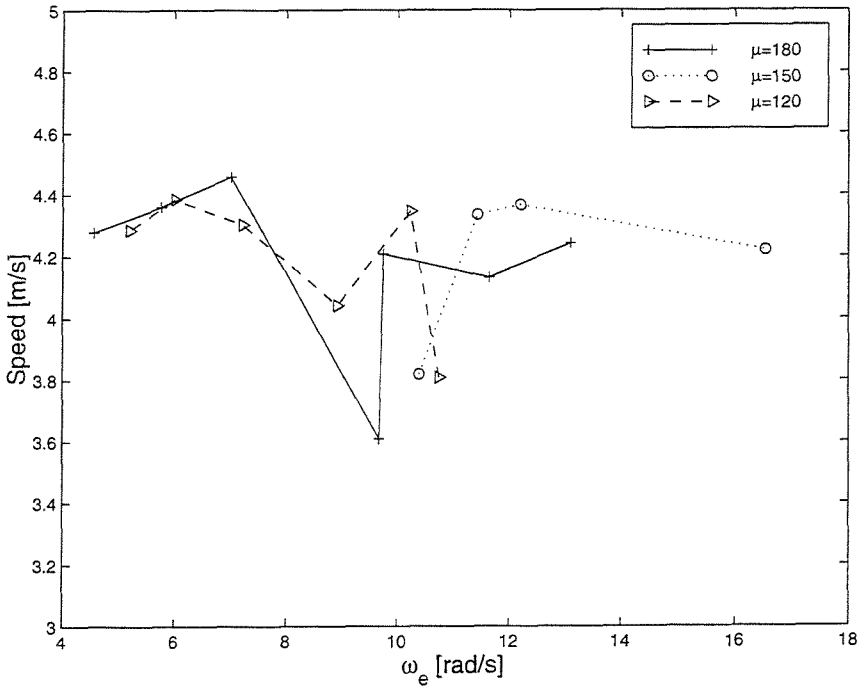

Figure 71: Model 5s, S/L=0.2 Speed Loss

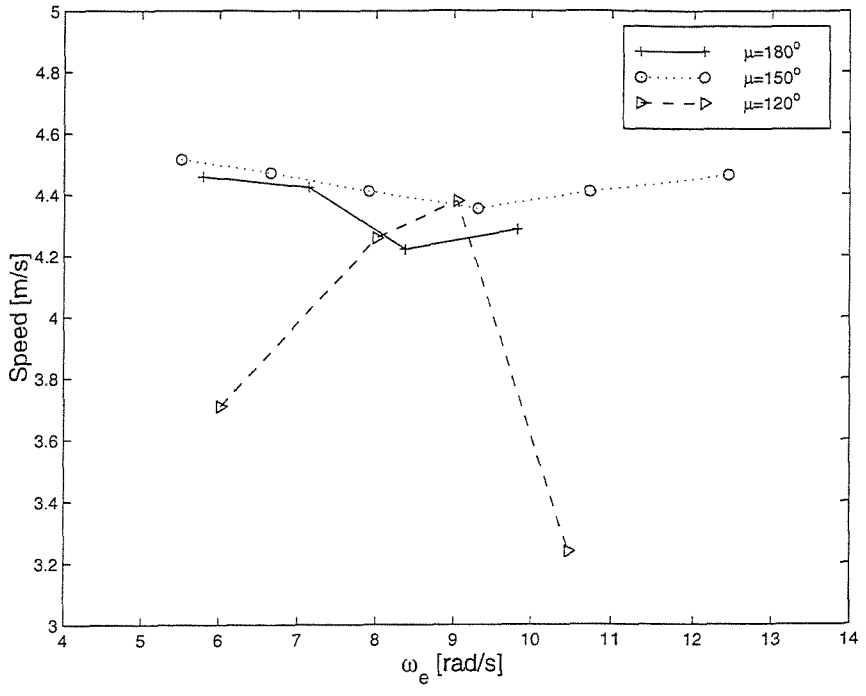

Figure 72: Model 5s, S/L=0.4 Speed Loss

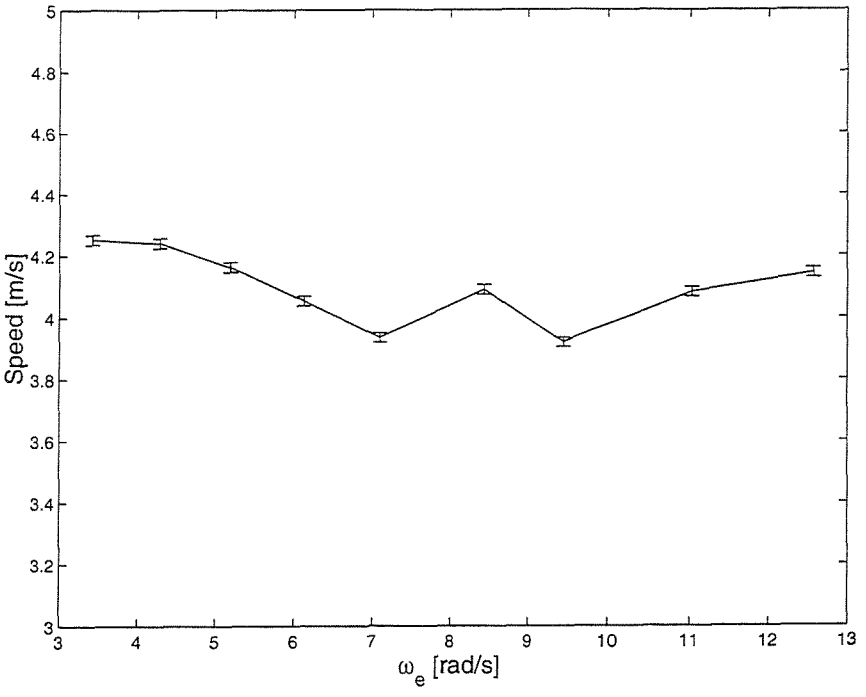

Figure 73: Model 5s, S/L=0.2, $\mu = 180°$, Effect of 5° change in heading on speed loss

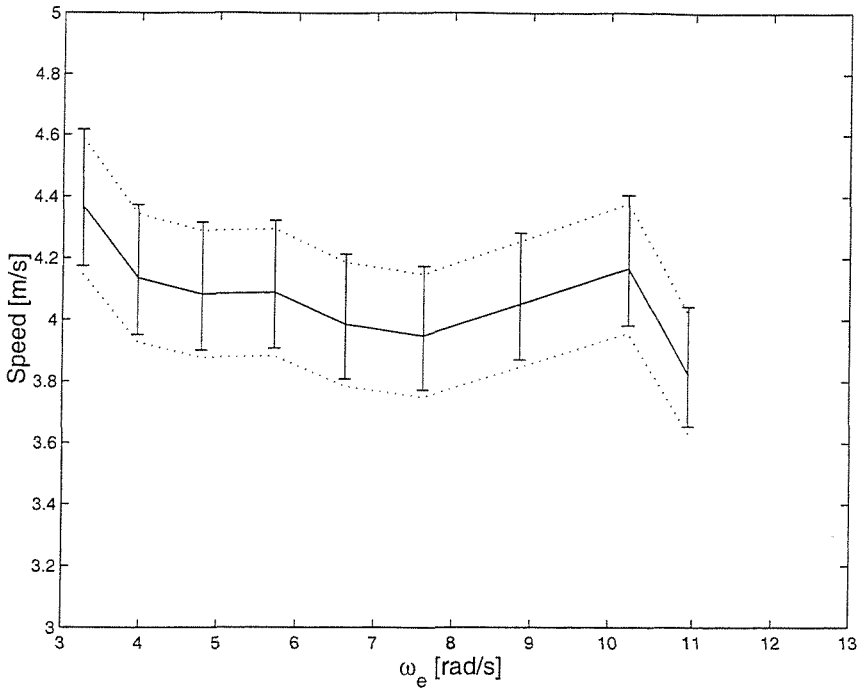

Figure 74: Model 5s, S/L=0.2, $\mu = 150°$, Effect of 5° change in heading on speed loss. Dotted lines show $du/d\mu$.

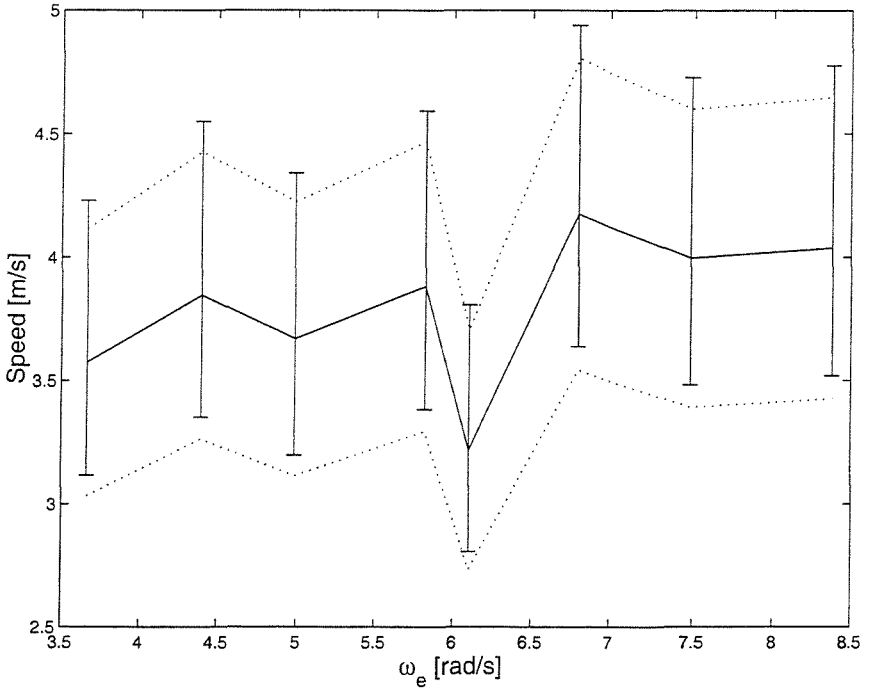

Figure 75: Model 5s, S/L=0.2 $\mu = 120°$, Effect of 5° change in heading on speed loss. Dotted lines show $du/d\mu$.

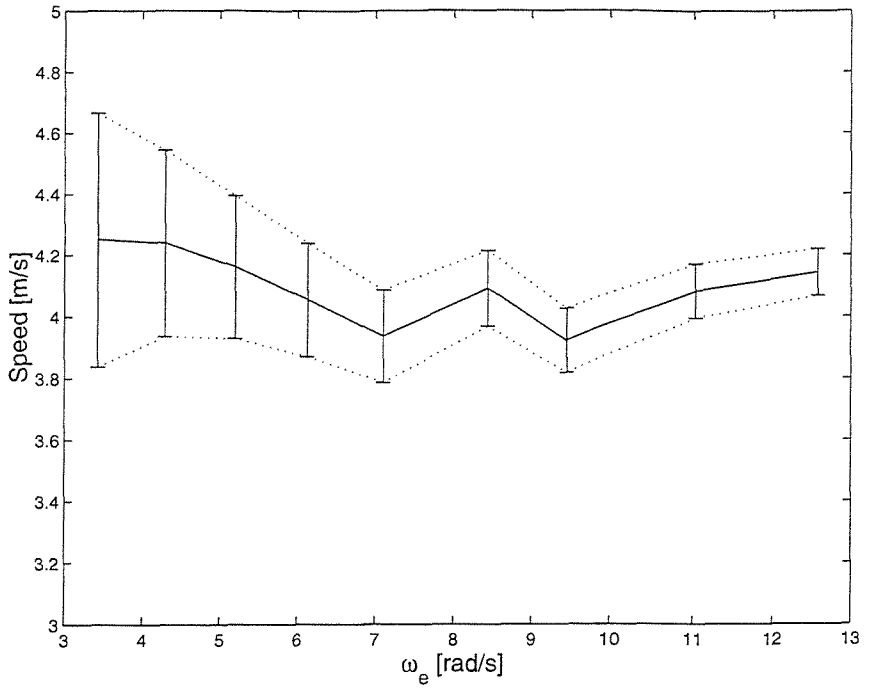

Figure 76: Model 5s, S/L=0.2, $\mu = 180°$, Effect of ω_e change on speed loss. Dotted lines show $du/d\omega_e$.

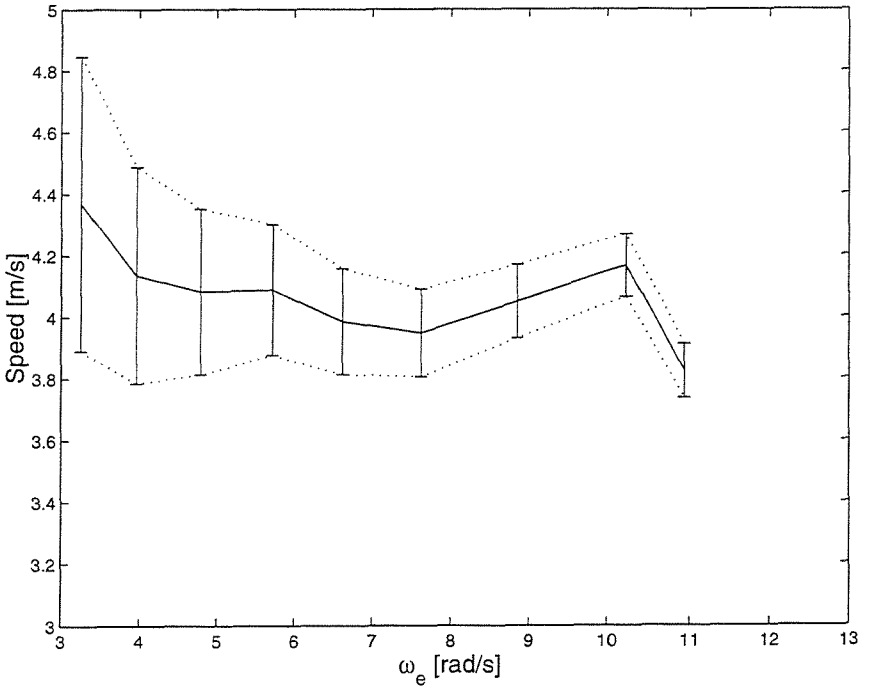

Figure 77: Model 5s, S/L=0.2, $\mu = 150°$, Effect of ω_e change on speed loss. Dotted lines show $du/d\omega_e$.

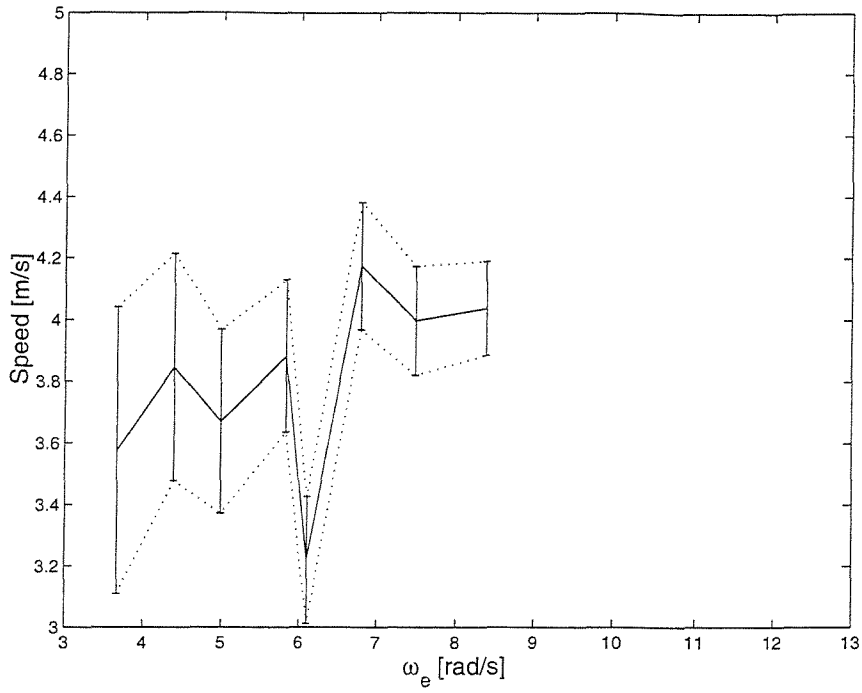

Figure 78: Model 5s, S/L=0.2, $\mu = 120°$, Effect of ω_e change on speed loss. Dotted lines show $du/d\omega_e$.

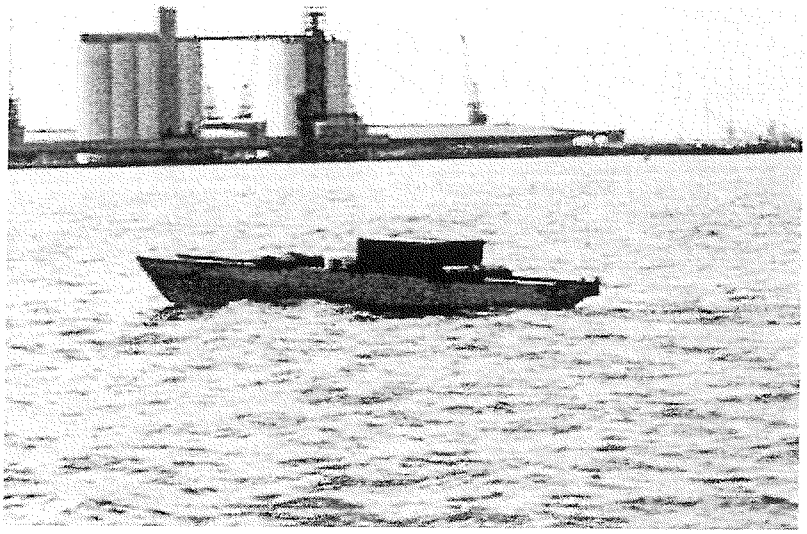

Figure 79: Model 5b, S/L=0.2 on Southampton Water.

Figure 80: Wave Buoy

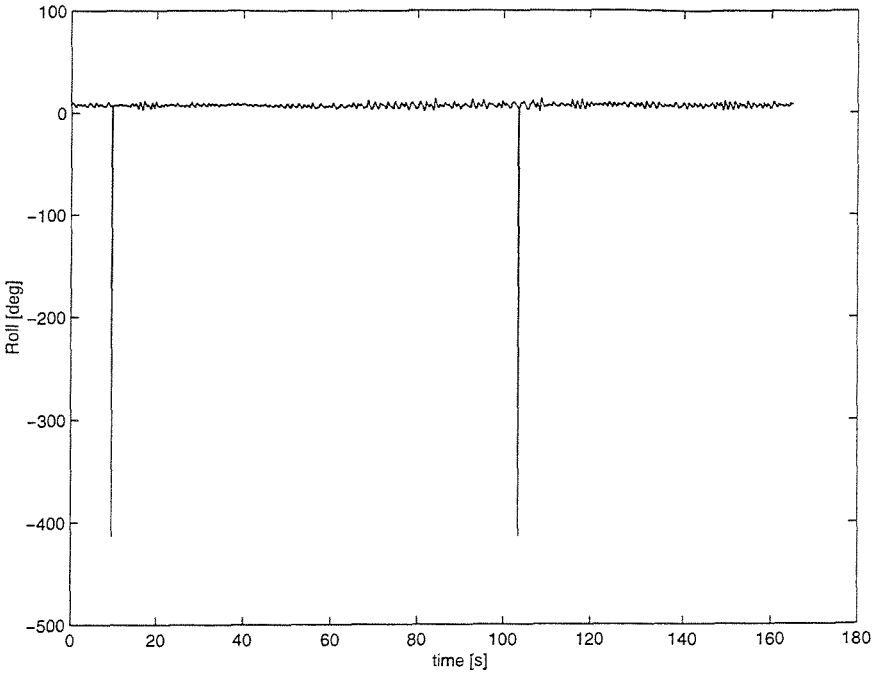

Figure 81: Typical Roll Time History

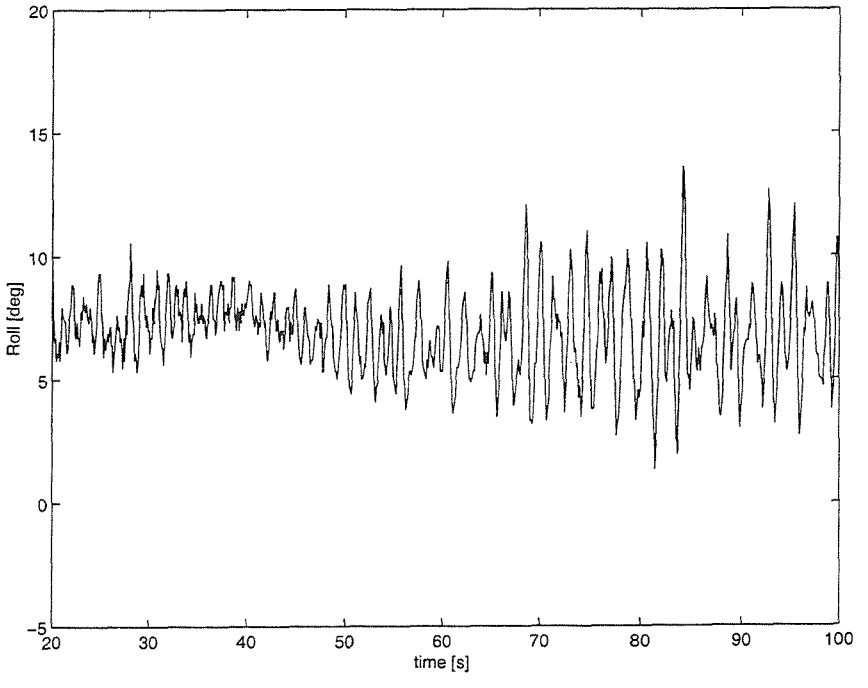

Figure 82: Windowed Roll Data

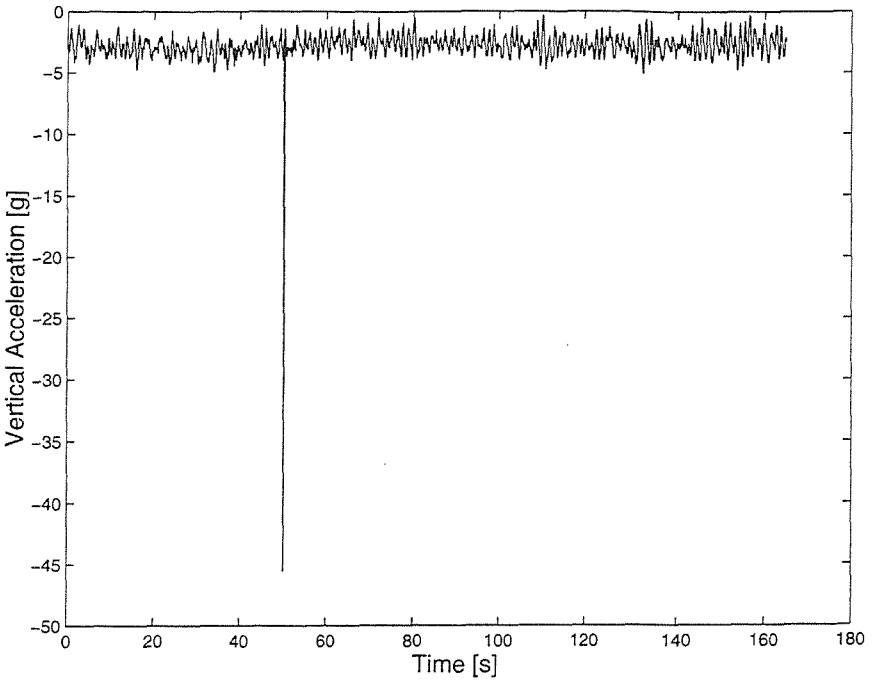

Figure 83: Typical wave buoy Time History

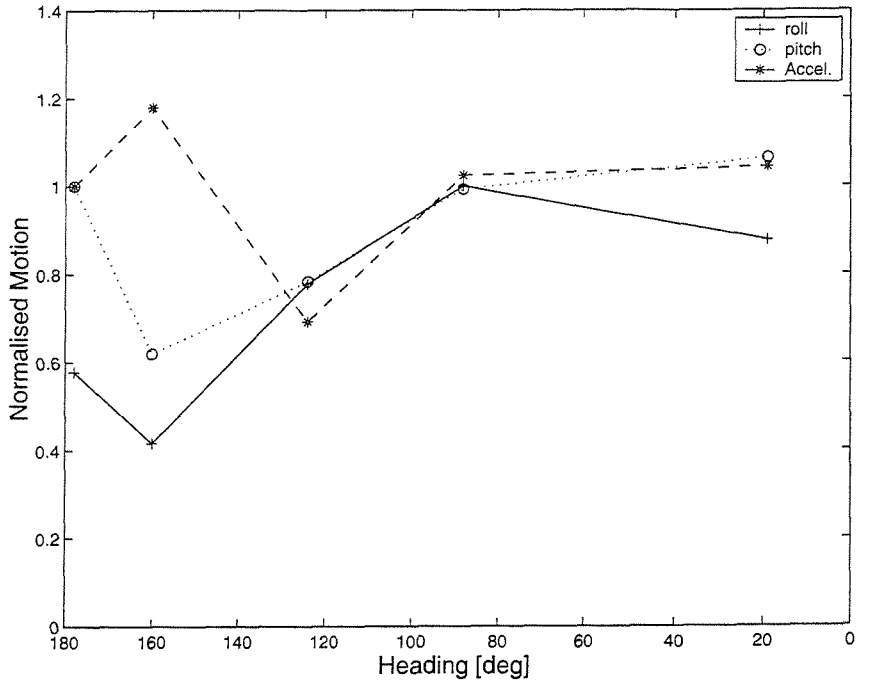

Figure 84: Normalised RMS Roll, Pitch and Acceleration for Model 5b, S/L=0.4, in Irregular open Seas.

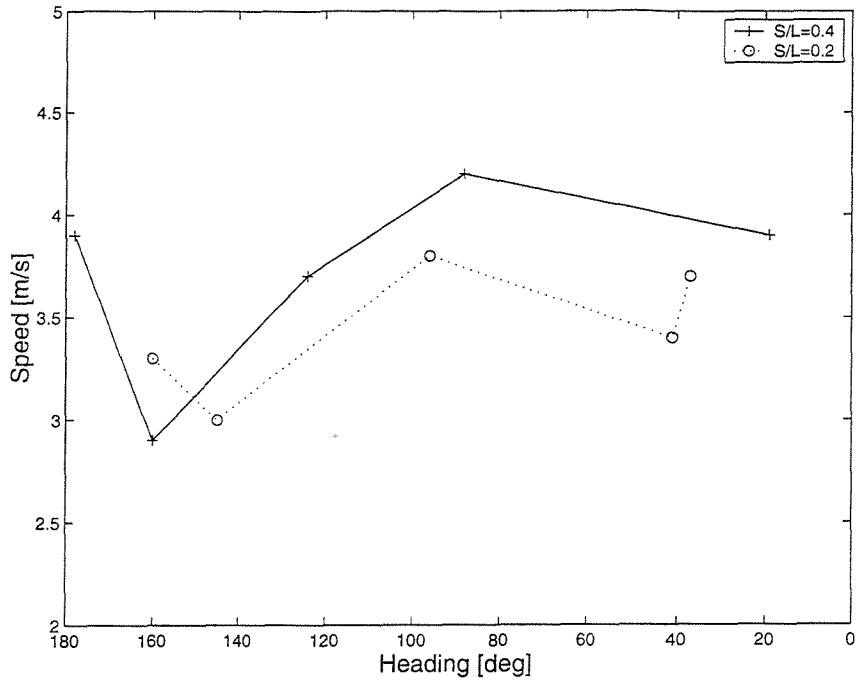

Figure 85: Speed Loss with Heading for Model 5b, in Irregular Seas.

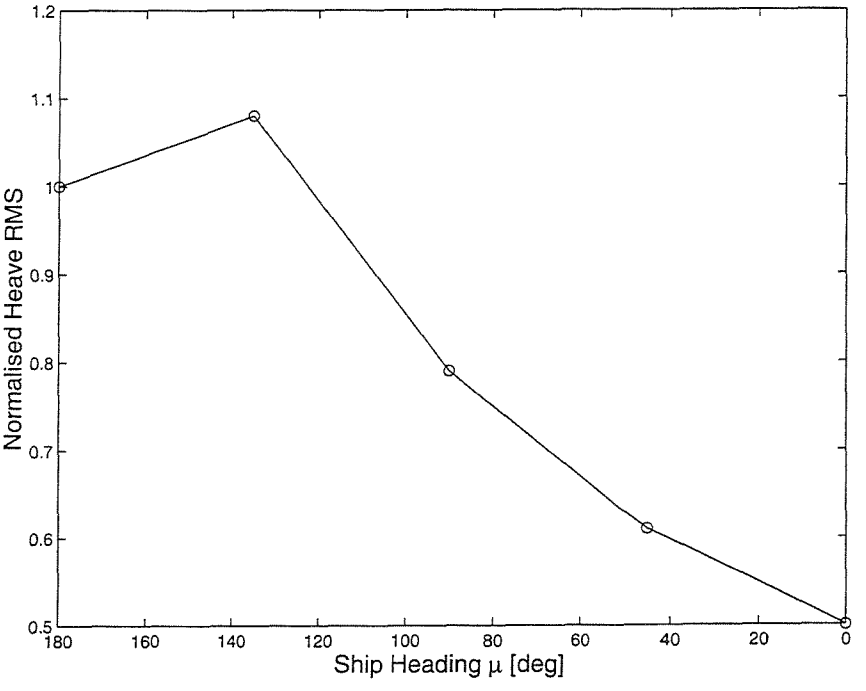

Figure 86: Normalised Heave for an FBM Tricat at 35 knots

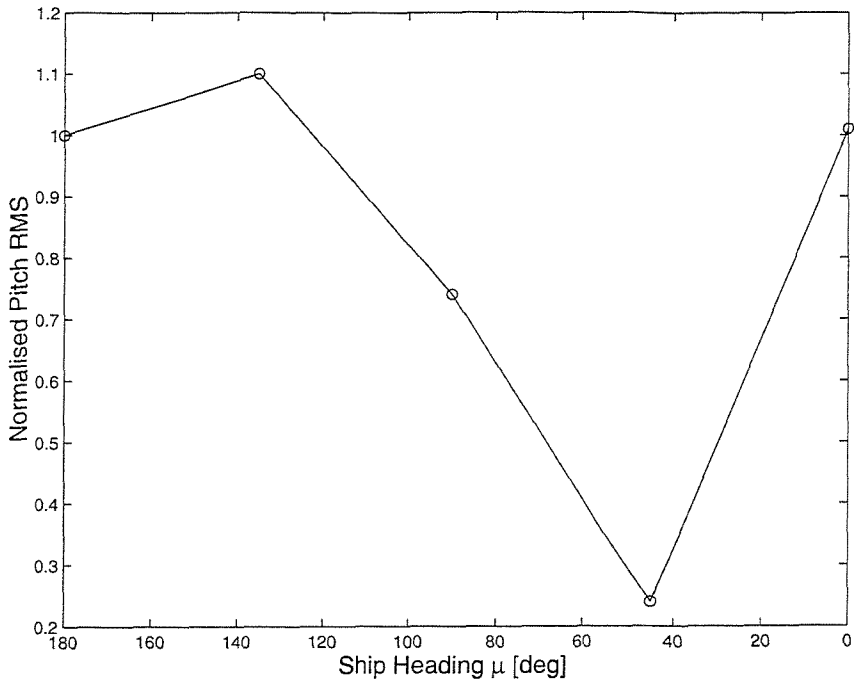

Figure 87: Normalised Pitch for an FBM Tricat at 35 knots

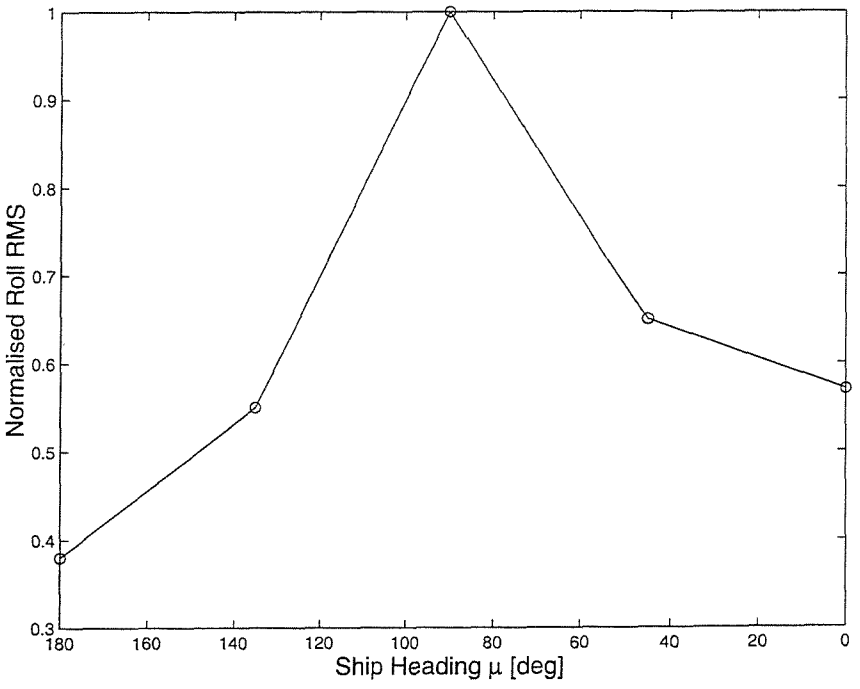

Figure 88: Normalised Roll for an FBM Tricat at 35 knots

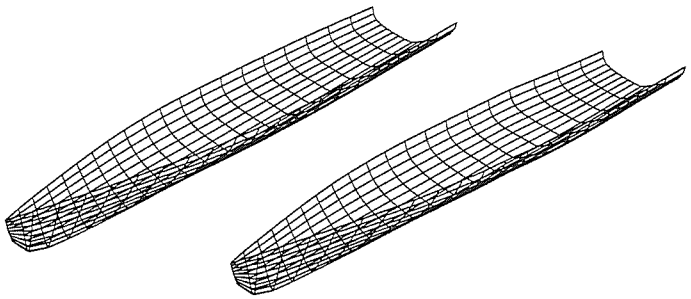

Figure 89: Model 5b S/L=0.2, panelled hulls

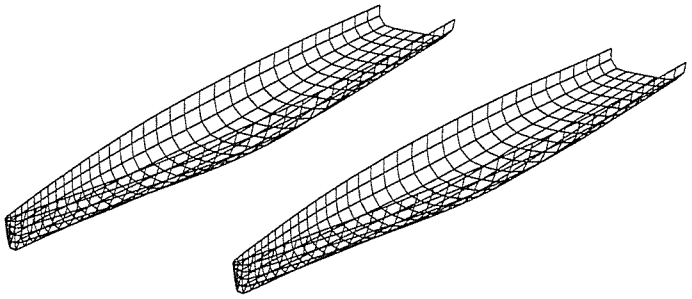

Figure 90: Model 5s S/L=0.2, panelled hulls

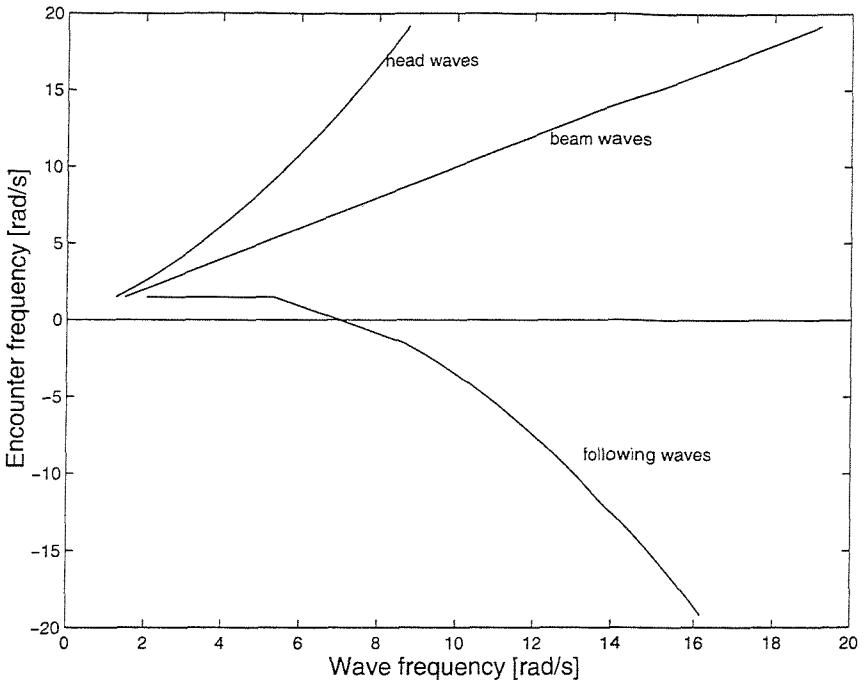

Figure 91: Encounter frequency and heading at the lowest Froude number of 0.2

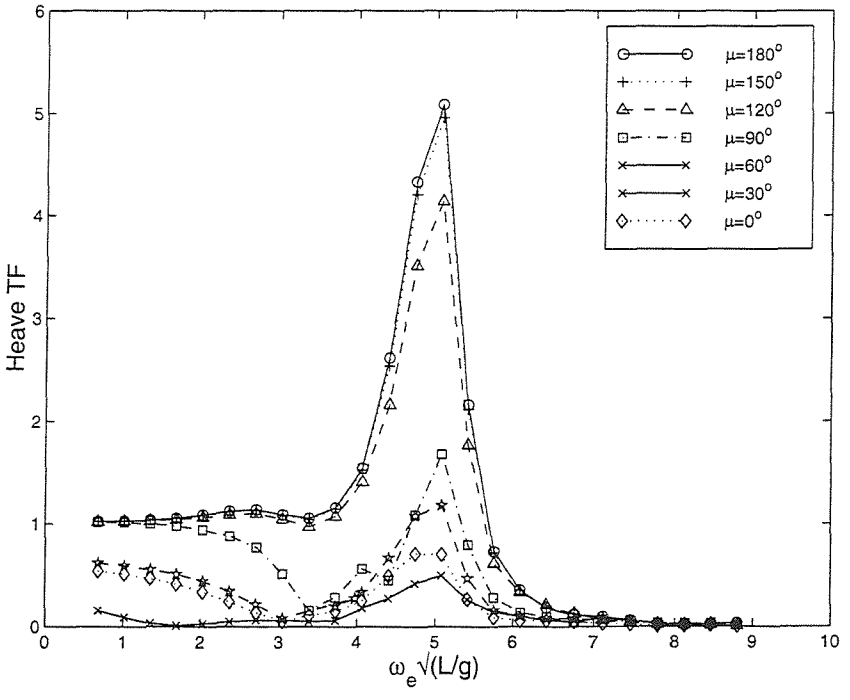

Figure 92: Theoretical heave transfer functions for Model 5s, S/L=0.2, Fn=0.65 at all headings

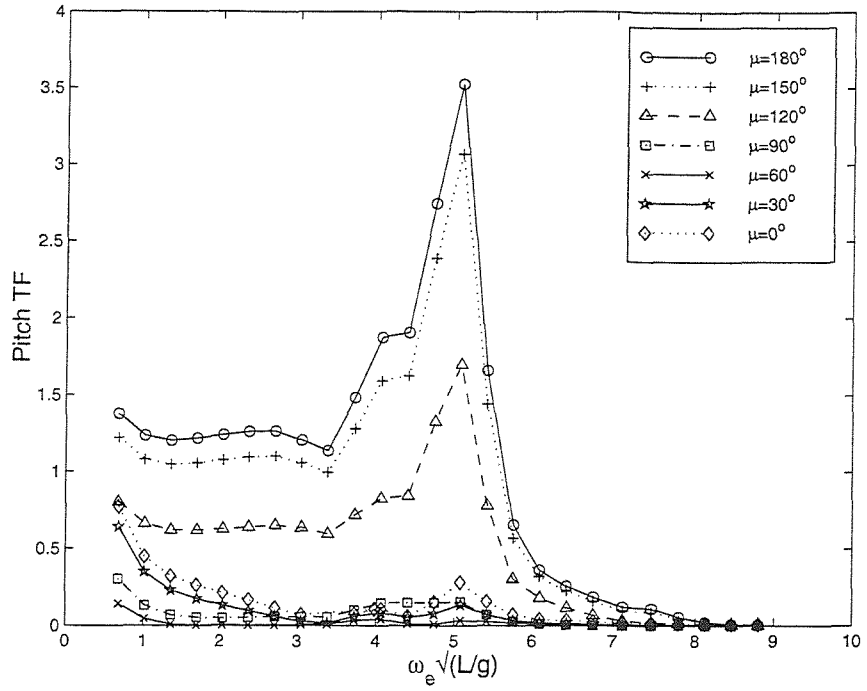

Figure 93: Theoretical pitch transfer functions for Model 5s, S/L=0.2, Fn=0.65 at all headings

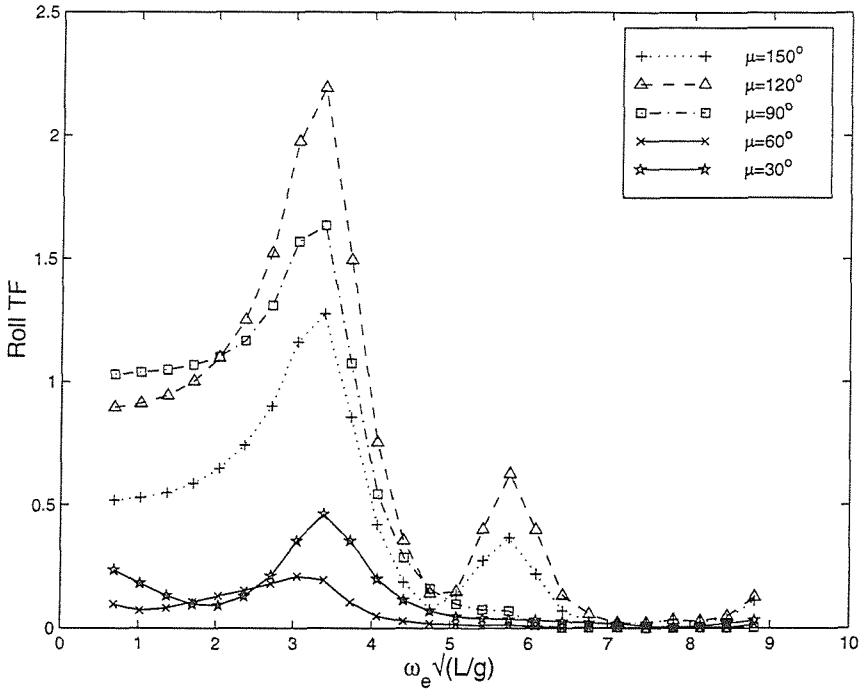

Figure 94: Theoretical roll transfer functions for Model 5s, S/L=0.2, Fn=0.65 at all headings

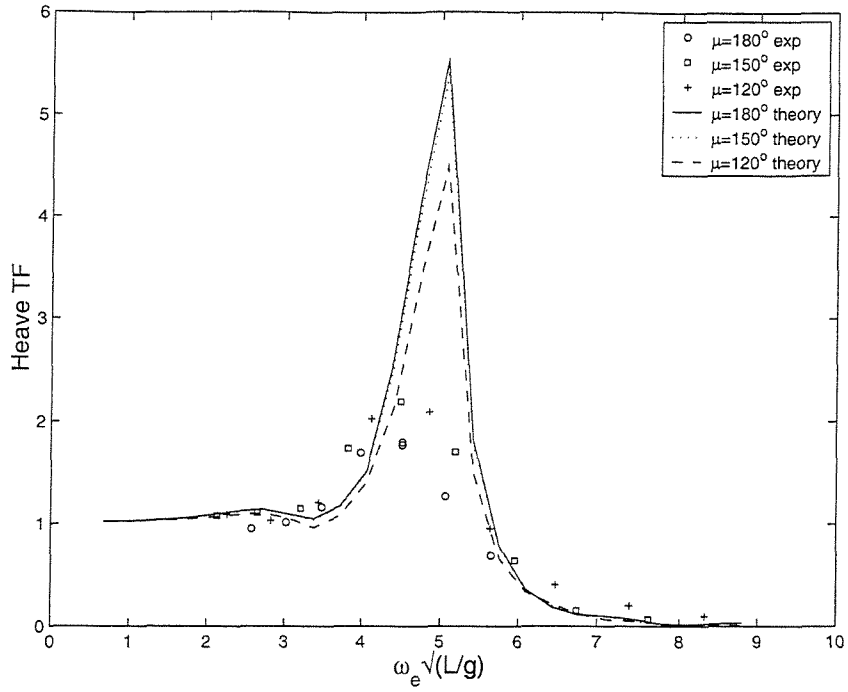

Figure 95: Comparison of experimental and theoretical heave transfer functions for Model 5s, S/L=0.2

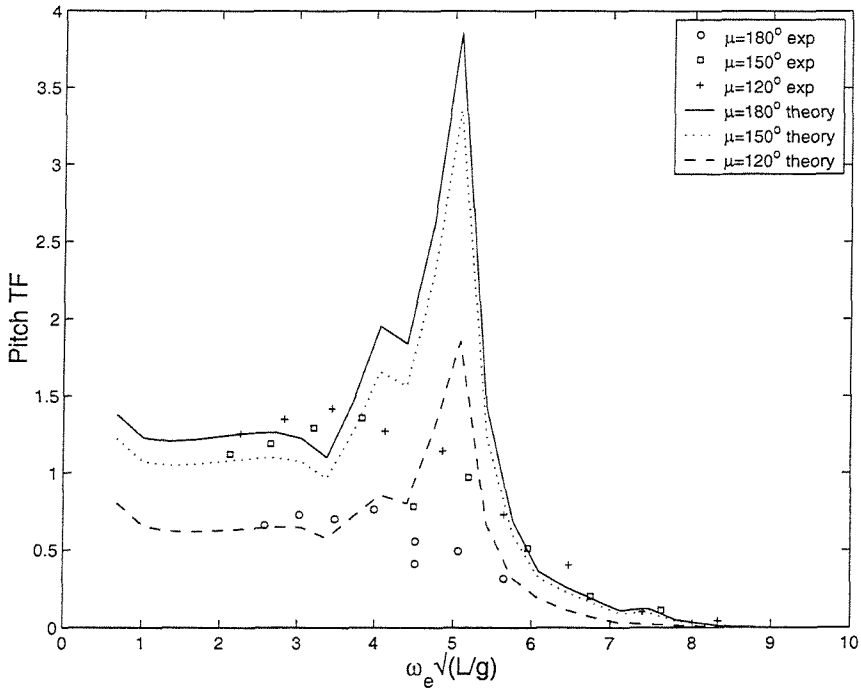

Figure 96: Comparison of experimental and theoretical pitch transfer functions for Model 5s, S/L=0.2

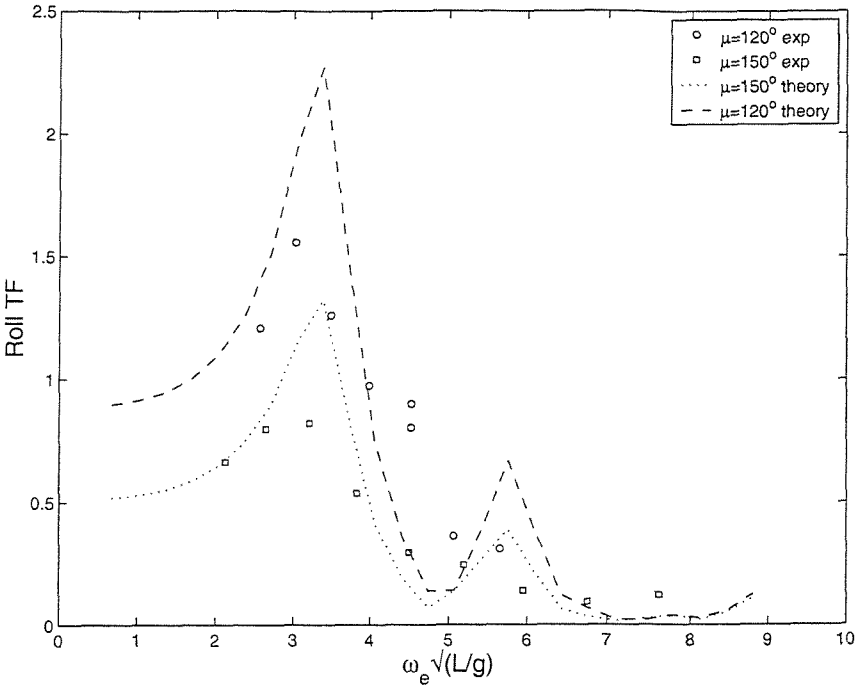

Figure 97: Comparison of experimental and theoretical roll transfer functions for Model 5s, S/L=0.2

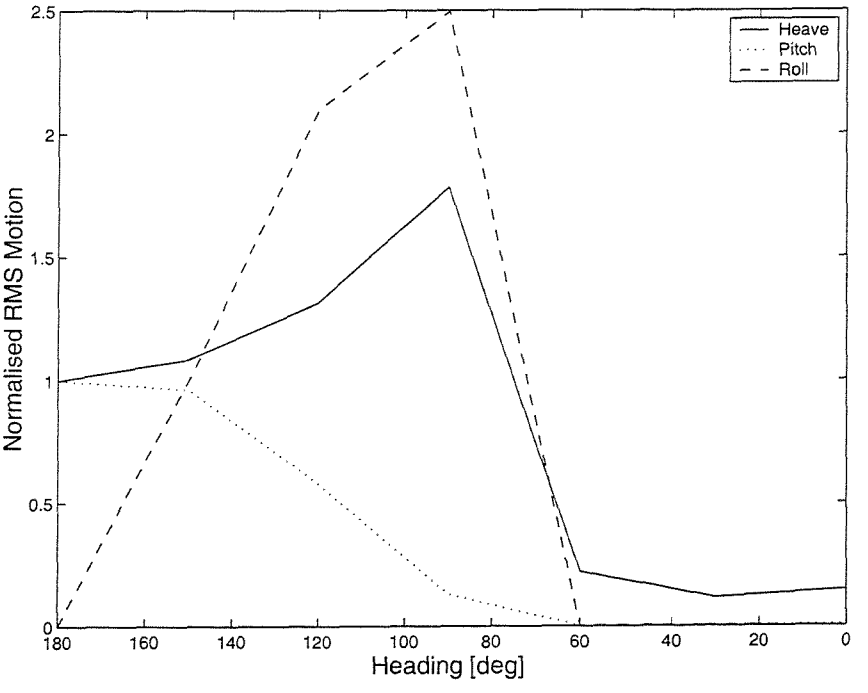

Figure 98: Normalised RMS Motions for Model 5s, S/L=0.2, Fn=0.2

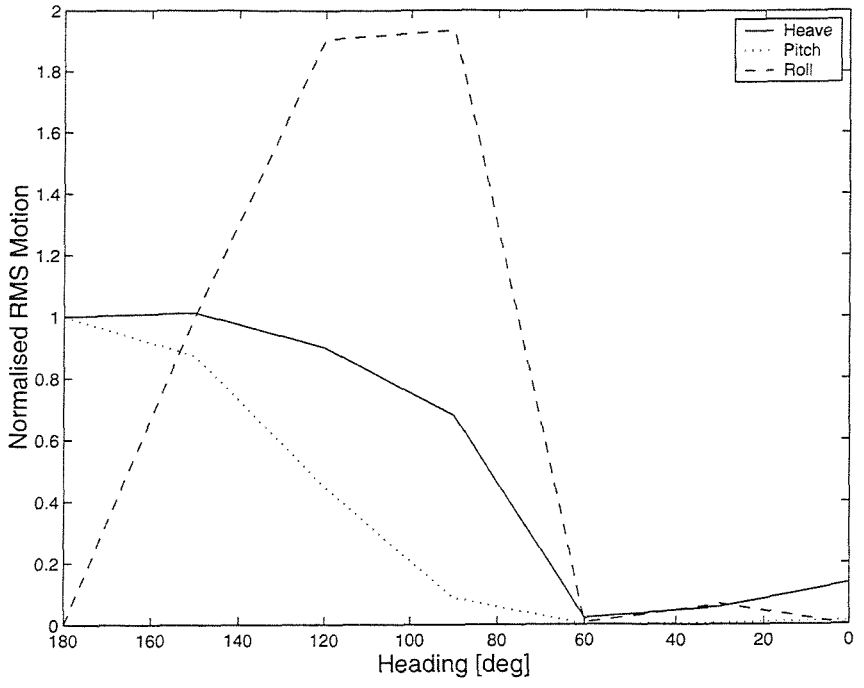

Figure 99: Normalised RMS Motions for Model 5s, S/L=0.2, Fn=0.3

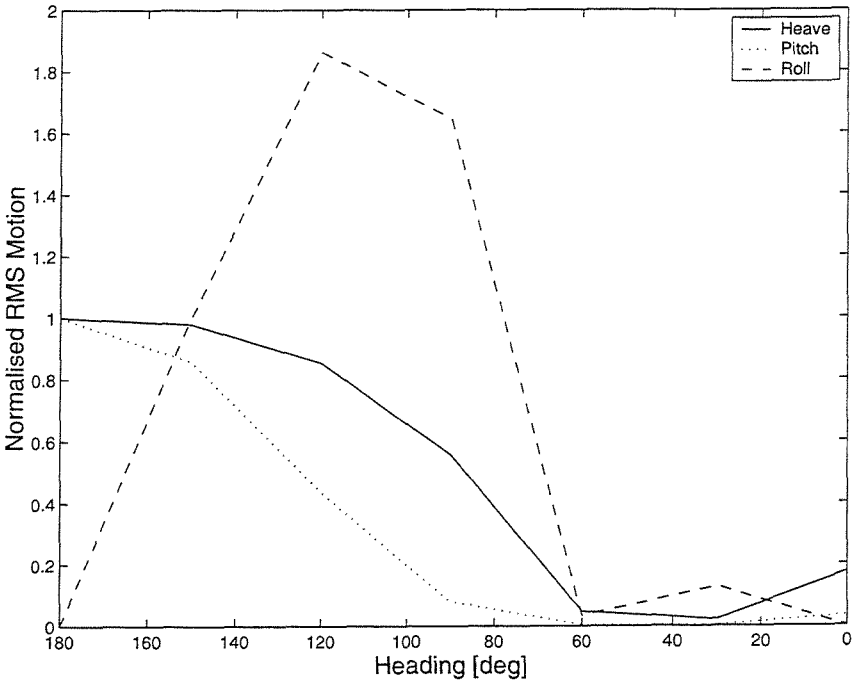

Figure 100: Normalised RMS Motions for Model 5s, S/L=0.2, Fn=0.4

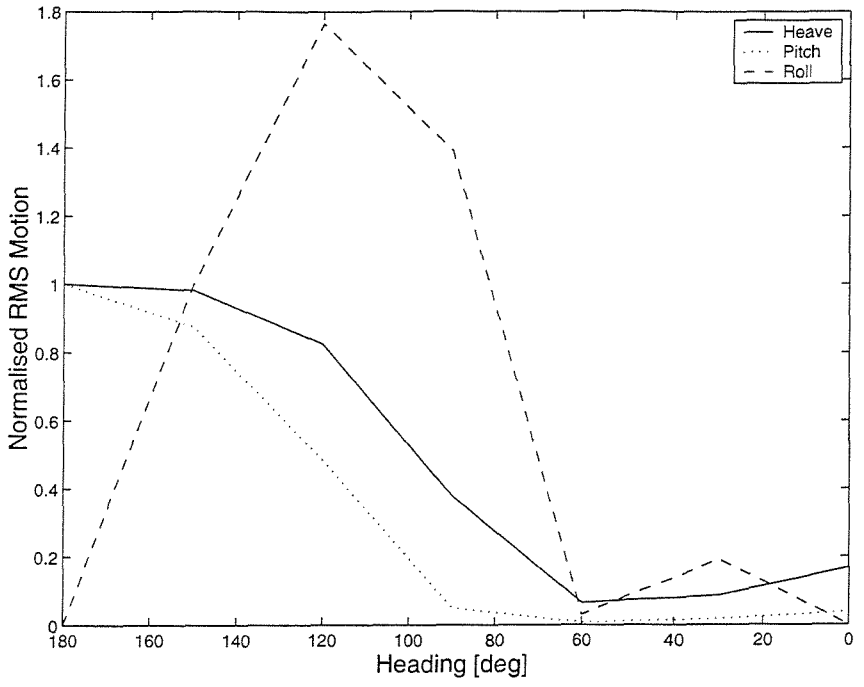

Figure 101: Normalised RMS Motions for Model 5s, S/L=0.2, Fn=0.53

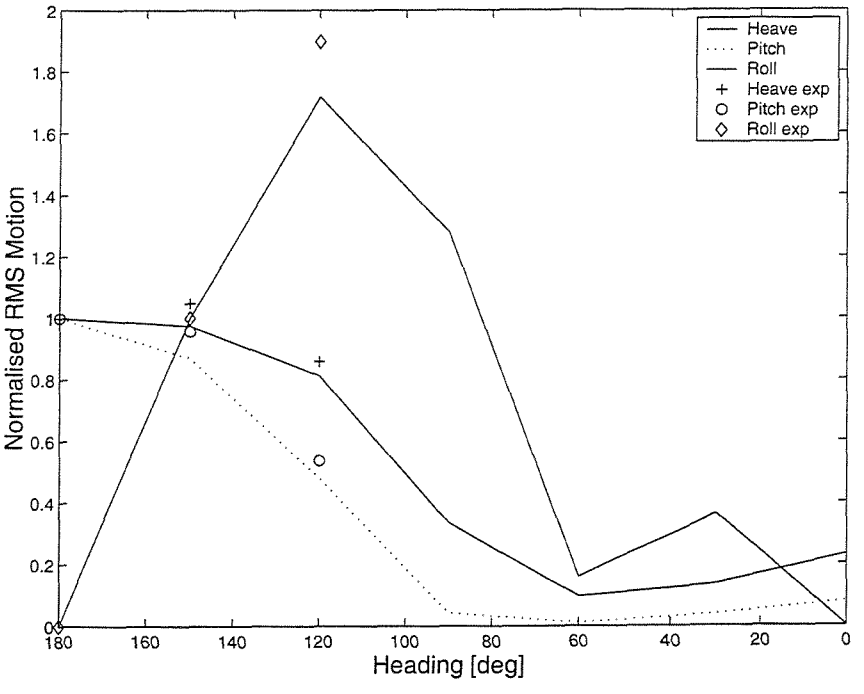

Figure 102: Normalised RMS Motions with experimental points, for Model 5s, S/L=0.2, Fn=0.65.

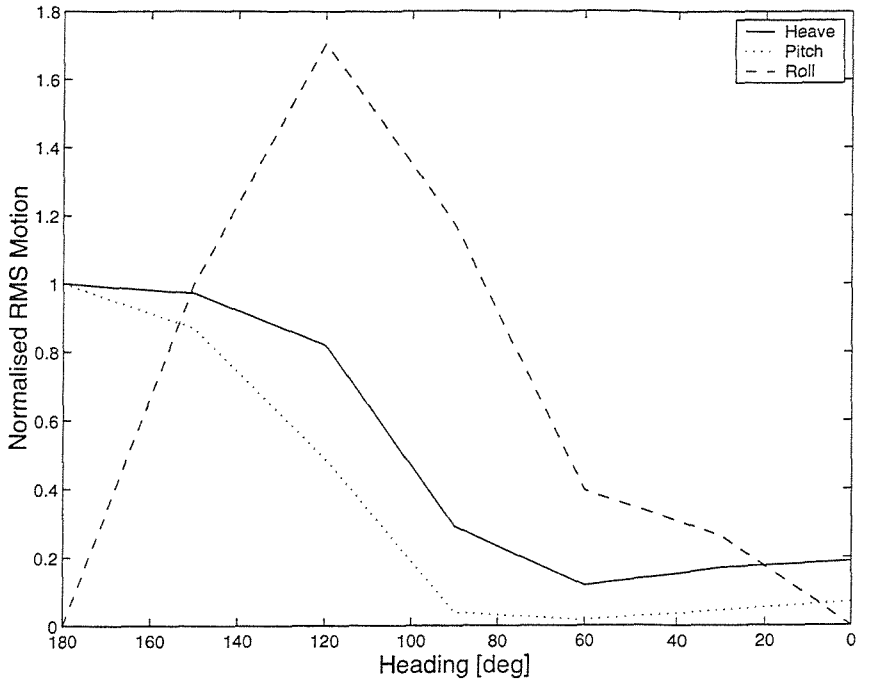

Figure 103: Normalised RMS Motions for Model 5s, S/L=0.2, Fn=0.8

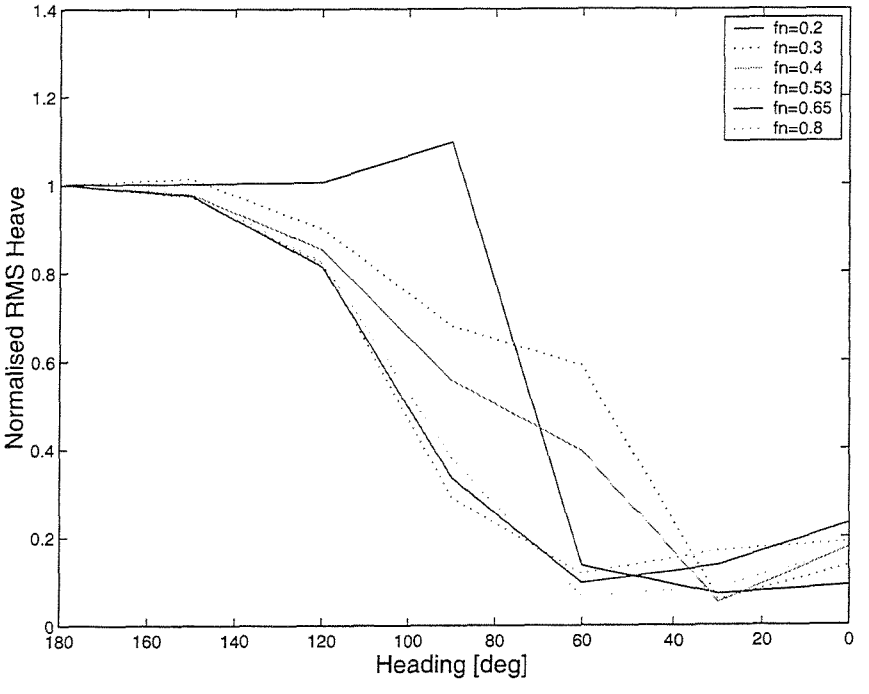

Figure 104: Influence of Froude number on the Normalised RMS Heave for Model 5s, S/L=0.2

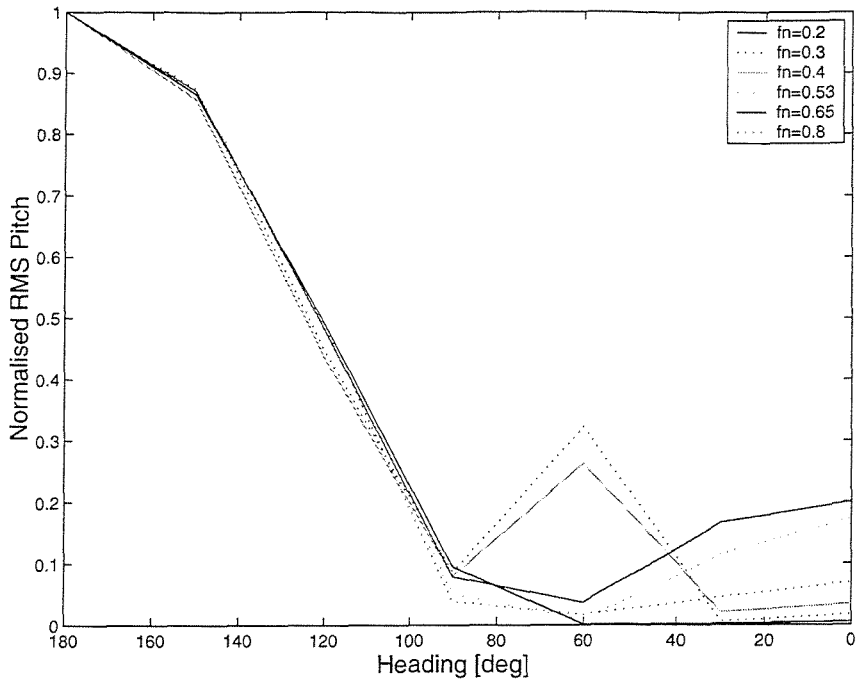

Figure 105: Influence of Froude number on the Normalised RMS Pitch for Model 5s, S/L=0.2

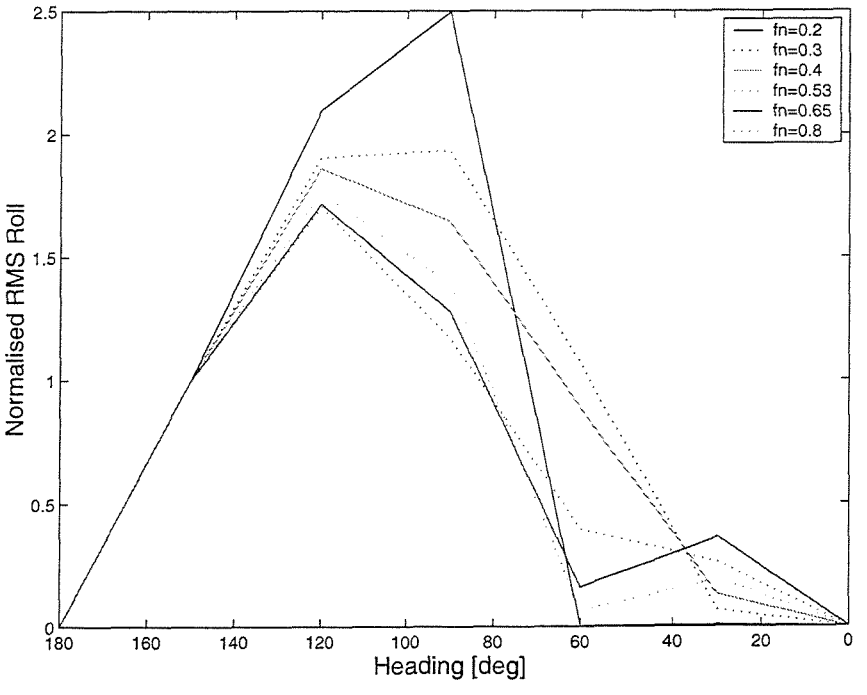

Figure 106: Influence of Froude number on the Normalised RMS Roll for Model 5s, S/L=0.2

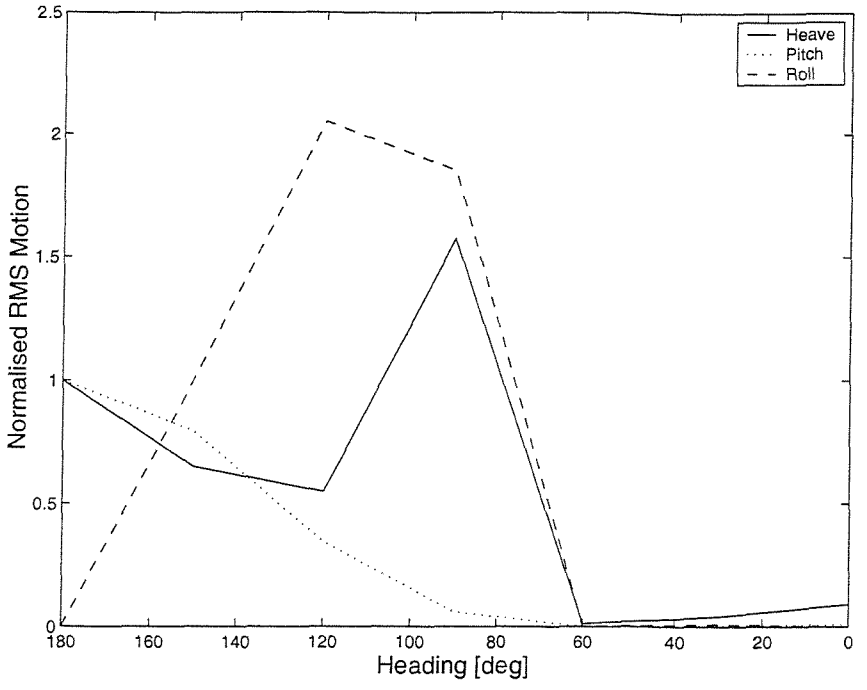

Figure 107: Normalised RMS Motions for Model 5s, S/L=0.4, Fn=0.2

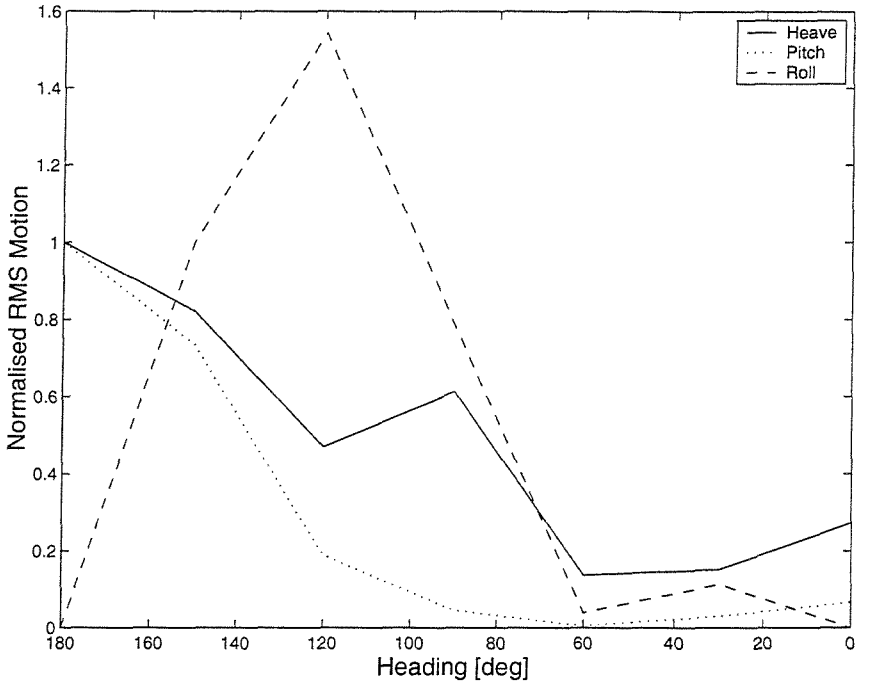

Figure 108: Normalised RMS Motions for Model 5s, S/L=0.4, Fn=0.53

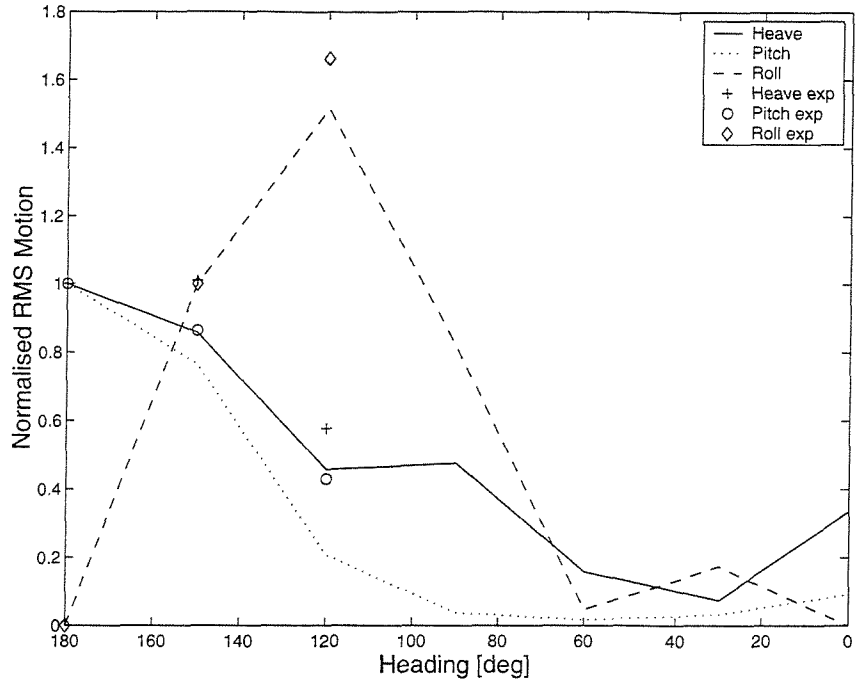

Figure 109: Normalised RMS Motions with experimental points, for Model 5s, S/L=0.4, Fn=0.65.

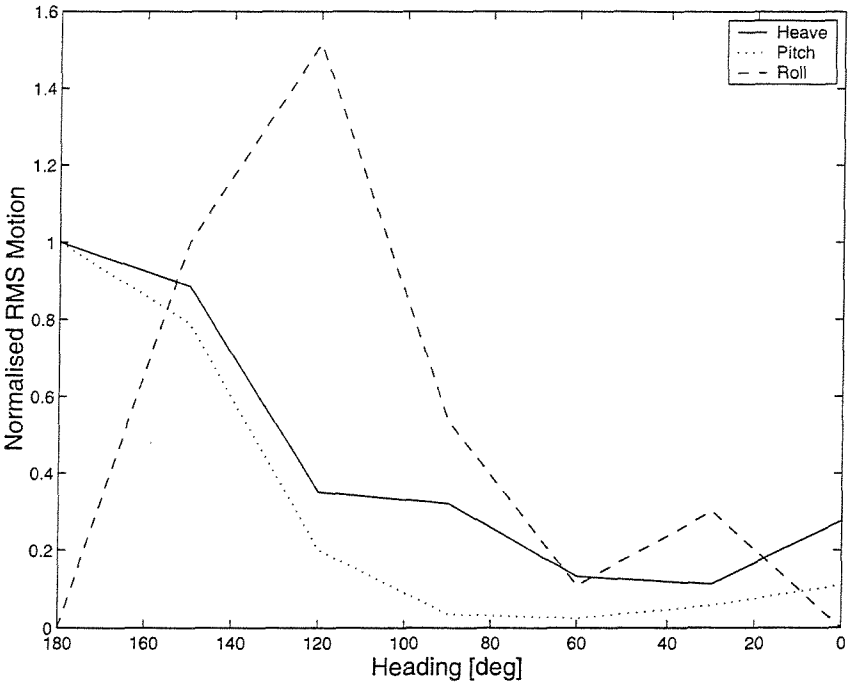

Figure 110: Normalised RMS Motions for Model 5s, S/L=0.4, Fn=0.8

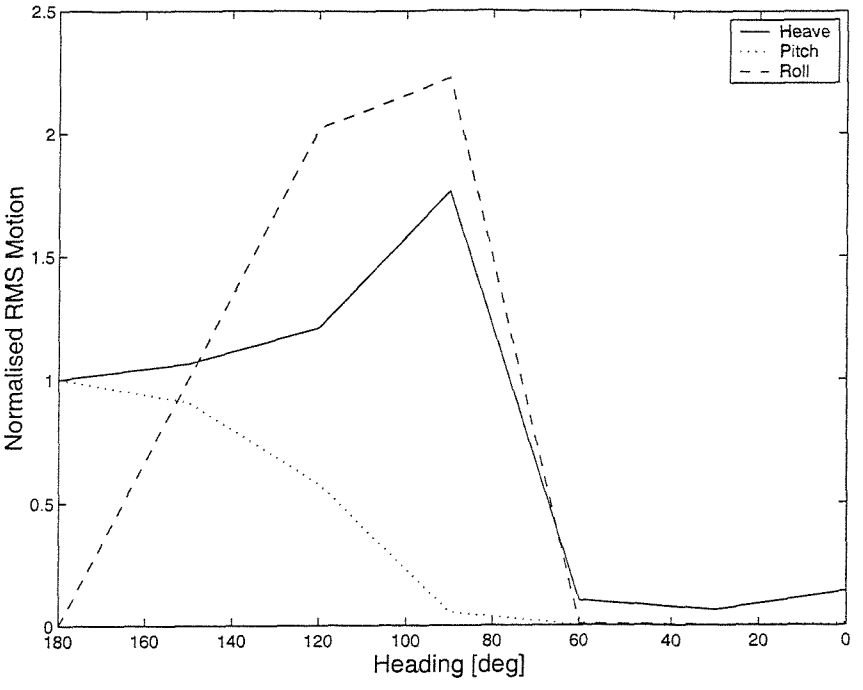

Figure 111: Normalised RMS Motions for Model 5b, S/L=0.2, Fn=0.2

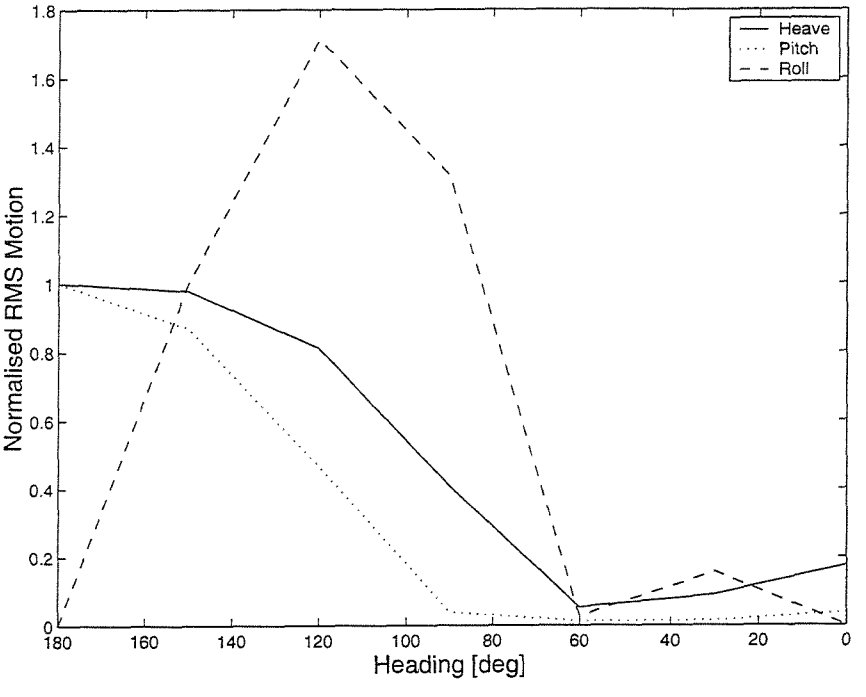

Figure 112: Normalised RMS Motions for Model 5b, S/L=0.2, Fn=0.5

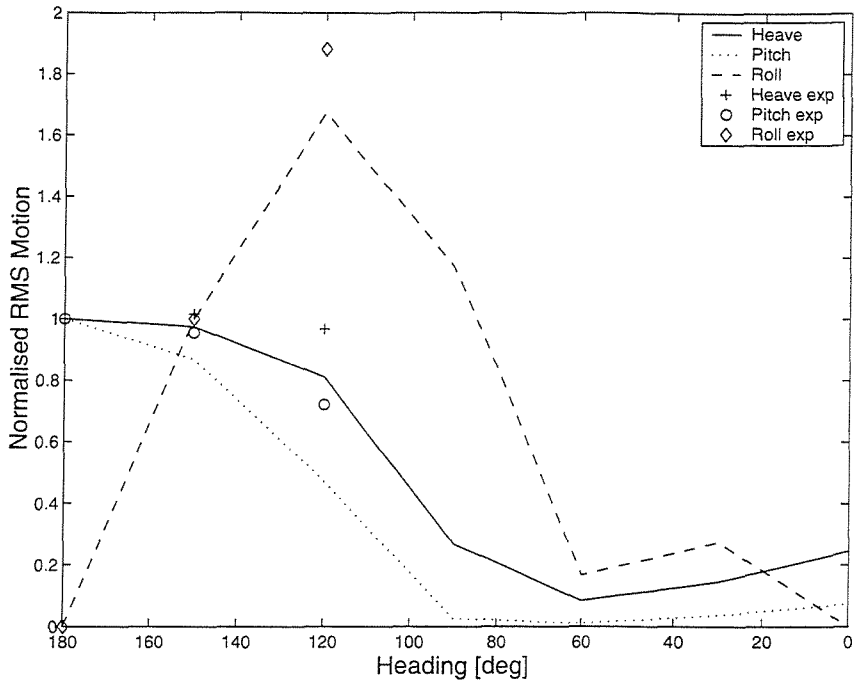

Figure 113: Normalised RMS Motions with experimental points, for Model 5b, S/L=0.2, Fn=0.65.

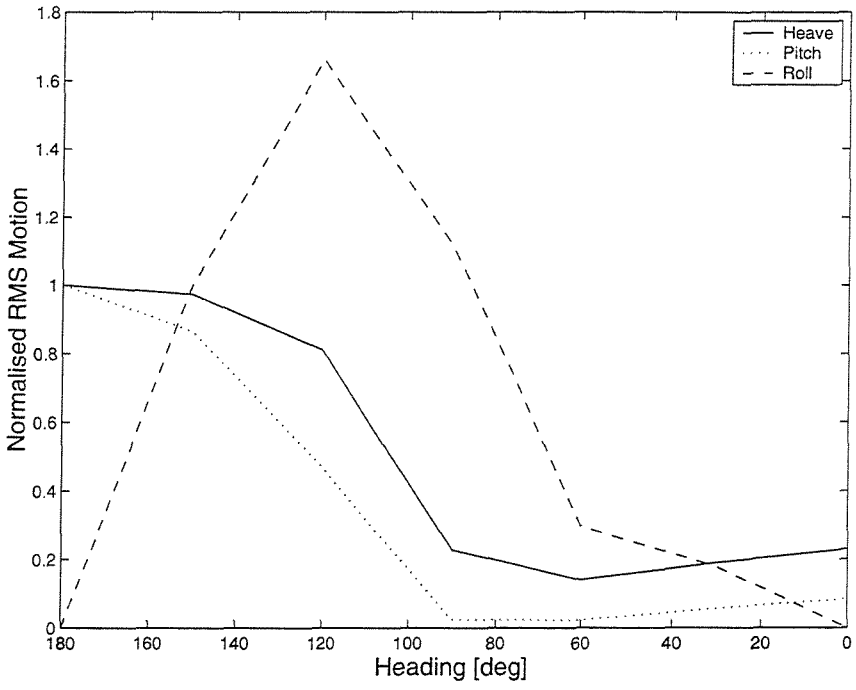

Figure 114: Normalised RMS Motions for Model 5b, S/L=0.2, Fn=0.8

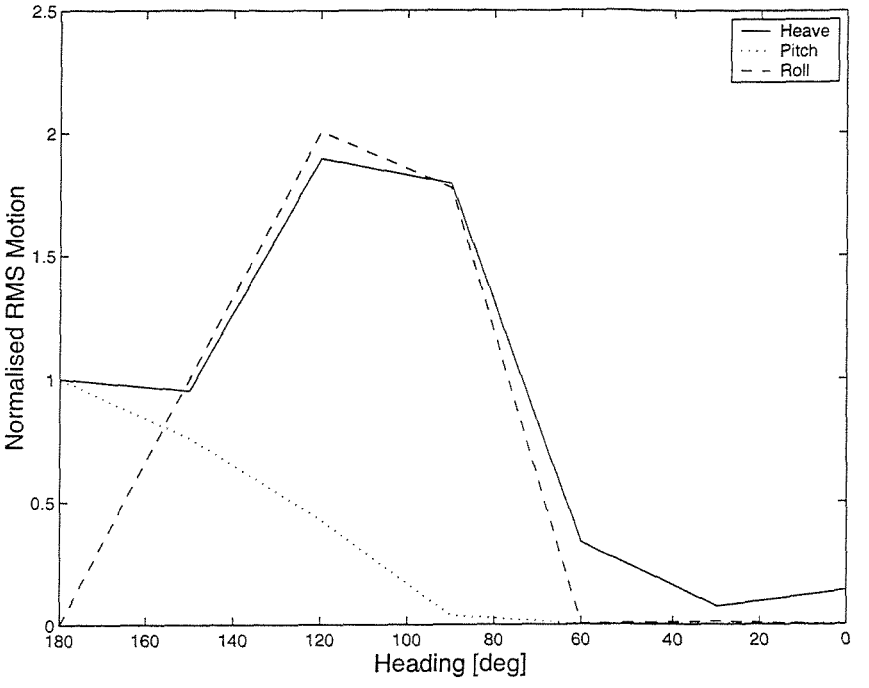

Figure 115: Normalised RMS Motions for Model 5b, S/L=0.4, Fn=0.2

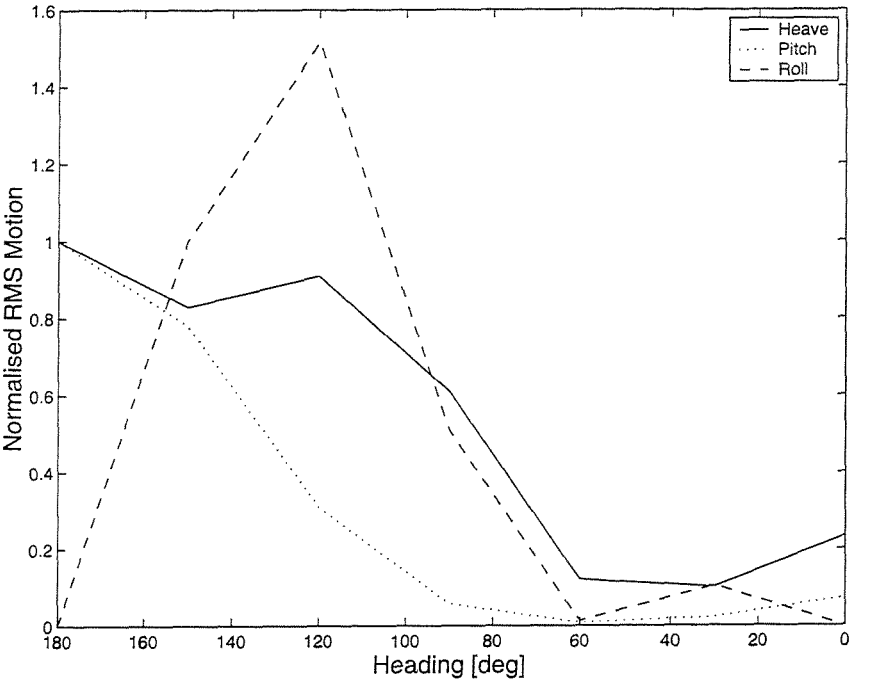

Figure 116: Normalised RMS Motions for Model 5b, S/L=0.4, Fn=0.53

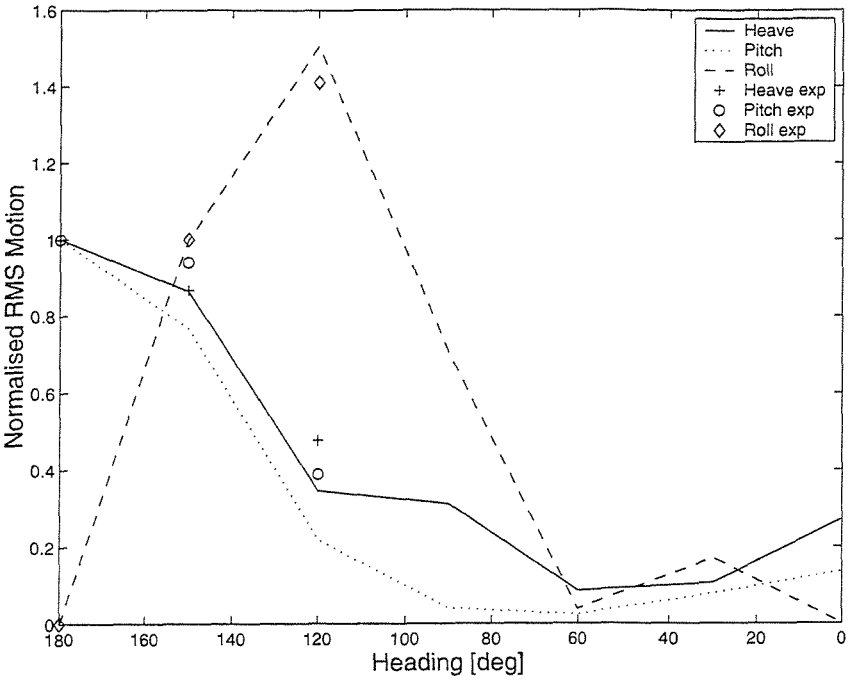

Figure 117: Normalised RMS Motions with experimental points, for Model 5b, S/L=0.4, Fn=0.65.

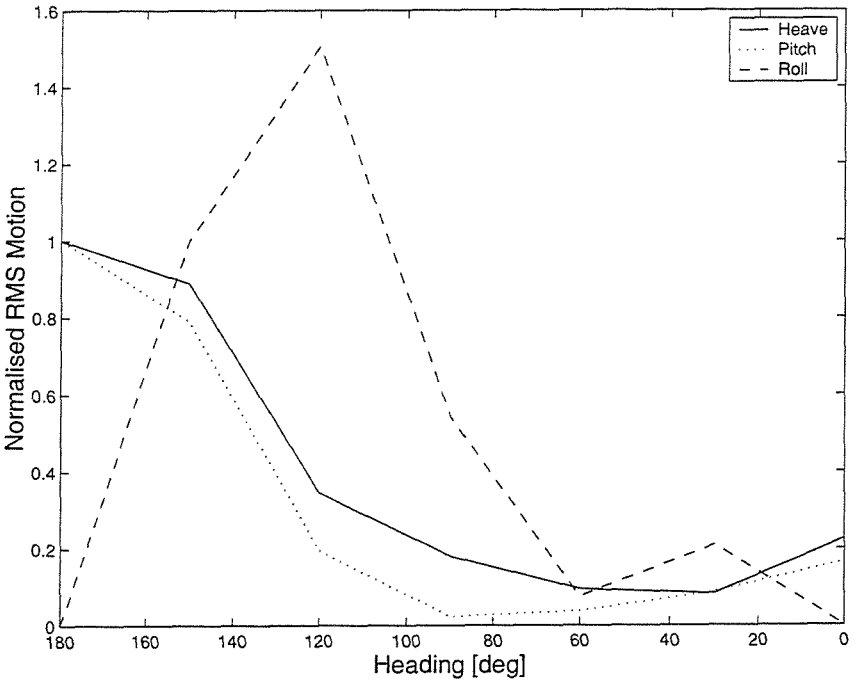

Figure 118: Normalised RMS Motions for Model 5b, S/L=0.4, Fn=0.8

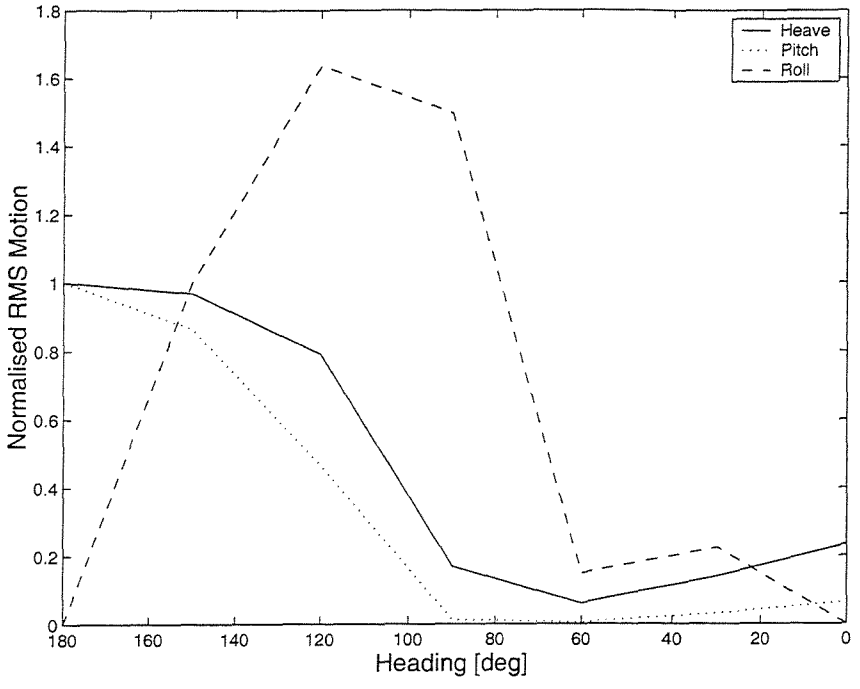

Figure 119: Normalised RMS motions for Model 4b, S/L=0.2, at Fn=0.65

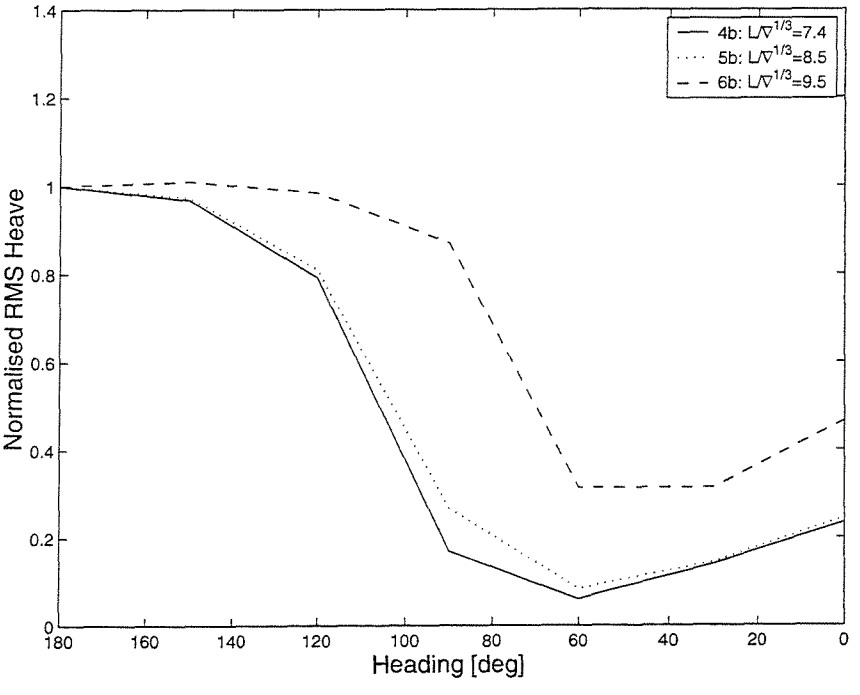

Figure 120: Influence of $L/\nabla^{1/3}$ on normalised heave motion, at Fn=0.65

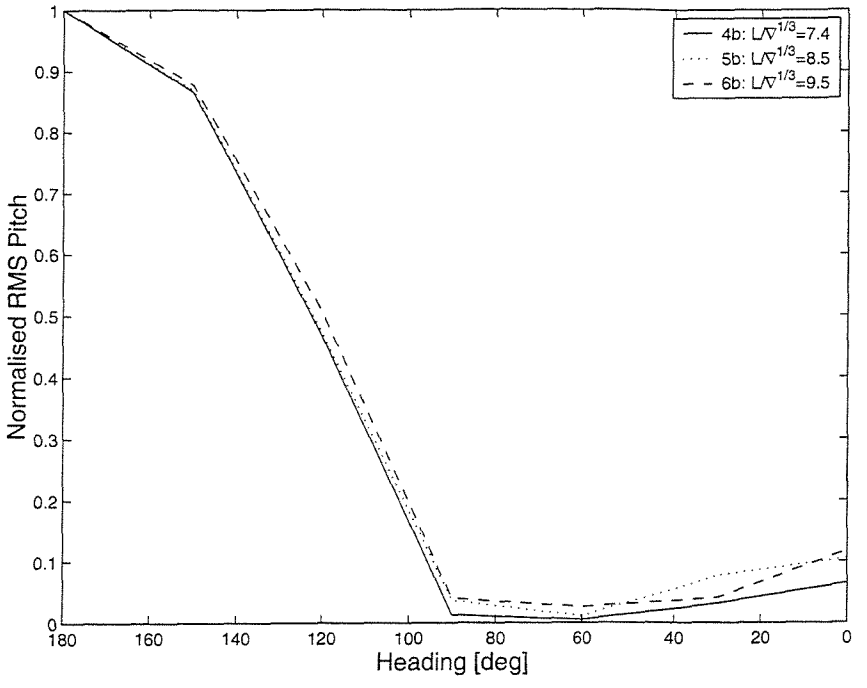

Figure 121: Influence of $L/\nabla^{1/3}$ on normalised pitch motion, at Fn=0.65

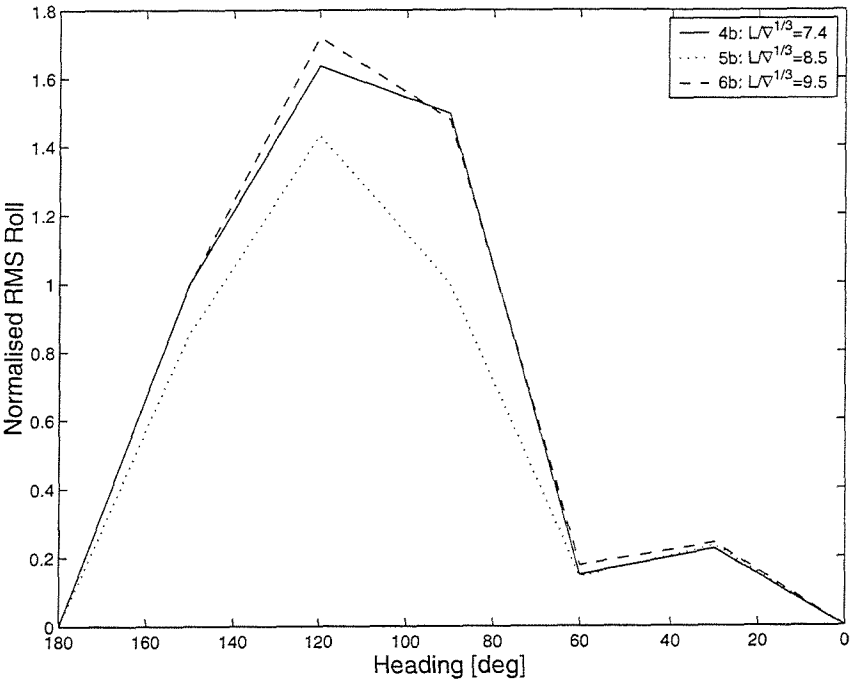

Figure 122: Influence of $L/\nabla^{1/3}$ on normalised roll motion, at Fn=0.65

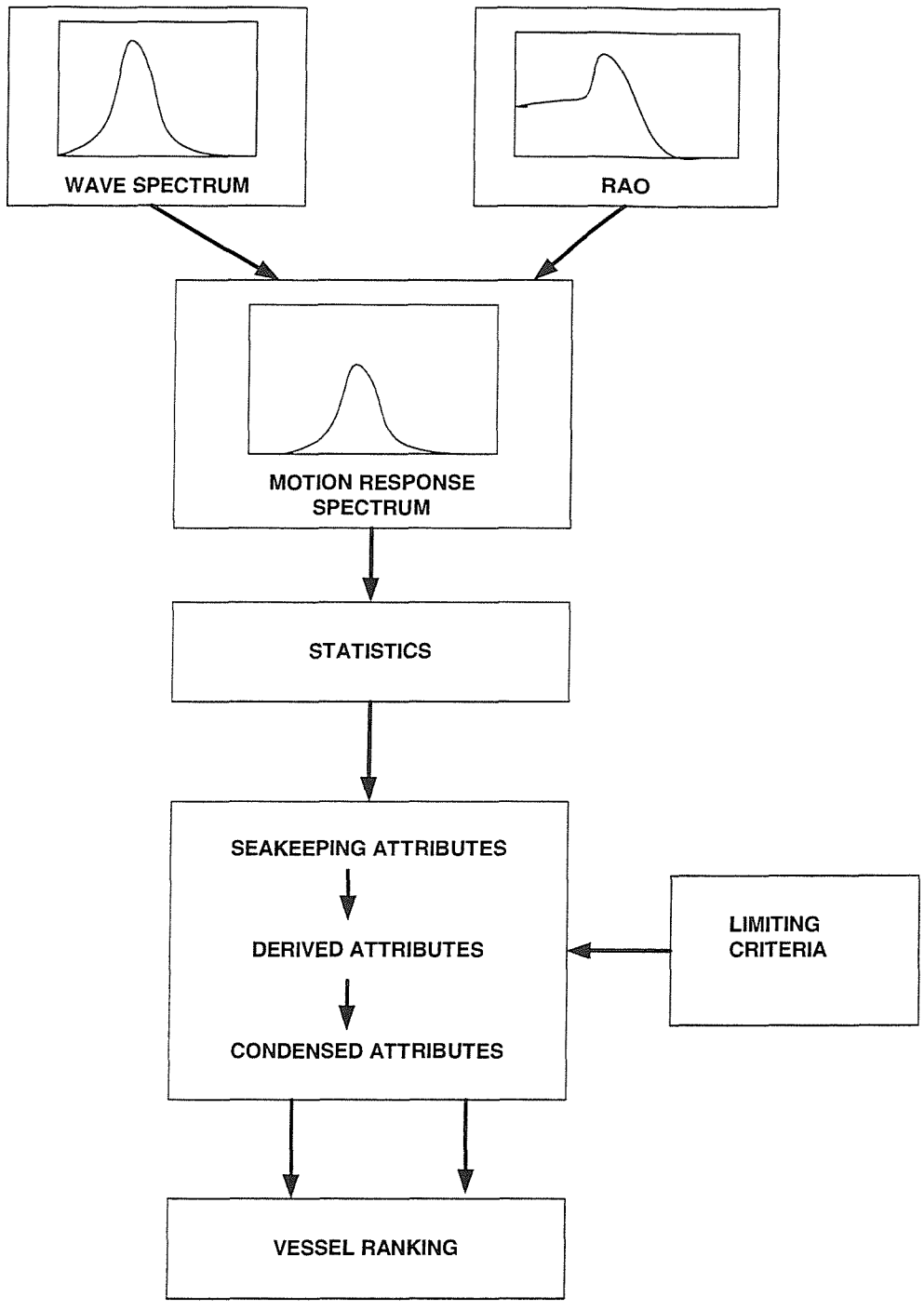

Figure 123: Methodology

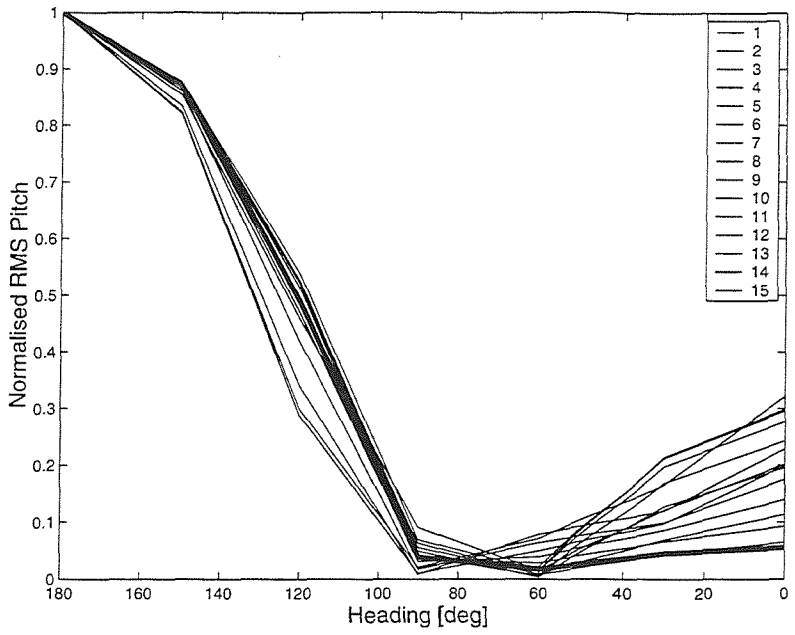

Figure 124: Frequency variation of normalised motion

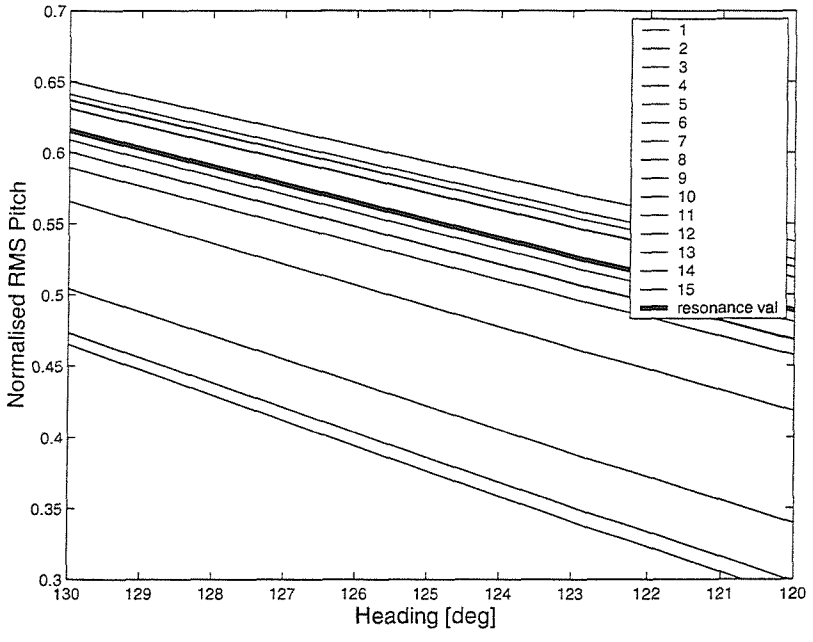

Figure 125: Frequency variation of normalised motion between 120° and 130°

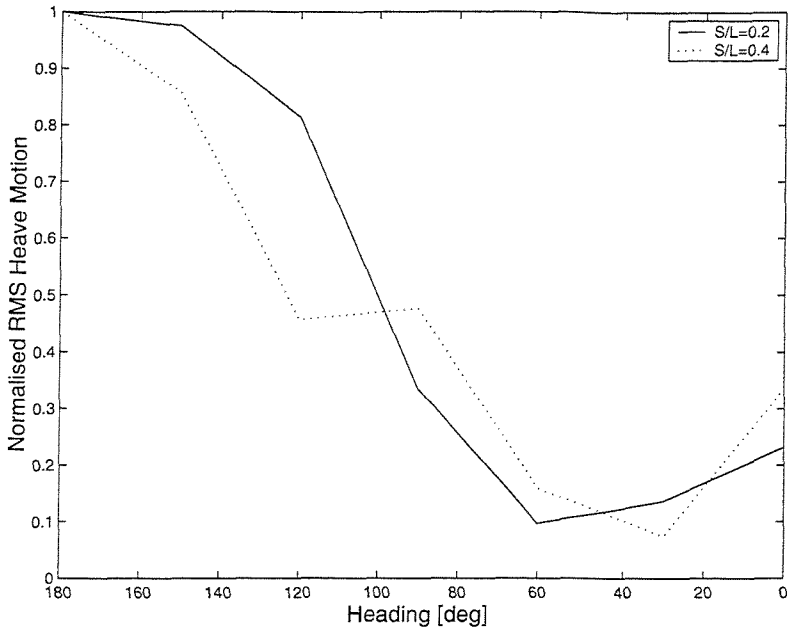

Figure 126: Influence of S/L on normalised heave motion

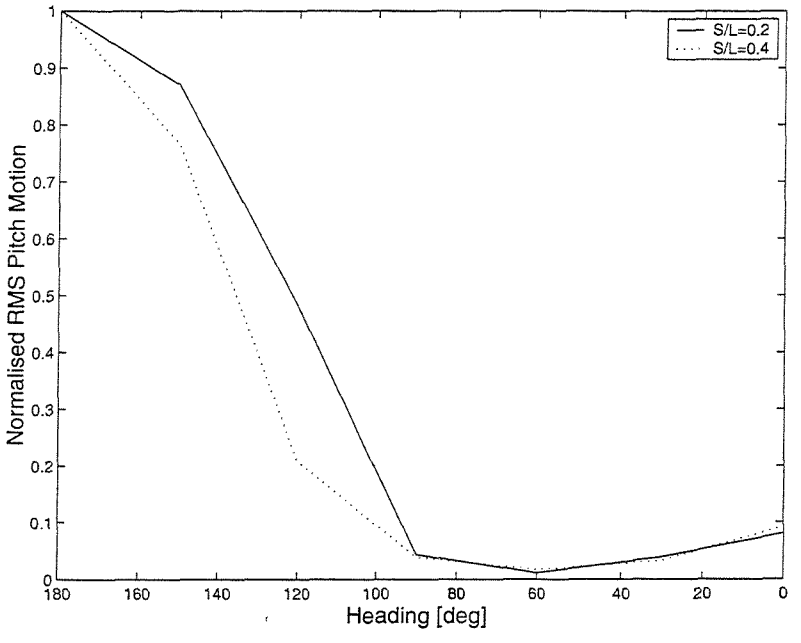

Figure 127: Influence of S/L on normalised pitch motion

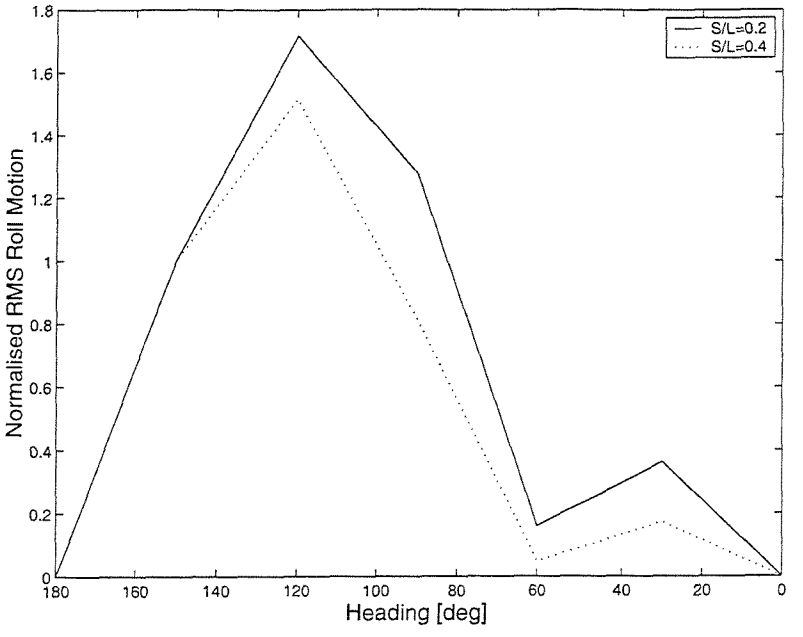

Figure 128: Influence of S/L on normalised roll motion

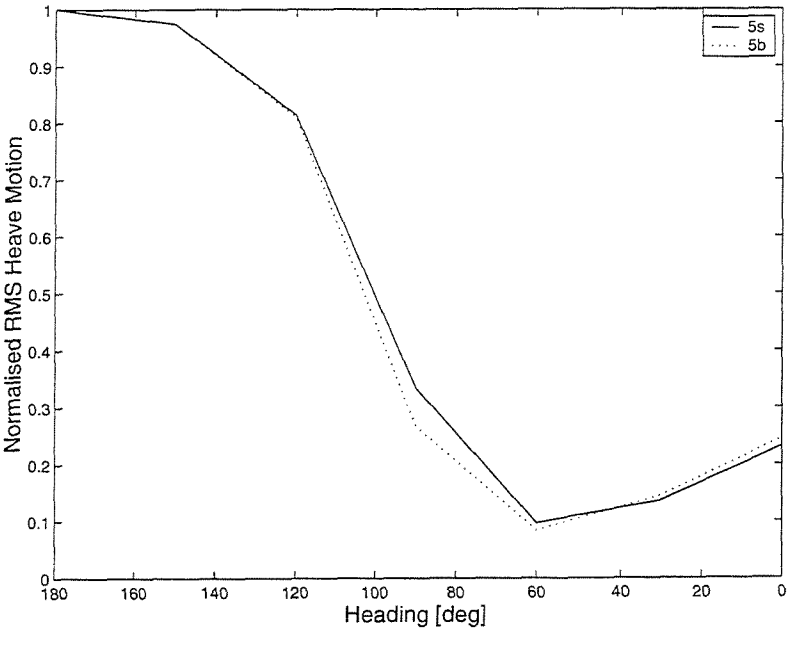

Figure 129: Influence of hull form on normalised heave motion

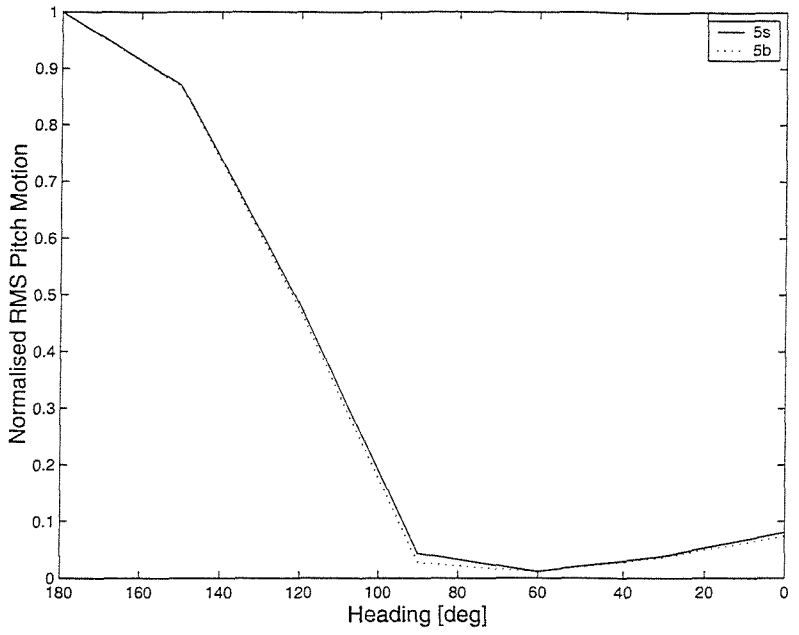

Figure 130: Influence of hull form on normalised pitch motion

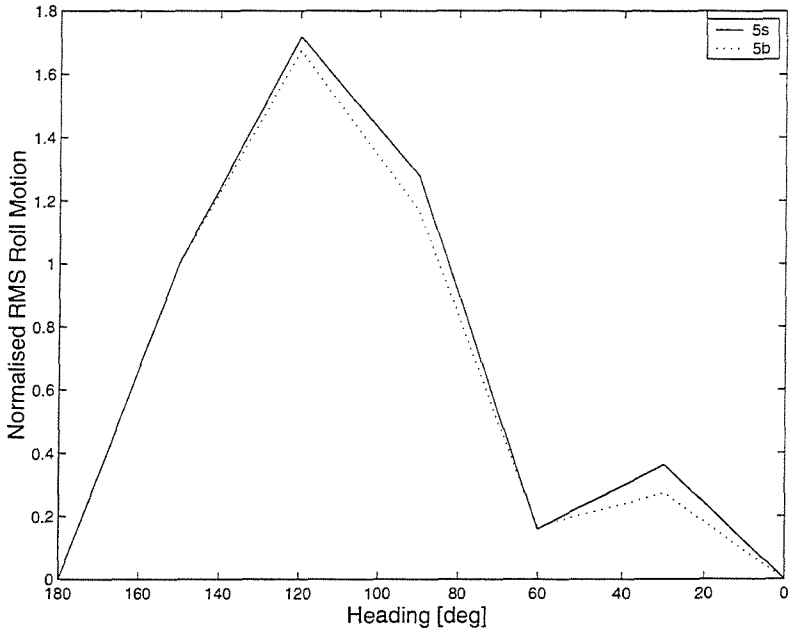

Figure 131: Influence of hull form on normalised roll motion

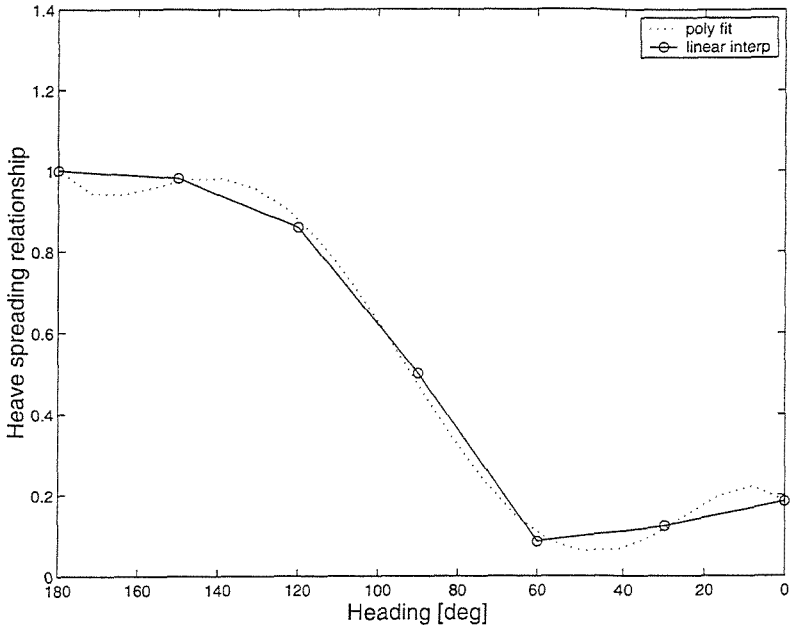

Figure 132: Polynomial fit to spreading relationship

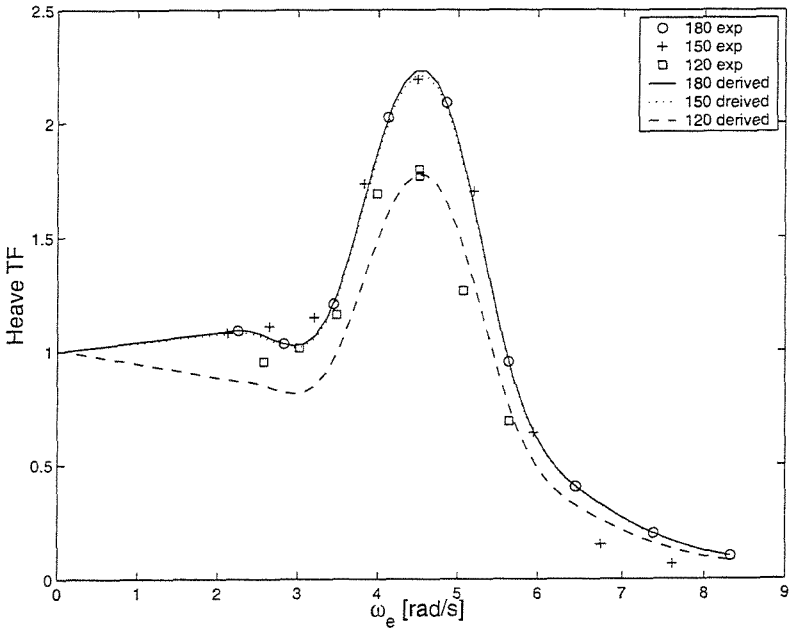

Figure 133: Comparison between experimental data and data generated using the spreading relationship.

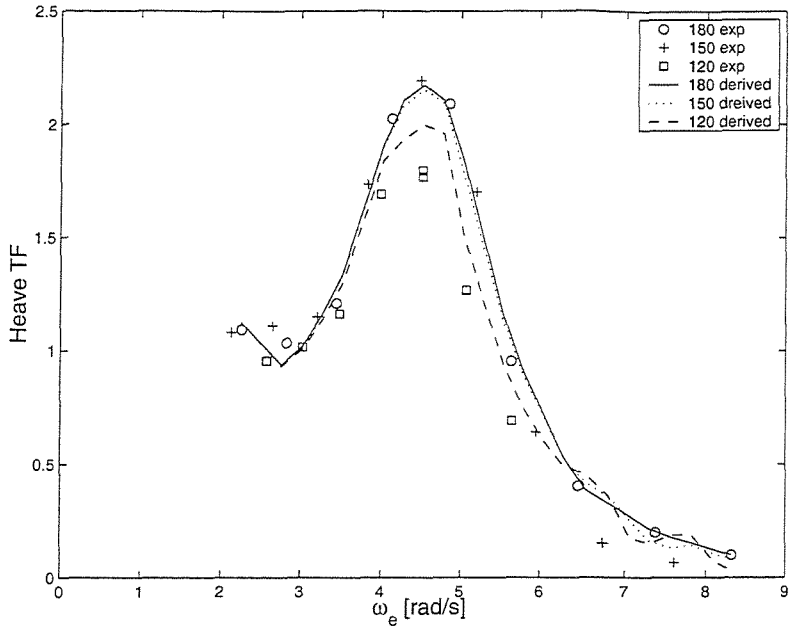

Figure 134: Comparison between experimental data and data generated using the frequency by frequency spreading relationship.

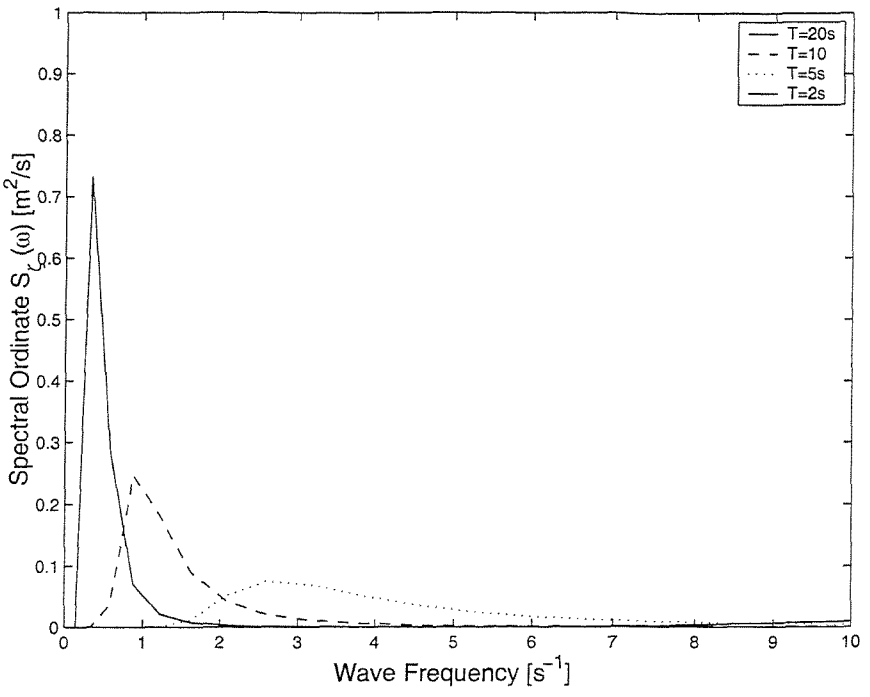

Figure 135: Influence of wave period on band width of spectrum

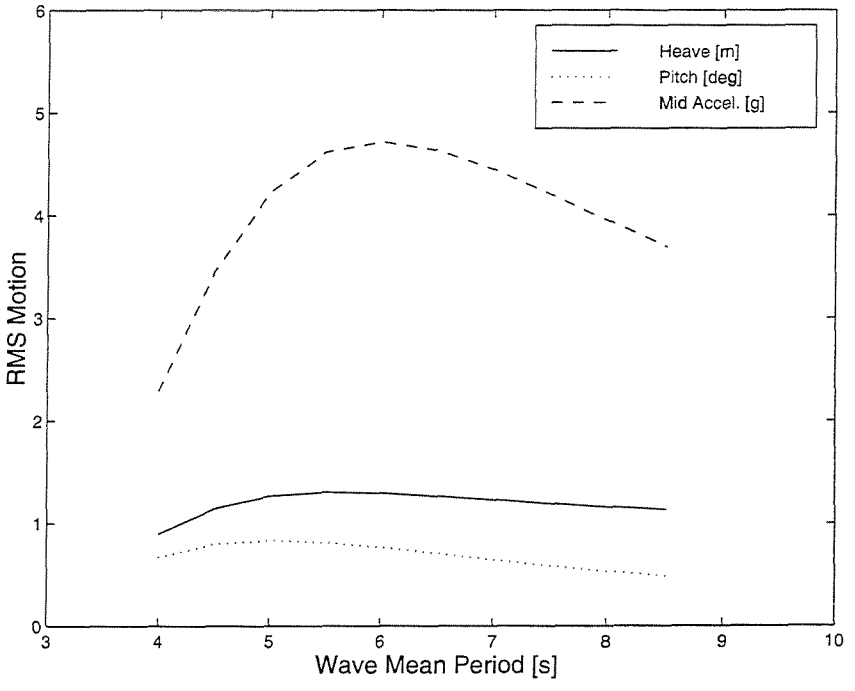

Figure 136: Influence of $\overline{T}$ coinciding with resonant period of transfer function

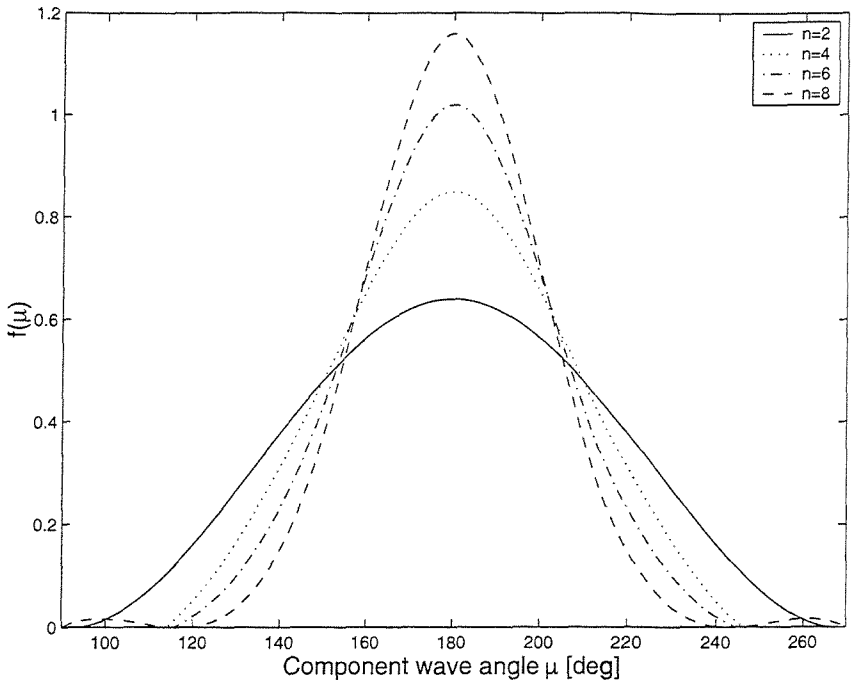

Figure 137: Influence of n on Cos^n spreading function

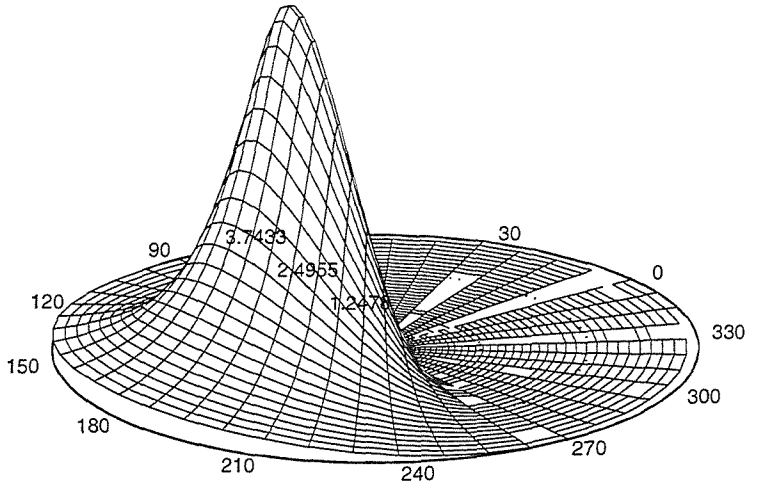

Figure 138: Example of a 180° short-crested wave spectrum.

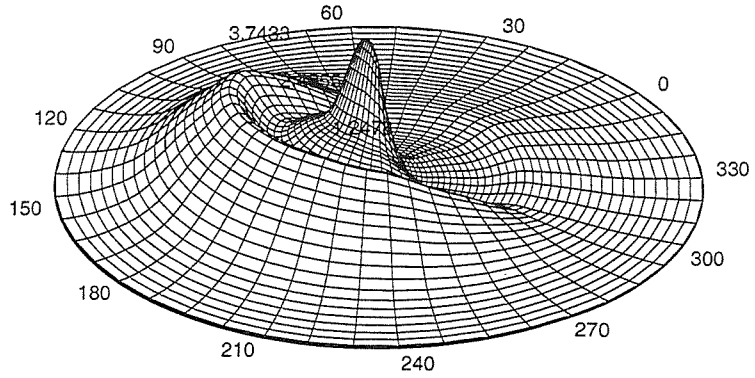

Figure 139: Example of a 180° 3D mid accel. transfer function.

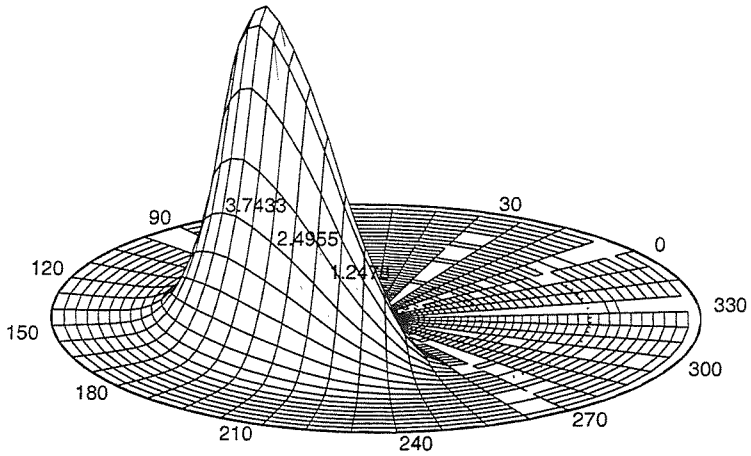

Figure 140: Example of a 180° 3D mid accel. response spectrum.

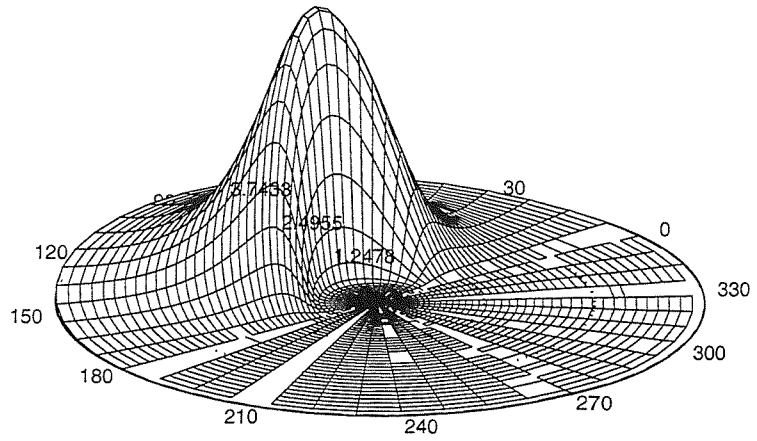

Figure 141: Example of a 90° short-crested wave spectrum.

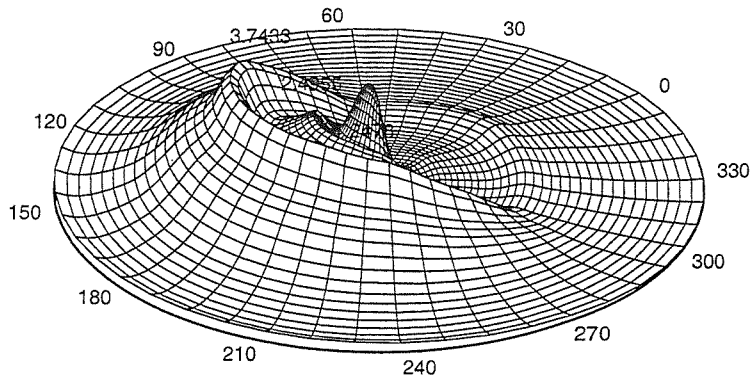

Figure 142: Example of a 90° 3D heave transfer function.

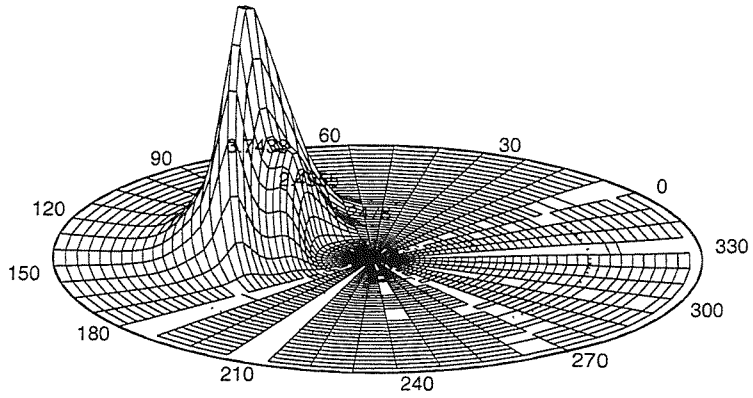

Figure 143: Example of a 90° 3D heave response spectrum.

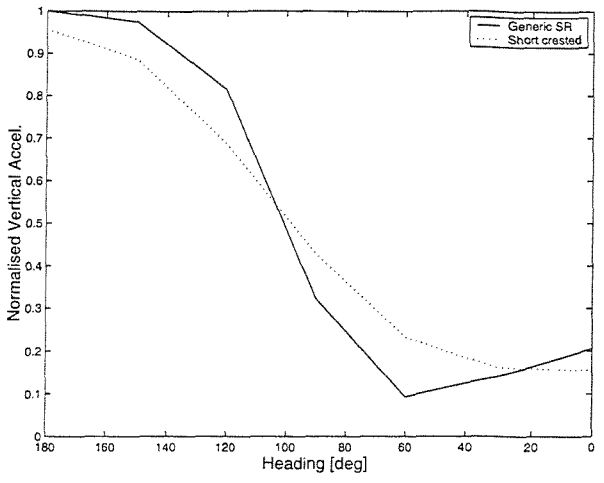

Figure 144: Comparison between short-crested and long-crested generic normalised vertical accelerations.

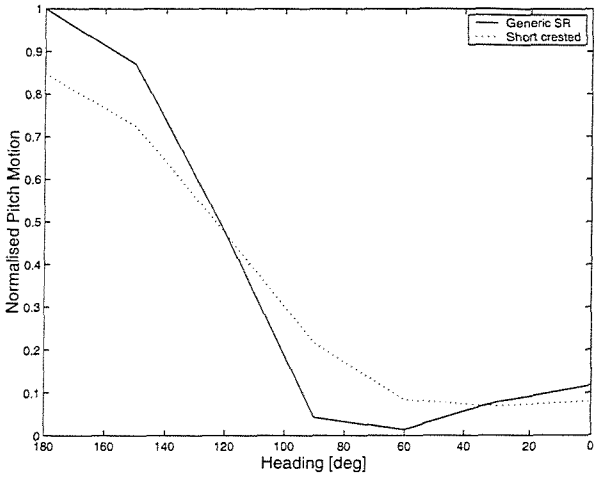

Figure 145: Comparison between short-crested and long-crested generic normalised pitch motion.

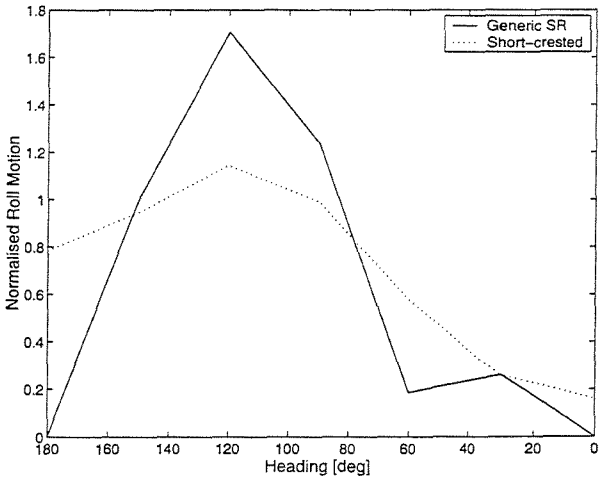

Figure 146: Comparison between short-crested and long-crested generic normalised roll motion.

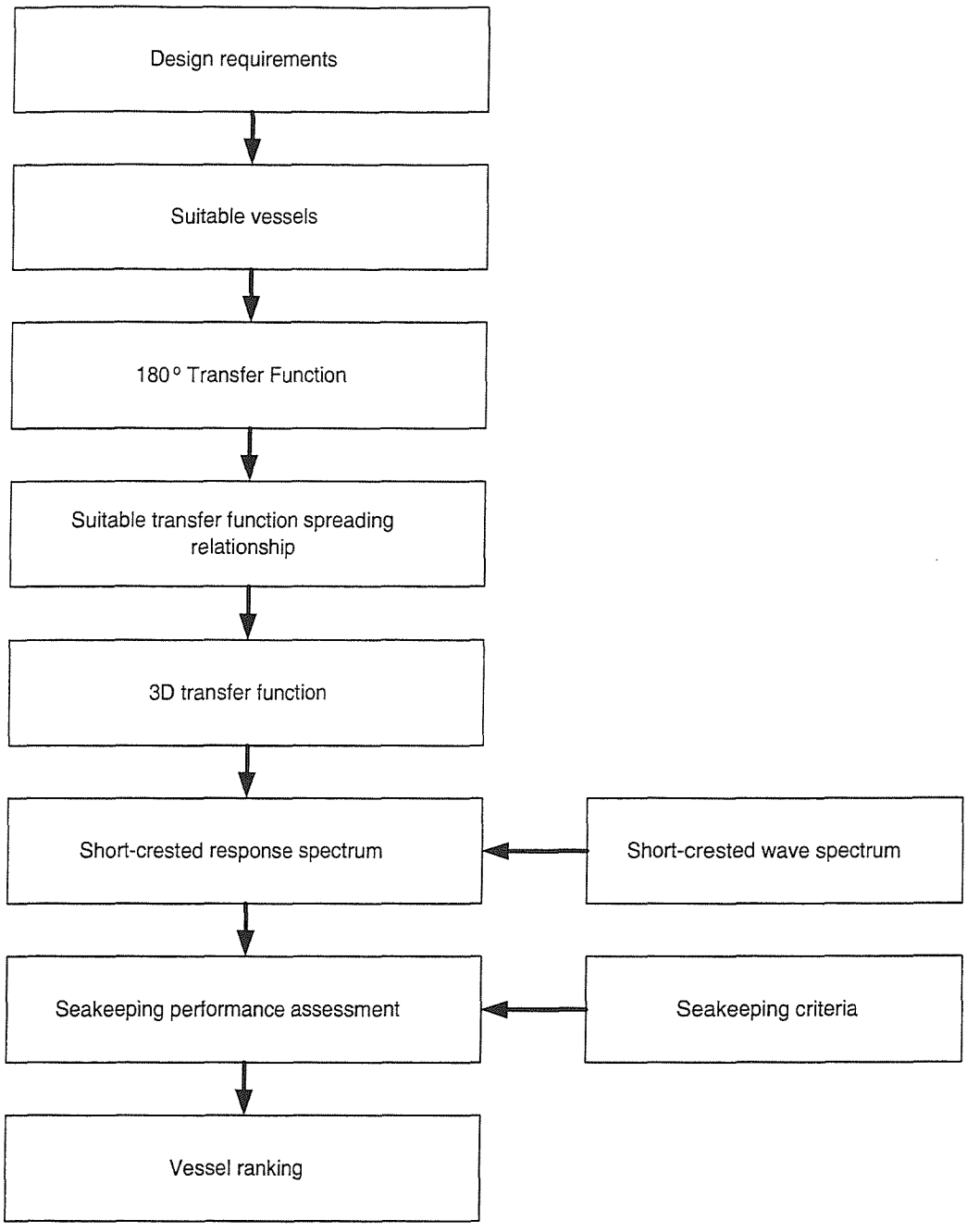

Figure 147: The application of the short-crested seakeeping assessment procedure to the designer.

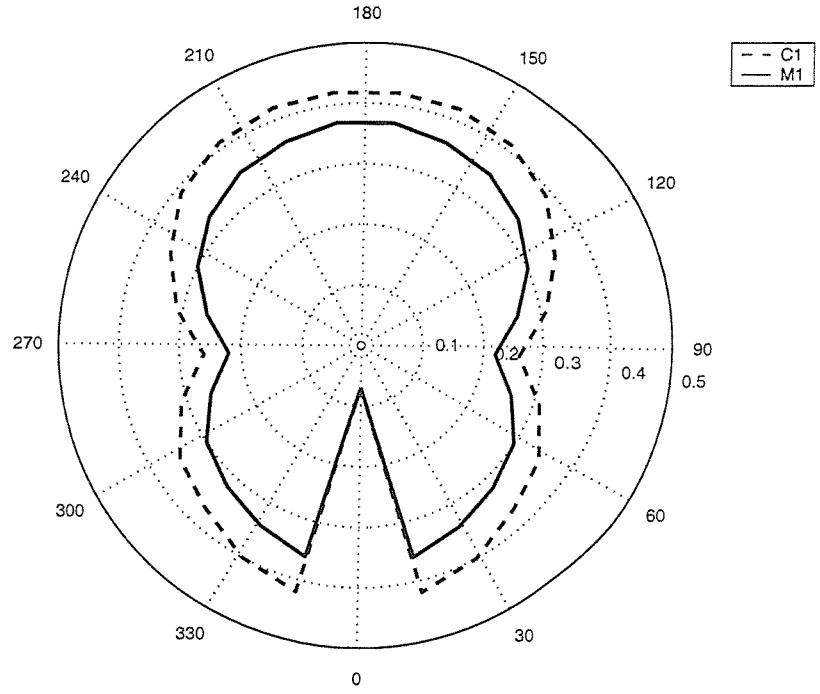

Figure 148: Comparison of heave performance for vessels M1 and C1 in short-crested seas.

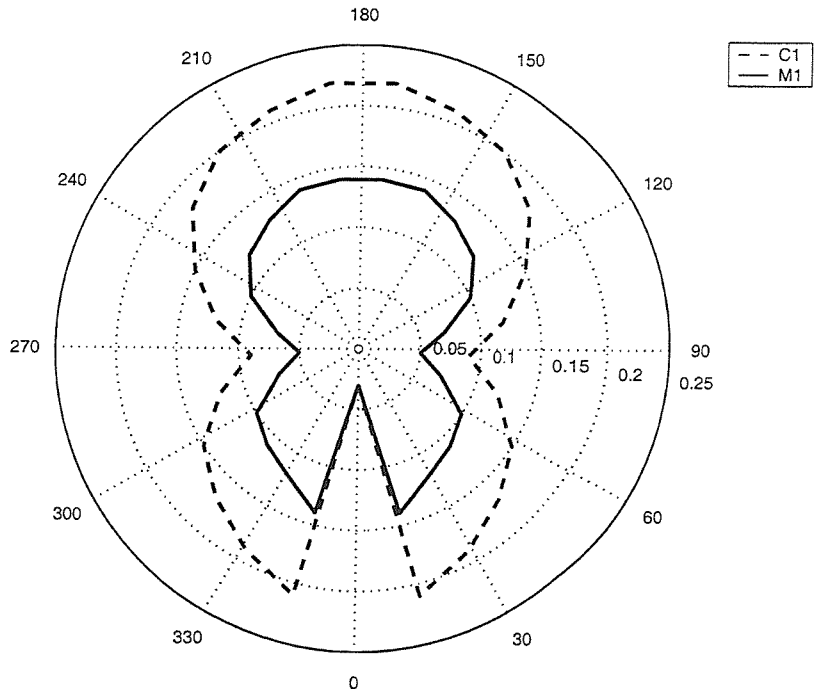

Figure 149: Comparison of pitch performance for vessels M1 and C1 in short-crested seas.

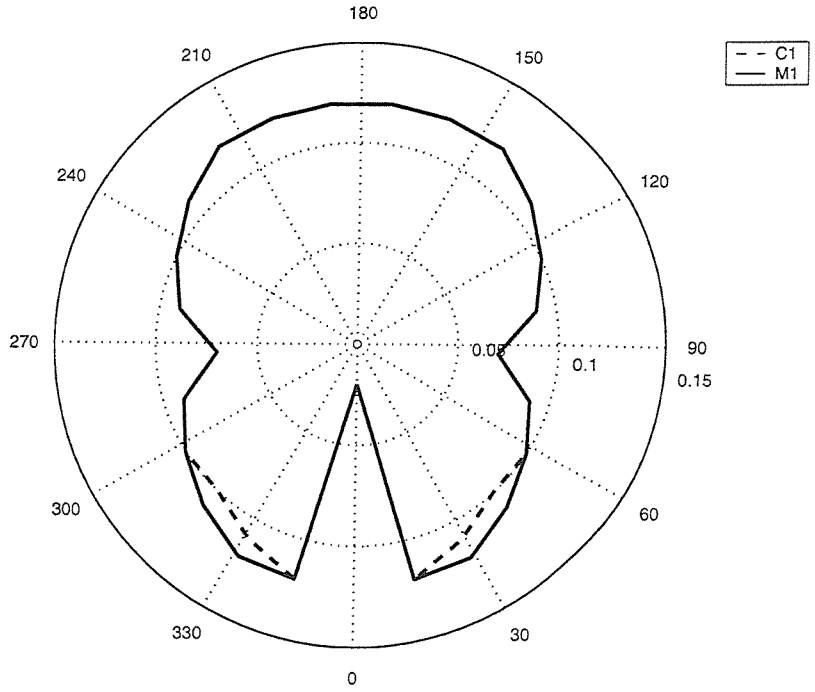

Figure 150: Comparison of midship acceleration performance for vessels M1 and C1 in short-crested seas.

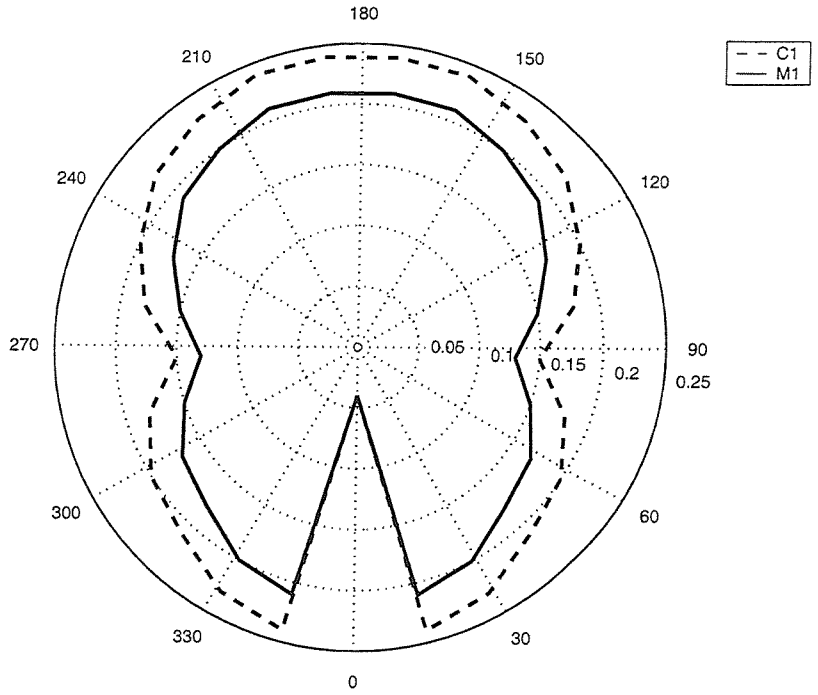

Figure 151: Comparison of forward acceleration performance for vessels M1 and C1 in short-crested seas.

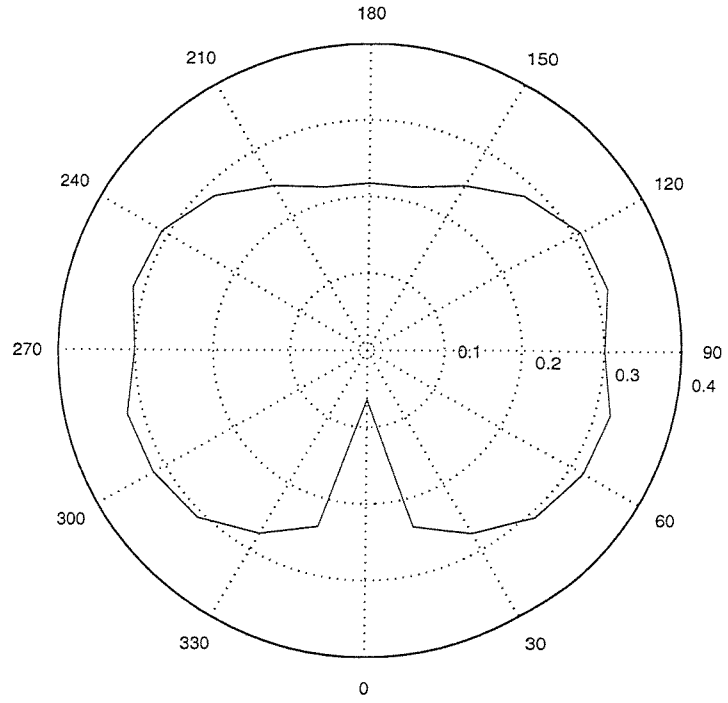

Figure 152: C2 RMS roll motion in short-crested seas

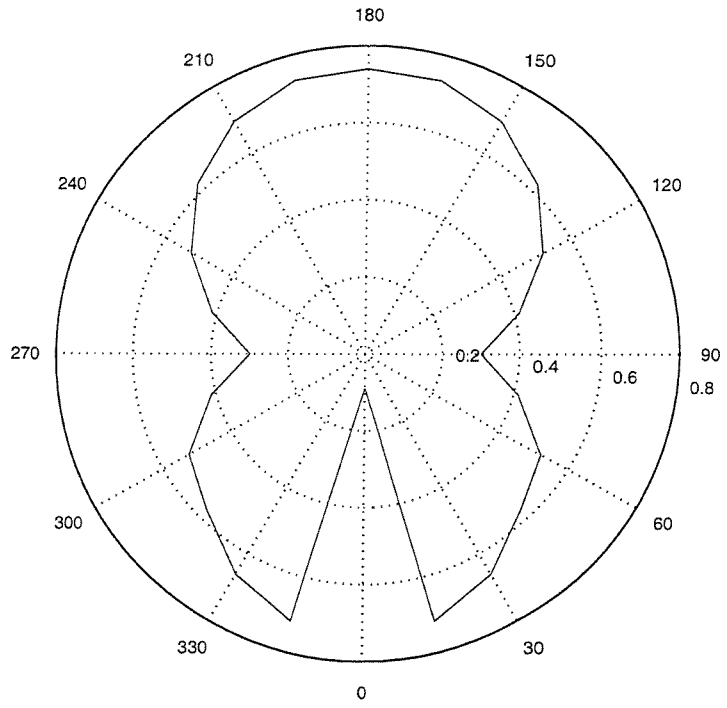

Figure 153: C2 RMS pitch motion in short-crested seas

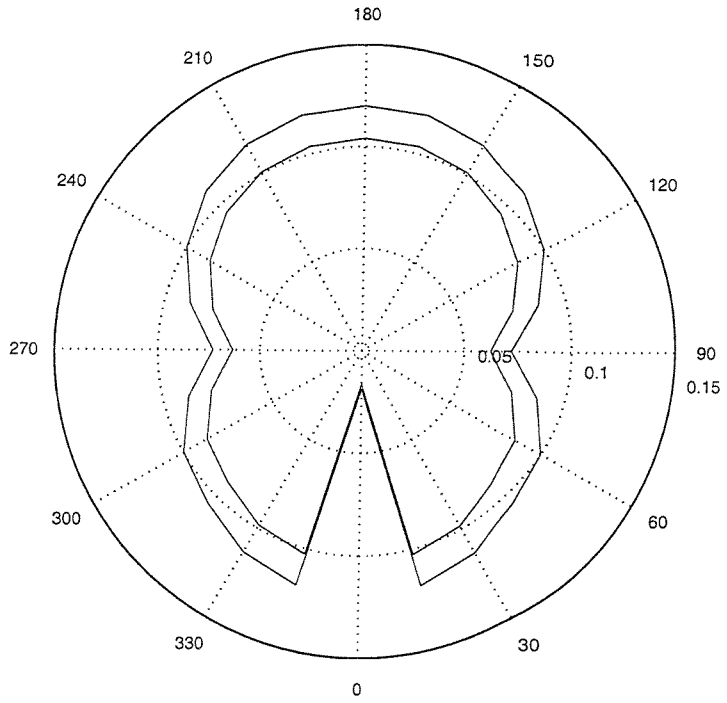

Figure 154: C2 RMS midship vertical acceleration and reduced frequency weighted acceleration in short-crested seas

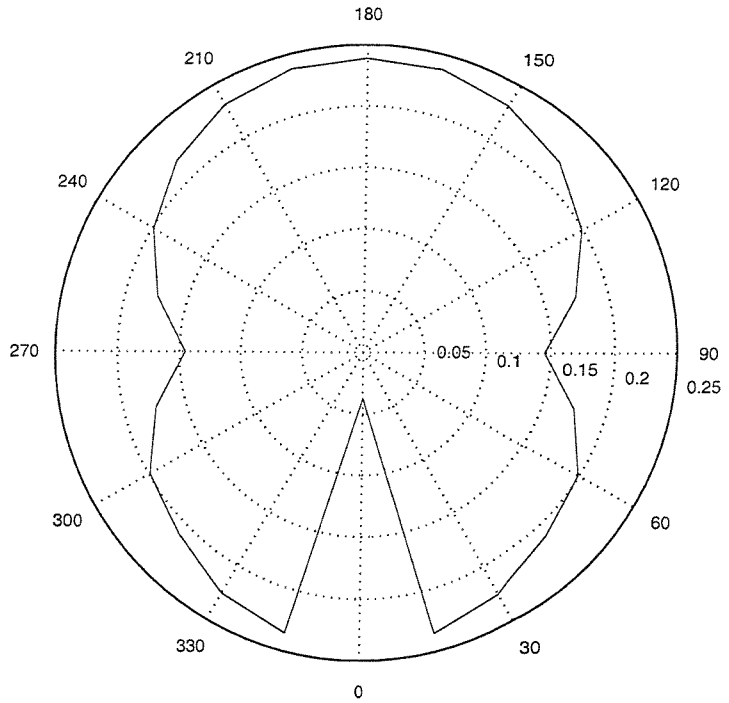

Figure 155: C2 RMS forward vertical acceleration in short-crested seas

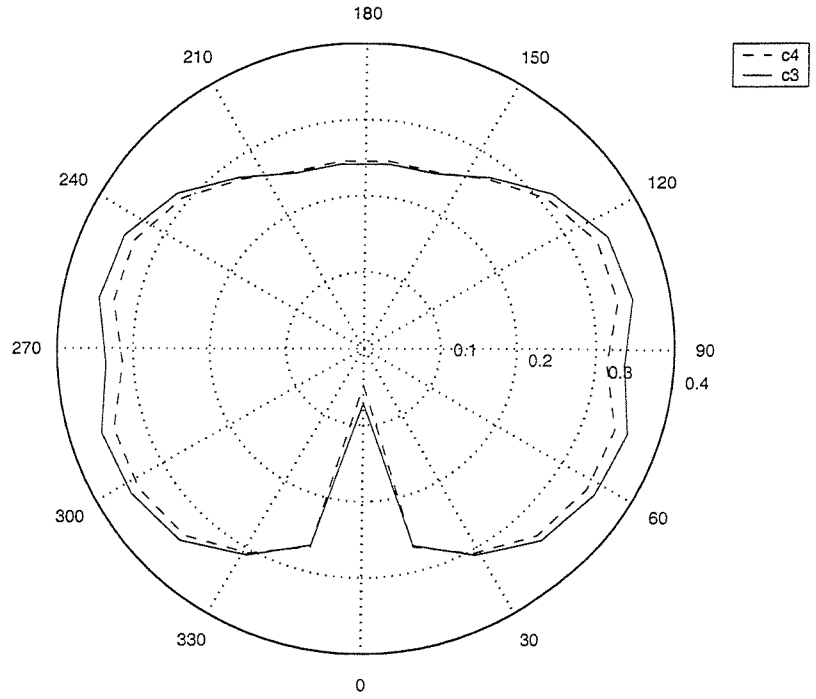

Figure 156: Comparison of C3 and C4 RMS roll motion in short-crested seas

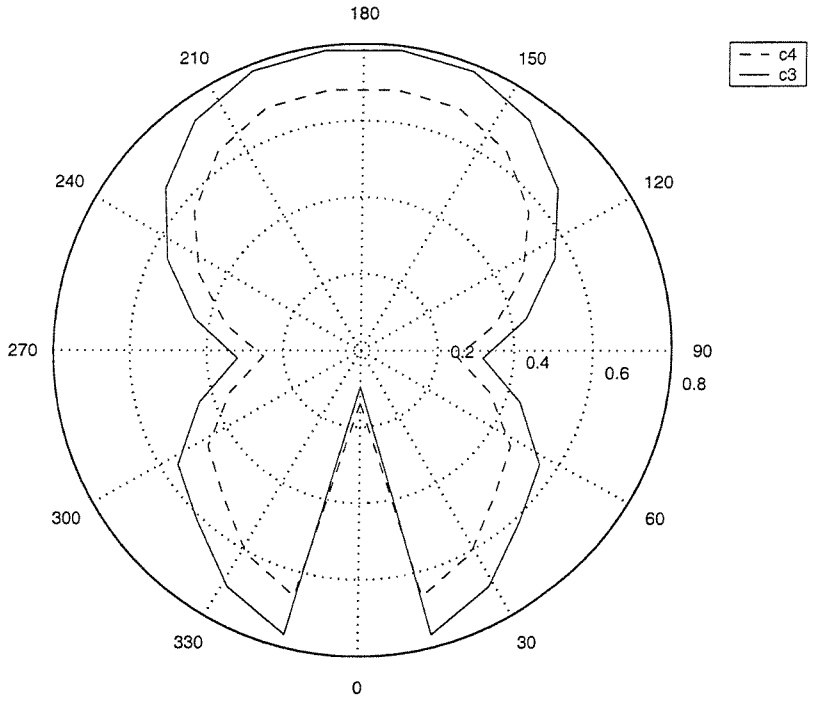

Figure 157: Comparison of C3 and C4 RMS pitch motion in short-crested seas

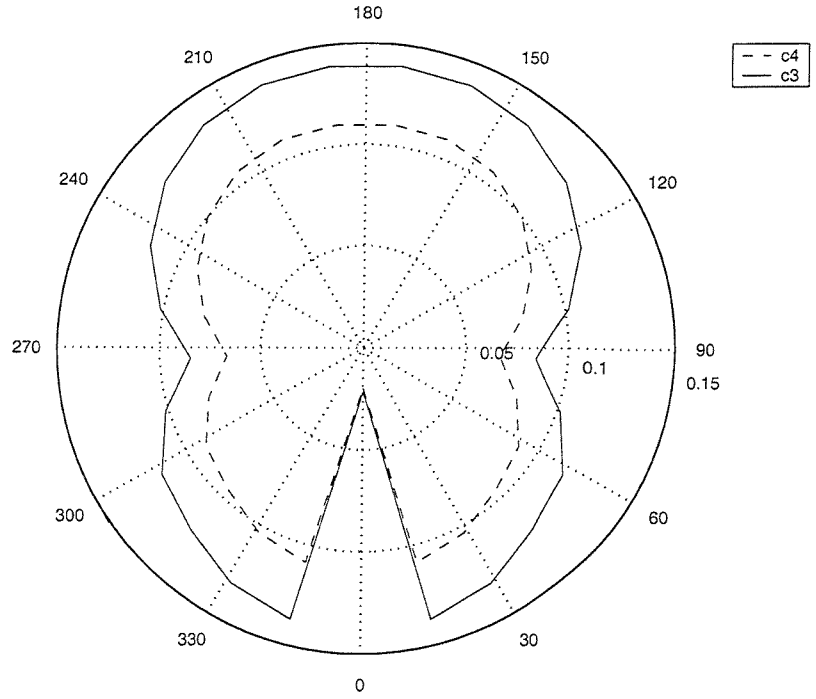

Figure 158: Comparison of C3 and C4 RMS midship vertical acceleration in short-crested seas

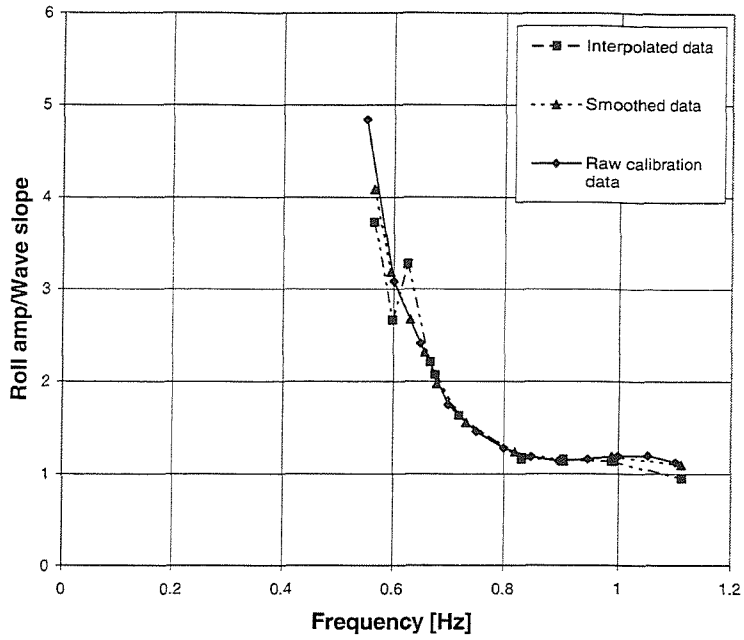

Figure 159: Buoy Roll Transfer Function

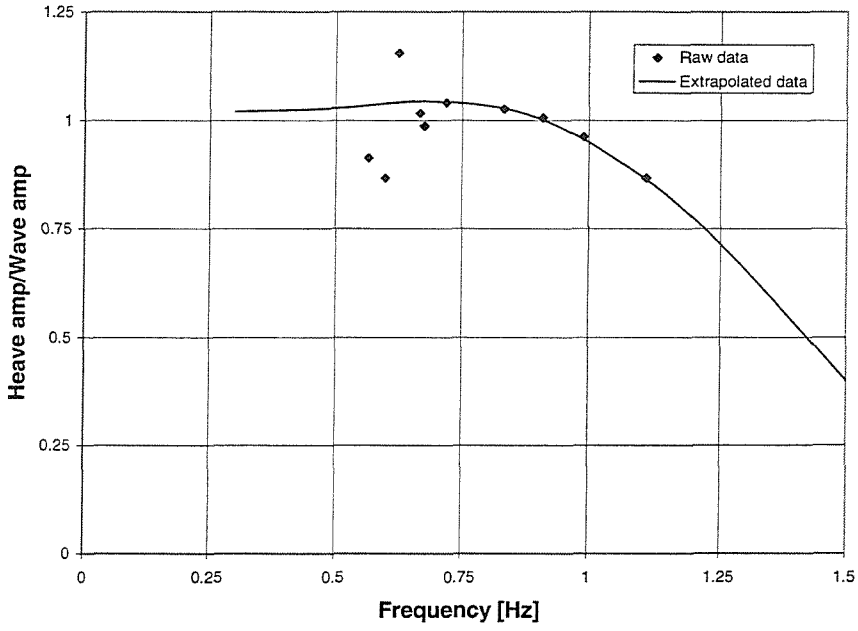

Figure 160: Buoy Heave Transfer Function

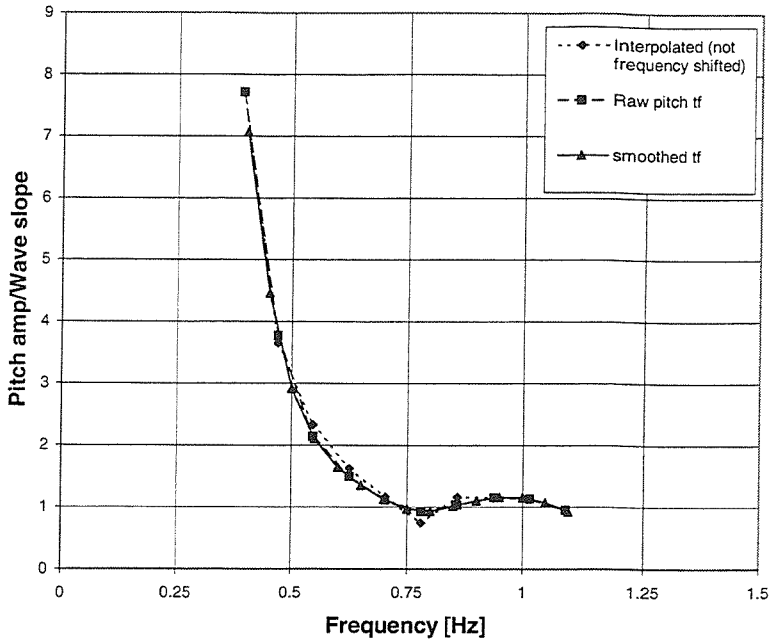

Figure 161: Buoy Pitch Transfer Function

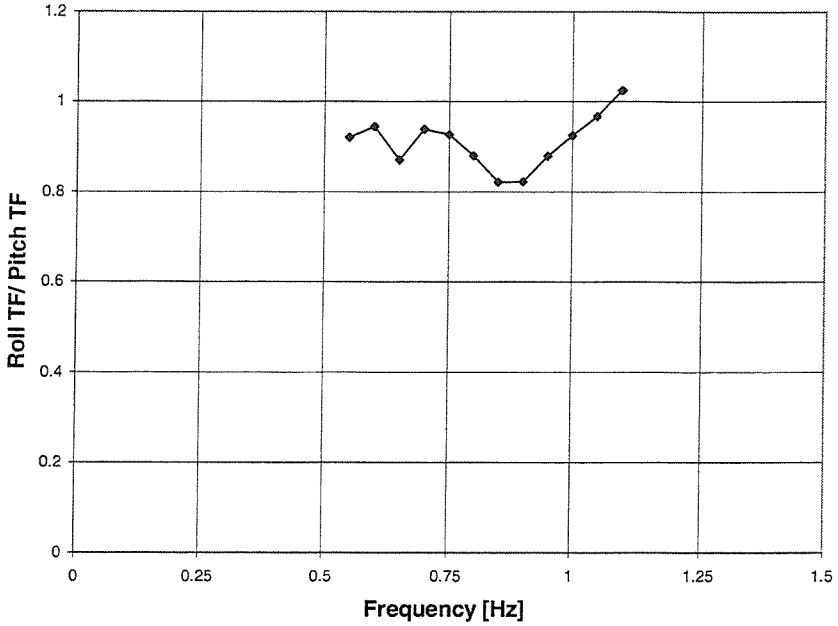

Figure 162: Buoy Roll TF/Pitch TF

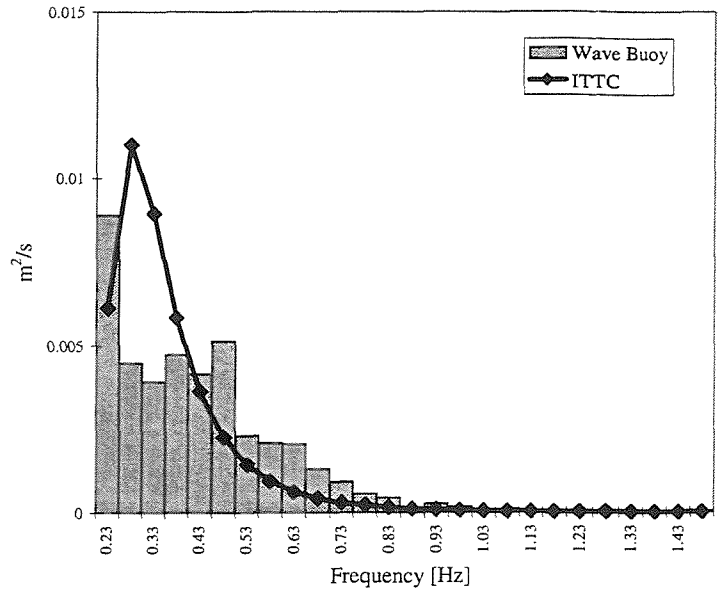

Figure 163: Acceleration Spectral Density

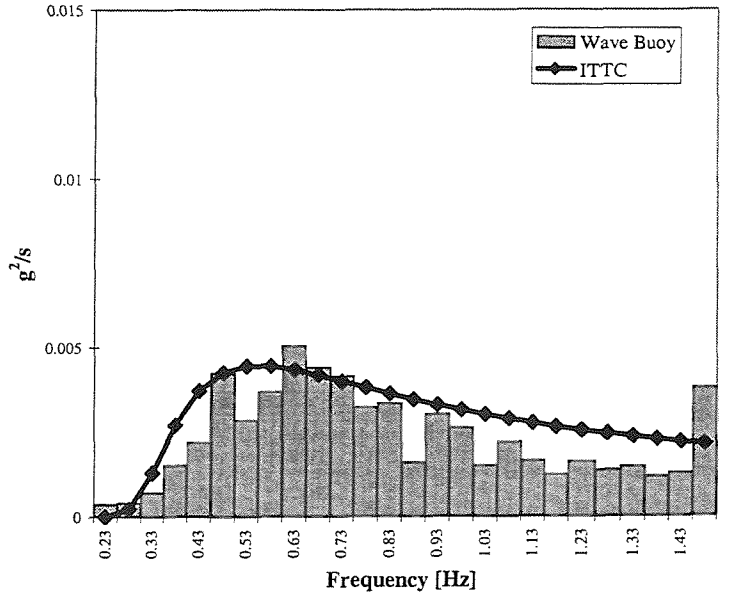

Figure 164: Amplitude Spectral Density

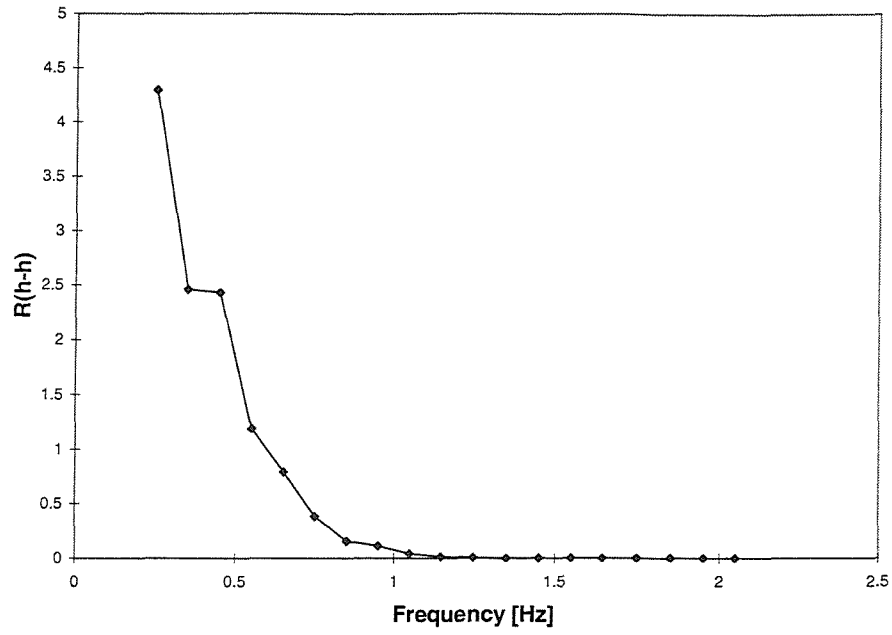

Figure 165: Heave Auto-correlation

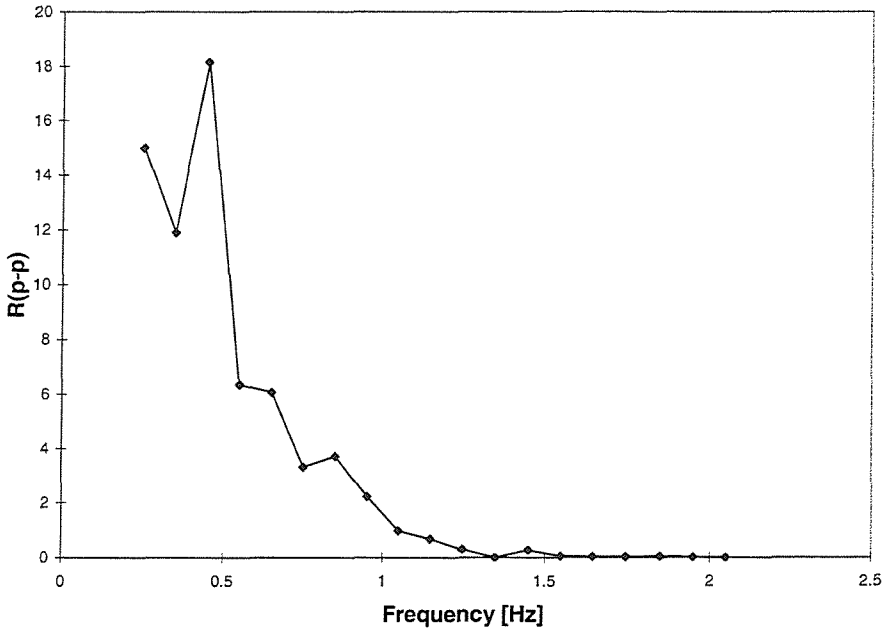

Figure 166: Pitch Auto-correlation

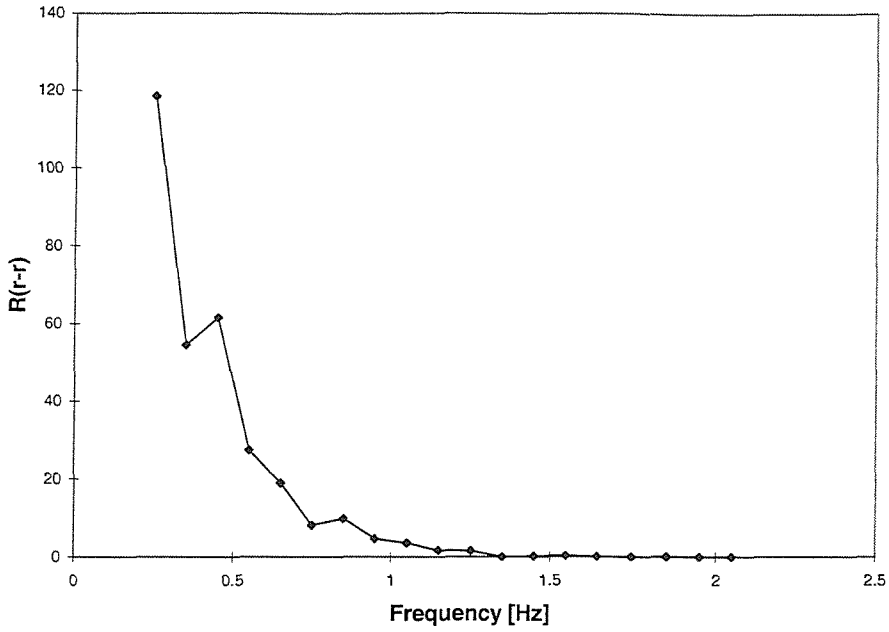

Figure 167: Roll Auto-correlation

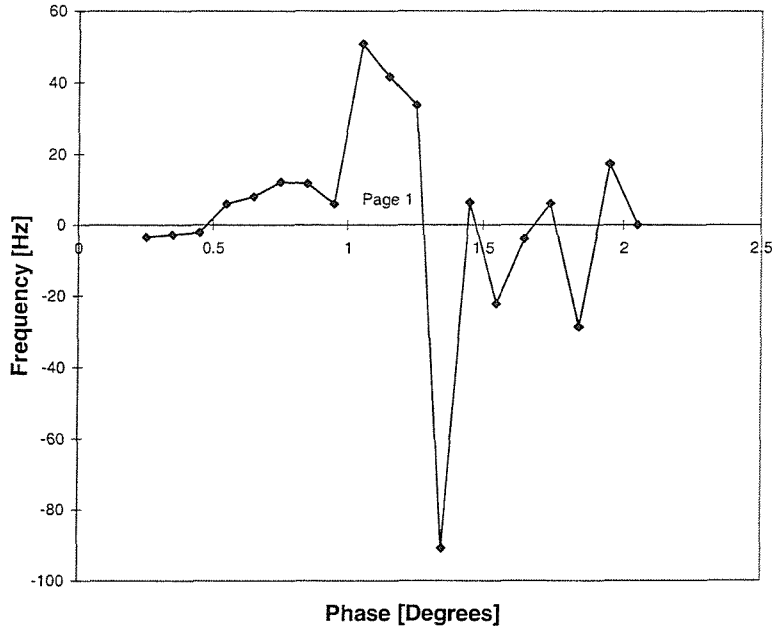

Figure 168: Roll-Pitch Phase

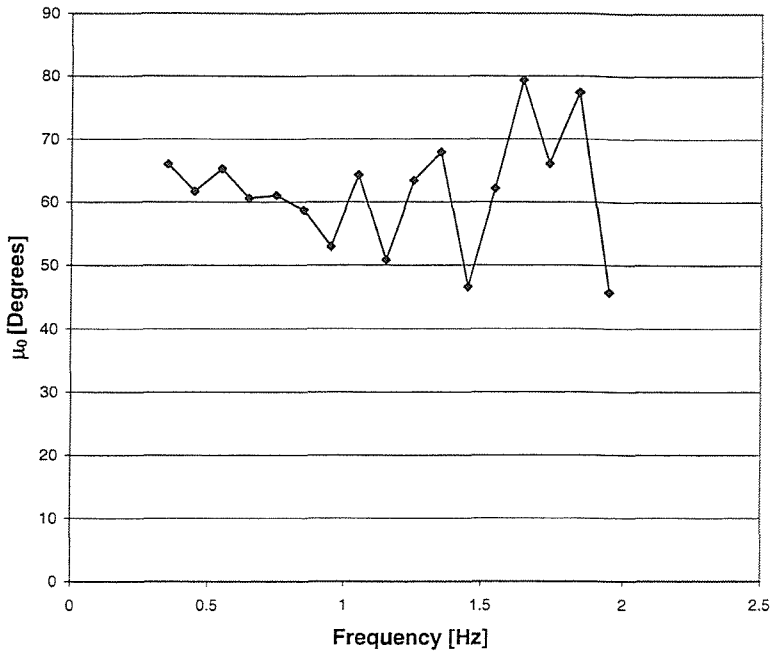

Figure 169: Mean Direction at Each Frequency Band

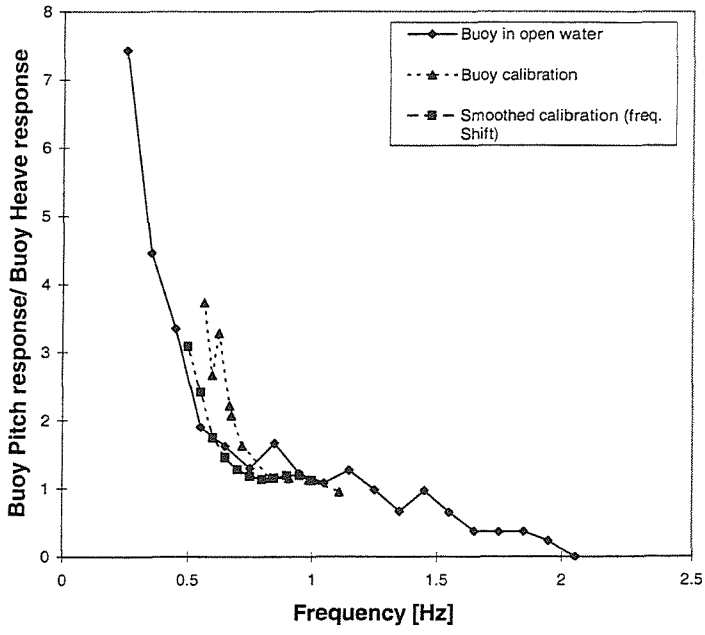

Figure 170: Pitch/Heave Amplitude

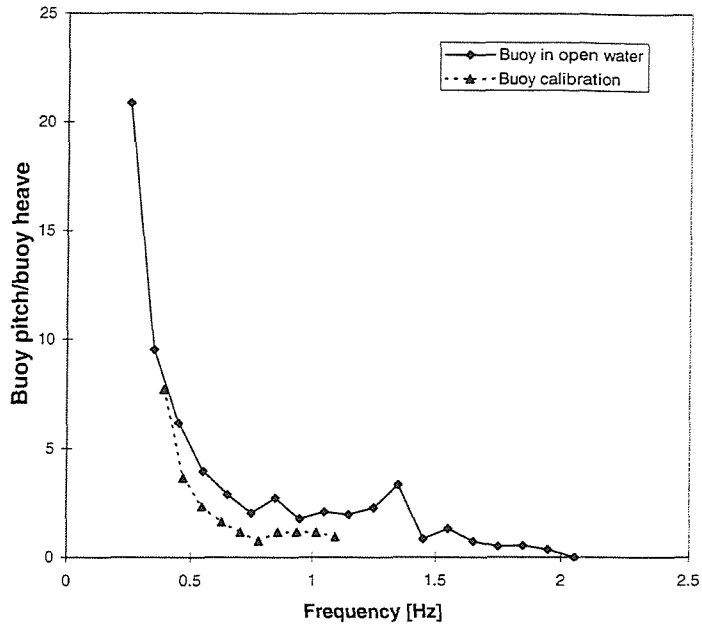

Figure 171: Roll/Heave Amplitude

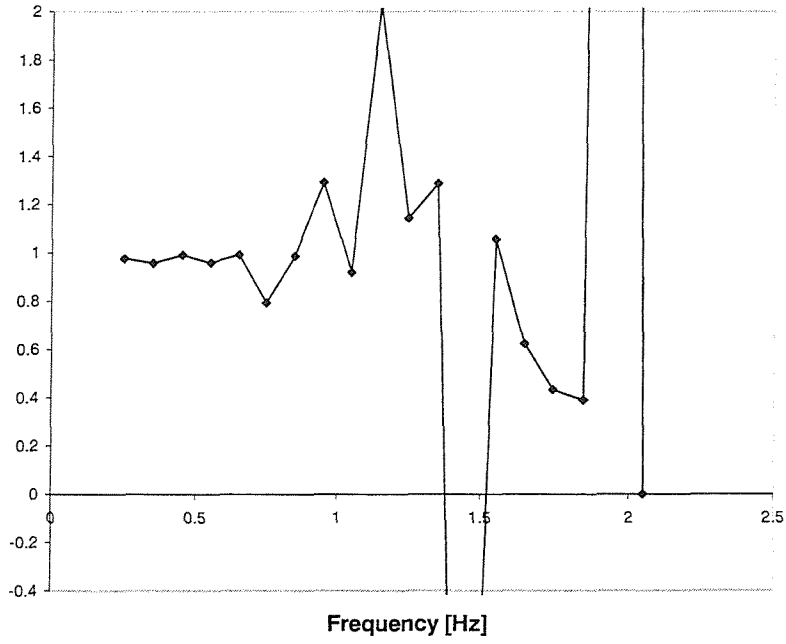

Figure 172: Spreading Function Integral

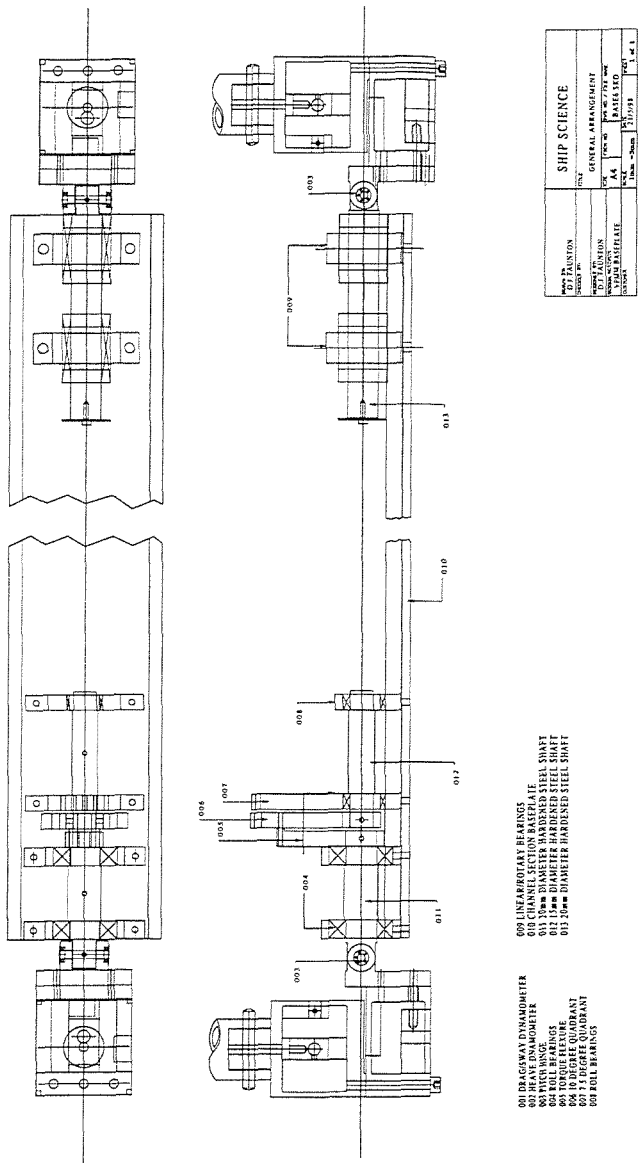

Figure 173: VPMM Baseplate arrangement

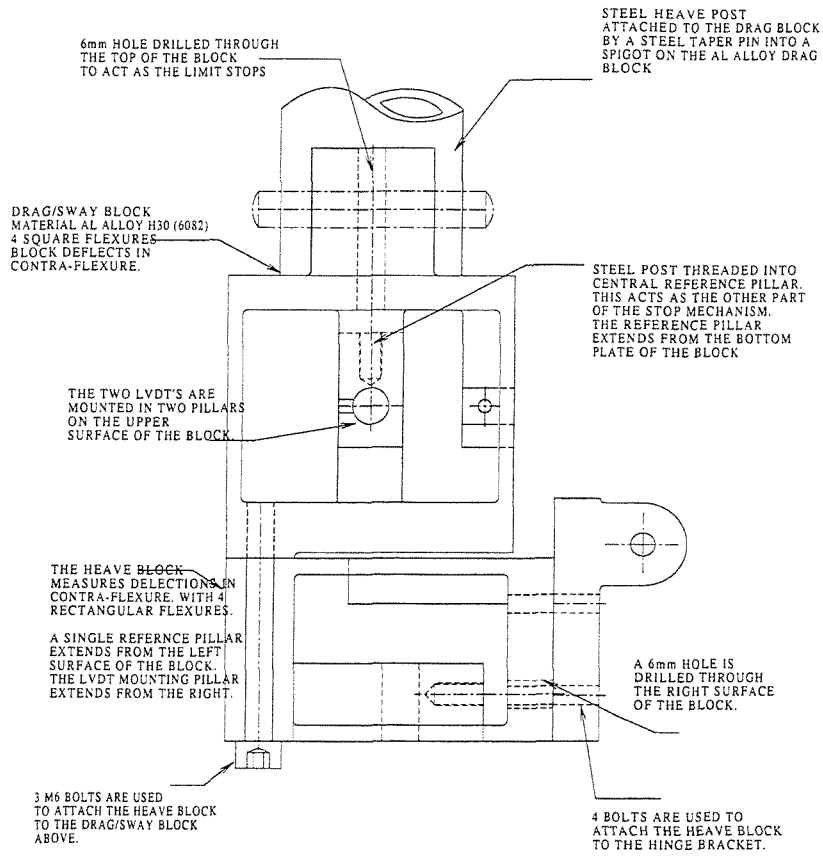

Figure 174: Dynamometer general arrangement

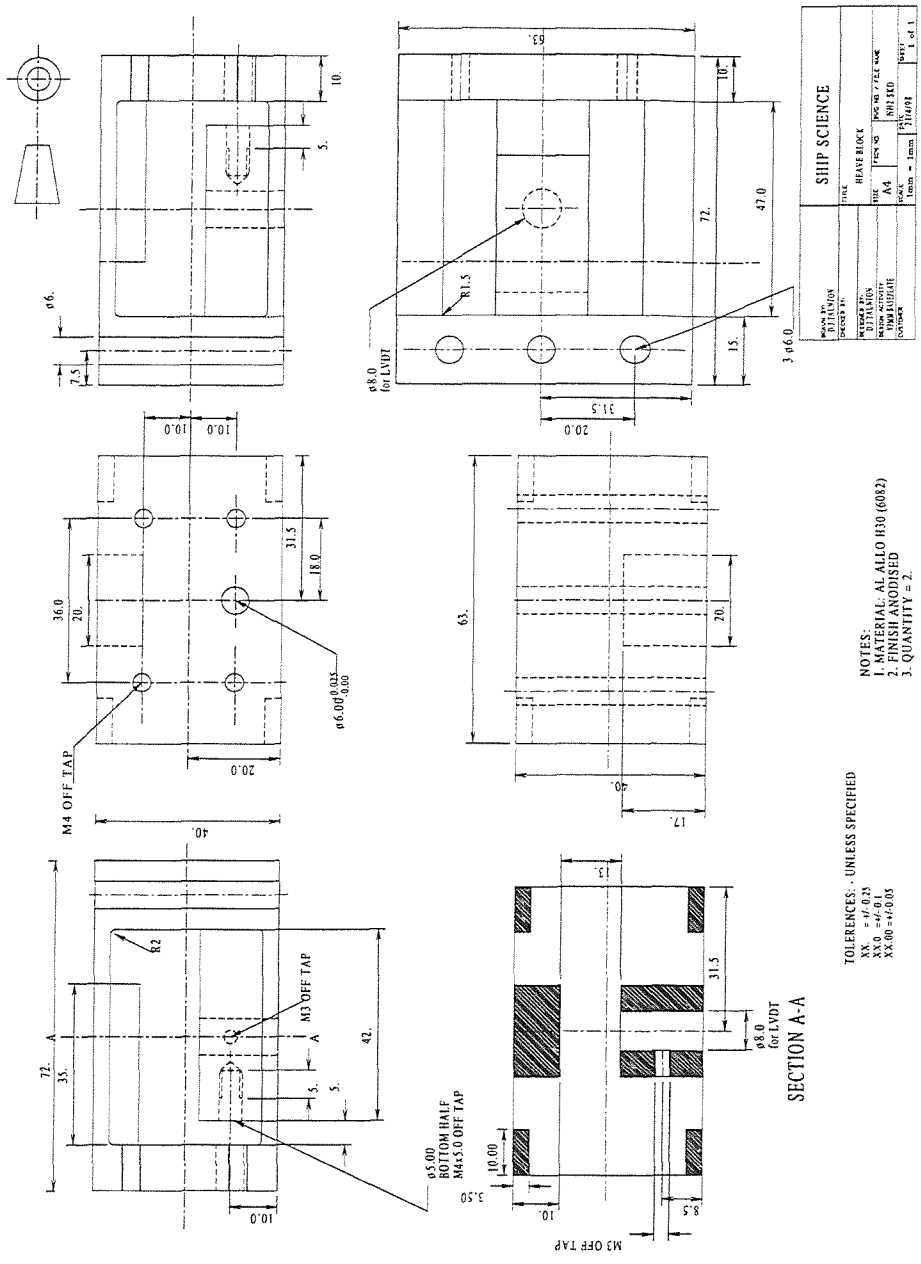

Figure 175: Heave Dynamometer

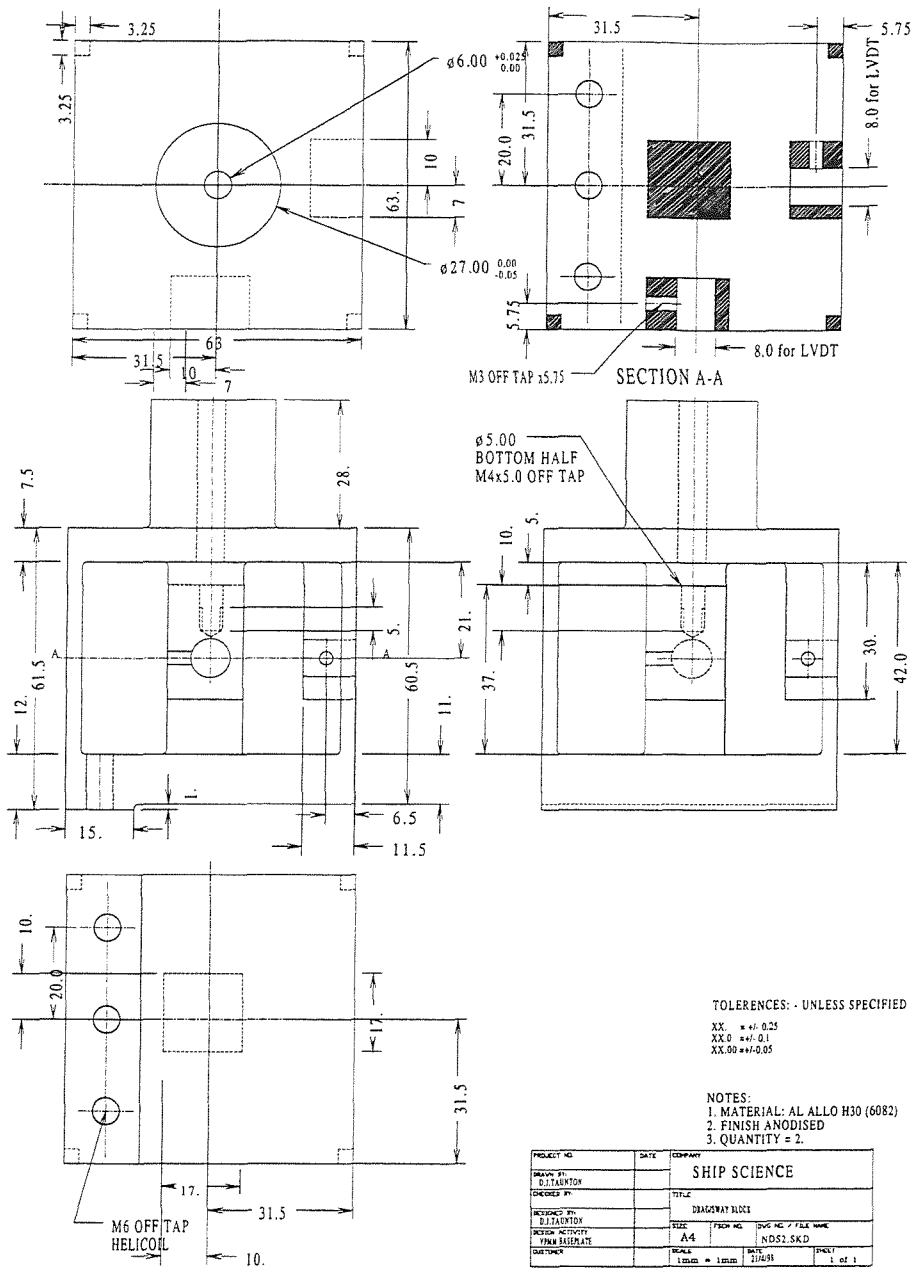

Figure 176: Drag/Sway Dynamometer

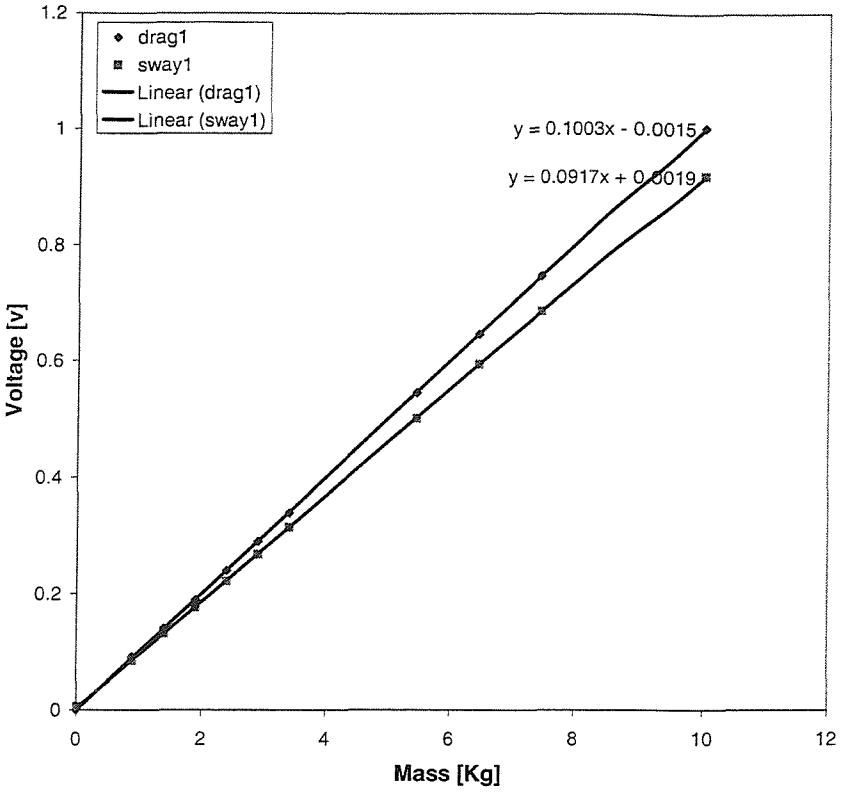

Figure 177: Drag/Sway Dynamometer 1: Mass-voltage relationship

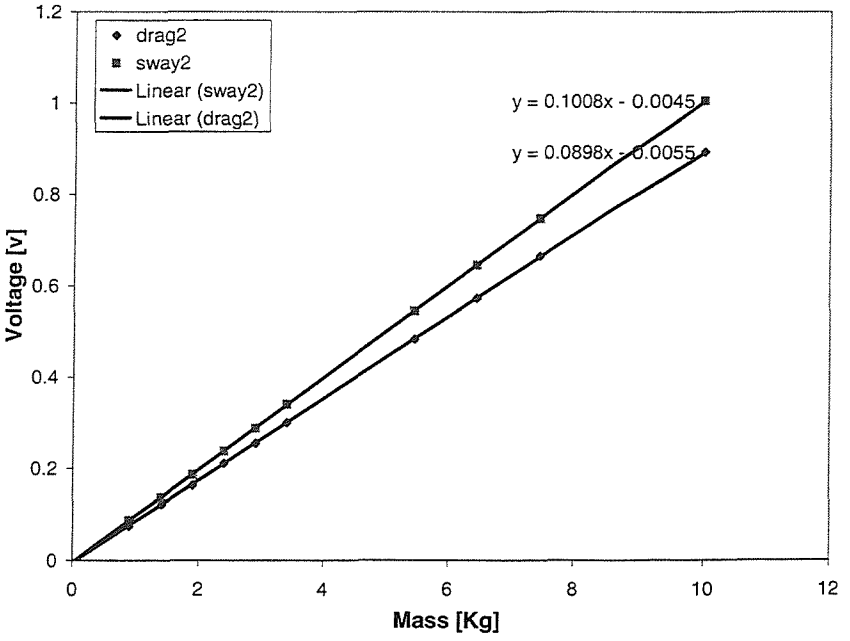

Figure 178: Drag/Sway Dynamometer 2: Mass-voltage relationship

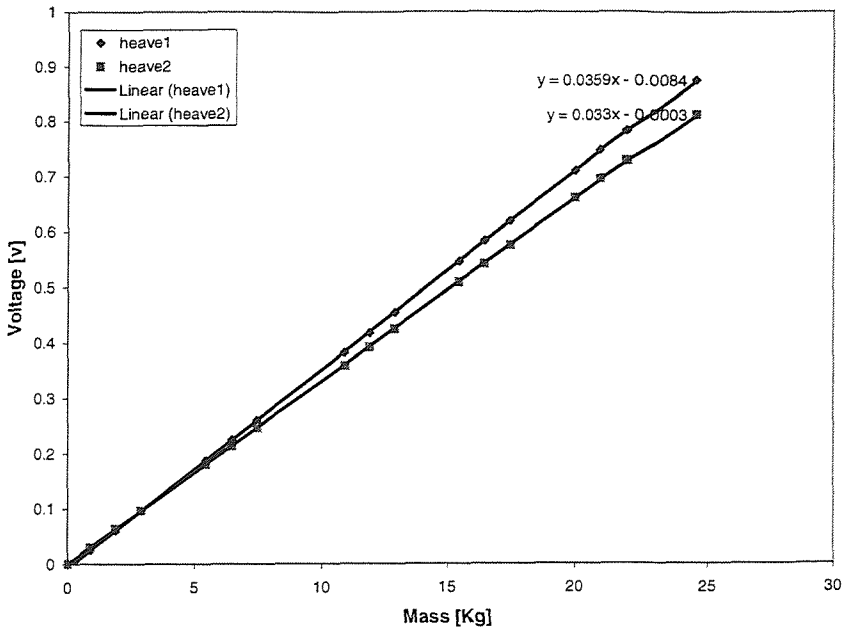

Figure 179: Heave Dynamometers: Mass-voltage relationship

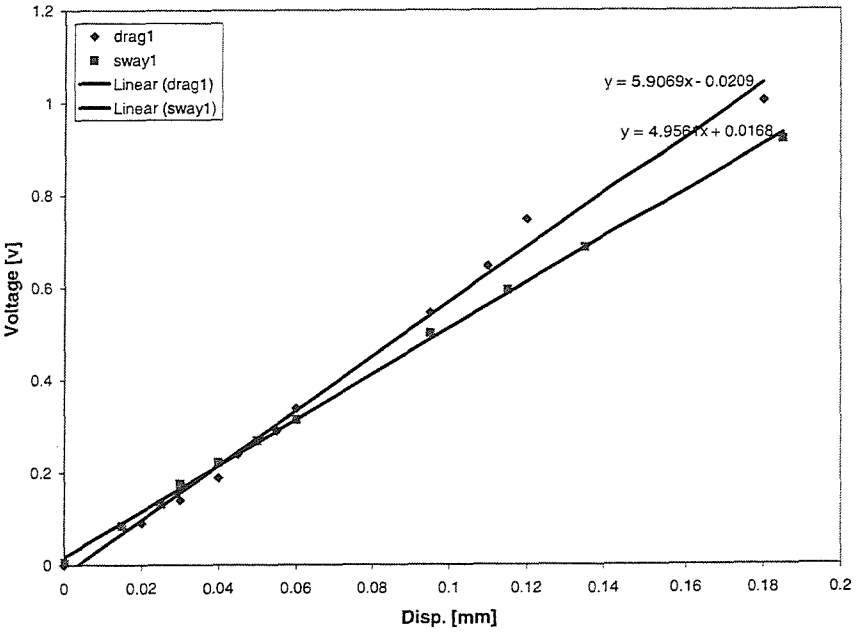

Figure 180: Drag/Sway Dynamometer 1: Deflection-voltage relationship

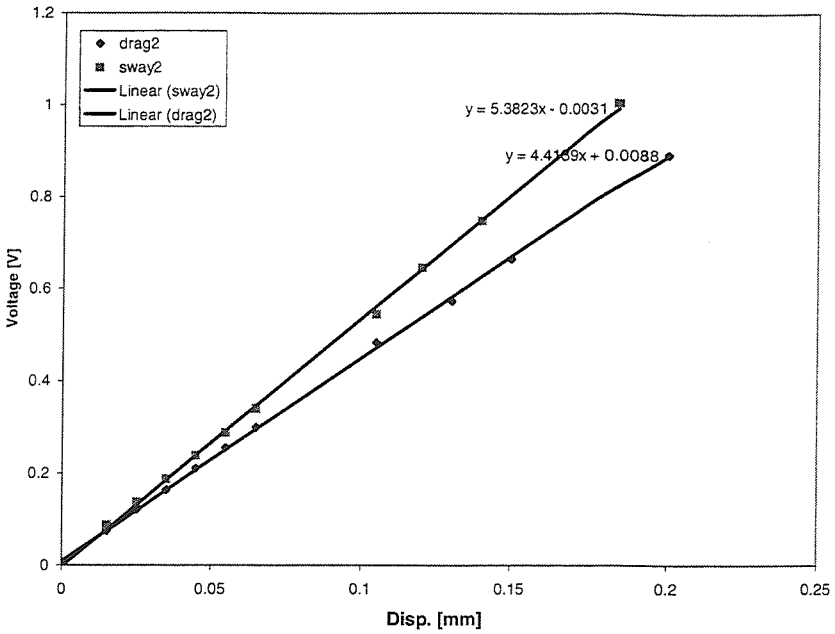

Figure 181: Drag/Sway Dynamometer 2: Deflection-voltage relationship

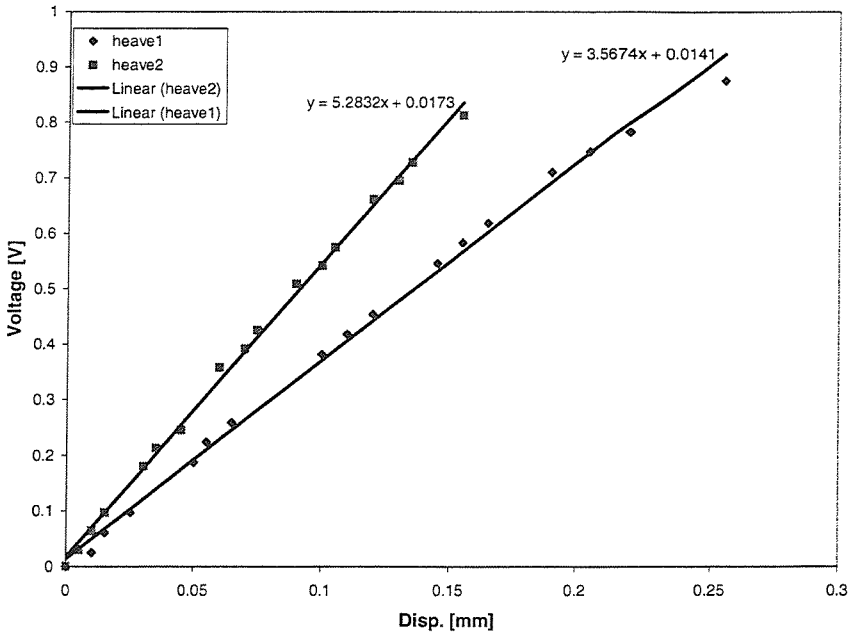

Figure 182: Heave Dynamometers: Deflection-voltage relationship

REFERENCES

[1] T. Karayannis, "A concept design and decision making model for alternative high speed ferries.,". PhD thesis, Department of Ship Science, University of Southampton, 1999.

[2] A.F. Molland and T. Karayannis, "Development of a concept exploration and assessment model for advanced fast marine vehicles.," The Sixth International Marine Design Conference, IMDC'97, vol. 1, Newcastle upon Tyne, U.K., 1997.

[3] A.F. Molland, T. Karayannis, and P.R. Couser, "Concept exploration and assessment of alternative high speed ferry types.," The Fourth International Conference on Fast Sea Transportation, FAST'97., vol. 1, Sydney, Australia., 1997.

[4] T. Karayannis, A.F. Molland, and Y. Sarac Williams, "Design data for high-speed vessels.," The Fifth International Conference on Fast Sea Transportation, FAST'99., vol. 1, Seattle, USA., 1999.

[5] G.E. Hearn, P.N.H. Wright, and W. Hills, "Seakeeping for design: Balance the vertical and horizontal motions of a catamaran.," The Third International Conference on Fast Sea Trasnport, FAST'95, vol. 1, Lubeck-Travemund, Germany, pp. 205–219, September 1995.

[6] N.K. Bales, "Optimizing the seakeeping performance of destroyer-type hulls," The 13th Symposium on Naval Hydrodynamics, Tokyo, pp. 479–503, 1980.

[7] ABCD Working Group On Human Performance At Sea, "Generating and using human performance simulation data to guide designers and operators of navy ships: Two large multinational programmes.," International Conference on Seakeeping and Weather., London, UK, 1995.

[8] R. Graham, A.E. Baitis, and W.G. Meyers, "On the development of seakeeping criteria," Naval Engineering Journal, pp. 259–275, 1992.

[9] A. Lawther and M.J. Griffin, "Prediction of the incidence of motion sickness from the magnitude, frequency, and duration of vertical oscillation," Journal of the Accoustical Society of America, vol. 82, pp. 957–966, September 1987.

[10] A. Lawther and M.J. Griffin, "The motion of a ship and the consequent motion sickness amongst passengers," Ergonomics, vol. 29, no. 4, pp. 535–552, 1986.

[11] A. Lawther and M.J. Griffin, "Motion sickness and motion charcteristics of vessels at sea," Ergonomics, vol. 31, no. 10, pp. 1373–1394, 1988.

[12] J.E. Conolly, "Ship motions in irregular waves," National Physical Laboratory Sea-Going Qualities of Ships, 1961.

[13] E.M.M. Wright, "Design applications of multihull motions data," Master's thesis, Department of Ship Science, University of Southampton, Sept 1996.

[14] J.J. Blok and W. Beukelman, "The high-speed displacement ship systematic series hull forms- seakeeping characteristics.," SNAME Transactions, vol. 92, pp. 125–150, 1984.

[15] G.J. Grigoropoulos and T.A. Loukakis, "Seakeeping characteristics of a series of fast monohulls," RINA international conference on high speed craft motions and manoeuvrability, 20 Feb 1998.

[16] E. Lahtiharju, T. Karppinen, M. Hellevaara, and T. Aitta, "Resistance and seakeeping characteristics of fast transom stern hulls with systematically veried from," Transactions of the Society of Naval Architects and Marine Engineers, vol. 99, pp. 85–118, 1991.

[17] J.F. Wellicome, P. Temarel, A.F. Molland, and P.R. Couser, "Experimental measurements of the seakeeping of fast displacement catamarans in long-crested head-seas.," Ship Science Report 89, Department of Ship Science, University of Southampton, 1995.

[18] M. Insel and A.F. Molland, "An investigation into the resistance components of high speed displacement catamarans.," Transactions of the Royal Society of Naval Architects, vol. 134, 1992.

[19] P.R. Couser, "An investigation into the performance of high-speed catamarans in calm water and waves.,". PhD thesis, Department of Ship Science, University of Southampton, 1996.

[20] C.G. Soares, N. Fonseca, P. Santos, and A. Maron, "Model tests of the motions of a catamaran hull in waves," RINA International Conference on the Hydrodynamics of High Speed Craft, vol. 1, London, November 1999.

[21] C. Boccalatte, G. Caprino, and L. Sebastiani, "Sea-keeping assessment of catamarans through numerical and experimental methods," RINA International Symposium on high speed vessels for transport and defense., London, November 1995.

[22] D. Rocco, L. Grossi, G. Caprino, and L. Sebastiani, "Comfort considerations in the design of fast monohulls," RINA International Conference on High speed craft motions and manoeuvrability, London, Feb 1998.

[23] D. Boote, M. Ragoone, and A. Sculati, "Seaworthiness of aquastrada class ships," The Third International Conference on Fast Sea Transport, FAST'95, vol. 1, Lubeck, Travemunde, Germany, pp. 165–178, September 1995.

[24] J. Kvålsvold, T. Svensen, and A. Braathen, "Comfort assessment of large high-speed catamarans," International Symposium on High Speed Vessels for Transport and Defence., London, 1995.

[25] H.S. Chan, "On the calculations of ship motions and wave loads of high-speed catamarans.," Internationl Shipbuilding Progress, vol. 42, no. 431, pp. 181–195, 1995.

[26] P.A. Bailey, D.A. Hudson, W.G. Price, and P. Temarel, "Theoretical and experimental validation of the seakeeping characteristics of high speed mono- and multi-hulled vessels.," The Fifth International Conference on Fast Sea Transportation, FAST'99, Seattle, Washington USA, pp. 429–442, September 1999.

[27] C.C. Fang, H.S. Chan, and A. Incecik, "Investigation of motions of catamarans in regular waves-1," Ocean Engineering, vol. 23, no. 1, pp. 89–105, 1996.

[28] C.C. Fang, H.S. Chan, and A. Incecik, "Investigation of motions of catamarans in regular waves-2," Ocean Engineering, vol. 24, no. 10, pp. 949–966, 1997.

[29] D. Kring and P. Sclavounos, "A new method for analysing the seakeeping of multi-hull ships.," The First International Conference on Fast Sea Transportation, FAST'91, vol. 2, pp. 429–444, 1991.

[30] S. Cook, P. Couser, and K. Klaka, "An investigation into wave loads and catamarans," RINA International Conference on the Hydrodynamics of High Speed Craft, vol. 1, London, November 1999.

[31] J.F. Wellicome, P. Temarel, A.F. Molland, and D. Hudson, "Theoretical prediction of the seakeeping charcteristics of two fast displacement catamarans in oblique seas.," Ship Science Report 113, Department of Ship Science, University of Southampton, 1999.

[32] Det Norske Veritas Classification, "Tentative rules for classification of high speed and light craft,". Det Norske Veritas Classification A/S, January 1991.

[33] "International code of safety for high-speed craft hsc code," 1994. sales no: IMO-187E.

[34] J.F. O'Hanlon and M.E. McCauley, "Motion sickness incidence as a function of the frequency and acceleration of vertical sinusiodal motion," Aerospace Medicine, vol. 45, pp. 366–369, 1974.

[35] ISO2631, "Evaluation of exposure to whole-body z-axis vertical vibration in the frequency range 0.1 to 0.63 hz, ISO 2631/3-1985," 1985.

[36] BS6841, "Measurement and evaluation of human exposure to whole-body mechanical vibration and repeated shock, BS6841," 1987.

[37] F. Perez Arribas, A. Lopez Pineiro, and J.A. Felgueroso Leon, "Movements in ro-pax ships. effect on security and comfort," International Conference on Ship and Shipping Research, vol. 1, Venice, September 2000.

[38] ISO2631, "Mechanical vibration and shock–evaluation of human exposure to whole-body vibration–part 1: General requirements," 1997.

[39] A.R.J.M. Lloyd, "Seakeeping: Ship behaviour in rough weather.,". ARJM Lloyd, 1998.

[40] R.N. Andrew and A.R.J.M. Lloyd, "Full-scale comparative measurements of the behaviour of two frigates in severe head seas," Transactions of the Royal Institution of Naval Architects, vol. 123, pp. 1–31, 1982.

[41] Ir. A.M. van Wijngaarden, "The optimum form of a hull for the North Sea area," Internationl Shipbuilding Progress, vol. 31, no. 359, pp. 181–187, 1984.

[42] H.S. Chan and A. Incecik, "Seaworthiness assessment of a trimaran ship," Internation Conference on High Speed Craft Motions and Manoeuvrability, London, February 1998.

[43] D. Bailey, "The NPL high speed round bilge displacement hull series.," Maritime Technology Monograph, Royal Institute of Naval Architects, vol. 4, 1976.

[44] H.Y.H. Yeh, "Series 64 resistance experiments on high-speed displacement forms.," Marine Technology, July 1965.

[45] J.F. Wellicome, A.F. Molland, J. Cic, and D.J. Taunton, "Resistance experiments on a high speed displacement catamaran of series 64 form.," Ship Science Report 106, Department of Ship Science, University of Southampton, 1999.

[46] A.F. Molland, J.F. Wellicome, P. Temarel, J. Cic, and D.J. Taunton, "Experimental investigation of the seakeeping characteristics of fast displacement catamarans in head and oblique seas.," Transactions of the Royal Institution of Naval Architects, no. W255(2000), 2001.

[47] J.F. Wellicome, P. Temarel, A.F. Molland, J. Cic, and D.J. Taunton, "Experimental measurements of the seakeeping characteristics of fast displacement catamarans in oblique waves.," Ship Science Report 111, Department of Ship Science, University of Southampton, 1999.

[48] J.F. Wellicome, P. Temarel, A.F. Molland, J. Cic, and D.J. Taunton, "Experimental measurements of the seakeeping charcteristics of fast 4.5m displacement catamarans in open irregular sea.," Ship Science Report 118, Department of Ship Science, University of Southampton, October 1999.

[49] J.F. Wellicome, P. Temarel, A.F. Molland, J. Cic, and D.J. Taunton, "The design, construction and calibration of a wave buoy for ship model tests in open water.," Ship Science Report 112, Department of Ship Science, University of Southampton, October 1999.

[50] R.E. Harris, J. Wolfram, and A. Aitken, "Measurement of standby vessel motions in storms," International Conference on Ship Motions and Manoeuvrability, London, U.K., February 1998.

[51] D.A. Hudson, "A validation study on mathematical models of speed and frequency dependence on seakeeping of high speed craft.,". PhD thesis, University of Southampton, 1999.

[52] R.E.D. Bishop, W.G. Price, and Y.S. Wu, "A general linear hydroelasticity theory of floating structures moving in a seaway," Philisophical Transactions of the Royal Society, Series A, vol. 316, pp. 375–426, 1986.

[53] "Seakeeping trials on board universal VI an FBM 35 metre solent class high speed catamaran tricat," October 1993.

[54] G.J. Goodrich, "Personal communication on transfer function spreading relationships." May 1999.

[55] T.H. Havelock, "Notes on the theory of heaving and pitching," Transactions of the Royal Institution of Naval Architects, vol. 87, pp. 109–122, 1945.

[56] N. Hogben, N.M.C. Dacunha, and G.F. Olliver, "Global wave statistics,". Old Woking, Surrey, GU22 0LH, England: Unwin Brothers Limited, 1986.

[57] A.F. Molland and D.J. Taunton, "Methods for assessing the seakeeping performance of competing high speed vessel designs," RINA International Conference on the Hydrodynamics of High Speed Craft, London, U.K., Nov 1999.

[58] Ir. C.C. Glansdorp, "Horizontal high frequency pmm-tests with a mariner model," Tech. Rep. 381 M, Laboratorium voor Scheepsbouwkunde, Technische Hogeschool Delft, July 1973.

[59] R. Pattendon, C. Shepherd, and M. Wittke, "The design and construction of a vertical planar motion mechanism.," Master's thesis, University of Southampton, 1997.

[60] T.B. Booth and R.E.D. Bishop, "The planar motion mechanism," admiralty experimental works, Admiralty experimental works, 1973.

[61] "Fast ferries," Shipping World and Shipbuilding, pp. 18–25, April 1996.

[62] C. Bertorello, "Trimaran hull performance for fast passenger ferries," International Conference on Ship and Shipping Research, vol. 1, Venice, September 2000.

[63] T. Karppinen, "Criteria for seakeeping performance prediction," VTT, ESPOO, 1987.

[64] E.V. Lewis, "Principles of naval architecture-motions in waves and controllability,", vol. 3. 601 Pavonia Avenue, Jersey City, New Jersey: The Society of Naval Architects and Marine Engineers, second revision ed., 1988.

[65] The Nordic Cooperative project, "Seakeeping performance of ships, assessment of ship performance in a seaway," 1987.

[66] K. Sariöz and E. Narli, "Seakeeping performance of high speed warship hull forms: Deep vee versus round bilge," International Conference on High Speed Craft Motions and Manoeuvrability, London, February 1998.